SYNTHESIS AND CHARACTERIZATION OF BIOACTIVE SOL-GELS AS ANTI-CORROSIVE/ANTI-FOULING STEEL COATINGS

BY

UBONG MONDAY EDUOK

A Dissertation Presented to the

DEANSHIP OF GRADUATE STUDIES

KING FAHD UNIVERSITY OF PETROLEUM & MINERALS

DHAHRAN, SAUDI ARABIA

In Partial Fulfillment of the
Requirements for the Degree of

DOCTOR OF PHILOSOPHY

In

CHEMISTRY

DECEMBER 2015

KING FAHD UNIVERSITY OF PETROLEUM & MINERALS

DHAHRAN- 31261, SAUDI ARABIA

DEANSHIP OF GRADUATE STUDIES

This thesis, written by **UBONG MONDAY EDUOK** under the direction his thesis advisor and approved by his thesis committee, has been presented and accepted by the Dean of Graduate Studies, in partial fulfillment of the requirements for the degree of **DOCTOR OF PHILOSOPHY IN CHEMISTRY**.

27/12/2015

Dr. MAZEN KHALED
(Advisor)

27/12/2015

Dr. ABDULAZIZ AL-SAADI
Department Chairman

27-12-2015

Dr. RAMI SULEIMAN
(Co-Advisor)

Dr. SALAM A. ZUMMO
Dean of Graduate Studies

27/12/2015

Dr. BASSAM EL ALI
(Member)

24/1/16

Date

27/12/2015

Dr. ABDALLA ABULKIBASH
(Member)

27-12-2015

Dr. AMJAD KHALIL
(Member)

I dedicate this work to the Almighty God, the source of wisdom, the light of understanding and inspiration, who has been the reason for my success in this program and in life; my strength in adversity and my maker, guidance and power

ACKNOWLEDGMENTS

I acknowledge and accord total reverence to my God for His faithfulness, drive and sustenance throughout my academic pursuits, for the completion of the doctoral research work, and subsequent award of the Doctor of Philosophy (Ph.D.) degree in Chemistry.

I wish to also acknowledge King Fahd University of Petroleum and Minerals (KFUPM) and the Ministry of Higher Education for providing the PhD scholarship (including funding of my research and conference trips, locally and internationally) of which I have benefited throughout my stay in this institution. Immense thanks goes to the rector of KFUPM (Dr. Khaled S. Al-Sultan) for hosting my PhD program; the past (Dr. A. Hamdan) and present (Dr. Al-Abdulaziz Saadi) Chairmen, Department of Chemistry, KFUPM for providing the needed facilities for my PhD education and research for these past years. I wish to thank the Dean of Graduate School, Dr. Salam A. Zummo for his encouragement in this program; his advises have helped in so many ways regarding the program schedules and general academic performance.

I express my deepest gratitude to my research advisors, Dr. Mazen Khaled and Dr. Rami Suleiman (co-advisor) for their instructive guidance and encouragements, constructive criticism and insights, and patience in training throughout the course of this work, in the prior and design phases as well as the execution and presentation of this work; I wish to say a big thank you. I wish to also express my appreciation to the members of my PhD thesis committee (Dr. Bassam El Ali, Dr. Amjad Khalil and Dr. Abdalla Abulkibash) for their assistance and advice in keeping with the progress of work on schedule and the reading/correction of this thesis. Special thanks goes to Dr. El Ali for his valuable

suggestions and critiques in the developmental stage of this research work that kept its progress on schedule. As the graduate adviser, his advises have helped in the selection of courses needed to foster a strong taught-research balance in my PhD research. Dr. Khalil is appreciated for his advice on the biological part of this research (the provision of the thermophilic *Bacillus licheniformis* and its isolation/identification procedures); I wish to say a big thank you. I wish to also acknowledge the assistance of the former Director, Center of Research Excellence in Corrosion (CORE-C), KFUPM, Dr. Zuhair Gasem, for hosting me and allowing the use of equipment at the Advanced Coating Laboratory, CORE-C, for my experimental work. CORE-C is also appreciated for sponsoring my summer research trips (2013 and 2014) to Sheffield Hallam University, UK as well as the 15th Middle East Corrosion Conference and Exhibition held at the Gulf Hotel, Bahrain from the 3rd to 5th February, 2014. A big thank you to other CORE-C members of staff. Many thanks to all the academic and non-academic staffs of the Department of Chemistry, KFUPM, for not just instructing and teaching Chemistry to me, but also raising a scholar worthy of character and learning. Taking several advanced theoretical and research courses in chemistry has helped my background in the science and has also fostered better thinking beyond narrow academic disciplines.

I wish to acknowledge the help and training provided by Mr. Deepak Aanand, Department of Life Sciences (Bacterial studies); Mr. Hatim Dallafa, Center for Engineering Research (Scanning electron microscopy and other material characterizations); Mr. Mohammad Arab and Mr. Mansour Al-Zaki, NMR Laboratory, Department of Chemistry (FTIR/NMR); Mr. Ahmed, Center for Engineering Research (Thermogravimetric analyses) and so many others member of staff and students too

numerous to mention**.** I wish to also acknowledge Prof. Thomas J. Smith (Biomedical Research Centre, BMRC, Sheffield Hallam University, UK) and Prof. Robert Akid (Corrosion and Protection Centre, School of Materials, University of Manchester, UK), for hosting me and providing the needed advice, reagents and facilities for the work during my research visits. Immense thanks goes to Dr. Jeanette Gittens for instructing and teaching me, especially on the advanced bacterial part of this work with confocal scanning laser microscopy, field analyses (at Whitby Harbour, UK) and making my stay at BMRC, UK, comfortable; many thanks to Prof. Ron for his advice on sol-gel synthesis. I express my deepest gratitude to Dr. Saviour A. Umoren and Dr. Ime B. Obot for their encouragements throughout the work; their successes in the corrosion field has been a source of great inspiration, and I wish to also thank them for mentioning and recommending KFUPM to me in 2011. Assuredly not the least, I wish to thank and appreciate the members of my dear family for being there for me in times of need, their ceaseless prayers have sustained me throughout the program; my mother and brother (Barr. Mrs. Sylvia and Udeme Eduok) have been sources of inspiration and peace. The advices, prayers and support of my fiancée, Ms Blessing, will never be forgotten. The Nigerian community at KFUPM has also been a source of moral support.

TABLE OF CONTENTS

LIST OF TABLES

LIST OF FIGURES

LIST OF ABBREVIATIONS

SEM	:	Scanning electron microscopy
AFM	:	Atomic Force Microscopy
EDX	:	Energy dispersive x-ray
CLSM	:	Confocal laser fluorescence microscopy
EIS	:	Electrochemical impedance spectroscopy
NMRS	:	Nuclear magnetic resonance spectroscopy
FTIR	:	Fourier transform infra-red
CFU	:	Colony-forming units
EPS	:	Extracellular polymeric substance
PDMS	:	Polydimethylsiloxane
FRC	:	Foul release coating
ATR/IR	:	Attenuated total reflectance Fourier transform infrared spectroscopy
ATCC	:	American Type Culture Collection
XRD	:	X-ray Diffraction
XPS	:	X-ray photoelectron spectroscopy
OCP	:	Open circuit potential
CAM	:	Contact angle measurement
TGA	:	Thermogravimetric analysis
R_p	:	Polarization resistance

ABSTRACT

Full Name : [Ubong Monday Eduok]

Thesis Title : [Synthesis and characterization of bioactive sol-gels as anti-corrosive/anti-fouling steel coatings]

Major Field : [Chemistry]

Date of Degree : [December 2015]

Series of new protective sol-gel type coatings have been synthesized in this study from simple silanes (alkoxysilanes and organoalkoxysilanes) and reactive silicone precursors, carefully chosen to give the needed bulk and surface properties. Sol-gel syntheses focus on the combination of inorganic and organic functionalities to produce protective hybrid coatings with rigid bulk properties. The bulk of these sol-gel materials has also been incorporated with viable *Bacillus licheniformis* endospores as well as micro-sized anticorrosive pigments. The presence of the bacterial endospores in the coatings (biotic) is found to increase barrier protection and foul resistance compared to the abiotic ones within the immersion periods in this study. This has been attributed to the characteristic antibiotic biofilm produced by this bacterium, also found to increase the hydrophobicity of the sol-gel coatings in the presence of the bacterial endospores after incorporation. By altering the surface wetness of these coatings, bacterial spore accumulation prevents the diffusion of corrosion ions through the coating to mild steel surface thereby increasing the coating resistance while also reducing the degree of water uptake. This study reveals a novel corrosion/biofouling mitigation approach by an axenic thermophilic strain of *B. licheniformis* isolated from Saudi Arabia.

الملخص

الاسم الكامل: أبونغ موندي إيدويك

عنوان الرسالة: توليف وتوصيف طلاءات هلام ذائب فعالة بيولوجية في حماية حديد الصلب من التآكل والعفونة

التخصص: الكيمياء

تاريخ الدرجة العلمية: كانون الأول ٢٠١٥

أُصطنعت في هذه الدراسة سلسلة جديدة من طلاءات الهلام الذائب الواقية من مركبات السيليكون البسيطة (السيليكون العضوي وهيدروكسيد السيليكون) ومولدات (سلائف) السيليكون التفاعلية، التي اختيرت بعناية من أجل الحصول على الخصائص الكلية والسطحية المطلوبة.

ركزت توليفات الهلام الذائب على الجمع بين الوظائف العضوية وغير العضوية لإنتاج طلاء واقي هجين مع خصائص كلية وصلابة. الكتلة الكلية من مواد الهلام الذائب دمجت مع عصيات قابلة للحياة(*Bacillus licheniformis* endospores) وكذلك خُضُب صغيرة الحجم مضادة للتآكل. وُجد في هذه الدراسة أن تواجد بعض أبواغ البكتريا في الطلاء الحيوي يزيد من حماية السطح ومقاومة العفونة مقارنة بتلك غير الحيوية خلال فترات الغمر. ويعزى ذلك إلى الغشاء الحيوي الرقيق المميز المضاد الحيوي الذي تنتجه هذه البكتريا ووجدت أيضاً زيادة في خصائص الكره للماء لطلاء الهلام الذائب بعد دمج الأبواغ البكتيرية. تراكم أبواغ البكتيريا يمنع انتشار الأيونات المسببة في التآكل من خلال الطلاء الخفيف لسطح الفولاذ وبالتالي زيادة مقاومة الطلاء وأيضا تقليل درجة الترطيب عن طريق تغيير رطوبة سطح هذه الطلاءات. وتكشف هذه الدراسة نهجا جديدا في تخفيف التأكل وتراكم القاذورات الحيوية من قبل مزرعة حرارية (ممحوضة) لسلالة ب. ليشينيفورميس (*B.licheniformis*) المعزولة في المملكة العربية السعودية.

CHAPTER 1

INTRODUCTION

1.1 Sol-gels

These are hydrolysis/condensation products formed from catalyzed reaction of linear and cyclic organoalkoxysilane and alkoxide (not restricted to only siloxanes) with water; also involving hydrosilylation if Si─H bonds are added across unsaturated bonds. The term "sol-gel" means that nanometer sized sol particles are disperse in a soluble suspension phase made of colloidal gel depending on the viscosity of this solution. Depending on the precursors employed for the syntheses, many sol-gel materials are designed to possess unique functionalities hence varying surface/bulk properties specific for some applications. For instance, the quest for synthesis of antifouling sol-gel materials with improved adhesion on metal substrates involving the establishment of the Si-O-M bond while maintaining the amphiphilic properties for surfaces designed to resist settlement and adhesion of marine foulers. Hydrophilic and hydrophobic surfaces are known to foul-release ulva and algae spores, respectively, and this can be achieved from sol-gel chemistry made from PDMS and alkoxide [1]. Though other treatments may abound in some cases, these sol-gel materials attain remarkable surface and bulk properties when they are rightly cured at temperatures unique to their chemistries. Hydrophobic coatings (including some sol-gel types) reduce the adhesion of foulers due to their low surface

energies; and this is foul-releasing property is greatly aided by the sheer stress initiated by the speeding of the marine vessel in the seawater. This is common among fluoropolymeric and PDMS-based antifouling coatings [2]. The antifouling and fouling-release properties of an organically modified silicate (ORMOSIL) synthesized from tetraethoxysilane and octyltriethoxysilane, hydrolyzed with water and isopropyl alcohol has been reported according to Equation 1.1 (R= *n*─octyl group) for a typical marine application [2,3].

$$Si(OEt)_4 + RSi(OEt)_3 + H_2O \longrightarrow [R\text{-}SiO_nH_m(OEt)_q]_p + EtOH \qquad (1.1)$$

Figure 1.1 shows a small marine vessel at Irondequoit Bay, northeastern Monroe County, New York (US) whose hull was coated with this tetraethoxysilane─octyltriethoxysilane sol-gel antifouling paint (left:without and with mild polishing:right). The vessel was resistant to fouling on re-introduction into the seawater on the 20th May 2006, and after being coated (at the hull) and cured at ambient temperature for two days. This coating is now widely applied to larger ships and other marine vessels on Lake Ontario at the southwest by Canadian province of Ontario.

Moreover, since sol-gel materials are made of nano to micro size pores inherent in the bulk of the coating, they can be encapsulated with other active materials (proteins, enzymes, bacterial cells and spores, corrosion inhibitors, nanocomposites etc.) so as to enhance the properties to which they are prepared for: bulk strength, wetness, anticorrosive/ antifouling abilities, controllable permeability or porosity etc) [4].

Figure 1.1 The vessel hull coated with tetraethoxysilane─octyltriethoxysilane sol-gel antifouling paint at Irondequoit Bay (US); without (a) and with (b) polishing [3].

1.2 Sol-gel chemistry

Generally, the process by which solid materials are made from smaller molecules of precursors is known as sol-gel process. Sol-gel synthesis takes place at low temperatures. Sol-gel synthesis dates far back the 1800's with the pioneer work reported by Ebelmen M. (a French chemist) involving the synthesis of silicon tetraisoamyloxide from silicon tetrachloride and isoamyl alcohol [5]. His later work [6] involved the synthesis of boron amyloxide, boron ethoxide and boron methoxide using isoamyl alcohol, ethanol and methanol, respectively, with boron trichloride. Authors attributed the success of the synthesis route to the polarity of the main element: with alkoxides forming by reaction of electropositive metals with corresponding alcohols [7]. Earlier works from Ebelmen were reported from Manufacture de Ceramiques de Sevres in France [8], though other sol-gel researches had been developed from these reports in the late 1800's and middle 1900's. Similar sol-gel synthesis can also be found in nature. Attia et al. [8] have also reported the formation of chalcedony minerals from polycondensation of aqueous siliceous. Basically in sol-gel synthesis, interconnected networks of glass or glass-like material (even

ceramics) are formed from condensation reactions involving nanometer sized sol particles previously formed by hydrolytic conversion of adequate precursors (e.g. metal oxide, metal alkoxide, organoalkoxysilane etc.) via either catalyzed (acid or basic) reaction with water, usually with alcohol employed to aid precursor dissolution in the media. Figure 1.2 and 1.3 show typical sol-gel processes where ceramics are formed as stable gels from adequate precursors when heated to a high temperatures (sintering), and as moderate glass structures at room temperature curing of gels from simple silanes. Also in this process, critical drying temperatures will form noncrystalline and aquagels. The early stages of the gels are called aquagel since they are usually filled with other liquids like water (hydrogels) and alcohols (alcogels); aerogels are formed when these liquids are displaced by air without altering the rigid network structure [8].

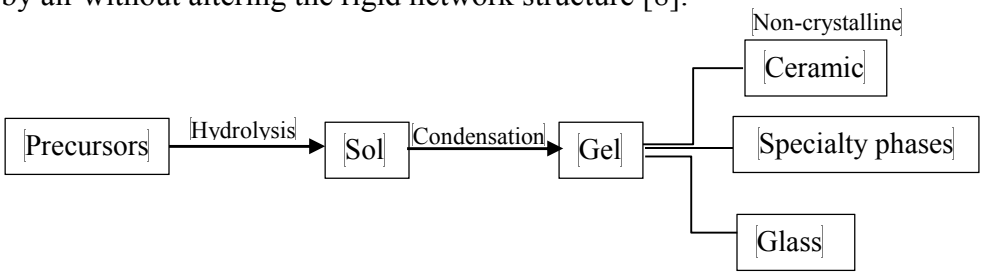

Figure 1.2 A typical sol-gel process, and products obtained from different drying phases.

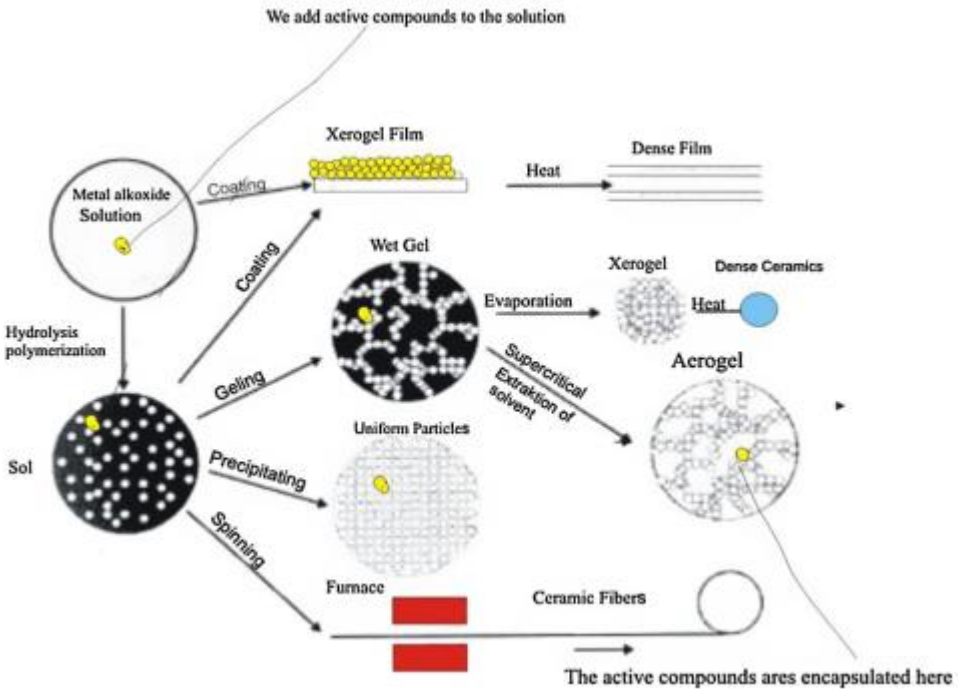

Figure 1.3 Possible sintered and dried gelled products derived from sol–gel synthesis [9].

Just before gelation, a pseudo-particulate growth stage involving the agglomeration/ nucleation of the sol-gel polymer structures is formed. A full gel structure is observed to form subsequently in the solution mixture when it thickens throughout the medium. Condensation reactions continue far after gelation, as the material cures depending on the temperature. During drying, excess water and alcohol molecules are removed as well as unreacted precursors thereby giving a glassy material as the silica network (in the case of silanes and siloxanes) shrinks. The sol-gel route for a gel network depends on the structure of the sol in two distinct mechanisms. The first mechanism is based on the growth of sol particles into macromolecules coming together into infinite network; this is common in acid-catalyzed hydrolysis of tetraalkyl silicates. The other mechanism is based on aggregation of particles into an intermediate colloidal sol phase before gelling [8]. It is also well known that the final structures of these gels are dependent on the kinetics of the stepwise hydrolysis and condensation reactions; with metal alkoxides ($M(OR)_n$) widely

reported to produce glass and ceramic materials from very stable gels with high degree of chemical homogeneity. The rate of hydrolysis, as well as the overall sol-gel process, is affected by pH, the ratio of water to M groups in the precursors (such as alkoxides of V, Si, Ti, Zr etc), the network-forming element (M; e.g. Si, Ti, Zr, Al, Fe, B) as well as the nature of the alkoxy groups including the size of R, concentration of other precursors, amount of solvents and dopants (e.g. organic dyes and rare earth elements), catalysts, temperature and degree of mixing. According to Equation 1.2, exchange reactions with alcohols can bring about unique routes for preparing higher alkoxides (even multicomponent systems) bearing simpler $M(OR)_n$; and altering the hydrolysis rate of alkoxy precursors also promotes homogeneity of final material [9,10]. Further reactions that condenses molecular water and alcohol are regarded as condensation since they lead to the formation of gelled (M─O─M) networks in the final materials (Equation 1.3).

$$M(OR)_n + R'OH \longrightarrow M(OR)_{n-1}(OR') + ROH \qquad (1.2)$$

$$2\ M(OR)_{n-1}(OH) \longrightarrow (OR)_{n-1}\ M{-}O{-}M\ (OR)_{n-1} + HOH \qquad (1.3)$$

Attia et al. [8] has opined that condensation of hydrolytic products of tetraalkoxy silanes like tetraethyl orthosilicate (TEOS) yield 3D connected silica networks (Equation 1.4); with two moles of water required per mole of TEOS.

$$Si(OEt)_4 + 2\ H_2O \longrightarrow SiO_2 + 4\ C_2H_5OH \qquad (1.4)$$

The conversion of TEOS to silica is not as simple as expressed in Equation 1.4, this process involves a more complicated mechanism (Equations 1.5─1.8) especially since hydrolysis is entirely stepwise. Normally condensation reactions commence before the hydrolysis is completed, therefore, condensation is possible via H─OH exchange as well as ROH (Equation 1.9; where $x+y=3=v+w$) from partially hydrolyzed precursors.

$$Si(OEt)_4 + H_2O \longrightarrow Si(OH)(OEt)_3 + C_2H_5OH \quad (1.5)$$

$$Si(OH)(OEt)_3 + H_2O \longrightarrow Si(OH)_2(OEt)_2 + C_2H_5OH \quad (1.6)$$

$$Si(OH)_2(OEt)_2 + H_2O \longrightarrow Si(OH)_3(OEt) + C_2H_5OH \quad (1.7)$$

$$Si(OH)_3(OEt) + H_2O \longrightarrow Si(OH)_4 + C_2H_5OH \quad (1.8)$$

$$(OH)_x(OR)_ySiOH + ROSi(OH)_v(OR)_w \longrightarrow (OH)_x(OR)_ySi{-}O{-}Si(OH)_v(OR)_w + ROH \quad (1.9)$$

Munoz-Azuado and Gregorkiewitz [10] has opined that condensation reaction in sol-gel is possible through two other routes (Equation 1.10 and 1.11):

$$\equiv Si\text{-}OH + HO\text{-}Si\equiv \longrightarrow H_2O + \equiv Si\text{-}O\text{-}Si\equiv \ (Water\ condensation) \quad (1.10)$$

$$\equiv Si\text{-}OR + HO\text{-}Si\equiv \longrightarrow R\text{-}OH + \equiv Si\text{-}O\text{-}Si\equiv \ (Alcohol\ condensation) \quad (1.11)$$

Since not all sol-gel precursors are alkoxides, the functional group chemistry determines the kinetic of a particular sol-gel type reaction. Depending on the rate of hydrolysis/condensation, the final gel material formed is diphasic with its morphology appearing between discrete particulates (mixed liquid phase) and continuous polymer network (semi-solid phase). The understanding of the structures of these organic-inorganic hybrid materials in relation to synthesis and processing is the success of sol-gel chemistry. The abundance of precursors and their unique chemistries allows for the development of materials with tunable chemical and mechanical properties. Common in this class of sol-gel materials are those prepared from organically modified alkoxides bearing polymerizable organic functional groups (e.g. epoxy rings). The chemistry of this class of precursors is difficult since it is almost impossible to track the number of imminent major and side reactions. To control these systems to yield materials with better properties, researchers worldwide employ the of Lewis catalysts (e.g. BF_3, $ZrCl_4$, $TiCl_4$, $SnCl_4$, and $AlCl_3$ etc) for accelerate the epoxy ring-opening reaction and while controlling the

polycondensation reactions. Many epoxy-bearing alkoxides (e.g. 3-Glycidyloxypropyl trimethoxysilane) require curing agents like amines for similar reactions of which allows for the formation of highly crosslinked modified silica structures [11]. Sol-gel chemistry has become a productive route for the preparation of countless materials with electronic, optical and magnetic properties for various applications ─ ranging from the development of stationary phase materials for chromatography, anticorrosive coating for industrial metals, materials for mounting active bioagents and substances for biomedical applications, amphiphilic coatings with antifouling potentials, to mention but a few.

1.3 Protective sol-gel coating

1.3.1 Corrosion overview

Metals employed for use in many industrial service environments corrode. The economics of maintenance and repairs of these metals is huge, and so much is being expended annually by multinationals as well as developed countries as consequences of corrosion, including the inspection, monitoring and control of this evitable degradation process. More than $100 billion is being expended annually as a result of corrosion in the United States of America alone. Annually, in a global scale, approximately one-fifth of global energy making 4.2% of gross national product is lost to corrosion [12]. Depending on the metal substrate, metal corrosion as an electrochemical process is best explained using the Pourbaix diagram. Pourbaix diagrams of metals aid in the understanding of factors that could promote corrosion in terms of pH and it show how these metals are susceptible to corrosion as a function of potential and pH. Solution pH and surface chemistries are known to hugely affect the rate of metal corrosion, and by understanding these factors,

adequate control procedures and method can be proposed to revert corrosion degradation kinetics.

The degradation of metals by corrosion is a spontaneous process involving the reaction of the metal with its environment, catalyzed by moisture and oxygen. Figure 1.4 shows photographs of corroded surfaces of metals; steel oxidizes to rust, and the process continues until the metal block/mass has been totally degraded depending on a number of surface and environmental factors. Classified as electrochemical reaction, the first stage in the process is the anodic area surface dissolution with Fe^{+2} ions from the metal going into the bulk of the solution mixture. Pairs of electrons from the metallic anode is taken by the cathode, here hydrated hydroxyl ions are formed as Fe^{+2} ions react with molecular water and oxygen. The red hydrated ferric oxide (rust) is the formed when freshly generated Fe^{+2} ions reacted with hydroxyl ions in solution. The corrosion behavior of steel working electrodes in the acidic solution is shown in Equations (1.12-1.14). On a prolong period of time, corrosion product's growth of the microstructure stifles the surface by relative polarisation effect, thus a new metallic/anodic sites is formed furthering the process (http://www.steelconstruction.info/Corrosion_of_structural_steel). This could result in uniform corrosion if the surface degrades uniformly, but other forms of corrosion may also occur, ranging from: localized, crevice, pitting, galvanic, stress corrosion, etc.

$$Fe + 3O_2 + 2H_2O \longrightarrow 2Fe_2O_3H_2O_{(aqu)}\,(\text{rust}) \qquad (1.12)$$

$$Fe_{(s)} \rightarrow Fe^{+2}_{(aq)} + 2e^- \quad \textit{anodic reaction} \qquad (1.13)$$

$$2H^+_{(aq)} + 2e^- \rightarrow H_{2(g)} \quad \textit{cathodic reaction} \qquad (1.14)$$

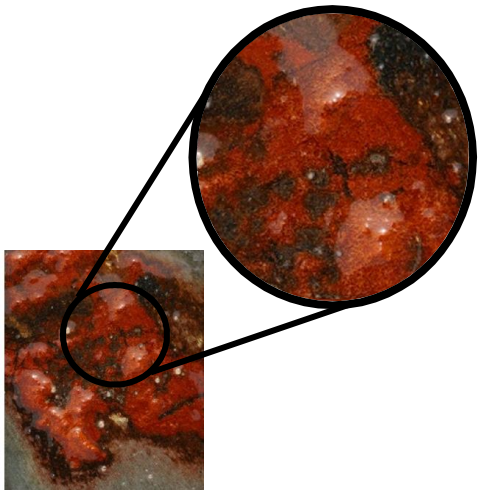

Figure 1.4 A photograph of a submerged corroded steel surface in the sea.

1.3.2 Protective sol-gel coatings and modifications

Several methods have been reported worldwide in preventing corrosion, or at least minimize its spontaneous dynamics, and the use of chromate conversion coating is a very popular technique against steel corrosion and the passivation of other metals and their alloys. Chromate products are known to be carcinogenic, and because of environmental safety concerns as well as their impact on man's health and ecological balance, their usage is regulated by very strict environmental legislation. The use of protective sol-gel coatings is one of the most applied greener control strategy as an alternative to industrial chromate coating. Organic-inorganic hybrid sol-gel coatings are easily synthesized as organosilicic acid esters ($R'_nSi(OR)_{4-n}$) as they act in dual protection capacity: corrosion inhibition and physical barrier against corrosive ions and molecules [13]. Alkoxy groups (RO─) on silanes/siloxanes are readily hydrolysed to silanol groups (Si-OH), and the presence of this hydrophilic Si-OH aids the formation of hydrogen bond on a hydroxyl-treated metallic surface. During curing, silica sol-gel coatings bind to metal substrates via a metallo-siloxane (Si─ O─M) bond with van der Waals forces and the adherence of the coating on the metal surface is increased. The silica rich M-oxide film on these industrial metals (M),

further barriers inherent pores by forming passive and highly corrosion-resistance layer to prevent passage and leaching of corrosive ions and molecules [14,15]. Figure 1.5 shows a representative illustration for this assertion. This unique barrier property is possible with silica composed of pure inorganic network and those with organic/inorganic hybrid network structures, all made from varieties of precursors. Protective sol-gel coatings made from organic/inorganic precursors have more robust and reliable strengths since they combine both inorganic (e.g. scratch, wear resistance, durability and impact strength) and organic (flexibility, low temperature curability and adhesion) properties [14].

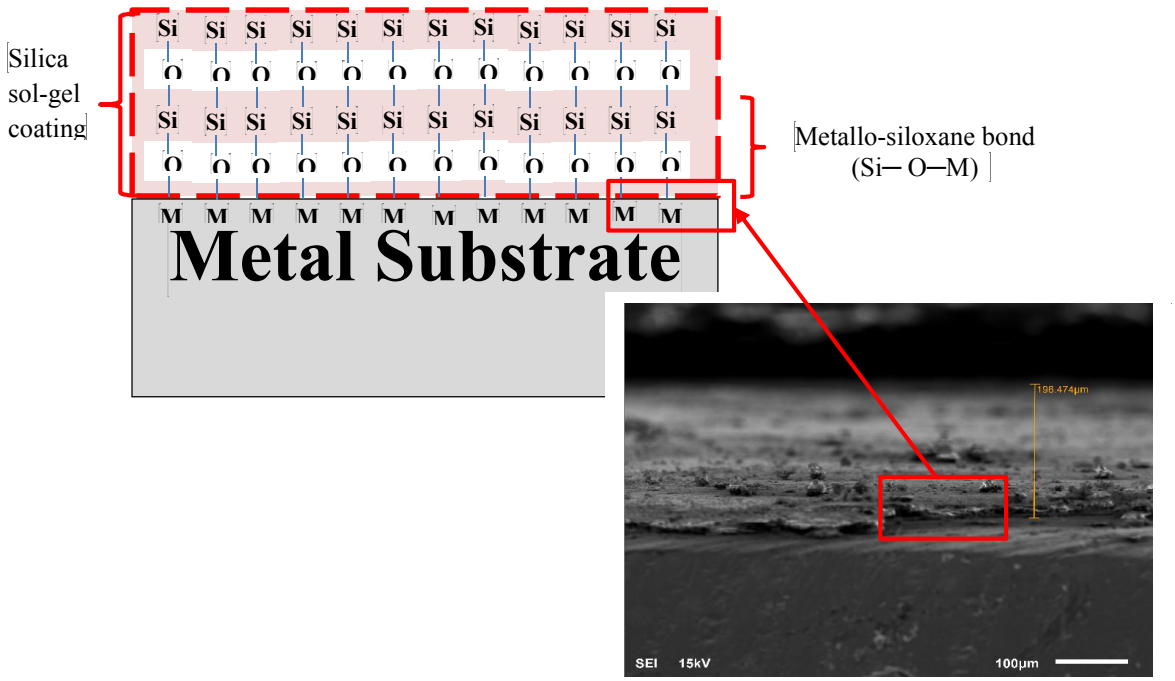

Figure 1.5 Annotated and SEM representation: Silica sol-gel coating bound to metal substrate via a metallo-siloxane (Si─ O─M) bond.

Table 1.1 presents some of the most reported precursors used in the synthesis of protective sol–gel coatings for industrial metals [12]. The abundance of sol-gel precursors allows for changes in coating chemistry, thereby creating versatility in the final materials endowed with tunable properties. Also counted as an advantage of this process is the ease of coating

application on substrates, and several syntheses of organic-inorganic hybrid sol-gel coatings have been reported for a number of large area substrates via sol–gel method [16─19]. The morphology of organic-inorganic hybrid sol-gel coatings reveals nano to microsize fissures and pores; pathways through which corrosive ions and molecules can get to the metal surface. Protective films of this class lack prolonged active inhibition against corrosion as they are susceptible to cavitation and pitting at increased exposure period to aggressive ions. They also prone to minor/major surface damages and defects, and these may persist expect the sol-gel coating has rigid bulk mechanical properties or possesses self-healing ability. To reduce this limitation, sol-gel coatings are either physically or chemically modified to confer the needed active protection. Sol-gel coatings can be chemically modified by encapsulating within its bulk low surface energy materials capable of rendering it hydrophobic to water molecules. These modification instills reduced wetness to the surface the coating thereby disallowing the passage of water through it. Another chemical modification method is the synthesis of sol-gel materials with higher surface contact angle (θ_w) hence, increased water impact resistance. Among useful sol-gel additives and precursors offering hydrophobic properties, Mahltig et al [20] has mentioned polysiloxanes with increasing chain-length of alkyl groups, monomeric alkylsilanes, as well as fluorinated compounds, for metallic and non-metallic (e.g. functionalized textiles) substrates. Polytetrafluoroethylene precursors and those of chloride substituted silanes have been reported [21]. The anticorrosive applications of sol-gel materials encapsulation TiO_2─CeO_2/ carbon nanotubes [22,23], nanosized alumina and clay [24,25] as well as nanoscale CeO_2, graphene and zeolite [26─28] have been earlier reported. Incorporating corrosion inhibitor pigments into the bulk of the coating is another

method; anticorrosive graphene [28] and aluminum pigments [29–33], organic corrosion inhibitors [34], inorganic non-chromate corrosion inhibitors [35,36] and zinc aluminum polyphosphate [37–41], zinc aluminum phosphate [38], strontium aluminum polyphosphate [39], zinc phosphate [40,41], and aluminum tri-polyphosphate [42]. The presence of these non-chromate and phosphate/polyphosphate inhibitor pigments further modifies the bulk properties of the sol-gel coating, and also spontaneously aids the formation of passive oxides layers in the coating thereby reducing the passage corrosive molecules and ions across to the metal surface [39].

Table 1.1 Some of the most reported linear and cyclic silane precursors used in the synthesis of protective sol–gel coatings for industrial metals: Chemical structures and names/abbreviations.

Chemical Structure	Chemical name	Chemical Structure	Chemical name
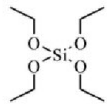	Tetraethyl orthosilicate (TEOS)	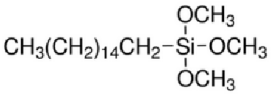	Hexadecyltrimethoxy silane (HDTS)
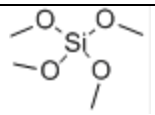	Tetramethoxysilane (TMOS)	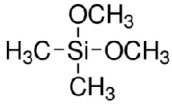	Dimethyldimethoxysi lane (DMDS)
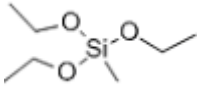	Methyl-triethoxysilane (MTES)	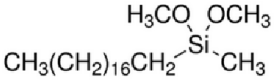	Dimethoxymethyl octadecylsilane (DMOS)
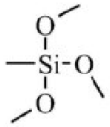	Methyl-trimethoxysilane (MTMS)	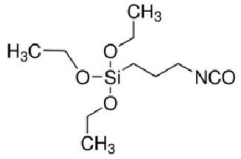	3-(Triethoxysilyl)propyl isocyanate (ICPTES)
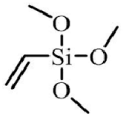	Vinyl-trimethoxysilane (VTMS)	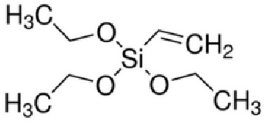	Triethoxyvinylsilane (TEVS)

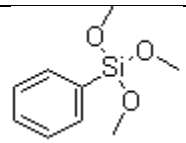	Phenyl-trimethoxysilane (PTMS)	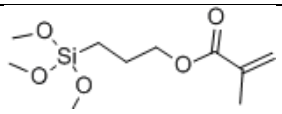	3-(Trimethoxysilyl)propyl methacrylate (TMPM)
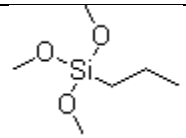	propyltrimethoxysilane (PTMOS)	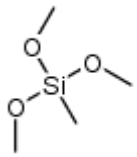	Trimethoxymethylsiloxane (TMMS)
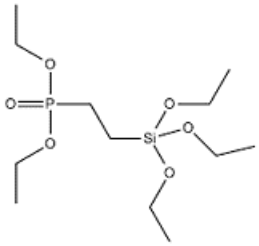	Diethylphosphonatoethyltriethoxysilane (PHS)	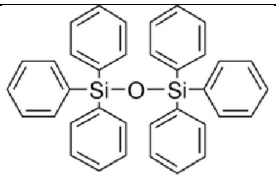	Hexaphenyldisiloxane (HPDS)
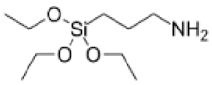	3-Aminopropyltrimethoxysilane (APS)	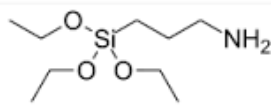	γ-aminopropyl triethoxysilane (APS)
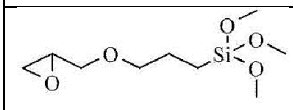	3-Glycidoxypropyltrimethoxysilane (GPTMS)	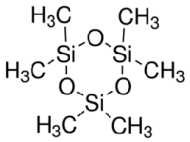	Hexamethylcyclotrisiloxane (HMCS)
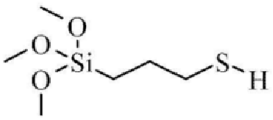	Methacryloxypropyltrimethoxysilane (MAPTS)	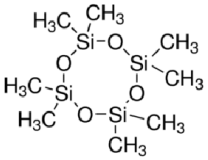	Octamethylcyclotetrasiloxane (OMCS)
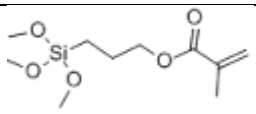	Mercaptopropyltrimethoxysilane (MPTMS)	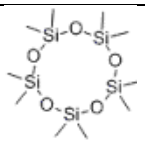	Decamethylcyclopentasiloxane (DMCS)

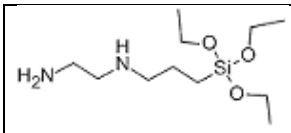	3-(2-Aminoethyl)aminopropyl trimethoxysilane (AEAPS)	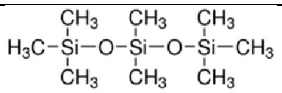	Octamethyltrisiloxane (OMTS)
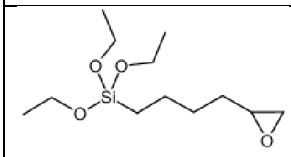	5,6-epoxyhexyltriethoxysilane (EHTS)	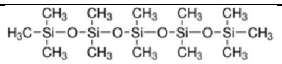	Dodecamethylpentasiloxane (DMPS)
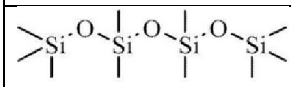	Decamethyltetrasiloxane (DMTS)	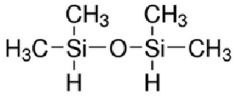	1,1,3,3-Tetramethyldisiloxane (TMDS)
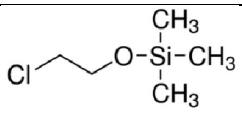	2-Chloroethoxytrimethylsilane (CETS)	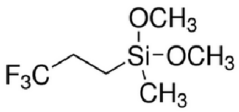	Dimethoxy-methyl(3,3,3-trifluoropropyl)silane (DMTS)
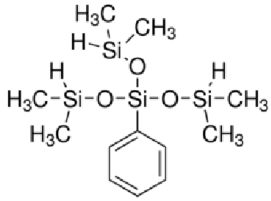	Tris(dimethylsiloxy)phenylsilane (TDPS)	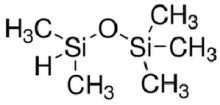	Pentamethyldisiloxane (PMDS)
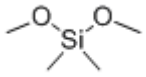	Dimethyldimethoxysilane (DMDS)	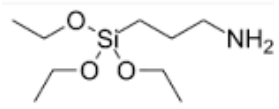	Aminopropylethoxysilane (AMEO)
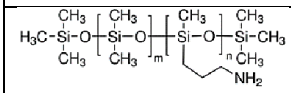	2–4% aminoethylaminopropyl-methylsiloxane dimethylsiloxane (APDMS) copolymer	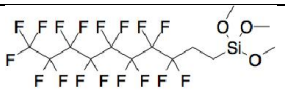	(Heptadecafluoro-1,1,2,2-tetrahydrodecyl)triethoxysilane (FTEOS17)

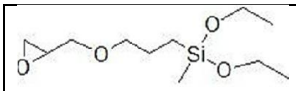	(3-glycidoxypropyl)methyl diethoxysilane (GPMD)	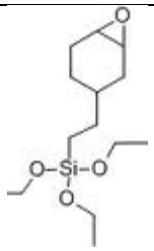	2-(3,4-epoxycyclohexyl)ethyl -trimethoxysilane (ECET)

1.4 Electroanalytical methods for monitoring corrosion

Corrosion monitoring strategies and methods are designed to observed trends in external or internal corrosion episodes; including the rates of degradation (e.g. wall loss) in metal-based infrastructures. Most above-ground electroanalytical based techniques run by the principles of direct current (dc) or alternating current (ac).

1.4.1 Electroanalytical dc techniques

The dc techniques monitor current responses once potential has been applied to a metal substrate. Though effective in corrosion monitoring, these dc based techniques are stricken with inevitable interferences (e.g. current stray from aligning structures like rectifiers, power sources etc.). Some of the most commonly used dc based techniques are [43]:

1. Close potential survey,
2. Voltage gradient,
3. Cathodic protection current requirement,
4. Coating conductance determination.

1.4.1.1 Close potential survey

This technique involves the measurement of potential of metal structures relative to the medium (e.g. soil or water) and the range stays within the bounds of a set aside cathodic

protection criteria. A copper-copper sulfate reference electrode is normally employed in most field-based studies to monitor the potential of the structure with a voltammeter.

1.4.1.2 Voltage gradient (dc) technique

Just like Close potential survey, voltage gradient technique measures dc potential but it employs the use of two reference electrodes to evaluate the voltage gradient between them. With a coated pipeline metal, its center line must be traced to have a good survey before applying a current that will detect coating delamination (and even micro-cracks).

1.4.1.3 Cathodic protection current requirement

The current requirement of cathodic protection method involves the evaluation of current (in amperes) required to protect a metal structure. This cathodically depends on the quality and quantity of the coating, but this involves the initial measurement of corrosion potential perturbation throughout length of the metalloic structure as a result of current application from a source (even via a temporary anode). This technique simply measures cathodic polarization.

1.4.1.4 Coating conductance determination

Just like cathodic protection current, this technique measures the resultant current from current application but specifically, the potential drop within the coated metal (and in turn the information involving coating conductance is derived from the applied current by Ohm's law). Associated techniques are potential and current attenuation methods.

1.4.2 Electroanalytical ac techniques

While dc technique measures potential response on application of current (or vice versa), ac techniques evaluates attenuations caused by currents or measures voltage drop. Some of the most commonly used ac based techniques are [43]:

1. Voltage gradient,
2. Pearson survey and electromagnetic current attenuation,
3. Transwave system,
4. Electrochemical impedance spectroscopy.

1.4.2.1 Voltage gradient (ac) technique

In a field-based ac survey, the resultant voltage gradient (relative to the earth) from the application ac signal is monitored between electrodes (a reference and a working electrode, like a pipeline metal) place within a defined distance. The voltage gradient is measured in decibels once the center line of the pipeline has been traced. Inherent surface or bulk cracks or pores on the coating can be revealed by monitoring the trend in electrochemical response as being related to the voltage gradient.

1.4.2.2 Pearson survey and electromagnetic current attenuation

Pearson survey involves the application of ac audio signal within a fixed frequency range depending on the thicknesses of protective coatings on test metal substrates. The fluctuation in the applied audio signal reflected from the coated pipeline (as displayed by the receiver) connected between probes estimates coating defects. Electromagnetic current attenuation technique directly measures the electromagnetic field generated by underground coated pipelines when ac current is applied along its length. For a given signal frequency, soil resistivity, and structure characteristics (e.g., pipe diameter, wall

thickness, and depth), the electromagnetic field is a function of coating quality. Inherent surface or bulk cracks or pores on the coating can be revealed by monitoring the fluctuations in the electromagnetic field (directly related to the coating defects).

1.4.2.3 Transwave system technique

The transwave system technique monitors streams of generated waveforms from rectifiers to which installed readers analysis them within a distance. The generated results (attenuations) are affected by the type of metal as well as the coating applied on it, medium (e.g. soil), frequency of wave, etc. The quality of the coating is assessed from the transwave signal attenuations.

1.4.2.4 Electrochemical impedance spectroscopy

Impedance is the resistance to the flow of current (in an ac circuit) when a minute amplitude sinusoidal excitation signal is applied across a metal surface. In simple circuits, the resultant quantity relates the potential applied to the measured current (by Equation 1.15). This assertion is different in more complex circuitry as deviations abound shifting the boundaries to non-linear conditions; here, electrochemical impedance re-defines the resistance to this current flow (1.16).

$$R = E/I \qquad \text{(1.15; for ideal resistors)}$$

$$Z = \frac{E_t}{I_t} = \frac{E_o sin(\omega t)}{I_o \sin(\omega t + \emptyset)} = z_o \frac{\sin(\omega t)}{\sin(\omega t + \emptyset)} \qquad \text{(1.16; complex non-linear circuits)}$$

;where resistance, potential and current are denoted as R, E and I, respectively; E_o and I_o are magnitudes of amplitudes of potential and current; ω is the angular frequency (rad. per sec.= $2\pi f$); $\emptyset$ and f are phase separation/shift and the frequency of phase, respectively. Both potential (E) and current quantities are modified from Equations 1.17 and 1.18:

$$E_t = E_o \sin(\omega t) \quad (1.17)$$

$$I_t = I_o \, sin \, (\omega t + \emptyset) \quad (1.18)$$

Electrochemical impedance spectroscopic technique relies on the theoretical fitting of impedance data in circuit models in order to obtain *Z;* and depending on the circuit components, magnitudes of Z could be redefined as being resistive, capacitive or inductive. Unlike other electroanalytical techniques employed for corrosion monitoring, electrochemical impedance spectroscopy is a lab-based technique with a more complex principle and instrumentation to which the level of result obtained from it could also depend on the dexterity of the experimenter. Normally coated pipelines are electrochemically modeled with complex networks of resistors and capacitors characteristic of the circuitry making the coating. Here, the behavior of the coated pipeline system, for instance, is monitored by applying a very small amplitude perturbation between ranges of frequency (measured in Hz).

1.4.3 Other electroanalytical techniques

1.4.3.1 Linear polarization resistance

By using the Stern-Geary relation, this technique involves the application of a potential within a range enough to polarize a test electrode (e.g. metal) in the solution of an electrolyte while a certain amount of current is needed to keep a defined potential shift (which is also proportional to the rate at which the electrode surface corrodes). Corrosion rate measurement is instantaneous with this technique [44].

1.4.3.2 Potentiodynamic polarization

Just like Linear Polarization Resistance, potential is also applied, but current response is monitored within extremes of anodic and cathodic potential ranges versus open circuit potential at defined scan rate; also known as Tafel experiment. Lower values of corrosion current density denotes deduced corrosion rate for this type of polarization measurements.

1.4.3.3 Galvanic monitoring

Simply known as zero resistance ammetry (with probes), this technique involves the use of two dissimilar metal electrodes immersed in corrosive electrolytes to monitor the potential between them. Corrosion rate is directly related to the current generated between the applied potential difference.

1.4.3.4 Galvanic cathodic protection

In this technique, the potential of the anode is relatively more negative than that of the cathode (the test metal). Normally for steel, its surface is polarized with more negative voltage values; at this juncture, the driving corrosion force is removed while the galvanic anode slowly degrades, in turn "protecting" the cathode. Electron transfer phenomenon is a key to the design of a perfect protecting system.

1.4.3.5 Cathodic shielding

In this technique, the "protective" current from the cathode is shielded from anodic metal by means of a resistive film; a "shield". It allows for the exterior coating to further protect metal surfaces from episodes of corrosion.

1.4.4 Other electrical resistance methods

Other resistance monitoring techniques employ electrical resistance probes (Flush or cylindrical-type probes are common) which the measurement basis of metallic mass loss *in situ* the reaction cell after exposure. The resultant electrical resistance is linked with the length and cross sectional area of the corroded metal substrate.

CHAPTER 2

LITERATURE REVIEW

2.1 Sol-gel: Antifouling applications

Organic/inorganic hybrid sol–gel materials have been greatly exploited in mitigating fouling due to its potential ability to resist adhesion of foulers derived from their unique surface chemistries and topologies [4]. The flexibility of this method could also be linked to its process chemistry and abundance of sol-gel precursors to which those with organo-fluorine have been widely reported. Apart from the foul-resistant chemistry of the surface, enhanced antifouling properties could be introduced to sol-gel material by encapsulating within its matrix, secondary active additives with characteristic foul-resistance abilities (e.g. biomolecules like enzymes, proteins, bacterial cells, etc; and chemicals, etc.). Successful encapsulation is due to inherent pores within their solid gelled matrices.

2.1.1 Antifouling activity initiated by the coating chemistry and morphology

Sol-gel coatings can be synthesized to introduce within their matrices, properties that could enhance antifouling to suit desirable applications in marine environments. Since sol-gel process and its associated reactions involved in synthesis greatly depend on precursor types, those made for this application are careful chosen. Against micro and macro foulers, the use fluorinated antifouling sol-gel coatings have been reported with their halogenated moieties combining reduced surface energy/ surface tension and

hydrophobicity with foul-resistant properties [45]. Sol-gels of this class are relatively non-wetting and with unique architectures characterized with film morphologies and topographies capable of resisting attachment and settlement of marine organisms. Their surfaces are foul-releasing in nature [46]. Berglin et al. [47] have synthesized a fluorinated sol-gel coating from TEOS and FTEOS17 crosslinked dihydroxy-PDMS sol-gel coatings. The coating was characterized with electron spectroscopy for chemical analysis, ATR/IR, SEM and AFM before evaluating the aqueous contact angle after 3 months immersion in water for both TEOS and FTEOS17 PDMS coatings. Due the relatively stable surface morphology and reduced cracks/ erosion pits for the TEOS and FTEOS17 PDMS coatings, respectively, these set of coatings were concluded as having the potential for antifouling ─ with the fluorinated coated assumed to be the better coating due to it halogenated siliceous phase. In another study, Marabotti et al. [48] have reported the antifouling properties of a fluorinated sol-gel coating synthesized from monomethacryloxypropyl-terminated PDMS, trifluorotoluene, poly(diethoxy siloxane), bis(silanol)-terminated PDMS and 1*H*,1*H*,2*H*,2*H*-Perfluorodecyl acrylate. The process route was probed with NMR analyses and the synthesized coating characterized with XRD/XPS, contact angle measurements, DSC and mechanical analyses. The coating possessed low modulus character and surface tension. The attachment and settlement of Ulva spores, Balanus Amphitrite and cyprids were studied against varying concentrations of fluorinated siloxanes of this modified PDMS coating. Experimental results revealed that the adhesion of these marine foulers reduced in the presence of the synthesized antifouling coating, though fouling was not dependent on the concentration of the fluorinated siloxanes. Glass slides were used as the substrate immersed in larger stationary

tank of aerated deionised water for the 60 day barnacle adhesion test, and also with less than 10 ml of 1×10^6 Ulva zoospores/ml suspension in Quadriperm dishes. Grunlan et al. [49] have synthesized another fluorinated sol-gel coating via hydrosilylation of oligosiloxanes and oligofluorosiloxanes using allyl glycidyl ether and the resultant sol-gel material was later crosslinked with bis(3-aminopropyl)PDMS. The film was later characterized for dynamic mechanical thermal behaviour and TGA before measuring its resistant against the settlement of Ulva spores. Results revealed sufficient spore adhesion resistant, and authors attributed this to increased storage modulus, reduced wetness as well as the foul-resealing properties of coating in the presence of the fluorinated siloxane moiety in the sol-gel coating. Fouling studies were conducted for all coated substrates immersed in deionized water and seawater containing Ulva spores immersion for 4 h. A fast curing fluorosilicone sol-gel coating grafted with a nonfluorinated organopolysiloxane resin have been synthesized and coated on adequate dimensioned glass substrate prior to a 15 month immersion at Chesapeake Bay to study its antifouling ability. Field results demonstrated reliable foul-resistance against newly metamorphosed barnacles and bryozoans on this class of sol-gel coating [50]. Damp sponge cleaning procedure was employed in removing all foulers except for strongly adhered bryozoans and barnacles. A research finding involving the grafting of an organohydrogenpolysiloxane-based coating with vinyl end diorganopolysiloxane and slilcone resins has been patented due to its enhanced fouling resistant ability against micro and macro fouling [51]. Spores of Ulva linza and diatom *Navicula perminuta* adhesion (attachment and settlement) studies have been studied using an antifouling sol-gel coating synthesized using polystyrene grafted with polyoxyethylene-polytetrafluoroethylene (via atom transfer radical polymerization).

Reduced adhesion was revealed for Ulva spores in the presence of the new synthesized coating with less strongly adhered *Navicula* cells on the same coating [52]. Another sol-gel coating has been synthesized against the surface settlement of macroalga Ulva linza and *Navicula perminuta* in a flow system of less than 60 pa wall shear stress. The coating precursor was poly(tetrafluoroethylene) with fluorinated side-chains grafted polystyrene-block-poly-(ethylene-ran-butylene)-block-polystyrene used in preparing amphiphilic surfaces. The algae and diatom revealed unequal adhesion on this antifouling surface, with algae and diatom being foul-released at the hydrophilic and hydrophobic surface, respectively [53]. Wouters et al. [54] have reported the synthesis of polysiloxane-silane coating encapsulated with sepiolite using amino-terminated and dodecyl PDMS, and GPTMS. The coating was appropriately characterized and then tested against the biofilm formation and adhesion of three bacterial strains (*Marinobacter hydrocarbonoclasticus, Vibrio alginolyticus, Cobetia marina*) after a seven days immersion in deionized water/artificial seawater. The coating demonstrated significant foul-release ability against the three bacterial strains, and authors attributed this result to the presence of sepiolite in the coating.

2.1.2 Antifouling activity initiated by viable bacterial endospores/cells encapsulating within sol-gel matrices

Apart from the unique surface chemistry of sol-gel coatings against marine fouling, they can also be synthesized to house active chemical and biomolecules capable to rendering improved antifouling abilities to the materials. Enzymes and proteins as well as bacterial cells/endospores can be encapsulated into the bulk of the film if the needed nutrients and water for the growth without denaturing these molecules are present. Mostly,

immobilization is done between gelation stages since encapsulation is not possible after the formed sol-gel material has totally gelled. The encapsulated molecules will still maintain their properties as along the environment to which they are deployed within the silica network is favorable (including temperature, solvent concentrations, pH, catalyst, etc). Akid et al. [55] has encapsulated vegetative endospores of *Paenibacillus polymyxa* (ATCC 10401) and *Paenibacillus fragi* (ATCC 4973) into a sol-gel coating synthesized from TEOS, MTMS and GPTMS using acetic acid as catalyst in ethanol. The resultant sol was encapsulated with nanosize alumina before adding freshly prepared bacterial culture previously harvested overnight, coated on Al 2024 substrate and divided into two parts to be analyzed in the lab and field. The lab samples were tested for their anticorrosion potential in the absence and presence of these two bacterial endospores electrochemically (after 12 days immersion in 3.5 wt% NaCl) while their antifouling properties were tested for after six months tidal immersion in a typical marine environment. In all, the presence of the bacterial endospores inhibited saline corrosion of Al compared to the sol-gel coating without these bacterial, and after immersion in a tidal estuarine environment throughout the period of under study. The reasons of the foul-resistance abilities of these bacteria are present in Table 2.1. Apart from these likely reasons that were not further investigated, the presence of an antibiotic, polymyxin, inherent in the bacterial biofilm, must have aided in the general resistant of the coating to marine fouling.

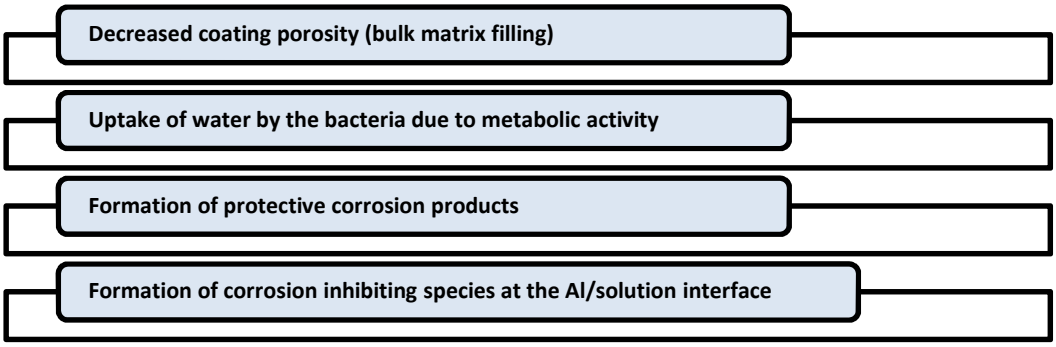

Table 2.1 Reasons for fouling-inhibition by the bacteria used in Ref. [125]

The use of glacial acetic acid as catalyst in a catalyzed hydrolysis/ condensation reaction of TEOS in the presence of ethanol has been reported [56]. The sol-gel coating was encapsulated with *Paenibacillus polymyxa* (ATCC 10401) and tested for its foul-resistance at Whitby harbor, River Esk, North Yorkshire, UK. Both abiotic and biotic coatings were characterized and spray-coated on AA 5005 panels before lab- and field-based studies. After 19 weeks immersion of these samples at Whitby harbor, the biotic coatings revealed remarkable resistance to fouling and also had higher corrosion protection for Al in artificial salt water (ASW) after 7 days immersion. The reasons for this unique bioactivity is as expressed in Ref. [55]. Premkumar *et al.* [57] had previously explained that these bacteria/gel material hybrids combine:

"physical properties and the biocompatibility of inorganic silicates with the ability of cells to respond to environmental stimuli and subsequently impeding fouling".

Authors were surveying the adhesion of some fluorescent bacteria in silicate films by gel encapsulation [57]. Ghach et al. [58] have reported the electrochemical-assisted encapsulation of five strains of *Escherichia coli* on ITO electrode surfaces by applying to it an anodic potential (of magnitude 1.3 V versus Ag/AgCl (3 M)) in the sol-gel solution. The ITO working electrode was sol electrolyzed with TMOS, PEG and chitosan at varying

pH. Results revealed remarkable thicknesses for the coating at adequate pH values where confocal laser fluorescence microscopy was employed in evaluating the viability of the immobilized bacterial cell using appropriate fluorescent dye. Bacterial cell encapsulation were successful only at positive potentials and longer deposition time ─ authors reported between 100 nm to 2 mm coating thickness at 10 and 60 s deposition periods.

2.2 Sol-gel: Anticorrosion applications

Barrier protection by silica type sol-gel coatings have been widely researched and reported in the literature in a huge volume of descriptive publications for various metal substrates and corrodent in divergent approaches. The interest in sol-gel research had already dominated late 1800's and early 1900's with particular interest in gel chemistry, but this era was also marked with sparse understanding of the elaborate physical and chemical properties of these materials [59]. There is barely no application in adsorption and corrosion science that has not the use of sol-gel or sol-gel type materials. Sol-gel coatings have been reported as reliable alternative for chromate coatings for pure metals and their alloys, and their unique chemical and physical bonding allows for a strong adhesion at the at the coating/metal interfaces [55].

2.2.1 General applications and modifications

There have also been several reports regarding protection of nobler metals/alloys in the literature though similar studies on pure ferrous materials are scare. Salahinejad et al. [60] have reported the anticorrosive effect of a double coat sol-gel coating; with $ZrTiO_4$–polymethyl methacrylate (PMMA) and $ZrTiO_4$ being the top and bottom coatings,

respectively, applied on stainless steel substrate (medical-grade) via spin coating at room temperature. Authors tested the corrosion resistance of this coating in a simulated body fluid using a dc-method. Results from Tafel polarization experiments revealed an aqueous protective synergy between both sets of coating compare to each of them, separately. Corrosion resistance was attributed to barrier protection in the presence of PMMA that contributed the needed bulk rigidity and ruggedness; filling possible pores against the passage of corrosive ions and molecules, but this also greatly affected the adhesion of the $ZrTiO_4$–PMMA coating on the steel substrate. Similar sol–gel spin-coating approach have also been reported by Norouzi and Garekan [61] using a combined ZrO_2/ZrO_2–PMMA coating on stainless steel (316L grade) in simulated body fluid. The corrosion tests were conducted using both dc and ac-techniques for both coating in the solution of the electrolyte. Cambon et al. [62] have studied the barrier protection of an organic–inorganic hybrid silicate film made from ring-opening polymerization of GPTMS using aluminum sec-butoxide for martensitic stainless steel (X13VD grade). Appropriate spectroscopic techniques were employed in studying the reaction routes. The coating's corrosion resistance and adhesion strength were improved by incorporating anticorrosive cerium salts. Corrosion tests were conducted in 0.1 M NaCl after an hour and a day immersion using electrochemical impedance spectroscopy. Improved resistance of the coating was attributed to the presence of the Cs ions drawn from their effect on the overall mechanical properties of the sol-gel coating tested by nanoscratch/indentation test. In another study [13], Cr^{3+} ions were doped in ureasilicates and amino-alcohol silicates coatings synthesized from ICPTES and GPTMS precursors at room temperature. Using the polarization resistance and macrocell current tests, corrosion resistance of the coatings

were found to increase in the presence of the Cr^{3+} ions, and this was attributed to formation is passive corrosion inhibiting oxide film in the coating after 137 days immersion in alkaline mortal environment. Scanning electron microscopy (SEM) results also complimented results collected from the electrochemical tests. Nanosize nanoclay composite have been encapsulated into a sol-gel coating to increase its barrier protection against the corrosion of hot-dip galvanized steel in 0.1 M NaCl [63]. The sol-gel coating was synthesized from hydrolysis/condensation reactions involving GPTMS, TEOS, MTES and sodium montmorillonite, and the effects of curing time and temperature on the corrosion resistance performance of the coating were investigated. Authors attributed the improved corrosion resistance of this clay/sol-gel hybrid coating to the presence of hydrophobic clay particle in the sol-gel matrix, and this was further aided by the dense Si-O-Si network in the material. Corrosion tests were based on monitoring of cathodic current density and the evaluation of pore resistance of the coating by means of potentiodynamic and impedance plots. In another work, sol-gel film synthesized from TEOS and 3(trimethoxysilyl)propyl methacrylate for the protection of AISI 304 and AISI 430 stainless steels in 3.5% NaCl has been reported [64]. Cerium nitrate was also added to improved corrosion protection and polyethyleneglycol (PEG) was used as the plasticizer. Potentiodynamic polarization and EIS tests revealed the extent of corrosion resistance of this class of coating while SEM and indentation of nanoscratches explained the morphologies and adhesion of the protective coatings on steel before immersion in the test solutions. Improved corrosion resistance of this coating was linked with its compacted silica bulk which had huge effect on the reduced corrosion current densities. Another epoxy-ring opening reaction of GPTMS using AMEO have been reported via sol-gel

reaction [65]. The sol-gel material was applied mild steel substrate by dip coating technique, cured at 200 ^{o}C before being tested for anticorrosive properties. Corrosion test were based on polarization and EIS techniques for the coated steel substrate in sodium chloride. SEM and FTIR were employed to study the morphology of the coating before and after immersion in NaCl corrodent and sol-gel chemistry, respectively. TEOS and MTES were employed in synthesizing the sol-gel coating and functionalized with bioactive strontium substituted silicate-glasses for stainless-steel (surgical grade; implant) [66]. The coated substrate was tested for bioactivity as well as corrosion resistance *in vitro* and *in vivo* for rat femur bone structure analysis with regards to corrosion. The coating was found to protect the steel substrate from corroding even after a month immersion in simulated body fluid. The presence of strontium ions improved corrosion resistance and bioactivity in the early immersion period, but reduced gradually; authors concluded that the presence of strontium ions in the coated implant improved corrosion resistance and aided bone regeneration. Criado et al. [67] have reported the synthesis of a polysiloxane type sol-gel derived from TEOS and TMPM in three molar ratios for carbon steel corrosion protection. After synthesis and curing of the coated substrates, polarization and EIS corrosion tests proceeded in carbonated synthetic solution employed to simulate carbonated concrete pore solution. The sol-gel coating demonstrated remarkable protection of the steel metal, and this was attributed to the cross-linked silica network in the bulk of the material as well as the adhesion of the coating on the steel substrate. Juan-Díaz et al. [68] have studied the anticorrosive properties of a sol-gel synthesized from acid-catalysed hydrolysis of MTES and TEOS (at different molar ratio) at room temperature. The corrosion resistance performance of the coating in 3.5 wt% NaCl was

attributed to the strength of Si-O-Si in the coating contributed by TEOS. Decrease in corrosion resistance with exposure time was attributed to the possible degradation process occurring in the coating at prolonged immersion in NaCl. In another study, Pavlovska et al. [69] have prepared a TiO_2–SiO_2 coating for enameled stainless steel against its corrosion in boiling oxalic acid/NaOH solutions. The mechanical strength of the coating was tested alongside its multilayered anticorrosion properties. The coating were found to resist corrosion in these media with remarkable chemical durability. The thickness of the coating was evaluated as well as its morphology using X-ray diffraction analysis (XRD), SEM and atomic force microscopy. The bioactivity and the corrosion resistance of a protective sol–gel coating for three surgical grade alloys: stainless steel 316 L, cobalt and titanium have been reported [70]. The sol-gel coating was prepared from MTES and TEOS then applied to the metal substrates by dip coating technique. Corrosion testing was conducted in a simulated body fluid environment using EIS and polarization technique, and the bioadhesion of tissue on the coated metal was evaluated. Resistance to corrosion was attributed to the hydroxyapatite formation form the test solution, this was confirmed using inductively coupled plasma mass spectroscopy (ICP-MS) after 12 months immersion. Three alkoxide precursors (TEOS, MTES, and GPTMS) have been used in synthesizing another sol-gel coating for stainless steel 304L protection in 3.5 wt% NaCl solution after 2 to 21 day exposure [71]. Nanoparticles of clay was encapsulated into the sol-gel to increase it bulk compatible, reduce the pores in the coating and also increase its hydrophobicity. Corrosion protection by this coating was attributed to the inherent Si-O-Si network in the coating well as its low wettability in the presence of the nanosized clay. The dispersion of clay in terms of the general coating roughness and morphology was

evaluated with SEM, AFM, XRD and FTIR. On stainless steel, Okner et al. [72] have reported a sol-gel route involving the electrodeposition of PEG/ICPTES polymerized coating. After spectroscopic and surface analytical evaluation of the coating for functional group chemistry, stability and morphology, its anticorrosion property was tested by potentiodynamic polarization. This hydrophilic coating was found to be stable in buffer phosphate and hence, reduced the cathodic corrosion current to a great extent compared to the bare steel substrate. In another study, the electrodeposition (at cathodic potential) of sol–gel coating on 316L stainless steel plates has been reported [73]. This protective coating was synthesized from APS, it was codeposited ion PTMS/PTMOS derived sol-gel. The coating was characterized by profilometry, goniometry and appropriate surface analytical techniques, before their elastic and adhesion properties were evaluated. Results from EIS for the coating revealed reliable corrosion resistance against the passage of hexacyanoferrate ion, this was attributed to the tunable physical and chemical properties of the coating and even dispersion of the microparticles via electrochemical-assisted deposition. Kiruthika et al. [74] have reported the anticorrosive properties of UV cured GPTMS/ZrO_2 sol-gel coating for mild steel applied by dip coating technique. In this study, authors were reviewing the effects of plasma surface treatment on the mechanical and protection properties of the hybrid coating. The adhesion and indentation properties were evaluated before aqueous corrosion test in 3.5 wt% NaCl using EIS and Tafel polarization. Its corrosion resistance for steel was attributed to mechanical strength and reduced wetness while surface pre-treatment with plasma greatly improved the adhesion of the coating to steel, thereby aiding inhibition of corrosive ion percolation. The presence of GPTMS/ZrO_2 sol-gel coating on steel reduced its corrosion rate with a factor more than

600 times that of the uncoated steel substrate due to the plasma treatment. A self-curing sol-gel coating synthesized from TEOS and alumina sol by acid-assisted hydrolysis in the presence of phosphoric acid catalyst has been reported [75]. An anticorrosive Ce salt was encapsulated into the bulk of the coating to improve inhibition of corrosive ions and molecules. The cerium doped matrixed demonstrated improved barrier protection due to the presence of this earth metal, increasing the hydrophobic nature of the coating and also hindering cathodic reduction by precipitating oxides and hydroxides of Ce in the coating. The undoped silica inhibited corrosion due to the rigid Si-O-Si in the sol-gel network from the corrosion test results obtained from EIS and salt spray experiment. In another study, Ruhi et al. [76] have investigated the anticorrosion properties of a zinc-phosphate pretreated mild steel surface coated with sol–gel alumina sintered a temperature greater than 200 ^{o}C. The protective sol-gel coating was synthesized using 1:100 molar ratio of aluminium iso-propoxide and water in an acidic medium. An electrochemical corrosion test was employed to evaluate the protective strength of the coating in 3.5 wt% NaCl using EIS. Better corrosion and wear resistance abilities were revealed for sol-gel sintered at 400 ^{o}C compared to a hundred degree lesser. Author attributed this to abundance of micro-cracks and fissures at higher temperature and the decomposition of organic functionalities required to provide the needed protection from corrosion. Studies regarding the barrier properties of another sol–gel Al_2O_3 has been reported for mild steel protection [77]. After synthesis, author studied the morphology and functional group chemistry of the coating using SEM, AFM, XPS and FT-Raman and X-ray photoelectron spectroscopies. The improved corrosion resistance of the coating was attributed to the presence of Al_2O_3 in the sol-gel matrix, and this was evaluated in 3.5 wt % NaCl solution using EIS, polarization

and OC potential tests. The presence of Al_2O_3 improved mild steel corrosion protection five time more than the undoped coating by the evaluation of cathodic corrosion current. The effect of amount of cloisite in organic-inorganic hybrid sol-gel synthesized using from TEOS, MTES and GPTMS has been investigated for the corrosion protection of mild steel in 0.1 M NaCl [78]. Silica matrix bound with cloisite content revealed improved protection from chloride ions thereby enhancing corrosion inhibition; this was attributed to reduced surface wetness with this material. Corrosion tests were conducted using EIS, polarization and electrochemical noise (EN) measurements. Electrochemical noise data were collected at a second rate of electrochemical sampling lasting 1024 seconds while EIS involved a 10 mV sine wave amplitude applied between 100 kHz to 0.01 Hz, and the dc test was performed last at ±200 mV at a millivolt scan rate per second. Cloisite content was evaluated using FTIR (functional group analysis), SEM (for surface morphology) and by aqueous water contact angle (for wetness evaluation in terms for hydrophobicity) measurements. A thin film of ZrO_2 has been prepared by sol-gel technique and deposited on 316L stainless steel by dip coating technique at different temperature [79]. It was characterized by TG/DTA, XRD, SEM and FTIR. This coating was found to inhibit acid-induced (1 M H_2SO_4) corrosion at 80 ^oC, evaluated using EIS and polarization techniques. The ZrO_2/sol-gel coating sintered at 500 ^oC demonstrated the best corrosion protection performance as results from SEM and AFM analyses revealed absence of surface cracks and reduced roughness, respectively. Authors opined that increased temperature must have allowed the formation of tetragonal (then to monoclinic) ZrO_2 phases in the coating at higher temperatures, thereby exposing the microstructure of the coating to corrosive attack. Wang and Akid [75] have reported the TEOS-based silica-alumina sol-gel,

TEOS/MTES-based silica sol-gel, TEOS/MTES-based silica-alumina sol-gel doped with cerium nitrate used for the protection of mild steel substrate in 3.5 wt% NaCl at room temperature. Their barrier protection on steel was tested using EIS with associated electrochemical parameters revealing improved corrosion inhibition for the coating in the presence of the cerium nitrate followed closed by the silica coating synthesized with TEOS and MTES. The reason for the reduced corrosion protection for the silica coating synthesized from TEOS over time was attributed to less Si-O-Si bond in the sol-gel matrix; the TEOS/MTES-based silica-alumina sol-gel doped with cerium salt combined its reduced wetness with and the presence of the cerium-based inhibitor. Hindrance of cathodic processes in the presence of the cerium nitrate was another proposed reason for corrosion inhibition involving this functionalized organic/inorganic hybrid coating. EIS experiments were accompanied with salt spray tests at prolonged immersion. A combined protective barrier properties for sol-gel and a conductive polyaniline-based coating has been studied [80]. The latter was synthesized from $(NH_4)_2S_2O_8$ oxidation of aniline in HCl solution. Corrosion tests were conducted by EIS and salt spray test with the coating applied to aluminium (AA2024 grade) substrate immersed for 24 months in acid, alkaline and saline media. The polyaniline/sol-gel protected against aluminium corrosion more in both acidic and saline electrolytes compared to the alkaline solution. Polyaniline/sol-gel hybrid coating exhibited self-healing properties (using Scanning Vibrating Electrode Technique) and resisted delamination and corrosion after 500 h exposure to salt spray. Scratch test as well as pull off and SEM analyses were employed in studying its surface morphology. Modified to induce scratch resistance with silica nanoparticles, the same hybrid coating has also been reported to inhibit magnesium (AZ31 grade) alloy corrosion

in Harrison solution [81]. EIS and salt spray tests were used for the inhibition corrosion evaluation. Author deduced from the experimental results that the presence of the silica nanobodies was the reason for the scratch resistance and self-healing of the coating, and the variation in the electrochemical parameters related to this coating revealed stable passive layer due to silica. The adhesion and corrosion resistance of this hybrid coating depends on the ratio of polyaniline to sol-gel in the broad matrix. An organic–inorganic hybrid sol-gel coatings synthesized from TEOS and GPTMS has been doped with alumina sol and cerium nitrate using similar procedure reported in Ref. [75] for Al–Cu and Al 2024-T3 alloys by dip-technique [82]. Corrosion tests were conducted using EIS and Tafel polarization with results revealing improved barrier protection in the presence of cerium nitrate in 3.5 wt% NaCl against the metal substrates; this was also confirmed with SEM prior to and after immersion. The presence of the corrosion inhibitor in the coating maintained superior barrier protection even after 456 h immersion in the saline electrolyte with reduced corrosion current density. May et al. [83] have incorporated alumina nano-fillers/nanoparticles into epoxy coating modified by sol-gel method using TEOS and MTMS precursors, and diethylenetriamine as the curing agent via acid catalyzed hydrolysis. The adhesion/shear and tensile analyses were carried out to study the effect of the alumina particles. The nanoparticle-doped epoxy/sol–gel coating showed excellent adhesion to the metal (Al2024-T3) substrate and with remarkable tensile strength at different temperatures and time only when they were used in small amount. Authors attributed this assertion to better adhesive cross-linking at smaller concentration of alumina and also with the formation of Si–O–M bonds in the sol-gel network.

2.2.2 Effects of phosphate and molybdate type anticorrosive pigments on the protection performances of silica sol-gel coatings

The presence of corrosion inhibitor pigments are known to act as fillers in the microstructure of sol-gel coating susceptible to surface and bulk mechanical faults (e.g. fissures and pores). By filling these pores with these pigments, the pathway through which corrosive ions and molecules could have passed through to reach the metal surface have been virtually sealed. This physical bulk modification actively protects the coating with a self-healing ability. The presence of these non-chromate phosphate and polyphosphate inhibitor pigments further modifies the bulk properties of the sol-gel coating, and also spontaneously aids the formation of passive oxides layers in the coating thereby impeding ionic current flow of corrosive ions. Aluminum/Zinc phosphate type compounds have become better alternatives and safe compounds for protective and barrier coatings. The presence of these non-chromate zinc-type phosphate inhibitor pigments spontaneously aids the formation of passive metal oxides and hydroxides [39]. These compounds have been opined to improve the physical properties of the sol-gel matrix by influencing surface adhesion and bulk rigidity. They replace organic corrosion inhibitors because of their reliable stability; the former are known to dissociate at extreme environmental conditions, like pressure and temperature. Metal phosphates are known to form stable oxides/hydroxides and even complexes when they dissociate. Few have been found in literature with regards to anticorrosion applications for industrial metals: with zinc aluminum pigments, zinc aluminum polyphosphate, zinc aluminum phosphate, strontium aluminum polyphosphate, zinc phosphate, and aluminum tri-polyphosphate widely reported. Lu et al. [42] have reported the influence of aluminum tri-polyphosphate primer

on the GPTMS coating synthesized to protect magnesium (AZ91D grade) alloy by measuring the galvanic coupling current between the bare and coated Mg substrate in 0.6 M NaCl. EIS based corrosion test was employed to ascertain the behavior of the coated system in NaCl by applying a 10 mV sine wave amplitude between 100 kHz to 0.01 Hz before polarization tests. The electrochemical results revealed reduced magnitude of corrosion current for the coating in the presence of the anticorrosive pigment; influencing by anodic and cathodic Tafel branches. SEM and XPS techniques were employed to analyze the coating morphology and the chemistry (with respect to the binding energies associated with P, O and Al in the pigments), respectively. The improved barrier properties of this pigment was attributed to its pH buffering effect as well as the formation of anticorrosive oxides/ phosphates of Mg at the metal/coating interface. Most recently, Ma et al [29] have studied the effect of aluminum (waterborne) pigments on the corrosion protection properties of a silica sol-gel coating synthesized from TEOS and AMEO with H_2O_2 employed for anchorage in the silica network. FTIR and XRD techniques were employed to characterize for functional groups and phase analyses, respectively. Results revealed that H_2O_2 oxidized aluminum thereby forming boehmite that anchored the Si-O-Si network in the coating. Aluminum substrate was better protected from silica coating synthesized at pH 9.5 for H_2O_2 and with 5.1×10^{-5} M aluminum pigments. Pi et al. [30] in a recent work have also reported the effect of similar Al composite particles in a sol-gel coating synthesized from GPTMS and acrylates (methyl methacrylate and butyl acrylate). TEOS was later added to the resultant colloidal sol to form a silica-Al composite. The anticorrosive of silica-Al composite was compared to raw Al at pH 14 by comparing the hydrogen evolution in the alkaline solution; the presence of the Al composited evolved

less gas compared to the bare Al after 24 hour immersion at that pH. Pull-off tests revealed better surface adhesion for the composites in the sol-gel coating. Pull-off test was accompanied by test for coating glossiness and surface morphology. Supplit and Schubert [32] have reported the studies of the effect of aluminum pigments in a barrier protection properties of silica sol-gel coating synthesized from TEOS and HDTS and DMDS. Corrosion test were conducted in alkaline and ordinary boiling water solutions, and the improved barrier properties in the presence of these pigments were attributed to a compact silica network and also the strong Al–O–Si bond contributing to the adhesion on aluminuim substrate. Modern researches on phosphate-based corrosion inhibitor pigments have been widely reported by researchers worldwide for different sol-gel coatings and metal substrates. Naderi and Attar [40] have studied the effects of varying pigment volume concentrations of zinc aluminum polyphosphate and zinc phosphate in an epoxy bisphenol A/ polyamide coating. EIS and EN ac-based techniques were employed to study their anticorrosion performance on mild steel. From the values of coating and charge transfer resistances, it was revealed that the phosphates pigments greatly improved the barrier resistance of the coating in 3.5 wt% NaCl after 175 day exposure period. The presence of the pigments also revealed huge fluctuations in the current noise, signifying better protection compared to the coating without them given to the formation of passive oxide layer formation. Author have also reported the individual corrosion inhibiting properties of these pigments without being encapsulated in a coating; the aqueous corrosion tests were conducted in 3.5 wt% NaCl corrodent using electrochemical and surface analytical techniques [41]. The same authors [37] have also studied the effect of these pigments on cathodic disbonding of an epoxy coating by applying −1V (vs.

Ag/AgCl) cathodic potential. EIS and pull-off tests to ascertain its barrier properties and adhesion were also evaluated. EIS results revealed improved mild steel corrosion resistance of the epoxy coating in the presence of these pigments after 30 and 175 days immersion in 3.5 wt% NaCl. The presence the phosphate pigments also improved reduced the cathodic disbonding and the enhanced the adhesion strength of the coating to the metal substrate; surface morphologies of the coatings were also evaluated. Authors made the same conclusions for both studies [37,40] regarding the barrier protection of the test substrate. Attar's group [38] have also reported the individual effects of zinc phosphate, zinc aluminum phosphate and zinc aluminum polyphosphate anticorrosive pigments (in varying ratios) on the barrier protection of epoxy/polyamide coating synthesized with bisphenol A and polyamide as the epoxy source and curing agents, respectively. The epoxy/amine coating functionalized with the pigments were individually coated on mild and tested for their protective properties in 3.5 wt% NaCl after 35 days of immersion using EIS and salt spray tests. Electrochemical results revealed increased corrosion inhibition in the presence of one pigment combined with another, but with superiority of protection depending on the concentration ratios of the pigments. This unique behavior was attributed to synergy of the phosphates pigments in the epoxy coating. The pigments also revealed better adhesion strength with reduced pull-off strength losses, with zinc aluminum polyphosphate showing better protection. In yet another work by Attar's group [39], authors have reported the combined effects of strontium aluminum polyphosphate and zinc aluminum phosphate in an epoxy/polyamine coating with the precipitated oxide layer on the surface of steel substrate evaluated by SEM.

Apart from phosphate anticorrosive pigments, another corrosion inhibitor pigments is zinc molybdate. Only few reports are available in the literature regrading inhibitor formulation with this compound; for reasons of the instability in the passive films it forms on metal substrates even when it as anticorrosive as phosphates and polyphosphates. Zinc molybdate is a major constituent of Molywhite pigments and grease; the former being solved in hydrocarbon/mineral oils in combination with some organic molybdenum compounds. Suleiman et al. [84] have reported the effect of incorporating this compound as Molywhite 101-ED (UK) (alongside zinc aluminium polyphosphate, Hfucophos ZAPP, UK) in a sol-gel coating synthesized from GPTMS, TEOS and APDMS via alkaline-catalyzed hydrolysis. Mild steel coating and corrosion electrochemistry followed after synthesis with the application of 10 mV perturbation between 10 m and 100 kHz at 10 points per decade. The dc-behavior of currents on application of ±0.2 V was also evaluated. The presence of the anticorrosive pigments improved the corrosion resistance of the coating with Molywhite showing greater activity compared to zinc aluminium polyphosphate for both ac and dc based methods in 3.5 wt% NaCl after 192 h immersion. The morphology of the sol-gel coating before and after immersion was evaluated with SEM. Suleiman et al. [85] have also reported the encapsulation of similar pigments and Shieldex (Ca^{2+} exchange silica pigment) into a sol-gel coating made from some simple alkoxides (TEOS and MTES). Divided into functionalized and bare coating, they were coated on mild steel panels and tested for their barrier properties in 3.5 wt% NaCl using EIS. Corrosion inhibition of the individual coatings were evaluated by comparison of values of corrosion/ charge transfer resistances as well as constant phase elements at 192 h maximum immersion period. Values of electrochemical parameters revealed superior

corrosion protection in the presence of these pigments compared to the coatings without them. This unique behavior from these doped sol-gel coatings was attributed to the formation more stable protective networks in the sol-gel matrix. In another report [86], an organic/inorganic sol-gel coating (synthesized from APDMS and 1,2-epoxybutane and a curing agent: 1,6-diaminohexane) has been encapsulated with cerium(IV) ammonium nitrate, Molywhite 101-ED and Heucophos ZAPP™). Similar steel substrate as well as corrodent and immersion period reported in Ref. [76,77] with dc and ac-based electrochemical corrosion test. Results from EIS and the variation in values of corrosion current densities (derived from potentiodynamic polarization) revealed that cerium (IV) ammonium nitrate was not an adequate corrosion inhibitor for this coating system.

2.3 Identification of research problems

2.3.1 Biofouling/ corrosion cost

Biofouling has been reported to cost the US Navy about USD 1 billion annually in losses and repairs, and the expenses in other sectors of the marine industries are huge as well [87]. Biofouling initiates corrosion by reducing localized molecular oxygen via associated cathodic reactions thereby creating differential aeration concentration cells on surfaces [88]. With foulers adhering and accumulating on surfaces of ship hulls over time, interfacial stress drag increases up to 60% due to frictional effects and other hydrodynamics factors between the ship and the seawater. This drag leads to more fuel consumption, since more of the fuel (approximately 40%) is needed to propel the engine in other to overcome the frictional drag. With this rate of bunker fuel consumption representing more than half of the cost of running the US marine transport sector, about

USD 60 billion is needed annually for fouling mitigation techniques, both research and applications [89] by the US Office of Naval Research (ONR). According to the International Maritime Organization (IMO), pollutant emission due to fuel burning is estimated to increase between 38 and 72% by 2020 for all greenhouse gases; but with the use of antifouling coatings, CO_2 and SO_2 emissions could widely reduce worldwide by 384 and 3.6 million tonnes, respectively, annually for both gases [90]. For metal corrosion alone, more than $100 billion is being expended annually as a result of corrosion in the United States of America alone. Annually too in the global scale, approximately one-fifth of global energy and 4.2% of gross national product is lost to similar problem [12]. In the Middle East, there seems not to be a reliable data/figure surrounding fouling and corrosion episodes, especially in Saudi Arabia, so one cannot ascertain the extent to which these problems have affected man and his environmental, in health implication, impact and cost. Metal corrosion and marine fouling are significant problems in Saudi Arabia due to the Gulf's climate, enormous oil and gas activities and associated pollution factors. The persistent increasing humidity, temperature and dusty winds immensely degrade engineering materials and adversely affect their structural components and end-use.

2.3.2 Environmental implication of most efficient antifouling technique

Biocidal chemical dispersion is among some of the most used and efficient antifouling technique employed against marine biofouling for ships and marine vessels. Because of their adverse effects on man and the ecological system, tributyltin oxide, triphenyltin fluoride and other organotin-based biocides have been banned and their usage are restricted by many countries, though this regulation is yet to be fully implemented and

enforced in some nations [91]. Organotins are carcinogenic biocidal chemicals. For corrosion inhibition, the inorganic chromate- and arsenates-based inhibitors and some of their hazardous organic counterparts, though effective for the reduction of metal corrosion at lower concertation, and they are carcinogenic as well. With the banning of these compounds, corrosion control procedures with greener inhibitor compounds (chromate-free inhibitor formulations) in most oil field applications are designed to effectively meet safety standards and also efficiently protect the targeted metal substrates in their service environments.

2.3.3 Ineffective protective coating alternatives

Sol-gel process has been used over the years to produce several protective coatings for metal protection for both anticorrosive and antifouling applications from very simple silane precursors. Protective coating of this class are susceptible to shrinkage at the surface while some do not have a strong adhesion on the metal substrates so they fail overtime. During curing procedure, excess water and alcohol molecules and unreacted precursors are removed from sol-gels thereby forming a shrunk glassy silica material with inherent bulk pores to which corrosive molecules can pass through. Modern anticorrosive sol-gel coatings lack the dual enhanced corrosion protection and antifouling properties, and their adhesion failures show a huge gap between process science and industrial engineering material applications. Some classes of sol-gel are endowed with improved barrier properties but are without stable surface inertness, film hydrophobicity and hydrolytic stability.

2.3.4 Susceptibility of steel to corrosion

Non-alloyed steel grades used in most industrial applications consist of more than 90% pure iron. The Pourbaix diagram (*E* vs pH) of iron aids in the understanding of factors that could promote the corrosion of this metal in terms of pH . This plot shows the susceptible of metals to corrosion as a function of potential and pH (Figure 2.1). For Fe (in steel) and Al, the extent of corrosion of each metal is greatly influence by pH, with more areas on the plot for Fe likely to corroded (compared to immunity and passivity regions) than Al. While Fe is thermodynamically unstable at acid and alkaline pH values, Al is passive between 3.8 and 13 ─ revealing why Fe (non-alloyed steel) will corrode faster than Al in many conditions [92]. This is a huge problem, and most reported works in the literature focus on the reduction of Al and alloyed steel corrosion with protective sol-gel coating and not pure or non-alloyed ferrous materials. Since solution pH and surface chemistry are known to hugely affect the rate of Fe corrosion, and it will be a challenging research goal to synthesized silica-based protective coating for Fe corrosion control.

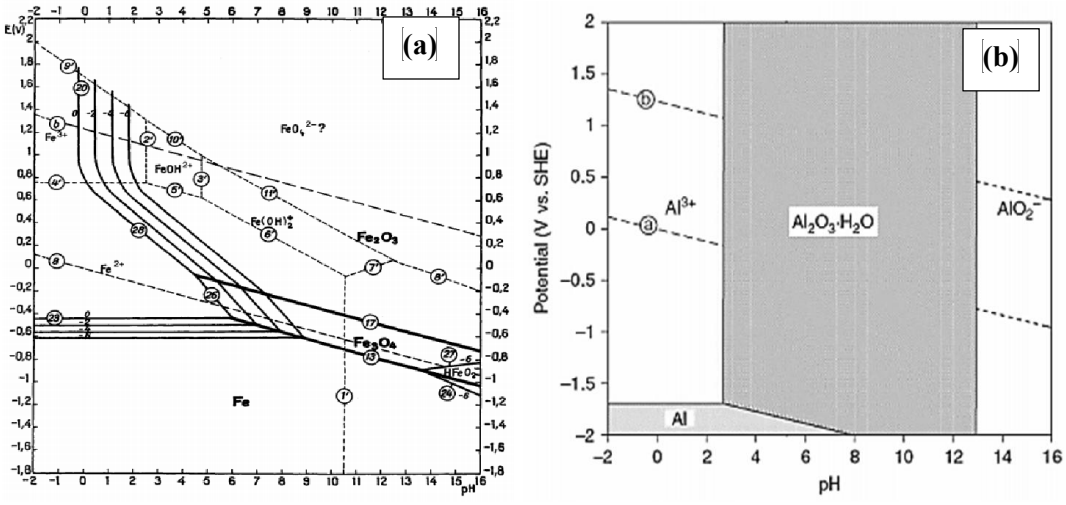

Figure 2.1 Pourbaix diagram (These plots derived from computations related to Nernst equations as well as solubility parameters of Fe and Al and their respectively ions) for the Fe- and Al-H_2O at 25°C.

2.4 Statement of research

To address channels of failed material application properties in chemical synthesis, series of protective sol-gel coatings are proposed based on simple siloxanes and organically modified polydimethylsiloxane (reactive silicones) copolymer precursors. Promoting surface adhesion *in situ*, these copolymers will co-react with the different siloxane functionalities from different monomer to form modified silica coatings. The microstructures of the protective film will be functionalized with some chromate-free phosphate-based corrosion inhibitors capable of forming passive layers made of metal complexes, oxides and/or hydroxides that can further reduce the passage of corrosive ions and molecules at the metal-solution interface. In addition, inoculum of spore-forming thermophilic bacteria isolated from Gazan geothermal springs (of the Arabian Gulf) with fouling and MIC resistant properties will also be encapsulated into the protective barrier coating. The assessment of the marine bioactivity of endospores of this bacterium encapsulated into these sol-gel coatings will be tested for potential antifouling properties after immersion of the coatings for a fixed period of time in a typical marine environment. This study proposes a corrosion protection method using safer technology and eco-compactible methods for environmental remediation and fouling control suitable for sustainable development in the Arabian Gulf.

2.5 Objectives of this work

For the first time, the foul-releasing potential of bacterial endospores of a thermophilic and non-pathogenic strain of *Bacillus licheniformis* whose enzymatic activities aids its adaptation and survival in the extreme hot climates of the Arabian Gulf (particularly the

hot Gazan springs) will be studied. Endospores of this thermophile will be encapsulated within some newly synthesized protective sol-gel coatings and tested for their potential against marine fouling and corrosion protection of S36-grade mild steel in saline medium. The bacterial biofilm of inoculums of this organism will also be cultured in appropriate medium on the mild steel substrate to further elucidate the mechanism of the fouling and corrosion resistance on the sol-gel films. This work combines the organic and inorganic functionalities of the various silane precursors to synthesis hydrid sol-gels with robust protective properties. Specifically, the following objectives are proposed in this work, for all protective sol-gel coating matrices:

(1) To design and synthesize some new organic-inorganic hybrid sol-gel protective coatings for corrosion protection of industrial S36 grade mild steel substrate. Synthesis of sol-gel polymers is via alchol-assisted and acid–catalyzed hydrolysis/condensation reaction involving normal- and organo-alkoxysilanes precursors in comparison with those synthesized from selected reactive silicones.

(2) Fourier Transform (FT) Infra-red, and liquid-state (^{1}H, ^{13}C and ^{29}Si) state Nuclear magnetic resonance spectroscopy (NMR) will be deployed to probe the extent of sol-gel reaction and also monitor the extent of hydrolysis.

(3) Each synthesized sol-gel coating will be functionalized with 5% w/v anticorrosive pigments; doped before coating (roller-coating technique) on mild steel substrate for the abiotic coating matrices; and in combination with freshly prepared *B. licheniformis* spore suspension. Recommended curing procedures will follow appropriately at recommended temperature ranges as well as surface morphology with SEM. The wetness of each coating surface will be measured for the magnitude of water contact

angle (θ_w) via static sessile drop method and the thermal stability of each sol-gel matrix will also be examined for under nitrogen atmosphere.

(4) Culturing bacterial endospores with appropriate microbiological procedures; subsequently testing its viability (using Invitrogen/BacLight staining protocol); preparing its standard solution and finally encapsulating these bacterium strains into the newly synthesized sol-gel coating matrices. The viability of the bacteria in the bulk of the coating will be further confirmed in the coating with appropriate microbiological assay.

(5) The protective ability of each coating (modified and unmodified) matrix will be evaluated by electrochemistry with each technique (ac and dc) studied for a defined surface area of the coating on steel in 3.5 wt% NaCl solution using a potentiostat. The variation of electrochemical parameters including coating resistance and capacitance for each coating corresponding to each immersion period will be evaluated.

(6) An on-field evaluation of the coated panels will be conducted in a hyper-saline Saudi Arabian Gulf waters, adjacent to KFUPM beach for fouling studies. The beach water is an unsheltered flow of body of seawater exposed to strong and hot winds of the Arabian Gulf (Figure 2.2). All coated samples will be continuously submerged in the seawater at more than 30 feet anchored from a dry dock/shore. Photograph images of both sets of coatings (including the bare steel) will be taken periodically and continuously for a couple of months. In some sol-gel formulations, the fouling studies in the hot Arabia Gulf will be compared with those of a warmer climate (precisely at Whitby Harbour, North Yorkshire, UK) for endospores of *Bacillus licheniformis* and *Paenibacillus polymyxa* encapsulated differently.

Figure 2.2. KFUPM beach at Half Moon bay, Al-Khobar, Saudi Arabia (source: Google map; Lat. 26º28', Long. 50º20').

CHAPTER 3

RESULTS AND CONCLUSION

Title: Assessing the effectiveness of immobilized bacterial (*Bacillus licheniformis*) endospores encapsulated in a doped organic-inorganic hybrid sol-gel coating for saline corrosion and marine fouling protection for steel

3.1 A brief overview

Most protective sol-gel coatings are suspectible to delamination from metal surfaces to which the applied to due to poor adhesion and because these coatings are synthesized from single-component silane precursors. Since a potential anticorrosion film is expected to be compact and without pores, the condensation and hydrolysis rates are normally controlled to yield the film with desired bulk properties. In this present study, the barrier protective ability of a multi-componenet organic–inorganic hybrid sol-gel coating with the bulk inorganic silica network synthesized from TEOS and TMMS with GPTMS crosslinking between molecular Si-O-Si chains of the final hybrid polymer matrix; GPTMS will also act an adhesion promoter. The synthesized sol-gel film will be doped with micro- and nano-sized zinc molybdate (MOLY) and alumina, before applying on mild steel substrate by roller coating technique. The sol-gel coating will also be encapsulated with endospores of *Bacillus licheniformis* for the same application, with and without MOLY. The anticorrosive and antifouling potentials of both modified and unmodified sol-gel coatings will be evaluated electrochemically (in 3.5 wt% NaCl) and in the field, respectively. The presence of alumina and the anticorrosive pigment (MOLY) in the coating will increase the bulk mechanical strength as well as impede limit the passage of corrosive molecules

and ions across the coating/electrolyte interface (by forming passive oxide/phosphate complex inhibiting layers ─ with MOLY due to the molybdate radical). The desire to inhibit non-alloyed steel corrosion using a protective sol-gel coating of this class is a huge challenge since Fe corrodes faster and it is thermodynamically unstable compared to Al. The available reports in the literature regarding organic-inorganic sol-gel coatings derived from alkoxysilanes and organoalkoxysilanes are focused on pure and alloyed Al and Mg metal substrates, Ti-based alloys, and stainless and galvanized steel grades. This work is a build up from Akid et al. [55] who reported the foul resistance of encapsulated vegetative endospores of *Paenibacillus polymyxa* (ATCC 10401) and *Paenibacillus fragi* (ATCC 4973) in the same organic–inorganic hybrid sol-gel coating for Al 2024 substrate.

3.2 Experimental

3.2.1 Reagents and pre-treatment procedures

Two alkoxysilanes (TEOS and TMMS) and an organoalkoxysilane (GPTMS) were purchased from Sigma-Aldrich (US) and used for the sol-gel synthesis without further purification. The molecular structures of these compounds are presented in Figure 3.1. Ethanol, nitric acid and alumina (Al_2O_3 nanopowder, <50 nm particle size) were purchased from Sigma-Aldrich (US); while Heucophos® Moly-white®S101-ED (a dirty yellow finely divided calcium zinc molybdate corrosion inhibitor pigment was obtained from Heucotech Ltd. Co. (US). Cold rolled steel (Low Carbon S36 type) SAE 1008 standard substrates were purchased from Q-panel standard substrates, Q-Lab Corporation (US) as one-sided ground/polished finish steel panels of dimension: 0.032”×3”×5”. The

ground/abraded steel surface gives better adhesion compared to the milled portions of the panel. The mild steel panels were properly pre-cleaned with absolutely ethanol and left to air-dried, labelled prior to coating and stored in a desiccator. Before coating, the microstructure of the metal substrate was studied by SEM (U9320A 8500 Field Emission Scanning Electron Microscope (Agilent Technology, UK)) after metal surface polishing.

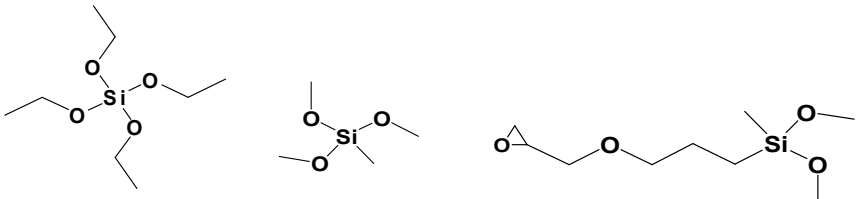

Figure 3.1. Chemical structures of the silane precursors used in this study.

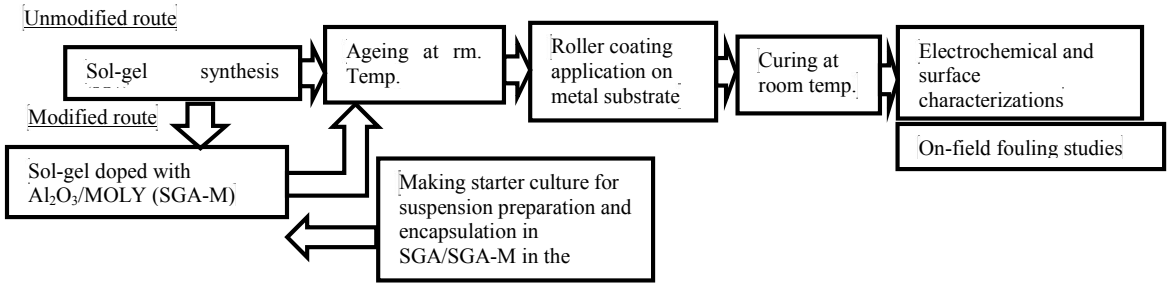

Figure 3.2 Summarized process route for the modified (doped with inhibitor pigment and bacterial endospores (SGA-M, SGA-6 and SGA-M6)) and unmodified (SGA) coating matrices on mild steel panels adopted in this study.

Table 3.1 Nominal (maximum %) chemical composition and mechanical specs data of SAE 1008 (S36 type) mild steel panels.

*Element	Mn	C	P	S
% composition	0.60	0.15	0.030	0.035
Mechanical Specs.				
Thickness	0.032"			
Finish	Ground			
Roughness (μ inches)	20-45			
Temper	1/4 hard			
Hardness (Rockwell)	B50-B65			
Tensile (psi)	55,000			

*The remaining percentage is allocated to Fe.

3.2.2 Sol-gel synthesis, modification and spectroscopic characterization

To synthesize the sol-gel organic–inorganic hybrid sol-gel coating, the three silane precursors were gently stirred (750 rpm) together for an hour without heating; prolonged agitation in a polar solvent is required before hydrolysis since GPTMS is only sparingly soluble in the mixture of TEOS and TMMS. To achieve the needed homogenization, 2 ml ethanol diluent was introduced into the silane mixture (TEOS, TMMS and GPTMS in a molar ratio of 10:6:1) thereby discouraging the possibility for liquid–liquid phase separation. Doubly distilled water (5 ml) was later added in drops into the solution and later, 0.5 ml 0.05 N HNO_3 to initiate the hydrolysis/ condensation reaction at room temperature. Hydrolysis reaction with water in the presence of these silane is endothermic, and reveals a cloudy appearance in the reaction vessel until the acid is added, then a clear and warm suspension begins to form, and remains this way throughout the reaction. A controlled and optimized ratio of diluted acid and water is needed since the rates of hydrolysis and condensation reactions depends of their molar amount (in volume) – increased amount of water as well as concentration of acid increase condensation and gelation kinetics. After an hour of continuous stirring, the solution becomes gradually viscous and remains indefinitely stable even after a week at room temperature; a prerequisite stability requirement for protective sol-gel coating. Synthesis was followed by spectroscopic characterization. The hydrolytic conversion of alkoxy groups of the silane (ethoxy and methoxy groups on TEOS and TMMS/ GPTMS, respectively) precursors to silanols as well as the ring-opening polymerization were monitored using Fourier Transform infra-red (FTIR) and liquid-state nuclear magnetic resonance (^{1}H, ^{13}C and ^{29}Si NMR using $CDCl_3$ as solvent) spectroscopies. Results obtained from these spectroscopic

techniques give an idea of the extent of hydrolysis/acidification reactions accompanying the sol-gel process. NMR was acquired with a Bruker 750 spectrometer (JOEL instrument, Japan) and FTIR with Nicolet 6700 Fourier Transform (FT) Spectrometer (Thermo Electron Corporation, UK) operating in transmittance mode. All chemical shift referencing in NMR was relative to TMS. IR absorption was recorded with the liquid state with a CaF_2 beam splitter measured with an InGaAs detector spectrometer with a ±4 cm^{-1} resolution at 64 scans.

The resultant colloidal sol (SGA) was divided into portions and some of them were modified accordingly with the 1.5% alumina (per 10 ml SGA), anticorrosive pigment and thermophilic bacterial endospores at pH more than 3. To a 20 ml sol-gel solution, 10 g Moly-white®S101-ED (MOLY) was added and sonicated to dissolve the pigments in the mixture before re-stirring and labeled (SGA-M) as modified sol-gel mixture. SGA-M solution was divided into two; to a potion, 0.5 mL of the bacterial endospore suspension was added and labelled (SGA-M6). The unmodified sol-gel solution was encapsulated with equal amount of the bacterial suspension as in SGA-M6 and labelled SGA-6. All labelled sol-gel solutions with "6" represents bioactive coating (i.e. SGA-6 and SGA-M6), with SGA and SGA-M denoting the sol-gel solution alone and sol-gel solution functionalized with MOLY. Prolonged sonication and stirring procedures were avoided for in the bioactive solution since mechanical mixing and homogenization could destroy/kill the bacterial endospores, rendering them unviable. Viability test was conducted to demonstrate the survival of the endospores in these solutions and growing vegetative cells were culture per micro litre in a Tetrathionate (TT broth) media at 50 ^{o}C.

The stepwise modification in this sol-gel process is represented in Figure 3.2 for all coating matrices.

3.2.3 Isolation and identification of *B. licheniformis*

Thermophilic microbes are among the few extremophiles commonly found in the geothermal areas of the world, and particularly, the few hot springs of Saudi Arabian deserts [93]. The uniqueness of enzymatic activity responsible for their adaptation and survival at these extreme climatic conditions is related to well define biochemical pathways and DNA conformations. Some thermophiles of the *Thermus* and *Bacillus* genera have been reported to be resistant to extreme pH and salinity [94,95]. The global market and demands for possible cellular and biocatalytic applications have increased since the isolation and characterization of the first thermophilic bacterial strains by Miquel's group in 1888, in food processing, waste recycling, pharmaceutics and antifouling activities [96,97]. In this work, the isolation of a thermophilic *B. licheniformis* strain (No. 6) and subsequent genotypic and phenotypic characterization is reported from the hot springs of the Gazan area (Lat. 43º15E', Long. 16º56N'), Eastern Province of Saudi Arabia. The collection of spring water samples, preservation and storing procedures employed in the work are similar to the ones previously reported by Khalil *et al.* [96,98]. Appropriate volumes of sterile containers, buffers and media used for the inoculation and culturing procedures were carried out at recommended incubation temperatures and durations in line with this bacterial strain. Single *Bacillus* colonies from the culture were streaked and picked onto TT agar plates, and then incubated for 48 h with gentle stirring (300 rpm) at 55─70 ºC. Distinctive colonies from the incubated TT agar were transferred and stored at ─80 ºC in fresh glycerol in TT broth [96]. Labelled as *Bacillus* strain, the

isolated wild type strain was identified by 16S rRNA gene polymerase chain reaction (PCR) and sequencing at KFUPM, Saudi Arabia. Its gene alignment was compared with the closest GenBank match at the highest degree of confidence, and later confirmed as *Bacillus licheniformis*. The elaborate non-specific 16S rRNA gene PCR amplification procedure with appropriate oligonucleotide primers have been previously reported [96,98].

3.2.4 Preparation of *Bacillus licheniformis* suspension

To obtain the bacterial endospore suspension for this study, the thermophilic strain of *Bacillus licheniformis* was collected from Department of Biology (identified by Prof. Amjad Khalil). Endospores were towed from ice previously used for storage after isolation from hot springs of the Gazan area (Lat. 43º15E', Long. 16º56N'), Eastern Province of Saudi Arabia. They were dissolved in sterile water and 100 µL of which was streaked in TT broth before being incubated overnight (at 50˚C, 180 rpm) in order to get the starter culture for suspension preparation the next day. Much growth in colonies was revealed in the media the next day showing viability of the bacterial endospores. The bacterial endospore suspension was prepared by collecting a loop-full (before a bacterial transferring a culture, a platinum wire is heated for some seconds then used to scoop the culture within the spoon-like loop) from discreet growth colonies on semi-solid TT broth surface in a plate into 9 ml of sterilized water. This suspension is repeatedly stirred to homogenize the crowed bacterial vegetative cells in the solvent.

3.2.5 Coating procedure and characterization

A neat coating of each sol-gel solution (both biotic and abiotic) was evenly applied on the previously pre-clean steel panels via roller coating technique (RK Print-Coat Instruments

Ltd, UK). The coated films on each labelled panel were allowed to cure completely at room temperature for 72 hours prior to surface morphology, electrochemical analyses, fouling field trail. Every coating was prepared in duplicates for both lab-based electrochemical and on-filed fouling studies. Thermogravimetric analysis (Perkin-Elmer TGA 7, US) was conducted on the unmodified sol-gel film (SGA) alone to determine the thermal behavior of this matrix under nitrogen atmosphere between 30 and 900 ^{o}C at 10 ^{o}C/ min. The degree of wetness (CAM Instrument DSA30, KRUSS, Germany) with respect to aqueous contact angle (θ_w) of each film surface was determined by static sessile drop method, and results presented in this study are single trails of every measurement taken in no predetermined order. The protective barrier evaluation was conducted in a saline corrodent (3.5 wt% NaCl) using electrochemical (GAMRY potentiostat/ZRA system, REF3000-19131, Gamry Instruments, US) and surface analytical techniques. A dc-based potentiodynamic polarization test was employed in for the evaluation of the anticorrosive abilities of these films, and this was accomplished by applying ±0.25V versus E_{oc} at 10^{-4} V/sec. Linear Tafel fitting was performed using EChem Analyst and appropriate polarization parameters were obtained and extent of barrier protection of each coating discussed with according to immersion period in 3.5 wt% NaCl. Electrochemical impedance spectroscopy (EIS) was also deployed in evaluating the protection of properties of both biotic and abiotic films on steel substrates and results were analyzed by studying the variation of values of electrochemical corrosion resistance and constant phase elements/ capacitances for each coating within the period of exposure in 3.5 wt% NaCl. Impedance measurements were performed by applying minute sinusoidal perturbation (±10 mV) signal versus E_{corr} at 10 points/ decade between 100 kHz and 10 mHz at

potentiostatic condition in a three electrode system (Figure 3.3). Surface analysis of the each protective film on steel mild substrate was evaluated by topology using atomic force microscopy (5420 Atomic Force Microscope, Agilent Technologies, US) operating at tapping mode, prior to and after exposure of each coating to 3.5 wt% NaCl at room temperature. The distribution of the bacterial endospores in the films before and after the encapsulation procedure was studied by scanning electron microscopy (U9320A 8500 Field Emission Scanning Electron Microscope, Agilent Technology, UK) operating at 10 kV SEM high voltage.

3.2.6 On-field fouling studies at Half-moon Bay, Saudi Arabia

The foul-releasing ability of each sol-gel coating matrix in the presence and absence of the bacterial endospores, was evaluated in the Half-moon (KFUPM beach) tributary of the Gulf River, Dhahran known for its all-season fouling and hyper saline conditions. This beach is unsheltered flow of body of seawater exposed to strong and hot winds of the Arabian Gulf known for its unique marine diversity, floral and faunal species, and complex aquatic ecosystems. All coated samples were continuously submerged in the sea water and photo-digital images of both biotic and abiotic coatings will periodically collected throughout the period of study.

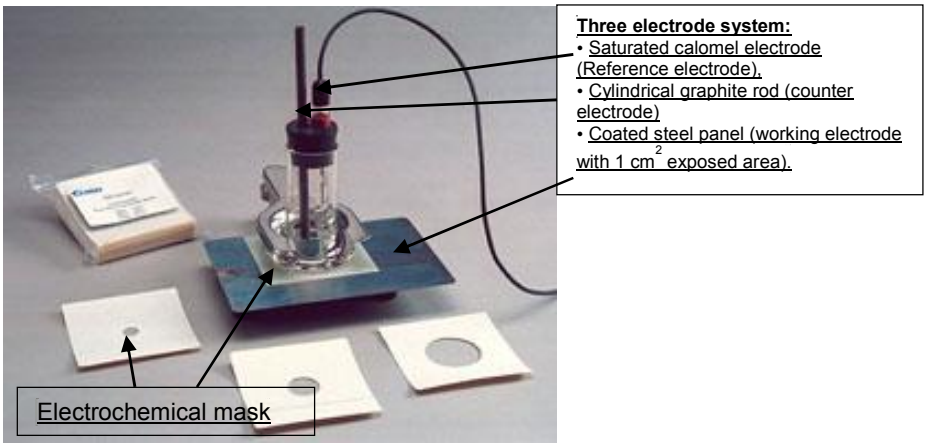

Figure 3.3 Photograph of a coated sample clamped to the PTC1 Paint Test Cell used in this study. The cell allows for the defining of distinct test areas for metal substrates using surface marks made of inert material (http://aseptec.com.my/index.php?cPath=25_35).

3.3 Results and discussion

3.3.1 The substrate's microstructure (by SEM)

The mild steel substrate used in this work is a S36 type grade specimen with the following chemical composition (wt.%): Mn 0.60, C 0.15, P 0.030, S 0.035 and the remaining percentage is allocated to Fe. To study the morphology of the substrate's microstructure, it was first mechanically cut into a 1 cm x 1 cm coupon and abraded with different grades of silicon carbide papers (between grit no. 120 and 800), repeatedly rinsed with absolutely ethanol before finally polished to mirror surface finish with micro-scaled alumina (gradually from 1 to 9 μm). Polishing was proceeded with acetone ultrasonication and later re-rinsed in the acetone and dried in warm air. Figure 3.4 displays the SEM microstructure of S36 mild steel grade imaged after sample polishing with relatively uniform distribution of phases. The SEM micrograph of this material displays predominantly areas rich in ferrite (bright patches) outlining the grain boundaries with those of pearlite (dark portion; a ferrite/cementite lamellar structure); typical of low carbon steel. The differences in the chemistries of these regions contribute to the corrosion

of mild steel due to galvanic effect as ferrite is most likely to be affected since the cementite content of pearlite is more electrochemically stable. The elemental mapping of the microstructure by scanning electron microscopy-energy dispersive X-ray spectrometry (SEM-EDS) reveals trace composition of Mn (0.75%), C (0.20%), P and S (<0.2%) with remaining percentage being dominantly Fe. The C content in most ferrite-pearlite steel grades as well as their grain sizes determine their microstructure and resulting properties [99].

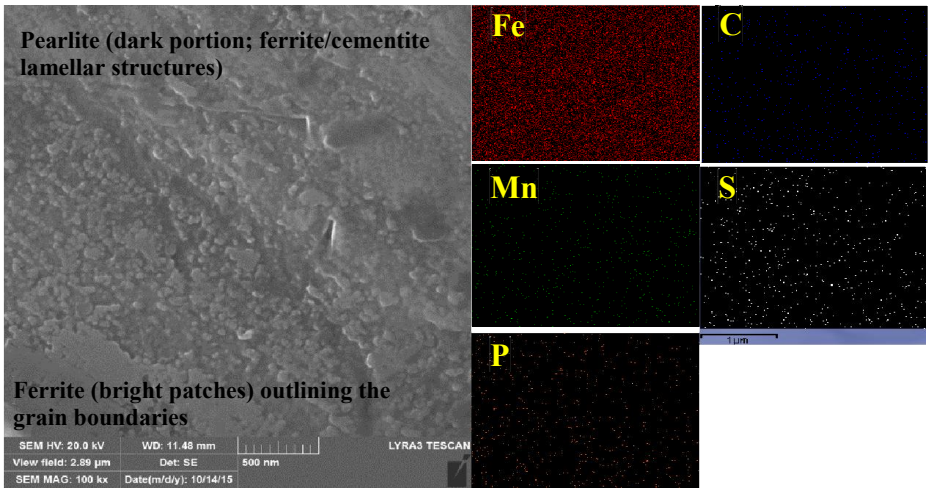

Figure 3.4 SEM micrographs of S36 mild steel grade showing its microstructure (left panel; 500 nm); EDX mapping (right panel; all micrographs are equally scaled (1 µm)).

3.3.2 Spectroscopic characterization of the sol–gel film

The extent of sol-gel reaction was probed by means of monitoring hydrolysis of active alkoxy groups on the silane precursors employed in the synthesis; Figure 3.5 shows the structures and NMR spectra ((a) ^{1}H and (b) ^{13}C) of these silane compounds. Sol-gel reaction was initiated by alcohol-assisted hydrolysis (acid-catalyzed) with minimal amount of water needed to prepare colloidal sol with partially hydrolyzed products and also capable to supporting metal surface adhesion. Apart from evaluating the extent of the hydrolytic conversion of ethoxy and methoxy functional groups on the silane precursors in

the stable prepared sol, NMR also monitored epoxy ring-opening polymerization in GPTMS precursor. To show evidence of hydrolysis/condensation reaction on the prepared sol-gel mixture, its NMR spectrum (Figure 3.6) were compared to those of the pure unreacted silanes. The disappearance of TEOS's ethoxy proton peaks at 1.23 and 3.84 ppm, triplet and quartet, respectively, shows successful hydrolysis, and well as those of methoxy groups at 3.43 ppm (for TMMS and GPTMS) ─ though showing peak broadening. The proton NMR spectrum of the sol-gel film also shows peak broadening of epoxidic protons at 2.51, 2.69 and 3.05 ppm (at position 3 and 5) being evidence of acid-catalyzed ring opening reaction on the epoxy ring. This is also confirmed on the carbon NMR spectrum (Figure 3.5 b) with reduced peak heights at 43.9 and 50.5 ppm being corresponding carbons at those positions. New carbon peaks between 60 and 70 ppm are associated to ring opening polymerization products; possibly aldehydes, enols or ketones [100]. More of these peaks are also visible at 9, 48, 56 and 63 ppm. Lee at al. [101] have reported that the presence of polymerization products corresponding to alkylether (between 9.0─9.5 and 70 ppm), diols (71 ppm) and polyethylene oxide (after 74 ppm) are responsible for these additional peaks on the sol-gel spectra. Innocenzi et al. [102] have opined that de pending on the sharp character of the NMR signals, there could also be indications of other chemical species characteristics of some oligomeric species in the same structure. Like the work by Lee et al [101], they also showed that peaks at 63 and 71; 72 and 73; 58 ppm are indicative of the presence of diols, polyethylene oxide and a terminal methyl ether produced by polymerization reaction between epoxide rings. However, the presence of the reduce carbon peak at 50.6 ppm is indicative of incompletely hydrolysed methoxy groups (from TMMS and GPTMS) absorbed on the silica; also

evident in the broad proton peak at 3.5 ppm. Peaks at 18.6 and 58.5 ppm possess reduced heights (compared to the NMR spectrum of TEOS) showing the hydrolysis of the ethoxy groups of TEOS actually took place in line with the result presented on the proton NMR. Figure 3.7 displays the liquid FTIR spectrum of the as-prepared sol-gel film with a distinct broad IR signal at 3300 cm^{-1} representing O–H stretching band from silanol groups from hydrolysis products (during the chemical conversions alkoxy groups) [102,103] ─ this could also have been from silica absorbed molecular water or excess alcohol condensation products. Successful condensation reaction of silanols yields silica with corresponding bands found at 1086 cm^{-1} and between 400─450 cm^{-1} for asymmetric Si–O–Si stretching and bending vibrations, respectively [104,105]. Absorption bands at 1272 and 2970 cm^{-1} are representative of C–H stretching vibrations while those between 1400 and 1410 cm^{-1} represent partially unhydrolysed (Si–C bonds) silanes and/or oligomers in the sol-gel. The reduced ring breathing of epoxy is found between 810 and 950 cm^{-1} affirm that ring-opening polymerization of GPTMS was successful; similar stretching absorption peak disappears at 1250 cm^{-1} being an asymmetric band of epoxy ring [103]. Apart from characterization with the carbon and proton NMR spectroscopies, the extent of sol-gel reaction was also monitored by ^{29}Si NMR (Figure 3.8). Since TEOS, TMMS and GPTMS possess ^{29}Si NMR peaks precisely at ─82.1, ─39.5 and ─42.0 ppm, respectively, it means that during reaction, any deviation of peaks from values different from those exhibited by individual precursors is suggestive of sol-gel reaction. The synthesized sol-gel film displayed ^{29}Si NMR peaks at ─63.7 and ─72.4 ppm assigned to T^2 and T^3 (in condensed cubic T_8 cage structures) species, respectively. These chemical species are derived from

the presence of hydrolysable silica network as the hydrolysis/condensation reactions occur bring about changes in the siloxane precursors' environments [102].

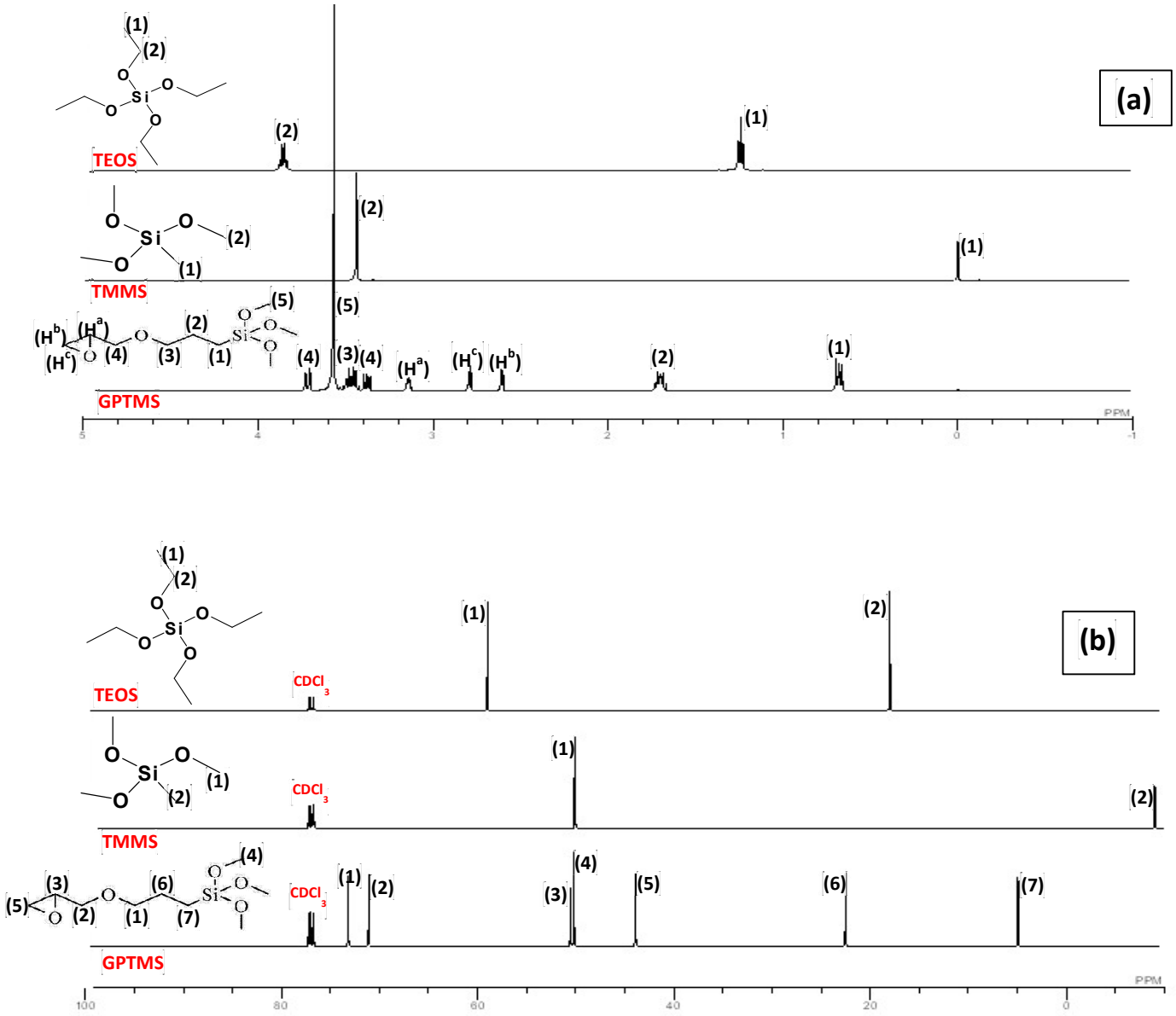

Figure 3.5 Liquid state NMR spectra (^{1}H (a) and (b) ^{13}C) of the precursors (TEOS, TMMS, GPTMS, respectively, from up to bottom) employed in this study (solvent: $CDCl_3$).

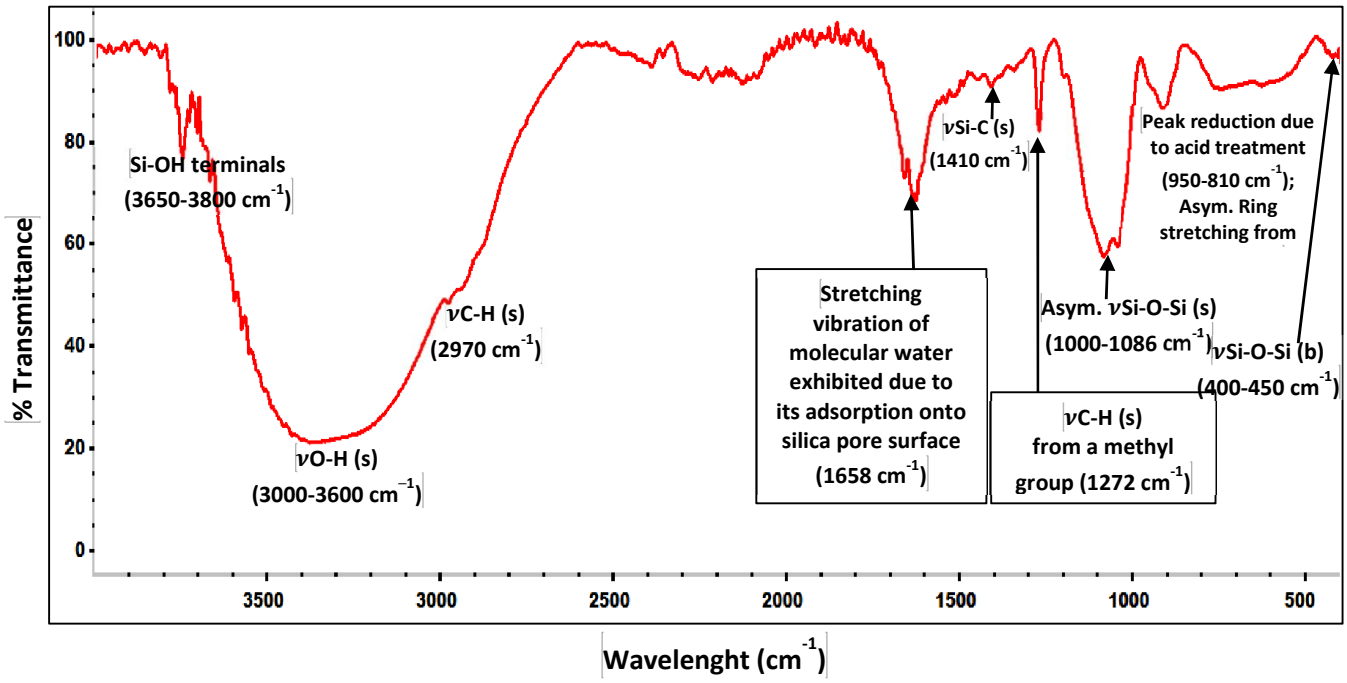

Figure 3.7 FTIR spectrum of the as-prepared and unmodified sol-gel coating before application on metal substrate and curing procedures

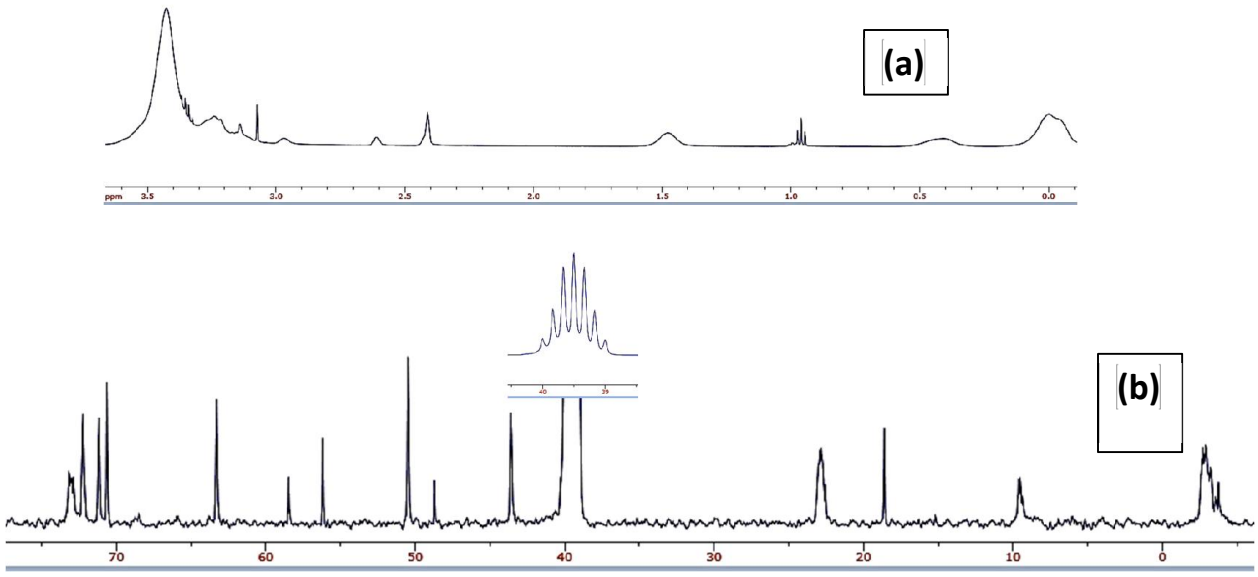

Figure 3.6 NMR (^{1}H (a) and (b) ^{13}C) spectra of the as-prepared and unmodified sol-gel coating before application on metal substrate and curing procedures

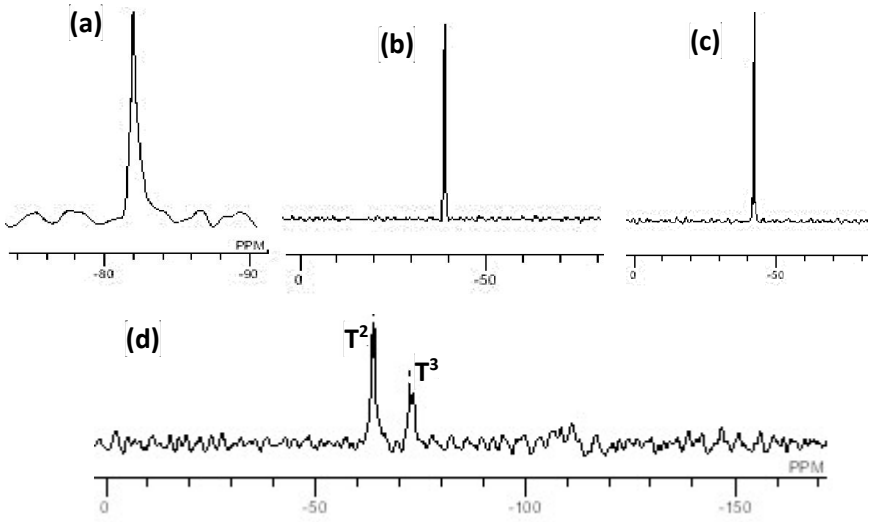

Figure 3.8 ^{29}Si NMR spectra of the silane precursors (above: a, TEOS; B, TMMS; and c, GPTMS) and the as-prepared and unmodified sol-gel coating (below) before application on metal substrate and curing procedures.

3.3.3 Bacterial viability test, thermogravimetry and contact angle measurement

The presence of viable bacterial cells in the biotic sol-gel matrices was evaluated by inoculation (per ml) in a TT broth media and culture overnight at 50 ^{o}C. The growth presence after 12 hours revealed several cluttered colony-forming units of viable vegetative bacterial cells signifying that both bioactive sol-gel coatings (SGA-6 and SGA-M6) contained viable or living bacterial cells. Figure 3.9 (a) shows viable bacterial cells in a plate carrying the media. After doping the sol-gel coating with abiotic and biotic additives as presented in scheme 1, each coating matrix was applied on pre-cleaned mild steel substrates and left to cure accordingly. Figure 3.9 (b) shows a photograph images of well distributed and continuous sol-gel films on steel, labelled according. Upon curing, the thermogravimetric analysis of the unmodified coating (SGA) alone was evaluated for stability under nitrogen gas between room temperature to 900 ^{o}C. Figure 3.10 represents the TGA curve of the sol-gel film with three distinct thermal regions corresponding to weight loss during the decomposition of the cured material. The evaporation of physically adsorbed (loosely bound molecular) water on silica occurs at before 250 ^{o}C of heating, and

this corresponds to 11% weight loss. Generally for sol-gel coatings, weight losses around 210 ^{o}C and 280 ^{o}C then to 580 ^{o}C and 650 ^{o}C are due to the pyrolysis of organic groups/chains in the silica matrix [106]. In this study, the sol-gel displays linear thermal decomposition 280 and 550 ◦C representing the highest weight loss (48%) while those between 600─900 ^{o}C represents a 10% loss due to disintegration of the Si-O-Si network and the formation of inorganic ash after 900 ^{o}C [107]. The degree of hydrophobicity of each coating sets of coating (biotic and abiotic), being a characteristics of potential protective coatings, was evaluated by static sessile drop method. The results presented on Figure 3.11 are those collected from single trails with the biotic coating matrices showing remarkably higher θ_w values compare to the abiotic coatings: SGA-M6 (91.72%)>SGA-M (89.72%)>SGA-6 (75.75%)>SGA(67.60). The reason for this this result were not further evaluated, but with the presence of the bacterial endospores in the coating revealing higher θ_w magnitude (hydrophobic), the abiotic system can be regarded as being hydrophilic with lower values of θ_w. The surface tension and wetness of surfaces are very important determining factors in the design of protective films with reliable barrier properties [108].

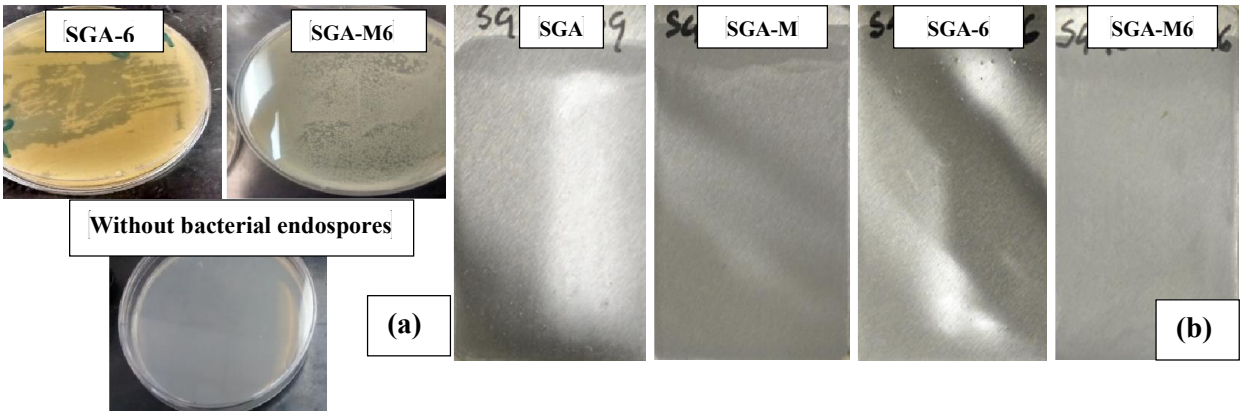

Figure 3.9 Viable bacterial growth on TT broth after an overnight incubation at 50 ^{o}C; the plate without bacteria has no growth (a); physical appearance of various cured sol-gel coatings.

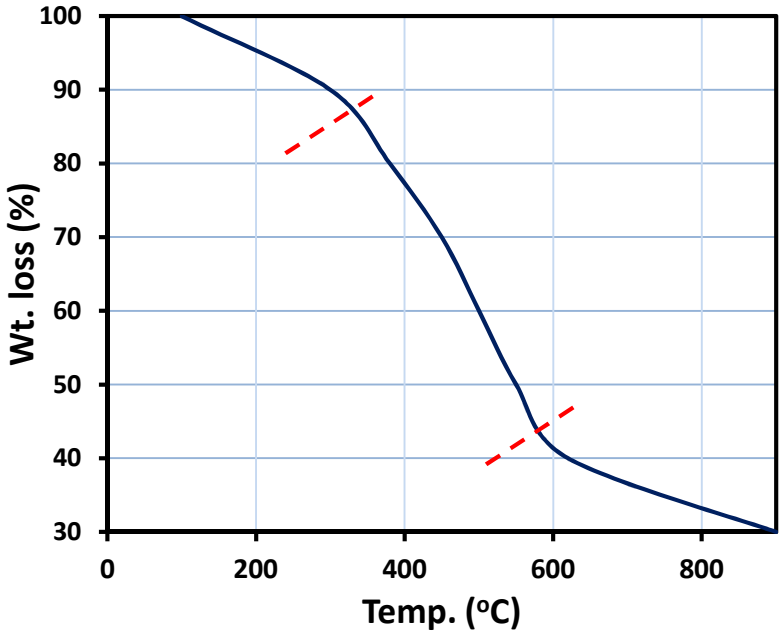

Figure 3.10 TG plot of the dried unmodified (SGA) sol-gel film collected under nitrogen atmosphere at 10 °C/min.

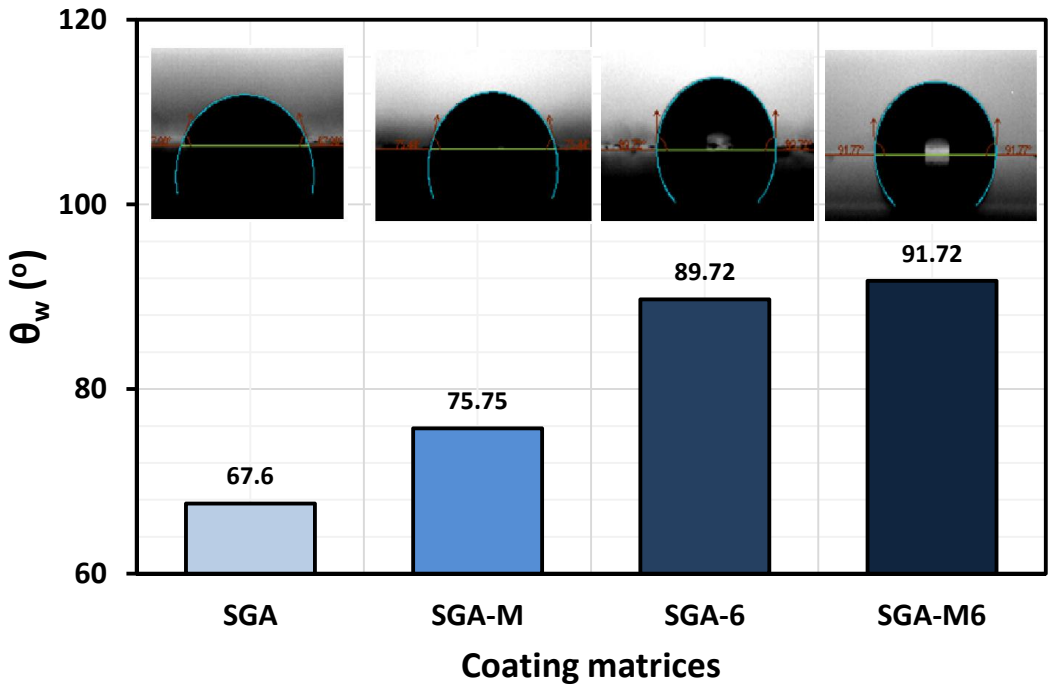

Figure 3.11 Aqueous contact angle (θ_w) values of static surface of both biotic and abiotic sol-gel coating matrices. θ_w for all coated electrodes are determined by static sessile drop method.

3.3.4 Electrochemical corrosion studies

AC and DC-based electrochemical techniques were used in evaluating the barrier protection properties of the various sol-gel coating matrices on mild steel in 3.5 wt% NaCl solution.

3.3.4.1 Potentiodynamic polarization

The corrosion behavior of mild steel working electrodes coated with the biotic and abiotic sol-gel films was evaluated by dc method with anodic and cathodic responses represented in current–potential (i-E) type relation in Figure 3.12. Potentiodynamic polarization technique employed for this studies involved the application of ±0.25V versus E_{oc} at 10^{-4} V/sec for each coated panel without replacement, neither for the same technique nor for the accompanied ac technique. Figure 3.12 displays the Tafel polarization curves for both sets of coatings on mild steel immersed in 3.5 wt% NaCl for (a) 24 and (b) 96 h. The plots show that the presence of the sol-gel coatings at all the immersion period decreased the corrosion rate indirectly by lowering the magnitude of current density. The passage of corrosive chloride ions to the metal surface by the coating was greatly impeded due to an improved interfacial barrier and the strength of the coated surfaces in the presence of the corrosion inhibitors. The values of potentiodynamic polarization parameters extrapolated from the Tafel curve of each coating after 24 and 96 h immersion are shown in Table 3.2. Values of E_{corr} were observed to be higher and nobler for superior sol-gel coatings, and a mark decrease in the corrosion current densities are also observed. For both immersion periods reported in this study, the modified coatings showed superior barrier properties compared to their unmodified counterpart; with SGA-M6 being the best. By exhibiting this corrosion inhibiting behaviour, this particular biotic coating matrix demonstrated a

synergy between the endospores and the molybdenum inhibitor molecules for reduction of mild steel corrosion in saline medium. A corrosion current density (i_{corr}) magnitude of 5.71 µA is recorded for SGA-M6 matrix after 24 h immersion in NaCl and 5.0 µA just after 96 h. From the i_{corr} values obtained, the corrosion protection behavior of these coating systems in 3.5 wt% NaCl solution decreased in this order: SGA-M6<SGA-M<SGA-6<SGA. It is the strength of the exocellular polymeric substances (EPS) secreted by the colonies of these organisms in coating and on metals that allow for simultaneously studies of corrosion protection and biofouling [56]. The anticorrosive pigment used in this work draws its unique ability to reduce corrosion by readily precipitating stable oxides and hydroxides that prevents cathodic reduction reactions at the working electrode surface in the solution of the electrolyte [40─42].

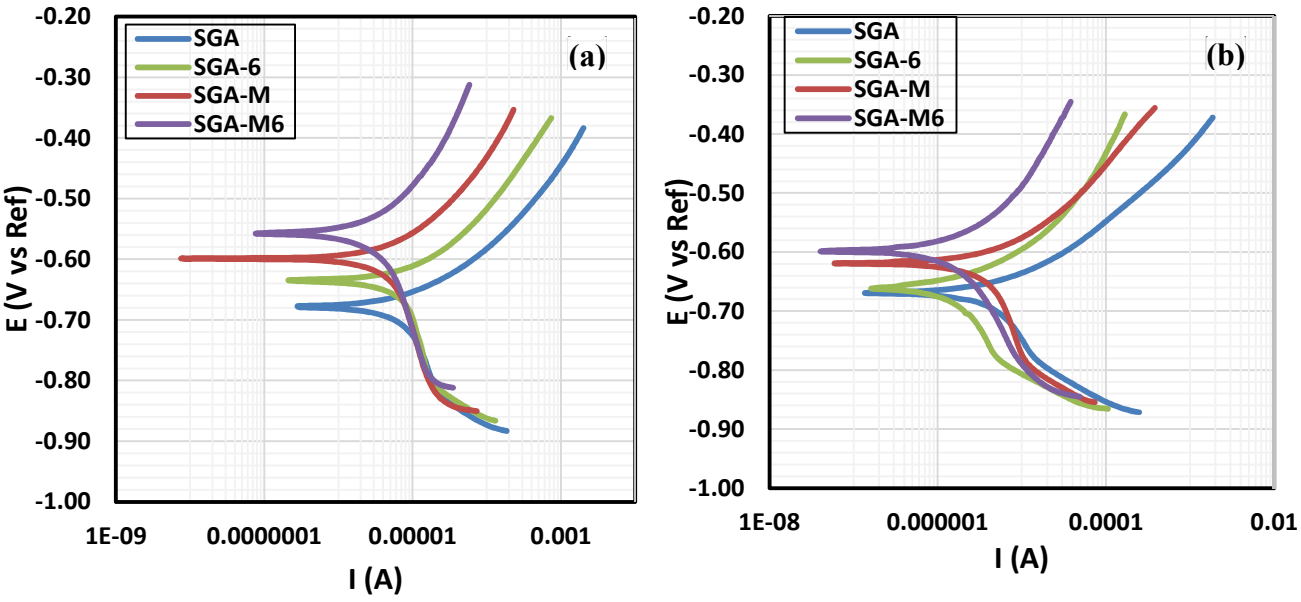

Figure 3.12 Tafel curves for biotic and abiotic coating matrices after 24 (a) and 96 (b) h immersion in 3.5 wt% NaCl.

Table 3.2 Potentiodynamic polarization parameters for the modifies and unmodified sol-gel coating on steel panels compared to the bare steel (uncoated) in 3.5 wt% NaCl after 24 and 96 hours immersion periods

Sol-gel coating	E_{corr} (mV/SCE)		I_{corr} (μA)		β_A		β_B	
	24 h	96 h	24 h	96 h	24 h	96 h	24 h	96 h
SGA	−678	−679	13.8	10.23	0.0753	0.0923	0.5117	0.3824
SGA-6	−635	−661	12.3	7.81	0.0974	0.1032	2.9505	0.5160
SGA-M	−610	−609	10.0	6.49	0.1468	0.1068	3.2071	1.1975
SGA-M6	−550	−558	5.71	5.00	0.2000	0.2031	4.8801	1.9690

3.3.4.2 Electrochemical impedance spectroscopy

In this study, the electrochemical behavior of each coating at a minute ac amplitude perturbation in the saline electrolyte has been evaluated. This technique was employed to further demonstrate the corrosion protection performance of the sol-gel films on the metal. Figure 3.13 displays the modules and phase angle (Bode curves) plots of biotic and abiotic sol-gel films on mild steel substrates after exposure in 3.5 wt% NaCl solution for (a) 24 (b) 48 and (c) 72 h. For all the immersion periods studied, the modified sol-gel films demonstrates superior protection to steel compared to the unmodified films due to the presence of anticorrosive species in bulk of these coatings. This can be deduced from the higher Z_{mod} values obtained at the range of frequencies under study. The variation in the magnitude of Z_{mod} is visible at lower frequencies, and throughout the three immersion periods at 0.01 Hz, the range of Z_{mod} is in this order: SGA-M6>SGA-M>SGA-6>SGA; with SGA-M6 being the most protective sol-gel coating. Z_{mod} values of 21.8 kΩ is recorded for SGA-M6 compared to 8.84, 6.09 and 3.42 kΩ for SGA-M, SGA-6 and SGA, respectively. For all the coating matrices, Z_{mod} values gradually decreased as the exposure period of the coated steel substrates in the saline electrolyte increased; with 15.9, 4.43, 4.12, and 1.35 kΩ recorded for SGA-M6, SGA-M, SGA-6 and SGA, respectively after 72 h. Higher Z_{mod} values denotes better corrosion resistance, and this has been observed for

the MOLY-doped biologically-functionalized coating (SGA-M6). EIS confirms the corrosion protection order previously shown in the dc-based electrochemical study. Barrier protection was also evaluated by means of evaluating the phase separation between the current and potential components (Phase diagram). The Bode phase (Z_{phz}) versus frequency plots for both biotic and abiotic sol-gel films on mild steel substrates after exposure in 3.5 wt% NaCl solution for (a) 24 (b) 48 and (c) 72 h are also presented in Figure 3.13. Phase angle curves are characterized by single maxima for all the sol-gel films towards the medium frequencies and with evidence of uncommon protection mechanisms. At 100 Hz for the 24 h immersion, the variation of Z_{phz} (Φ) magnitude are in this order: SGA-M6> SGA-6> SGA-M >SGA; with Φ values of the biotic coating being slightly higher than those of the abiotic films (−4.28, −4.10, −8.36 and −8.87^o observed for SGA-M6, SGA-6, SGA-M, SGA coatings, respectively). Φ values of −5.13, −2.13, −6.60 and −2.14^o are recorded for SGM6, SG6, SGM, SG coatings, respectively, at the highest frequency (100 kHz) after 72 h immersion, and without distinct maxima for SGA and SGA-M matrices on their Φ curves. Figure 3.14 displays the Nyquist curves for biotic and abiotic sol-gel films on mild steel substrates after exposure in 3.5 wt% NaCl solution for (a) 24 h (b) 48 h and (c) 72 h. All the curves are two-time constant (τ) semi-circles for the immersion periods under study, with wider capacitive loops for films with better barrier protection against steel corrosion. Full capacitive loops are obtained for all the systems of coating at higher frequencies. At all the immersion periods under study, the MOLY functionalized sol-gel coating encapsulated with the *B. licheniformis* endospores reveals widest semi-circle diameter and the unmodified sol-gel coating being the least. A two-time constant equivalent circuit model presented in Figure 3.15 was employed in

fitting experimental data for both sets of coatings at the immersion period studied using the EChem Analyst model editor software accompanying Garmy instrument. The electrochemical circuitry consist of resistors and constant phase elements in two phases: the first constant phase being a direct contribution of the coating (R_{po} and CPE_c) and a second phase denoting an interphase between the coating and the metal surface (R_p and CPE_{dl}), respectively. To characterize the barrier properties each constant phase, these resistance and capacitive components are extrapolated from the circuit model and are adequately plotted. The CPE (measured in μF cm^{-2} $s^{-(1-\alpha c)}$)), with impedance (Z_{CPE}) in Equation 3.1, was used in place of a pure capacitor in the equivalent circuit in order to show grounds for the adequate consideration of double layers' inhomogeneity and electrode surface irregularities [109,110]. CPE is a non-ideal dielectric properties of a protective barrier coating, and it is defined in Equation 3.2:

$$Z_{CPE} = 1/Y_o(j\omega)^{\alpha} \quad (3.1);$$

$$CPE = r.\varepsilon.\varepsilon_o A/d \quad (3.2);$$

where α is the system homogeneity factor, Y_o (CPE_o) is the pseudo-capacitance and ω is the frequency (measured in rads); ε_o and ε are the electrical permittivity and the surface film's dielectric constant; A is the exposed area of the metal, d is the thickness of the film while r is the film roughness factor [111]. Values of R_{po} and CPE_c representing the first phase were collected at higher frequencies. R_{po} being the pore resistance of the coating, represents the extent the sol-gel coating deteriorates as the ions and molecules of the corrosive NaCl electrolyte percolates through the bulk of the protective film. The magnitude of the film or coating capacitance (CPEc) contributes to electrolyte/water absorption and further explains the film's porosity in terms of its water uptake ability

[110]. After the fitting of impedance data with the equivalent circuit, the corresponding values of resistance and constant phase elements were also plotted for the first constant phase, and presented in Figure 3.16 a. Values of R_{po} improved remarkably after modifying the sol-gel coating with the MOLY inhibitor pigment and the bacterial endospores; and after 24 h of immersion in 3.5% NaCl solution at room temperature, R_{po} values for SGA, SGA-M, SGA-6 and SGA-M6 stands at 113.5, 347.9, 311.0 and 1231.0 Ω. The magnitude of R_{po} keeps decreasing gradually with the exposure immersion period in the saline solution as the corrosive ions percolates on prolonged immersion. This can also be attributed to the widening of micro-scale pores and cracks bulk of the silica network, allowing for the free passage of chloride ions to the metal surface [112]. Values of R_{po} for SGA, SGA-M, SGA-6 and SGA-M6 stands at 59.2, 225.3, 141.6 and 900.4 Ω after 72 h immersion in NaCl; with superior barrier protection being represented in this order: SGA-M6 > SGA-M > SGA-6 > SGA. Similar evaluation was done for the variation of CPEs with immersion period for all the coating matrices presented in Figure 3.16 b. As shown in this plot for all both sets of coating, the gradual increment in CPE values with immersion period reveals the rate of water absorption unto the protective coatings thereby leading to loss of their corrosion inhibiting ability in the saline electrolyte. Superior protective coatings possess smaller magnitude of CPEs; and judging from the CPEs values of every coating, MOLY functionalized sol-gel coating encapsulated with the bacterial endospores (SGA-M6) is a better barrier coating for mild steel in 3.5 wt% NaCl. Values of CPEs for SGA, SGA-M, SGA-6 and SGA-M6 stand at 47.8, 4.7, 10.1 and 0.1 μF cm^{-2} $s^{-(1-\alpha c)}$) after 24 h immersion in NaCl and gradually increases 72 h in the same order (546.8, 16.5, 94.2 and 0.9 μF cm^{-2} $s^{-(1-\alpha c)}$ for SGA, SGA-M, SGA-6 and SGA-M6,

respectively). Increased values of CPEs denotes increased water uptake through the protective coatings.

The variation in values of R_p and CPE_{dl} (resistances involved) representing the second constant phase were also collected at between the medium and lower frequencies. For both biotic and abiotic sol-gel coatings, these electrochemical parameters describes disbonding at the metal/coating interface. Figures 3.16 c presents the variation of R_p with immersion period for this class of protective sol-gel coating, and the trend in values of R_p is similar to those of R_{po}. R_p values for both sets of coating are observed to gradually reduce with immersion period and this could be due to defect in the coating as well as at the coating/metal interface. Values of R_p improved remarkably after modifying the sol-gel coating with the MOLY inhibitor pigment and the bacterial endospores. After 24 h of immersion in 3.5 wt% NaCl solution at room temperature, values of R_p for SGA, SGA-M, SGA-6 and SGA-M6 stand at 3.9, 10.4, 8.4 and 28.5 Ω, respectively but rapidly dropped: 1.5, 6.4, 5.7, and 23.9 Ω for SGA, SGA-M, SGA-6 and SGA-M6, respectively with superior barrier protection being represented in this order: SGA-M6 > SGA-M > SGA-6 > SGA. Since the corresponding values of R_p and R_{po} of SGA-M are greater than those of SGA-6, this indicates that the presence of MOLY inhibitor pigment in the protective sol-gel film/coating enhances corrosion inhibition compared to the thermophilic bacterial endospores. Higher values of R_p for SGA-M and SGA-M6 reveals that the stable inhibitor species in the silica coating contributed to bulk barrier against ionic and molecular diffusion of corrosive agents. The presence of this molybdate corrosion inhibitor pigment enhances corrosion inhibition by forming passive oxides films in the Si-O-Si network thereby providing a more compact bulk material devoid of microcracks and pores. Figure

3.16d displays the variation of values of the double-layer CPE and this parameter is observed to increase with immersion period in the NaCl electrolyte due to adsorption of the water /corrosive ion by the individual protective film. Higher values of CPE_{dl} for a coating denotes high absorptivity and ease of corrosive ions reaching the metal surface, hence poor barrier properties. By possessing lesser values of CPE_{dl}, SGA-M6 reduces the amount of water absorbed into the coating functionalized with the molybdate corrosion inhibitor and the bacterial endospores thereby maintaining a superior interfacial barrier compared to other sol-gel coating independent of the immersion period in 3.5 wt% NaCl. Values of CPE_{dl} for SGA, SGA-M, SGA-6 and SGA-M6 stands at 492.3, 173.1, 323.9 and 158.2 $\mu F\ cm^{-2}\ s^{-(1-\alpha c)}$) after 24 h immersion in 3.5 wt% NaCl and gradually increases after 72 h in the same order (699.8, 228.1, 530.4 and 200.6 $\mu F\ cm^{-2}\ s^{-(1-\alpha c)}$) for SGA, SGA-M, SGA-6 and SGA-M6, respectively). In this study, the electrochemical analysis has also collaborated with physical inspection of the films on the metal substrate; the appearance of the test area (1 cm^2) of each coated mild steel substrates after immersion in 3.5 wt% NaCl is presented in Figure 3.17. Huge corrosion product is observed in the unmodified sol-gel

coating on steel compared to the modified (biotic or abiotic); with SGA-M6 demonstrating superior barrier protection compared to SGA-M and SGA-6.

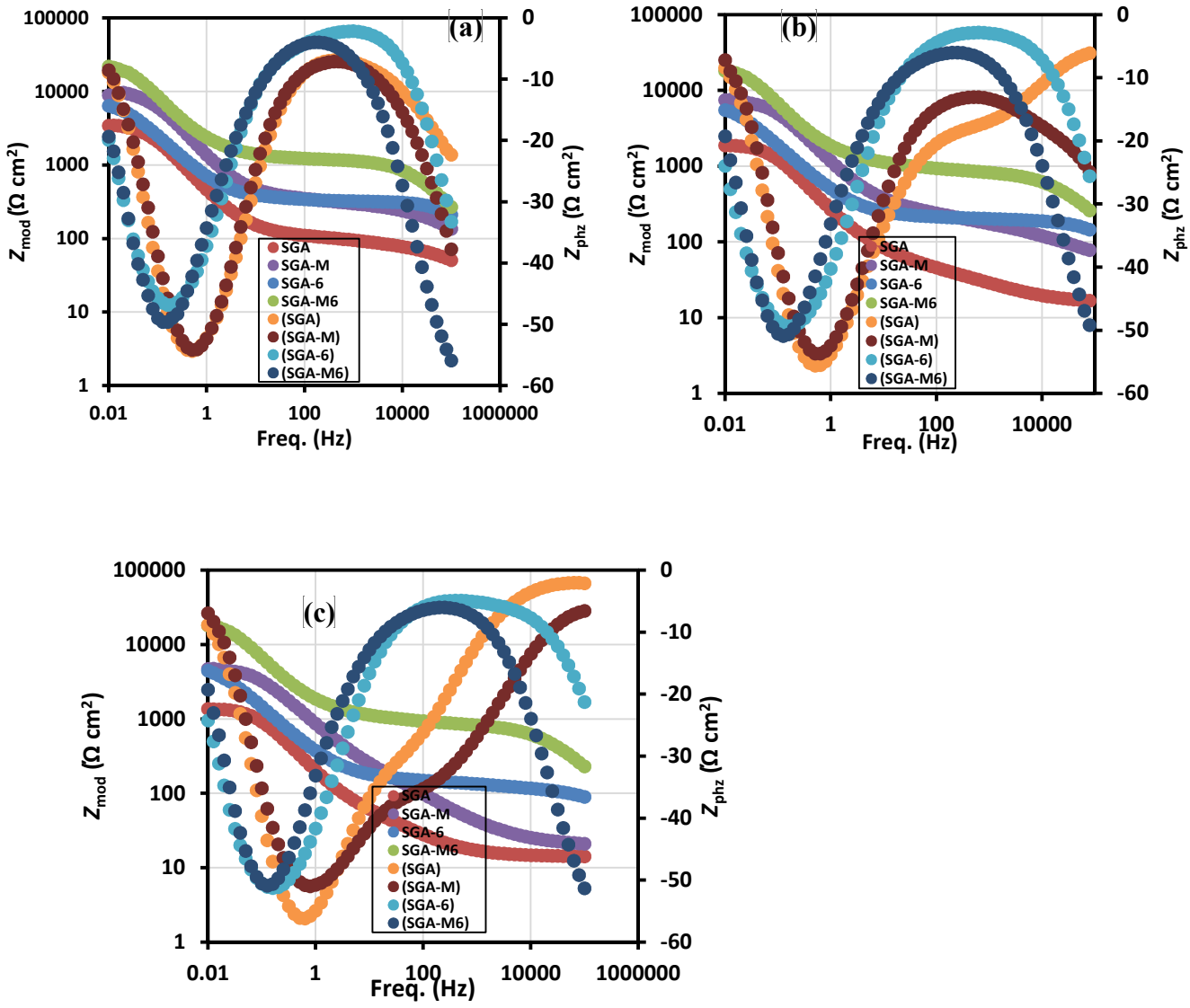

Figure 3.13 Modules and phase angle (Bode curves) plots of biotic and abiotic sol-gel films on mild steel substrates after exposure in 3.5 wt% NaCl solution for (a) 24 h (b) 48 h and (c) 72 h; Bracket () legends represent phase angle plots

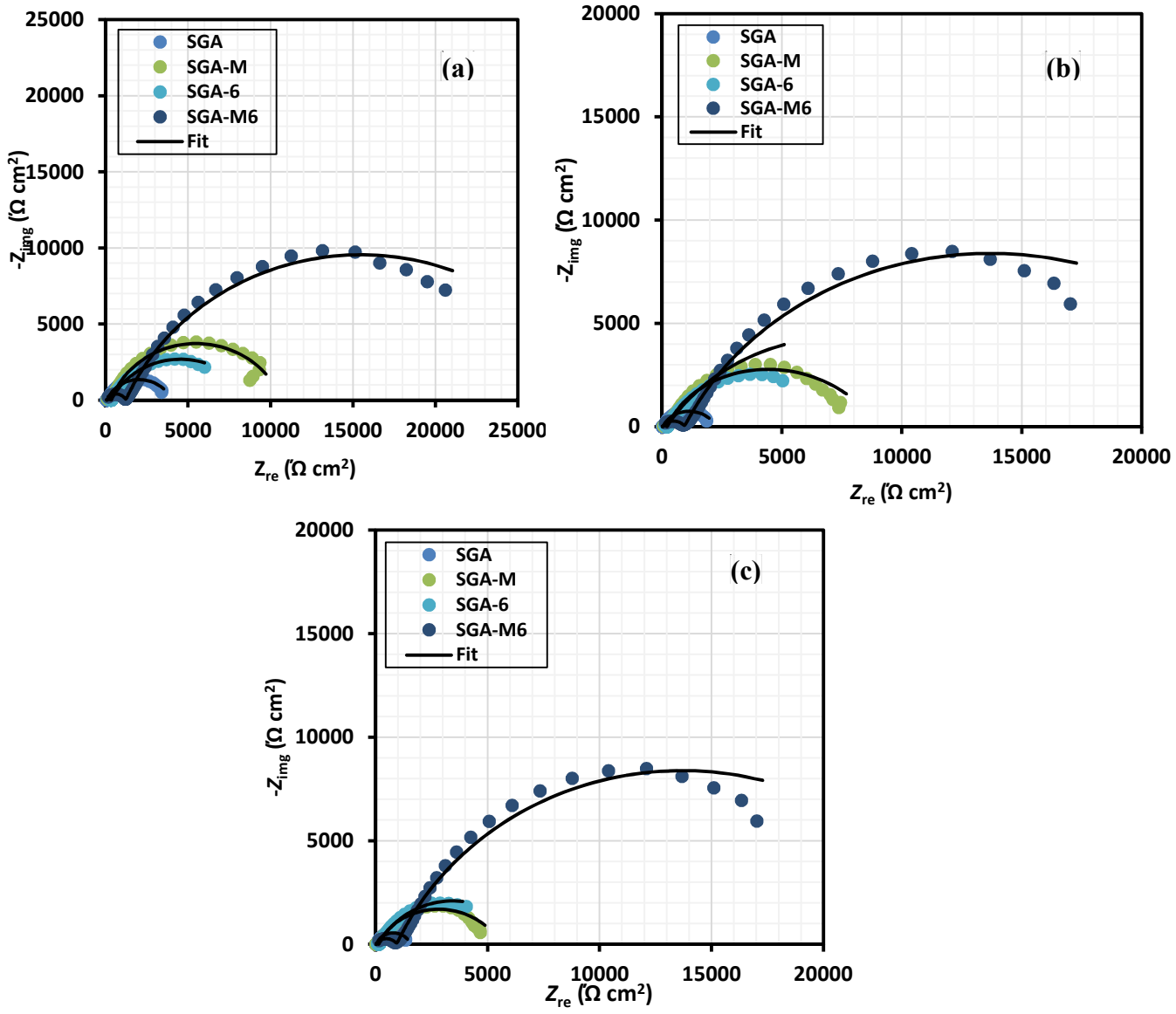

Figure 3.14 Impedance (Nyquist curves) plots of biotic and abiotic sol-gel films on mild steel substrates after exposure in 3.5 wt% NaCl solution for (a) 24 h (b) 48 h and (c) 72 h.

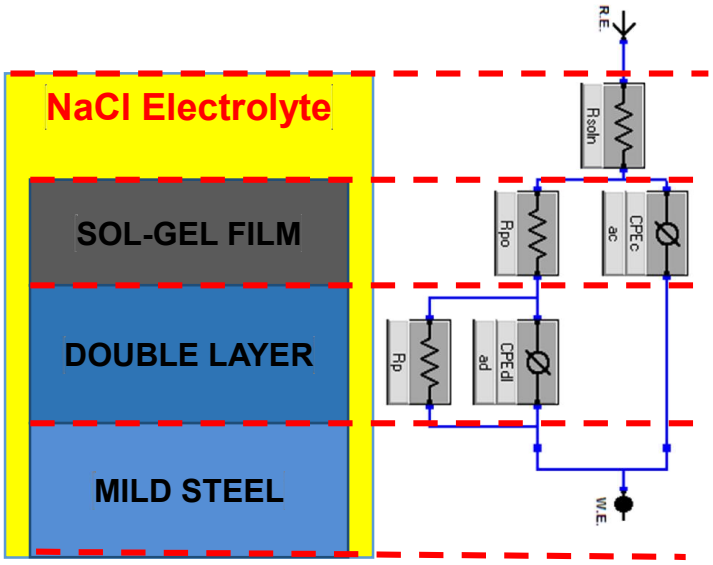

Figure 3.15 Equivalent circuit models [R(Q(R(QR)))] used in fitting the experimental impedance data (where R_{po} is the resistance of the sol-gel pore; CPE_c is the constant phase element's capacitive component of the coating; R_p and CPE_{dl} are the resistance and capacitive components of the interfacial coating/ metal layer.

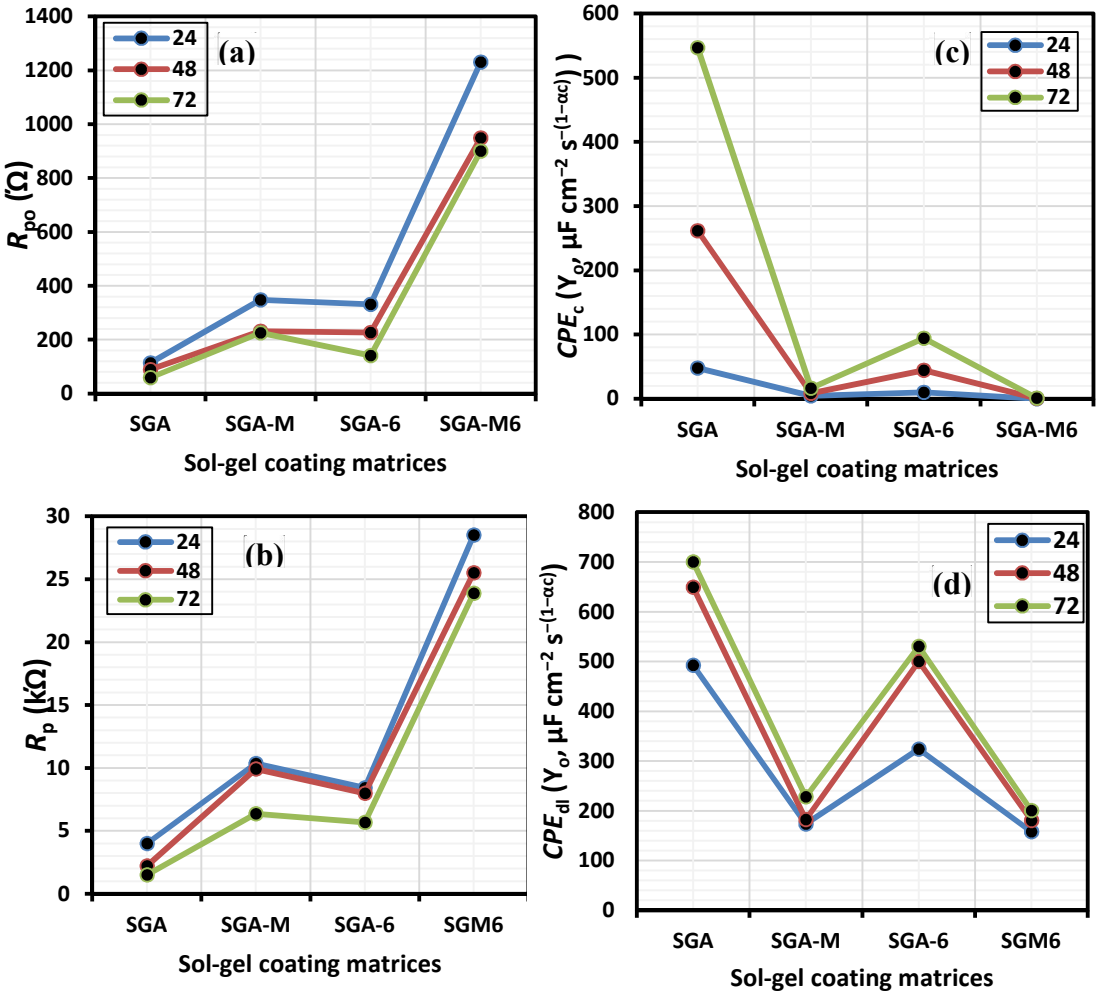

Figure 3.16 Variation in values of coating resistances (left panel) and capacitances (right panel) for biotic and abiotic sol-gel coatings with respect to immersion period (measured in hours) in 3.5 wt% NaCl. [(a) R_{po}, (b) CPE_c, (c) R_p, and (d) CPE_{dl})].

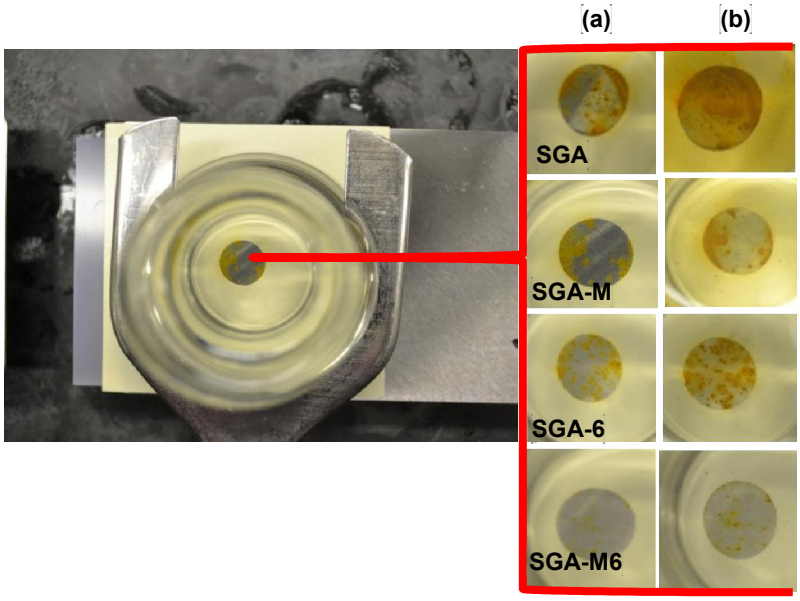

Figure 3.17 The appearance of the test area (1 cm^2) of each coated mild steel substrates after immersion in 3.5 wt% NaCl for (a) 24 and (b) 72 h.

3.3.5 Surface analytical evaluation

The evaluation of the surface morphologies of protective films/ coatings on metal surfaces could give further insight into interfacial reaction and adhesion as well as the effectiveness of the additives in the bulk of the coating. In this work, surface characterization of the microstructure of each coating matrix on mild steel has been examined using atomic force microscope (AFM). Figure 3.18 displays the AFM images of the sol-gel (biotic and abiotic) films on mild steel before (left panel) and after (right panel) immersion in 3.5 wt% NaCl solution for 72 h. The micrographs reveals uneven distribution on the film on the surface of the steel before immersion; this is characteristic of the technique of the coating application. Some degree of surface roughness and protrusions are observed evident of onset of delamination due to the passage of corrosive molecules and ions through the coatings. Micrographs of coatings with show less grooves, judging by the heights of the protrusions, after immersion in the saline corrodent display signs of resistance and hence might be considered superior to others. The surface of bare steel is very rough after immersion at the same immersion period, as it completely corrodes and

the surface appears charred with corrosion products. Enhanced surface FE-SEM images were collected for only biotic samples to show evidence of the thermophilic *Bacilli* cells in the coating and to show the secretion of exocellular polymeric substances (EPS), a biocorrosion inhibitive material from *B. licheniformis*. At this point, the further elucidation of the anticorrosive properties of the EPS of this bacterium has been elucidated, but it is widely reported that the presence of this organic complex act to reduce metal cathodic reduction and are also employed in Microbiologically-induced Corrosion inhibition (MICI) in various media [56]. Figure 3.19 A shows agglomeration of cells since they possesses equal charge in the colonies. Figure 3.19 B and C reveal the presence of bacterial cells in the bulk of the coating containing 0.5g MOLY in 10.0ml SGA on steel substrate after immersion in 3.5 wt% NaCl for 72 h. Samples were coated with a thin monolayer of conductivity gold before imaging to reduce the effect to surface charging.

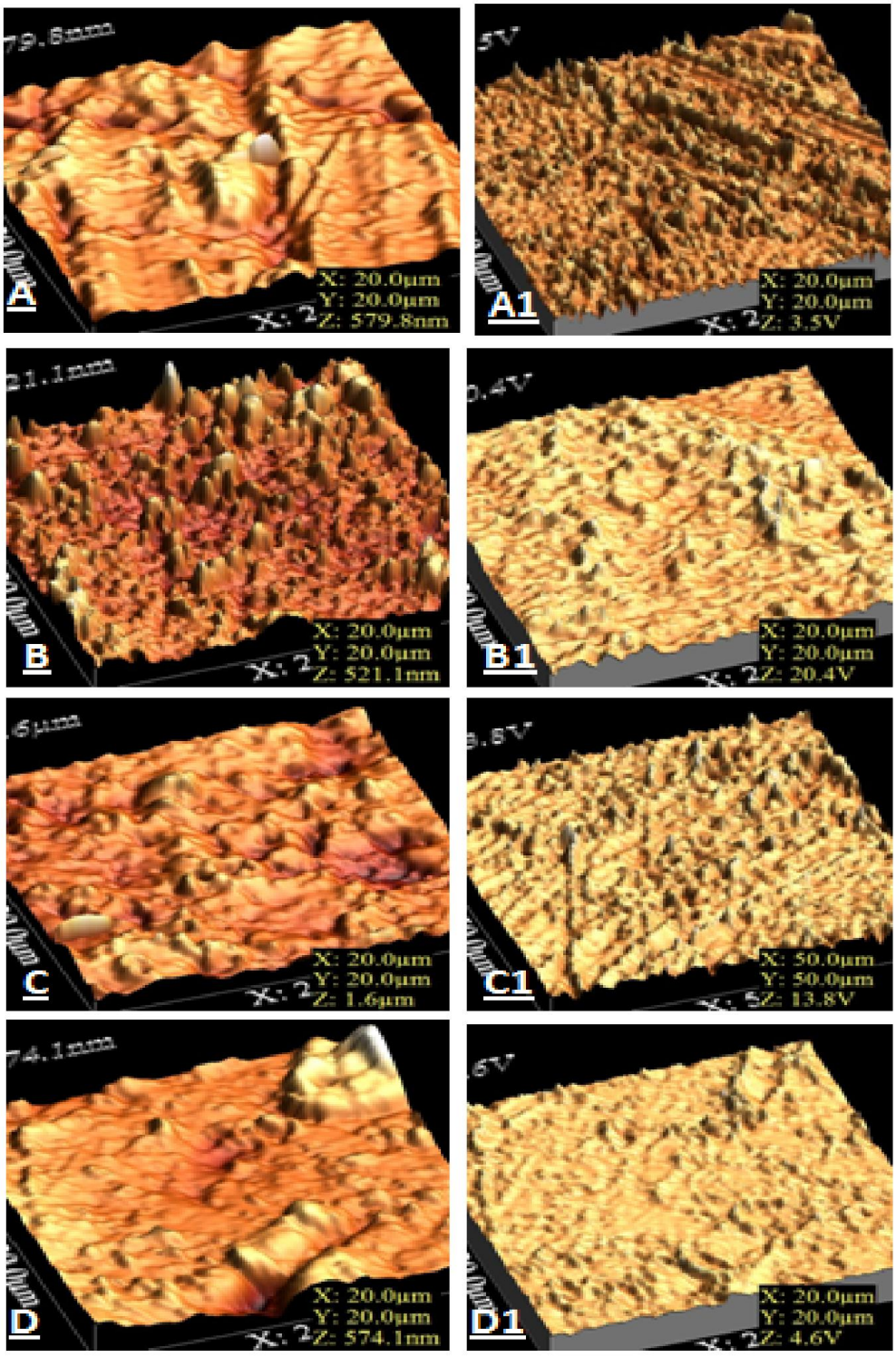

Figure 3.18 20µm-sized 3D-AFM images of (A) SGA-coating, (B) SGA-M, (C) SGA-6 and (D) SGA-M6 on the steel before and after immersion (in that order denoted by A1, B1, CI, and D1, respectively) in 3.5%NaCl at room temperature for 1 week.

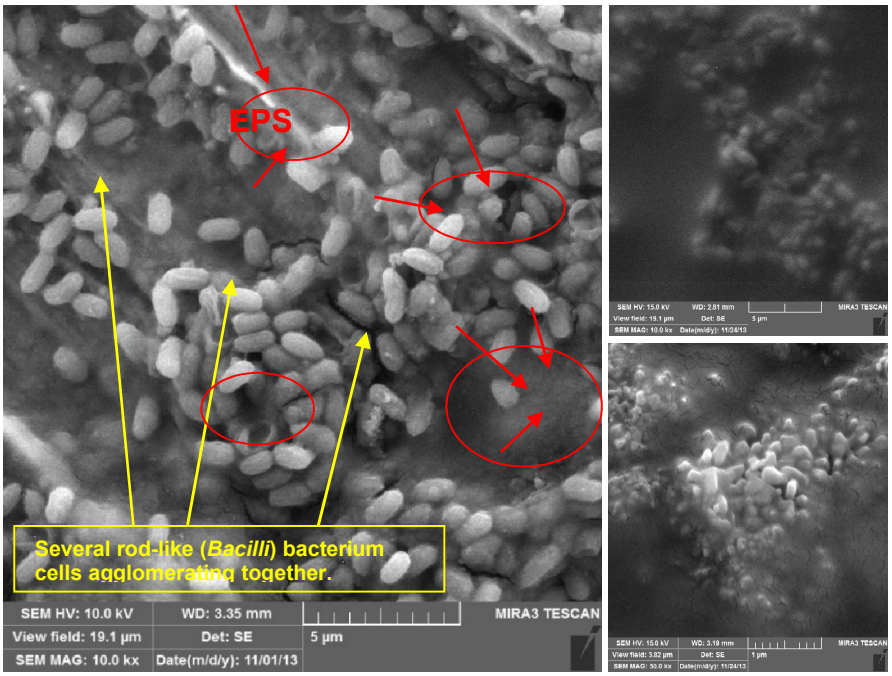

Figure 3.19 FE-SEM image showing [A] evidence of exocellular polymeric substances (EPS) secreted by *B. licheniformis*. The smaller images are FE-SEM images showing the presence of cells in the bulk coating with (B: SGA-M6) and without (C: SGA-6) 0.5g MOLY in 10.0ml SGA taken after immersion of the coated steel in 3.5 wt% NaCl for 1 week (Not shown). Red arrows show EPS while the yellow arrows show the live cells.

3.3.6 Foiling trail at Half-moon beach, Khobar, Saudi Arabia

The antifouling potential of the thermophilic bacterial endospores in the synthesized coating alongside the abiotic ones was evaluated at Half-moon beach, Khobar, after being applied in mild steel at ambient conditions. Figure 3.20 a shows coated mild steel samples submerged at sea water for 6 weeks with photographs collected continuously for two weeks. Compared to the unimmersed coated panels, the coated ones remarkably decolorized after two weeks of exposure in the seawater. Some surface defects could be observed on the protective sol-gel coating functionalized with MOLY inhibitor pigment, and huge delamination episodes on the unmodified sol-gel coating as well as the SGA-M6 matrix after two weeks. The reason for surface delamination could be attributed to poor adhesion due to excess amount to alumina, MOLY pigments and the bacterial endospores encapsulated in one matrix. Sol-gel films made from simple silanes can only be

functionalized to an extent since micro-cracks and swelling are bound to occur on extended curing periods thereby creating pathways for the passage of corrosive ions and molecules through the film. Surface delamination led to the corrosion after two weeks for the SGA-M6 matrix and the sample was replaced for the next two proceeding weeks. However, the presence of barnacles on the surface of the abiotic coating (compared to the biotic SGA-6 coating) is visible at the fourth week and more dominant at the sixth. The abundance of this macro-fouler on the surface of the abiotic coating at the sixth week compared to SGA-6 and SGA-M6 (even after replacement) shows that the biotic coatings possess foul-releasing properties. The presence of MOLY inhibitor pigments in the sol-gel coating matrix (SGA-M) demonstrates the anticorrosive properties of these powder on prolonged immersion in saline water. The foul-releasing properties of the bioactive coatings are due to the presence of *B. licheniformis* endospores and other authors have reported that the antifouling properties of such class of protective bacteria could be attributed to the production of exocellular polymeric substances (EPS) produced by the colony of this organism in the coating [55,56].

However, to remediate the problem to surface delamination for both sets of protective coatings, a primer (ACE oil-based primer) was applied to the steel panels and cured for three days before applying the same set of biotic and abiotic sol-gel coatings as top coats (Figure 3.20 b). Samples were labelled in duplicates, except for the negative control (the primer alone; without the sol-gel topcoat) before immersion in the same marine environment. Sampling in duplicates was necessary since fouling impact cannot be satisfactorily ascertained from a single trail experiment involving just one sample per coating. At the second week, the sol-gel matrices without MOLY inhibitor pigments

showed scratches and bulk cracks as a result of the inhomogeneity in the seawater filled with pebbles, sticks and gravels, etc. The surface integrity of other protective coatings remained intact until the fourth week except for the presence of newly metamorphosed barnacles observed on the surfaces of the primer and the abiotic sol-gel coating matrices. The growth of barnacles continued into the eight week of immersion in the seawater. Compared to the abiotic coatings, the protective biotic coatings show reduced adhesion of the adult barnacles at the eighth week due to the presence of the *B. licheniformis* endospores in the bulk of the coatings. The reasons for this unique bacterial-induced antifouling property has been previously reported [55,56]. Barnacles are observed to adhere more on the abiotic sol-gel coatings (SGA and SGA-M) and the negative controls (primer alone) compared to the protective coatings encapsulated with the bacterial endospores.

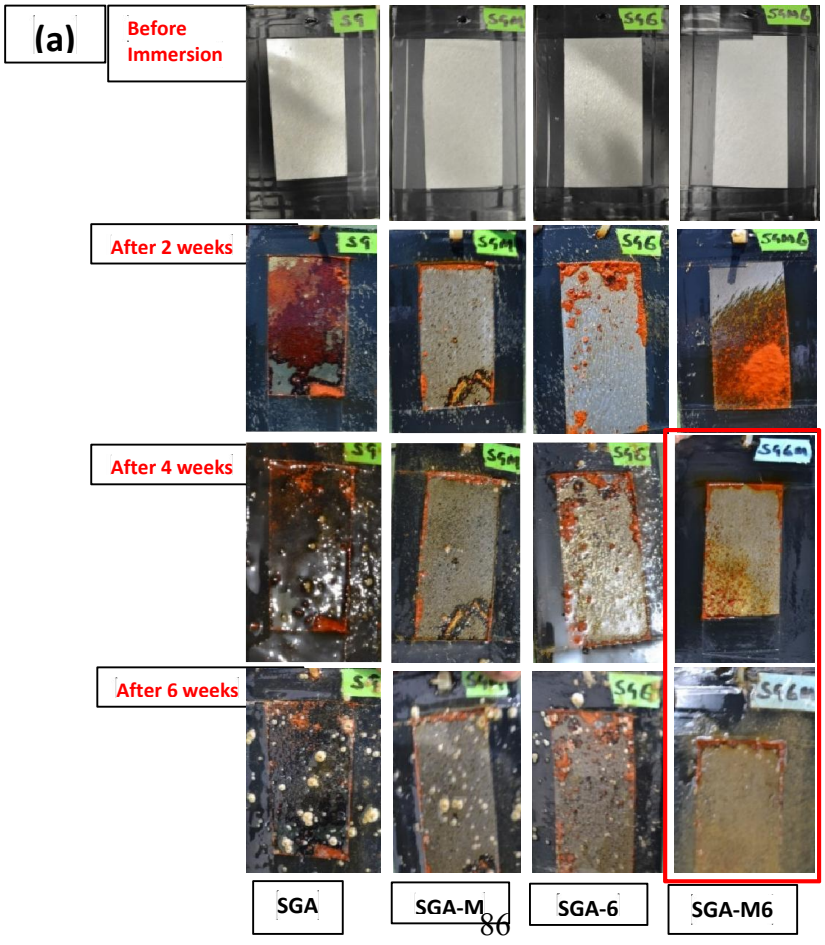

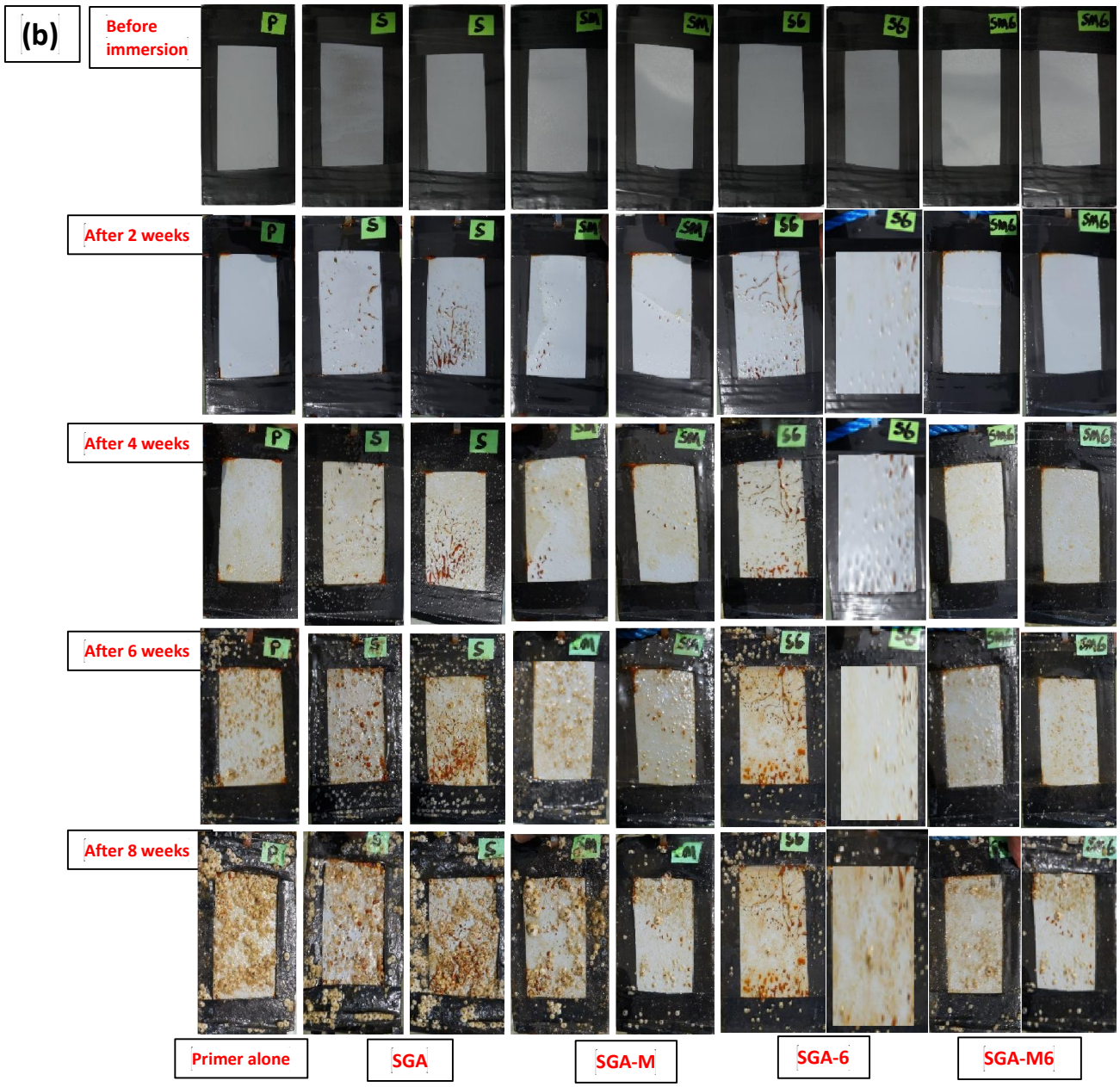

Figure 3.20 Coated mild steel samples (without (a) and with (b) primer) submerged at sea water (KFUPM Beach) for field trial for a defined period of immersion.

3.4 Summary

The following conclusions can be drawn from the results of the electrochemical and on-field fouling trails:

1. The presence of *B. licheniformis* endospores in the protective organic-inorganic hybrid sol-gel coating have demonstrated potentials towards reducing corrosion and fouling in hyper saline hyper medium judging from the results obtained from electrochemical experiments and field trail at Half-moon beach.

2. The antifouling properties of these bioactive coatings can be attributed to their foul-releasing potentials since reduced adhesion of marine foulers are observed after 6─8 weeks immersion at the same marine environment as the abiotic sol-gel coatings.

3. The bacterial endospores in combination with the MOLY inhibitor pigment demonstrated a synergistic anticorrosion/antifouling ability in the medium under study.

4. Electrochemical coating resistances of all the coating matrices are observed to gradually reduce in 3.5 wt% NaCl upon prolonged immersion; this could be attributed to the instability of the bulk silica network as micro-cracks and pores are created in the bulk sol-gel films thereby creating pathways for the corrosive ions and molecules. Specifically for the modified protective sol-gel coating matrices, increase in coating capacitances with immersion period could be ascribed to the increased water uptake into the coating to the metal surface due to the nature of the silica network as well as leaching of the anticorrosive pigments and the bacterial endospores.

5. The use of primers has reduced surface delamination in fouling trails to a great extent judging from the results collected from the field.

6. The choice of precursors for the synthesis of barrier protective coating should involve the selection of those that will yield more compact silica bulk network and hydrophobic surfaces (The average aqueous contact angle of the protective coatings in the current study is 81.2%; demonstrating hydrophilicity). Also, the study of the wider array of anticorrosive pigments and bacteria with antifouling potentials for a more stable sol-gel coating matrix is necessary.

CHAPTER 4

Title: Synergistic effect of chemical inhibitors/ bacteria endospores additives on the protective properties of a modified PDMS/silica sol-gel film for steel in 3.5 wt% NaCl solution

4.1 A brief overview

Protective coatings synthesized from polydimethylsiloxane (PDMS) are known possess improved adhesion on substrates, low wetness and surface energy improved flexibility and oxidative stability and heat resistance [113]. In this study, an organic/inorganic hybrid of PDMS/silica coating will be synthesized in which modified linear PDMS will be part of the silica network initiated via a two-step sol-gel reaction. By crosslinking the inorganic Si-O-Si core with PDMS, the bulk and surface properties of the material (e.g. metal adhesion and hydrophobicity) is improved. The coalescence of PDMS and the silica network synthesized from the pure silane monomers will bring about an improved bulk and surface properties to their composite/blended protective film. The effect of two anticorrosive pigments and two bacterial endospores additives on the barrier protection and antifouling properties of the PDMS/silica sol-gel coating will be evaluated in 3.5 wt% NaCl as well as in a typical marine environment. The application of compatible bioactive systems is a recent trend in corrosion protection and the mechanism of the interaction of some microorganisms with metal substrates is exploited in this view as the basis of this research.

4.2 Experimental

4.2.1 Materials and pre-cleaning procedures

Poly[dimethylsiloxane-co[3-[2-(2-hydroxyethoxy)ethoxy]-propyl]methylsiloxane (PDC2P) alongside two alkoxy silanes, trimethoxymethylsilane (TMMS) and tetraorthosilicate (TEOS) were purchased from Sigma-Aldrich (US) and used for the sol-gel synthesis without further purification. Their molecular structures are presented in Figure 4.1. Other chemicals sourced from Sigma Aldrich includes nitric acid, isopropyl alcohol (IPA), acetone and ethanol. Heucophos® ZAPP and SAPP (pure white finely divided corrosion inhibitor pigments) were obtained from Heucotech Ltd. Co. (US). The S36 mild steel substrates used in this experiment were pre-cleaned prior to use in order to remove the grease and rust inhibiting powder by ultrasonication (Vibra-Cell Sonics and Material INC., US). The cleaning solution contains 70% acetone (Sigma Aldrich) and 80% ethanol (Sigma-Aldrich). The panels were sonicated for 15 min, rinsed thoroughly with doubly distilled water and air-dried at room temperature.

4.2.2 Sol-gel synthesis

TMMS and TEOS were stirred in a 3:4 ratio (v/v) for 10 mins before adding a mixture of acidified water (0.05M HNO_3) and isopropyl alcohol (IPA) drop-wisely to the silane mixture. The reaction mixture was allowed to stir for an hour before adding the modified PDMS. The detailed stepwise synthesis of the sol-gel process is shown in Figure 4.2(a). This sol-gel reaction design involved a hydrolysis-condensation reaction of the alkoxy groups on the silane precursors at room temperature while the modified PDMS forms crosslinking polysiloxane links on the silica network.

4.2.3 Doping with anticorrosive pigments

The resultant colloidal organic-inorganic hybrid sol-gel (SGB) was continuously stirred overnight and 5ml of the final sol-gel mixture was then doped with Hfucophos®SAPP and Hfucophos®ZAPP 101-ED (5% w/v) each in separate vials; thoroughly stirring the powders in the colloidal solution for 2 hours, then sonicated for 30 mins. These modified coatings were labeled as SGB-Z and SGB-S respectively.

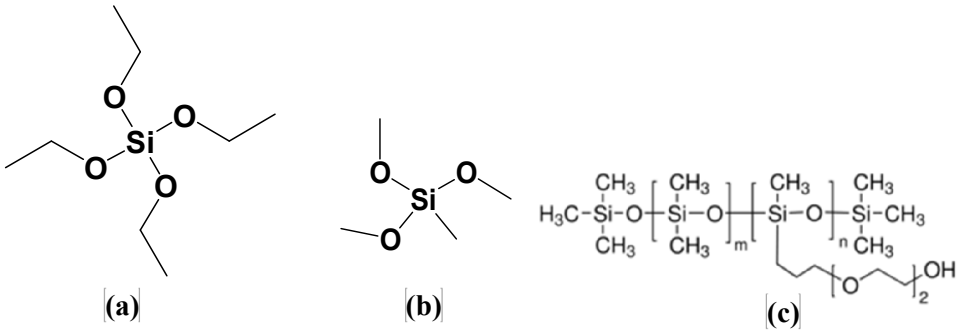

Figure 4.1 Molecular structures of the two siloxane precursors and polymer used in the synthesis of the sol-gel in this study (a) Trimethoxymethylsilane (TMMS) (b) Tetraorthosilicate (TEOS) (c) poly[dimethylsiloxane-co[3-[2-(2-hydroxyethoxy)ethoxy]-propyl]methylsiloxane (PDC2P) polymer.

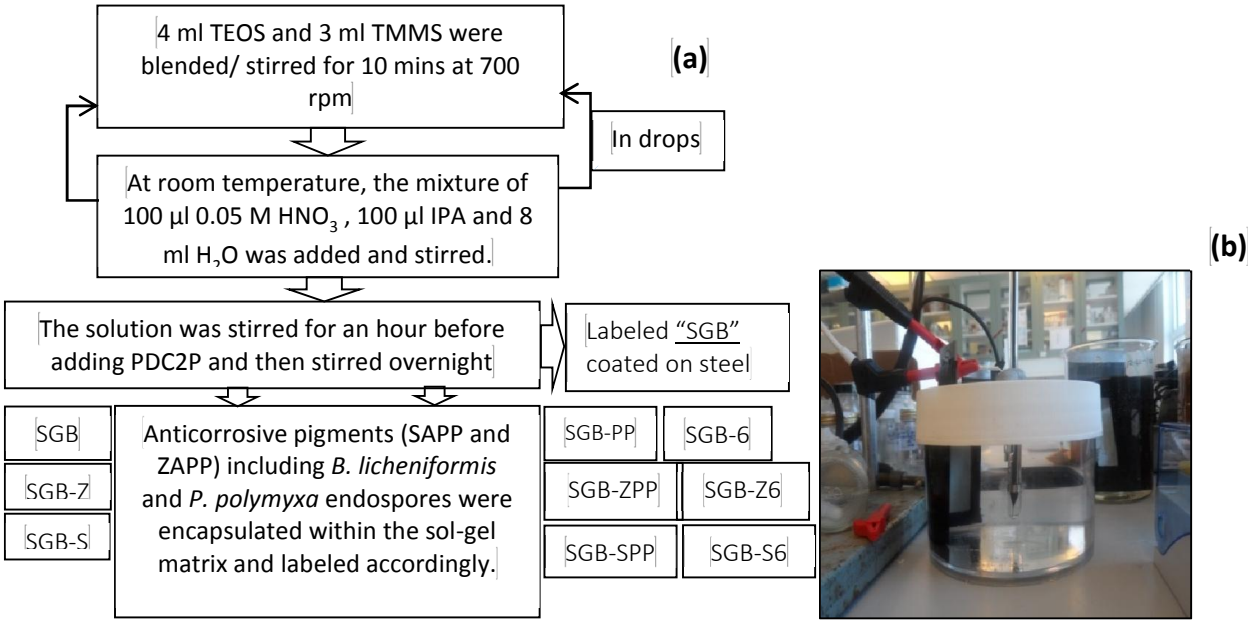

Figure 4.2 (a) Schematic diagram illustrating the processing route for the preparation of the sol–gel coating and (b) the laboratory-fabricated multiple-electrode conductivity cells used in this study.

4.2.4 Encapsulation of bacterial endospores

Endospore suspension of *P. polymyxa* and *B. licheniformis* were removed from storage (─20ºC), allowed to thaw on ice and divided into two portions. A portion was used to estimate the number of colony-forming units in the suspensions by serially diluting between (10^{-1}-10^{-7} ml) of the undiluted endospore suspension before 40 µl of each dilution was spread onto a quarter of NB2 (NB, Oxoid, Basingstoke, UK) Agar plate, and incubated at 45 ºC for overnight [56]. The number of growing colonies on each plate was then counted and recorded. To prepare the endospore-containing sol-gel mixture, the other portion was centrifuged at 13200 rpm for 10 mins. The supernatant endospore suspension was removed and the settled portion of the mixture was suspended in 5ml inhibitor-doped sol-gel mixture and sonicated at 40% of maximum power for 5 secs using a Jencon probe tip sonicator (Jencon, UK). These bioactive inhibitor-doped systems were labeled accurately for each of *B. licheniformis* (SGB-6, SGB-Z6, SGB-S6) and *P. polymyxa* (SGB-PP, SGB-ZPP, SGB-SPP), respectively for the doped inhibitors (SAPP, "*S"* and ZAPP, "*Z"*) in the sol-gel mixture. However, a neat layer of film (40 µm) of each prepared sample matrices (both biotic and abiotic) were evenly coated on the pre-clean steel coupons and panels and allowed cure at room temperature for 5 days under a Laminar flow hood at 30 ºC.

4.2.5 Lab-based electrochemical corrosion studies and on-field fouling trails

The corrosion cells used in this study were three-electrode laboratory-made propylene conductivity cell of 1300 ml capacity (Figure 4.2 b) with a Ag/AgCl,NaCl(3M) reference and platinized platinum counter electrodes connected to a VersaSTAT 3F potentiostat (Princeton Applied Research, US) work station. This cell has the ability of

carrying four working electrode coupons (3 cm × 12 cm). It was particularly designed for the simultaneous study of the electrochemistry of the bioactive samples; targeting the test of biocompactibility of bacterial endospores while avoiding cross-contamination at any immersion period in the study. All coating and electrochemical procedures were completed in a laminar flow hood at room temperature. Electrochemical impedance spectroscopy (EIS) test was performed at the end of 1, 6, 24, 48 h immersion periods at corrosion potential (E_{corr}) over a frequency range of 100 kHz to 10 mHz, with a signal amplitude perturbation of 10 mV leaving a 9 cm^2 area of the working electrode (mild steel) exposed to 3.5 wt% NaCl solution. The data were collected by using ZSimpWin software for data fitting, analyses and for other simulations. The linear Tafel fitting was done to extrapolate the necessary polarization parameters for the potentiodynamic polarization too at ±0.25 V versus OCP at 1 mV/s scan rate. On-field fouling trails for all sets of coatings were carried out in the open water with sample suspended from the dock at Whitby Harbour, North Yorkshire, UK.

4.3 Results and discussion

4.3.1 Viable endospores: CFU and CSLM

The lowest dilution concentration of the endospore suspension was chosen to estimate the number of colony-forming units (cfu) per volume of the cultured bacterial suspensions. The result collected is the quantity of countable colonies on the quarter NB2 (NB, Oxoid, Basingstoke, UK) Agar plate incubated at 30 ^oC in each biotic coating system (Table 4.1). The presence of growth in the media represents viable endospores of bacteria in each system available for corrosion inhibition.

Table 4.1 Colony-forming units (spore viability) per ml in each coating system after 30 ºC incubation in NB agar at 1×10^3 dilution.

Description	Number of colonies *N* (in 40 µl)	*N*/ ml	Standard deviation of *N*	SD of cfu (10^5)	cfu (10^5)/ml
P. polymyxa in SG	12	300	3.46	3.46	3.00
P. polymyxa in SG&ZAPP	6	150	2.44	2.45	1.50
P. polymyxa in SG&SRPP	15	375	3.87	3.87	3.75
B. licheniformis 6 in SG	9	225	3.00	3.00	2.25
B. licheniformis in SG&ZAPP	4	100	2.00	2.00	1.00
B. licheniformis in SG&SRPP	11	275	3.32	3.32	2.75

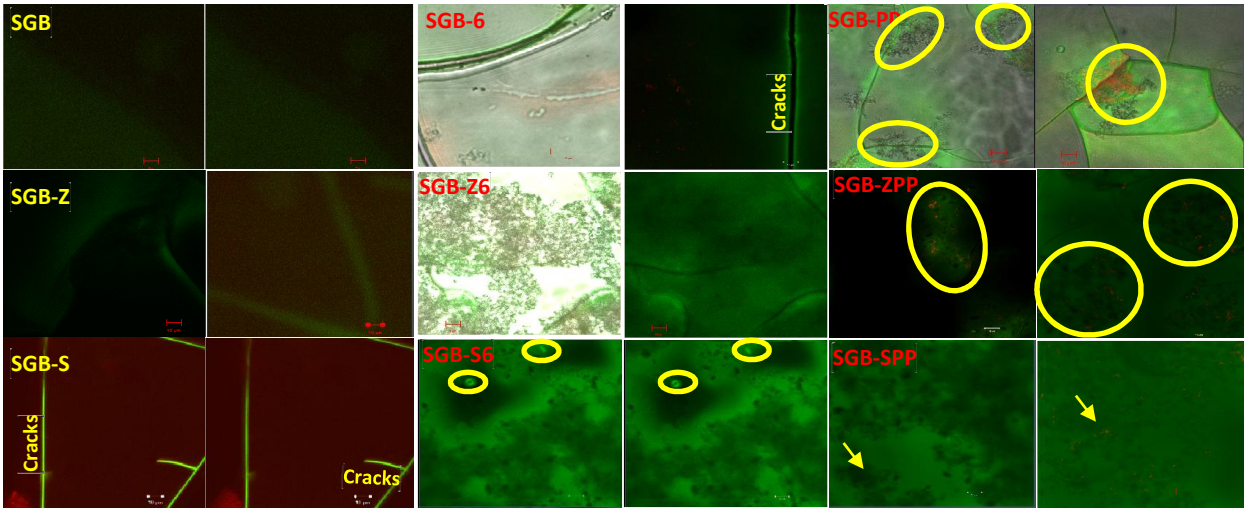

Figure 4.3 CLSM images showing live cells in the various biotic sol-gel coatings for both *P. polymyxa* and *B. lichenformis* endospores (this is no bacterial growth on the abiotic coating used in this study as negative control); CLSM micrograph for every coating matrix are presented in duplicates to show clarity.

Both sets of films were also coated on glass slides and incubated in NB2 at 30 °C overnight, stained with florescence probes in the Baclight™ Live/Dead bacterial viability stain kits (Invitrogen) and left to equilibrate in the dark for an hour before confocal laser scanning microscopic (CLSM) imaging (Zeiss AxioVision confocal scanning laser microscope, UK). CLSM images of both abiotic and biotic films on glass slide are presented in Figure 4.3, and viable vegetative cells are only found distributed in the biotic sol-gel matrices (circled). The dominant green florescence, even on the abiotic coating

micrographs, could be attributed to the adsorption of the Baclight™ Live/Dead bacterial dye by the silanol groups on the sol-gel coating, while the presence of micro-cracks on the coatings are due to their poor adhesion on glass compared to steel substrates. The bacterial endospores on the biotic films are oval-shaped in appearance found in coloured clusters though some have germinated to rod-like shapes while in contact with nutrients in the culturing step. For both *P. polymyxa* and *B. lichenformis* strains, clusters of rod-like cells represent early growth stages as presented the CLSM images. The presence of the anticorrosive pigments in the biotic coating further quenches the background fluorescence, so less number of bacterial cells are visible. Representative growths on Table 4.1 and those presented on the CLSM micrographs for the biotic coatings show the presence of viable bacterial cells in the coatings available for the needed physiology activity.

4.3.2 Inhibition by abiotic abiotic sol-gel coatings

The evaluation of the protective properties of the various abiotic coatings was observed electrochemically by ac and dc techniques for all mild steel coated samples in 3.5 wt% NaCl solution.

4.3.2.1 Potentiodynamic polarization measurements

Potentiodynamic scanning is a polarization technique often used for corrosion testing since its gives information about possibilities of corrosion of materials in specific medium, as well as rates and mechanisms of corrosion [114]. In this study, the rate of electron exchange at the electrode (or the change in current density) with applied potential was monitored by applying overpotential enough to initiate corrosion (±0.25V versus OCP at 1mV/s scan rate). The coating matrices on steel in the saline electrolyte maintain reduced current density at this range of potential, and are regarded as barrier protective films at the

earlier immersion period compared to the bare steel. The current–potential curves showing the kinetics of the mild steel electrodes coated with abiotic sol-gel coatings for both anodic and cathodic reactions are displayed in Figure 4.4. Inspection of the figures reveals that the presence of the coating on mild steel reduced the magnitude of current densities (i_{corr}) as well as the corrosion rate. This can be attributed to the barrier created by each sol-gel matrix against the passage of corrosive ions and molecules to the metal surface; coated surfaces with enhanced corrosion resistance possess reduced i_{corr} values relative to the bare steel. By far, the inhibitor-doped coatings performed better than the undoped coating at all immersion periods but corrosion rate for both set of coatings increased with immersion period. Magnitude of i_{corr} as low as 66.7 and 109.5 μA are recorded for the sol-gel matrices modified with SAPP (SGB-S) and ZAPP (SGB-Z), respectively, compared to the unmodified coating (126.8 μA) after an hour immersion. After 48 h, this values increased to 337.4, 352.7 and 379.4 μA for SGB-S, SGB-Z and SGB, respectively. Magnitude of E_{corr} gradually increased to higher and nobler values from the bare metal to the most protective coating: SGB-S (−490 and −638 μA) > SGB-Z (−560 and −679 μA) > SGB (−538 and −705 μA) > bare metal (−764 and −742 μA) after an hour and 48 h immersion in 3.5 wt% NaCl. Potentiodynamic polarization parameters collected from the i-E curves of each system after 1 and 48 h immersion are presented in Table 4.2. The enhanced corrosion protection in the presence of SAPP compared to ZAPP in the sol-gel coating at all immersion periods under study could be attributed to the stability of the passive oxides in SAPP. SAPP (strontium aluminium polyphosphate hydrate) is made of more stable SrO component compared to the presence of ZnO in ZAPP (zinc aluminium polyphosphate

hydrate); both anticorrosive pigments have in common Al_2O_3 and polyphosphate composition in relatively equal amount.

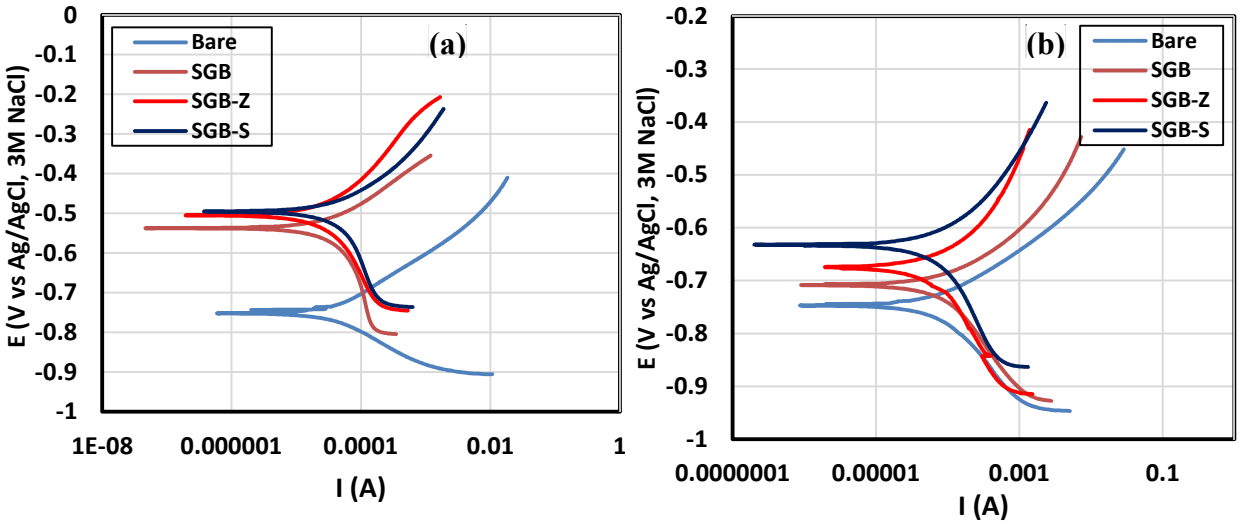

Figure 4.4 Potentiodynamic polarization plots of different abiotic coatings on mild steel compared to a bare steel (uncoated) in 3.5 wt% NaCl after (a) 1 h and (b) 48 h immersion periods.

Table 4.2. Potentiodynamic polarization parameters for the different forms of abiotic sol-gel coatings on steel panels compared to the bare steel (uncoated) in 3.5%NaCl after 1 and 48 hours immersion periods.

Coating system	E_{corr} (mV/Ag/AgCl, 3M NaCl $_{(sat)}$)		I_{corr} (μA)		β_c (mV)		β_a (mV)		%η	
	1 h	48 h	1 h	48 h	1 h	48 h	1 h	48 h	1 h	48 h
Bare	−764.5	−742.3	133.4	448.5	64.9	1.5	196.8	246.7	-	-
SGB	−538.3	−705.7	126.8	379.4	6.9	2.0	257.3	195.7	4.9	15.4
SGB-Z	−506.7	−679.5	109.5	352.7	2.1	3.9	532.7	368.8	17.9	21.4
SGB-S	−490.6	−638.9	66.7	337.4	65	5.0	104.3	408.6	50.0	32.9

4.3.2.2 Electrochemical impedance spectroscopy

To further demonstrate the corrosion protection performance of this set of sol-gel coatings, the ac based EIS technique was employed. Figure 4.5 displays the Bode modules (a), phase angle (b), and Nyquist (c) curves of the abiotic coatings on mild steel compared to a bare steel (uncoated) in 3.5 wt% NaCl after (a) 1 h and (b) 48 h immersion period. The Bode modules plot (Figure 4.5 a) reveals higher Z_{mod} values for the inhibitor doped sol-gel

coating throughout the frequency after an hour immersion in NaCl, with the coating functionalized with SAPP showing greater Z_{mod} value given after 48 hours. Variation in the values of Z_{mod} demonstrates corrosion resistance, and at 0.01 Hz, Z_{mod} values as high as 1365, 1116 and 399 Ω are recorded for the abiotic sol-gel coatings (SGB-S, SGB-Z and SGB, respectively, compared to the bare steel sample (179 Ω)). The decrease in the values of Z_{mod} after 48 h could be attributed to the initiation of corrosion caused by the passage of corrosive ions and molecules to the surface of the steel via the coating. The formation of stable oxide layers in the inhibitor-doped coatings could have contributed to their improved barrier protection in the bulk of the sol-gel coatings. At the same frequency after 48 h, Z_{mod} values also decease more than half; with 538, 293 and 224 Ω recorded for SGB-S, SGB-Z and SGB, respectively. As presented in Figure 4.5 b for both immersion periods, the abiotic coatings reveal single maxima towards the medium frequency and the magnitudes of Z_{phz} are without a defined trend at any frequency. The values of Z_{phz} for the bare steel (59^o) are greater than those of the coating at 1 Hz: 30^o, 34^o and 50^o observed for SGB-S, SGB-Z and SGB, respectively, after an hour immersion; but a slight variation in the trend after 48 h: 45^o, 59^o, 57^o and 54^o for SGB-S, SGB-Z, SGB and bare metal, respectively. As presented in the Nyquist plots (Figure 4.5 c), the diameters of the semicircles represent the extent of corrosion resistance of each coating in the saline corrosion. The figures display two-time constant curves with wider capacitive loops within the medium frequencies, with the SGB-S coating matrix representing the abiotic coating the highest corrosion resistance among others compared to the bare steel substrate. From these curves, appropriate equivalent model (Figure 4.6) was adopted in fitting and analyzing the impedance data for the respective abiotic coatings. The analysis of EIS data

with electrochemical circuit models was done using the ZsimpWin software, and from the fitting, respective electrochemical parameters derived from this model are presented in Figure 4.7.

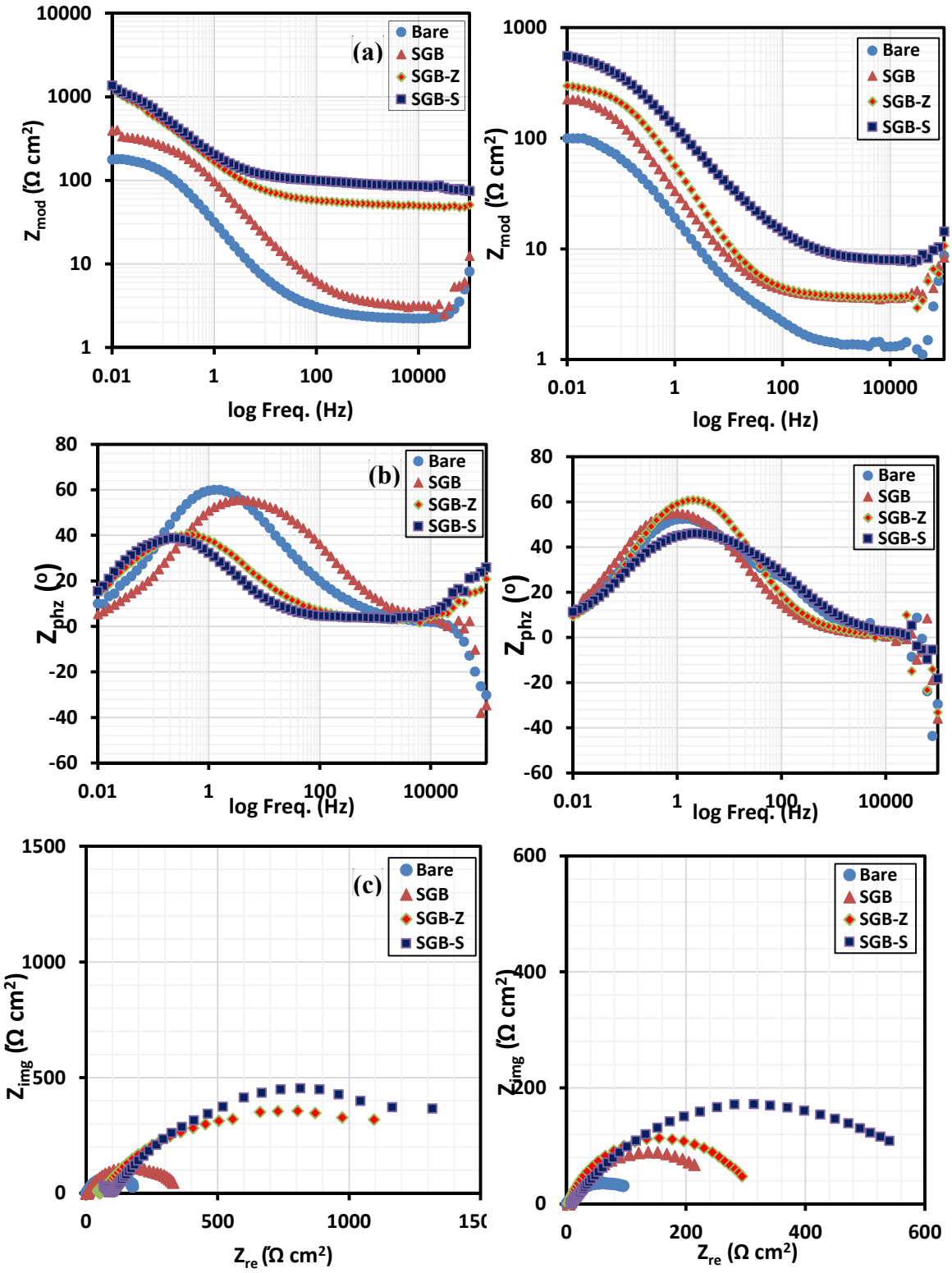

Figure 4.5 Bode module (a), Bode phase angle (b) and Nyquist (c) plots for different abiotic coatings on mild steel compared to bare steel in 3.5 wt% NaCl after 1 h (left panel) and 48 h (right panel) immersion periods.

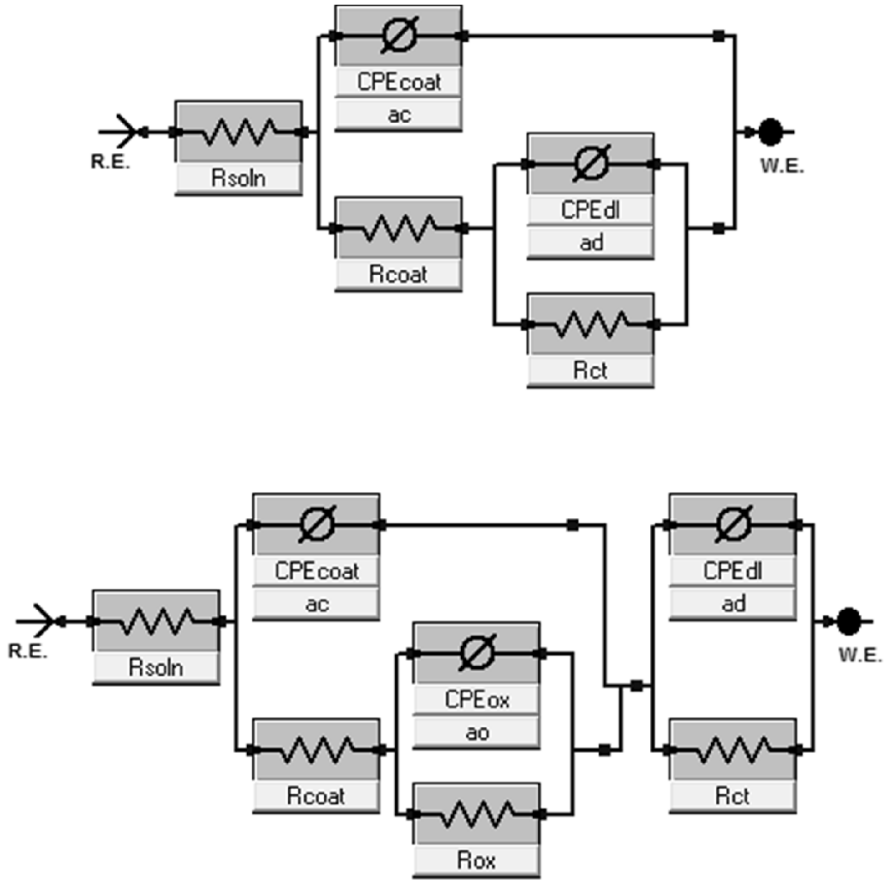

Figure 4.6 Equivalent circuit models used in fitting the experimental Nyquist curves; adopted from Garmy EChem Analyst software's model editor

Figure 4.7 presents values of resistance (left panel) and capacitance (right panel) derived from the phases proposed in the equivalent circuit models. The coating resistances (R_{coat}) induced by the respective abiotic films to the flow of ionic currents of corrosive species vary with immersion period. Values of R_{coat} as high as 835.6, 678.0 and 119.1 Ω cm^2 are recorded for SGB, SGB-Z and SGB-S, respectively (Figure 4.7 a) after the first hour of immersion in 3.5 wt% NaCl solution but drastically reduced at the second day (88.00, 62.09 and 33.57 Ω cm^2). This reduction in the values of R_{coat} with time could be attributed to the passage of corrosive ions and molecules via inherent pores and cracks in the sol-gel coatings (bulk deterioration of the coatings); with the most porous abiotic coating being the unmodified sol-gel film (SGB). The sol-gel coating functionalized with SAPP (SGB-

S) maintained higher magnitude of R_{coat} compared ZAPP modified coating (SGB-Z) due to the formation of more stable inhibitor layer in the coating matrix. Corrosion inhibitor pigments are known to form passive oxide films and barriers at metal surfaces as well as the protective coatings they modified. The R_{coat} values for SGB-S and SGB-Z at the 6th hour are 272.11 and 186.64 kΩ cm^2, respectively; 137.77 and 85.00 kΩ cm^2 after the 24^{th} hour of exposure in the saline electrolyte. Charge transfer resistance (R_{ct}) represents the resistance the interphase close to the metal surface and accounts for the reduction of active sites for corrosion reaction at the coating/electrolyte interface. This quantity is found to decrease as the coatings are exposed; with values up to 90.13, 126.7 and 146.00 kΩ cm^2 recorded for SGB, SGB-Z and SGB-S, respectively after 1 h as against 23.68, 27.48 and 36.56 kΩ cm^2 after 48 h. The R_{ct} values for the bare steel did not significantly change due to the simultaneous formation and degradation of corrosion products on the surface of the metal substrate in NaCl solution. The values of CPE_{coat} representing the capacitances of each coating show a gradual increase with immersion time due to the uptake of water by the immersed protective films in Figure 4.7 b. The least protective coating (SGB) records the highest values of CPE_{coat} compared to its modified counterpacts; with 0.33 and 0.29 μF cm^{-2} $s^{-(1-\alpha c)}$ recorded for SGB-Z and SGB-S while that of S is 0.68 μF cm^{-2} $s^{-(1-\alpha c)}$ after 1 h. These values increased to 2.04, 1.09 and 0.93 μF cm^{-2} $s^{-(1-\alpha c)}$ for SGB, SGB-Z and SGB-S, respectively at the 48 h. Like CPE_{coat}, similar trend was observed for CPE_{dl} being the capacitance of the double layer for each protective coating.

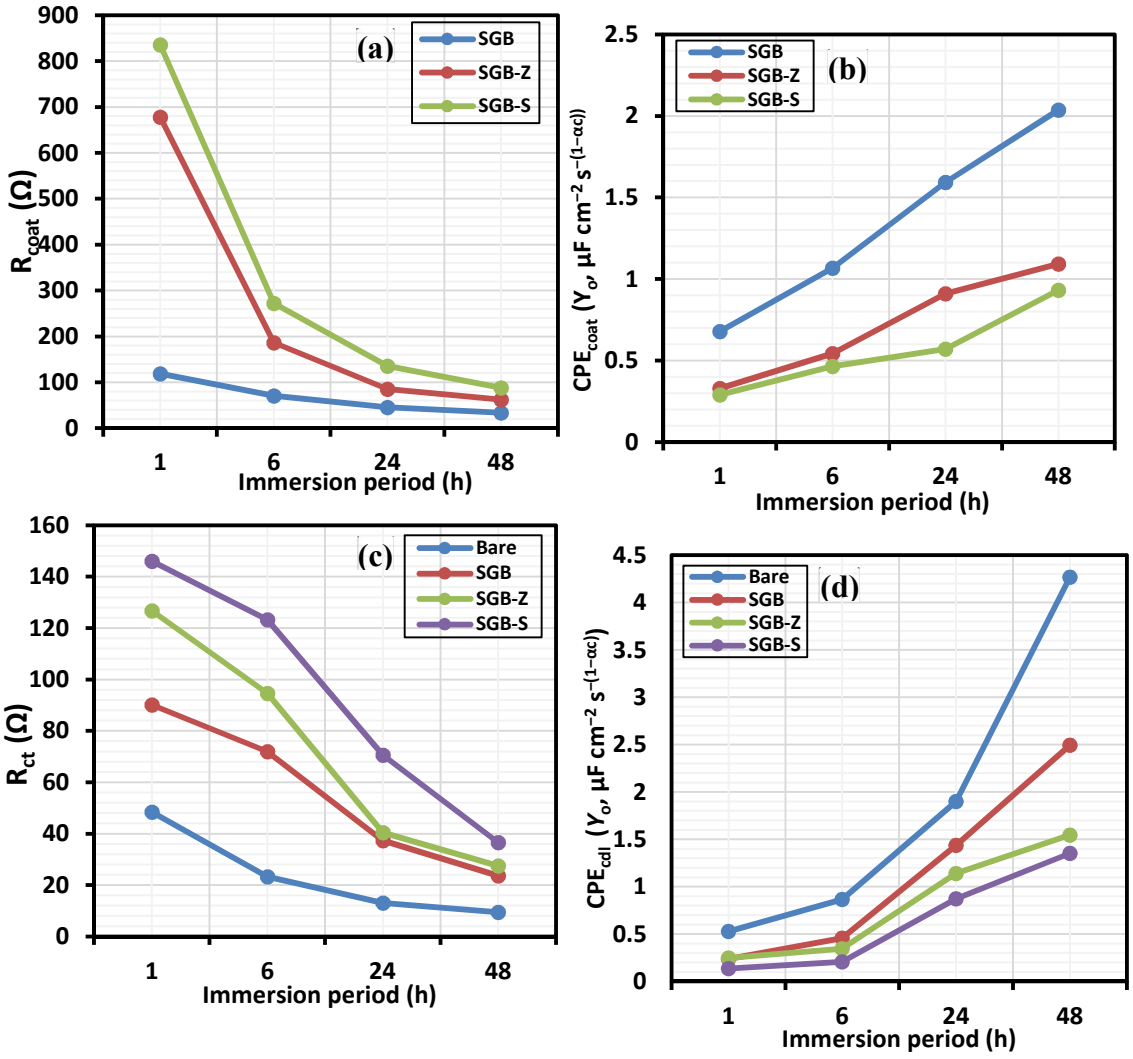

Figure 4.7 Variation in coating resistances (left panel) and capacitances (right panel) with exposure time (in days) with saline electrolyte for abiotic sol-gel coatings [(a) R_{coat}, (b) CPE_{coat}, (c) R_{ct}, and (d) CPE_{dl})].

4.3.3 Inhibition by biotic (endospore-loaded) sol gel films

Since the anticorrosion abilities of the two commercially available chemical inhibitors (SAPP and ZAPP) have been now ascertained in the sol-gel coating, their protective strengths in the presence of encapsulated endospores of viable bacteria in the same sol gel coating will be evaluated in order to study their synergistic effect. The evaluation of the barrier protective properties of the various biotic coatings (*B. licheniformis and P.*

polymyxa) was also observed electrochemically by ac and dc techniques for all coated samples in 3.5 wt% NaCl solution.

4.3.3.1 Potentiodynamic polarization measurements

The Tafel curves for the mild steel electrodes coated with these biotic sol-gel coatings are presented in Figures 4.8 and 4.9 (a). The presence of the bacterial endospores in the coatings on mild steel reduced the magnitude of i_{corr} (corresponding to the corrosion rate) compared to the bare steel substrate, denoting corrosion protection. This improved corrosion protection in the presence of these bacteria strains can be attributed to the secretion of exocellular polymeric substances (EPS) by respective colonies of these two organisms [115]. Values of i_{corr} as low as 55.0 and 40.7 μA are recorded for the inhibitor-doped sol-gel matrices encapsulated with *B. licheniformis*, SGB-Z6 and SGB-S6, respectively, compared to the undoped biotic coating (SB6; 64.4 μA) after an hour immersion (Table 4.3). Lower magnitudes of i_{corr} denoting reduced corrosion rate are obtained for the inhibitor-doped sol-gel matrices encapsulated with *P. polymyxa*: 17.1 μA (SGB-SPP) and 53.5 μA (SGB-ZPP) compared to the absence of the inhibitors (SPP; 56.9 μA) after an hour immersion (Table 4.4). These values increased gradually due to the passage of ion through the pores of each biotic coating after 48 h; with 174.9, 184.5 and 322.5 μA recorded for SGB-S6, SGB-Z6 and SGB-6 while 90.6, 117.5 and 147.2 μA are recorded for SGB-SPP, SGB-ZPP and SGB-PP, respectively. In the presence of the endospores of both bacteria, the sol-gel coatings with the inhibitor pigments demonstrate improved barrier performance due to a synergistic bulk protective barrier from corrosive ion and molecule across the coatings. The order of improved corrosion resistance, judging from the variation in the i_{corr} values is: SGB-S6 > SGB-Z6 > SGB-6 and SGB-SPP >

SGB-ZPP > SGB-PP; with *P. polymyxa* showing superior barrier performance to *B. licheniformis*. Higher values of E_{corr} are recorded for more stable and protective biotic coatings relative to the bare/uncoated steel substrate for both immersion periods.

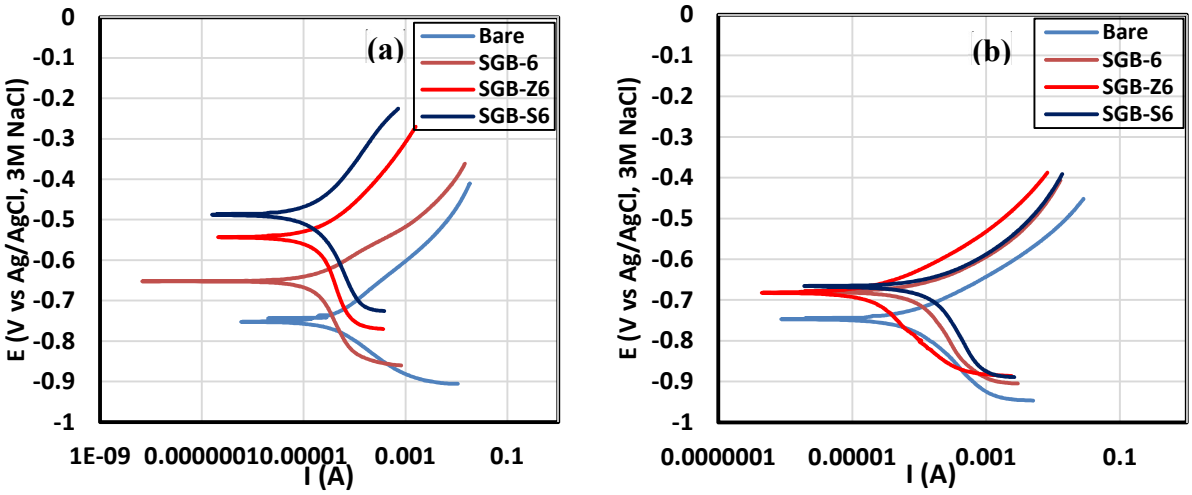

Figure 4.8 (a) Potentiodynamic polarization plots of different biotic (*B. licheniformis*) coatings on mild steel compared to a bare steel (uncoated) in 3.5 wt% NaCl after (a) 1 h and (b) 48 h immersion periods.

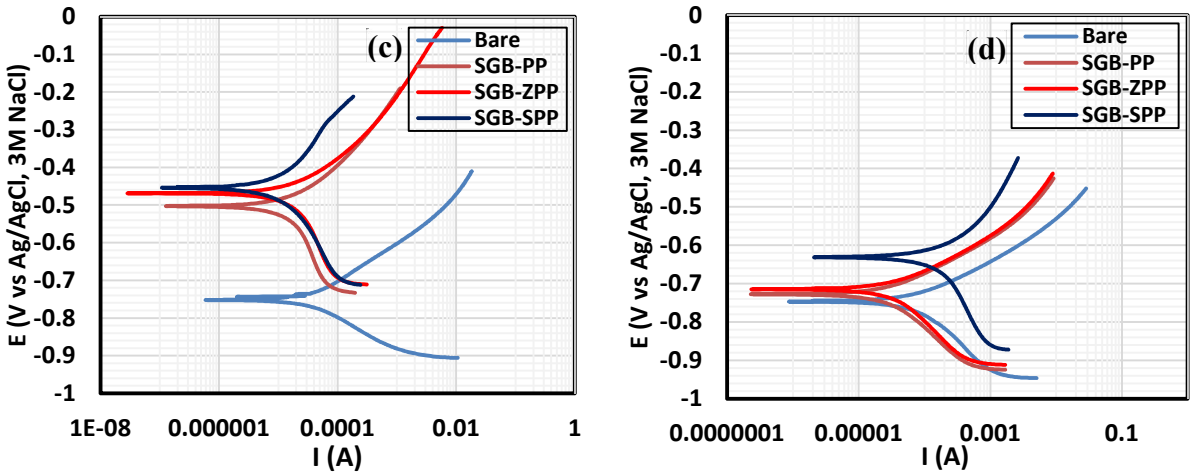

Figure 4.9 (b) Potentiodynamic polarization plots of different biotic (*P. polymyxa*) coatings on mild steel compared to a bare steel (uncoated) in 3.5 wt% NaCl after (a) 1 h and (b) 48 h immersion periods.

Table 4.3 Potentiodynamic polarization parameters for the different forms of *B. licheniformis*-containing (B6) sol-gel coatings on steel panels compared to the bare steel (uncoated) in 3.5 wt%NaCl after 1 and 48 h immersion periods.

Coating system	E_{corr} (mV/Ag/AgCl, NaCl $_{(sat)}$)		I_{corr} (μA)		β_c ($mVdec^{-1}$)		β_a($mVdec^{-1}$)		%η	
	1 h	48 h	1 h	48 h	1 h	48 h	1 h	48 h	1 h	48 h
Bare	−764.5	−742.3	133.4	448.5	64.9	1.5	196.8	246.7	-	-
SGB-6	−652.7	−685.9	64.4	322.5	1.24	2.98	126.2	183.5	51.7	28.1
SGB-Z6	−544.9	−679.5	55.0	184.5	1.27	3.4	201.3	213.6	58.9	58.8
SGB-S6	−486.2	−658.3	40.7	174.9	5.23	4.9	417.8	201.0	69.5	61.0

Table 4.4 Potentiodynamic polarization parameters for the different forms of *P. polymyxa* -containing (PP) sol-gel coatings on steel panels compared to the bare steel (uncoated) in 3.5 wt%NaCl after 1 and 48 h immersion periods.

Coating system	E_{corr} (mV/Ag/AgCl, NaCl $_{(sat)}$)		I_{corr} (μA)		β_c (mV)		β_a(mV)		%η	
	1 h	48 h	1 h	48 h	1 h	48 h	1 h	48 h	1 h	48 h
Bare	−764.5	−746.3	133.4	448.5	64.9	1.5	196.8	246.7	-	-
SGB-PP	−505.7	−728.1	56.9	147.2	5.2	188.6	270.2	108.4	57.4	61.0
SGB-ZPP	−468.9	−715.4	53.5	117.5	4.2	188.6	212.5	297.2	59.9	51.8
SGB-SPP	−435.2	−634.9	17.1	90.6	4.1	7.1	19.83	349.7	87.2	79.8

4.3.2.2 Electrochemical impedance spectroscopy

Just as evaluated for the abiotic coatings in 3.5 wt% NaCl, the corrosion resistance of those sol-gel coatings encapsulated with the bacterial endospores were tested by EIS, and the impedance plots for *B. licheniformis* and *P. polymyxa* are displayed in Figures 4.10 and 4.11, respectively. The Bode modules plot (Figure 4.10a) of the *B. licheniformis* encapsulated sol-gel coting reveals higher Z_{mod} values for both immersion periods (after 1 and 48 h) at both lower and higher frequencies; and the coating functionalized with SAPP in combination with the bacterial endospores (SGB-S6) reveal higher Z_{mod} values compared to SGB-Z6 and SGB-6. Similar trend is obtained for *P. polymyxa* in the same sol-gel coating (Figure 4.11 a): Z_{mod} (SGB-SPP) > Z_{mod} (SGB-ZPP) > Z_{mod} (SGB-PP) > Z_{mod} (bare steel) after immersion in the saline electrolyte for 1 and 48 h at room

temperature. Values of Z_{mod} higher than those of the abiotic sol-gel coatings are recorded at 0.01 Hz (after an hour immerison): 1790, 1060, 511 Ω for *B. licheniformis* and 2752, 2132, 900 Ω for *P. polymyxa;* this trend indicates that the presence of the bacterial endospores improved the barrier protection of the sol-gel coating. The passage of corrosive ions and molecules through the coating leads to the gradual decrease in the values of Z_{mod} with 294, 241 and 140 Ω recorded for SGB-S6, SGB-Z6 and SGB-6, respectively; and 324, 251 and 145 Ω for SGB-SPP, SGB-ZPP and SGB-PP, in that order. Figure 4.10 b reveals single maxima between 1 and 100 Hz for the "6" series for both immersion periods presented, except for SGB-S6 (appearing at much lower frequency after an hour). The values of Z_{phz} for the bare steel (59^o) are greater than those of the coating at their individual maxima: 38^o, 43.5^o and 43.1^o observed for SGB-S6, SGB-Z6 and SGB-6, respectively, after an hour immersion; but after 48 h, values up to 50^o, 43^o and 36^o are recorded in that order for *B. licheniformis*. For the other set of biotic sol-gel coating with *P. polymyxa,* 10^o, 20.0^o and 20.4^o observed for SGB-SPP, SGB-ZPP and SGB-PP, respectively (after an hour immersion) and then 62^o, 51^o and 42^o observed for the same coating in that order (after 48 h at their individual maxima). Figures 4.10 and 4.11 (c) displays Nyquist plots with two-time constant capacitive loops for each biotic coating; with wider capacitive loops obtained at medium frequencies. The diameter of the Nyquist curve semi-circles represents corrosion resistance, and by far, the sol-gel coating encapsulated with *P. polymyxa* are characterized with capacitive loops (with wider diameters) at higher range of impedance, compared to *B. licheniformis.* By physical inspection of the impedance plots, the biotic coatings with *P. polymyxa* demonstrates higher protection, but to affirm this, appropriate two-time constant equivalent model has

been used in fitting the experimentally derived impedance data for the respective biotic. From the circuit fitting, the respective electrochemical parameters derived from this model are presented in Figure 4.11.

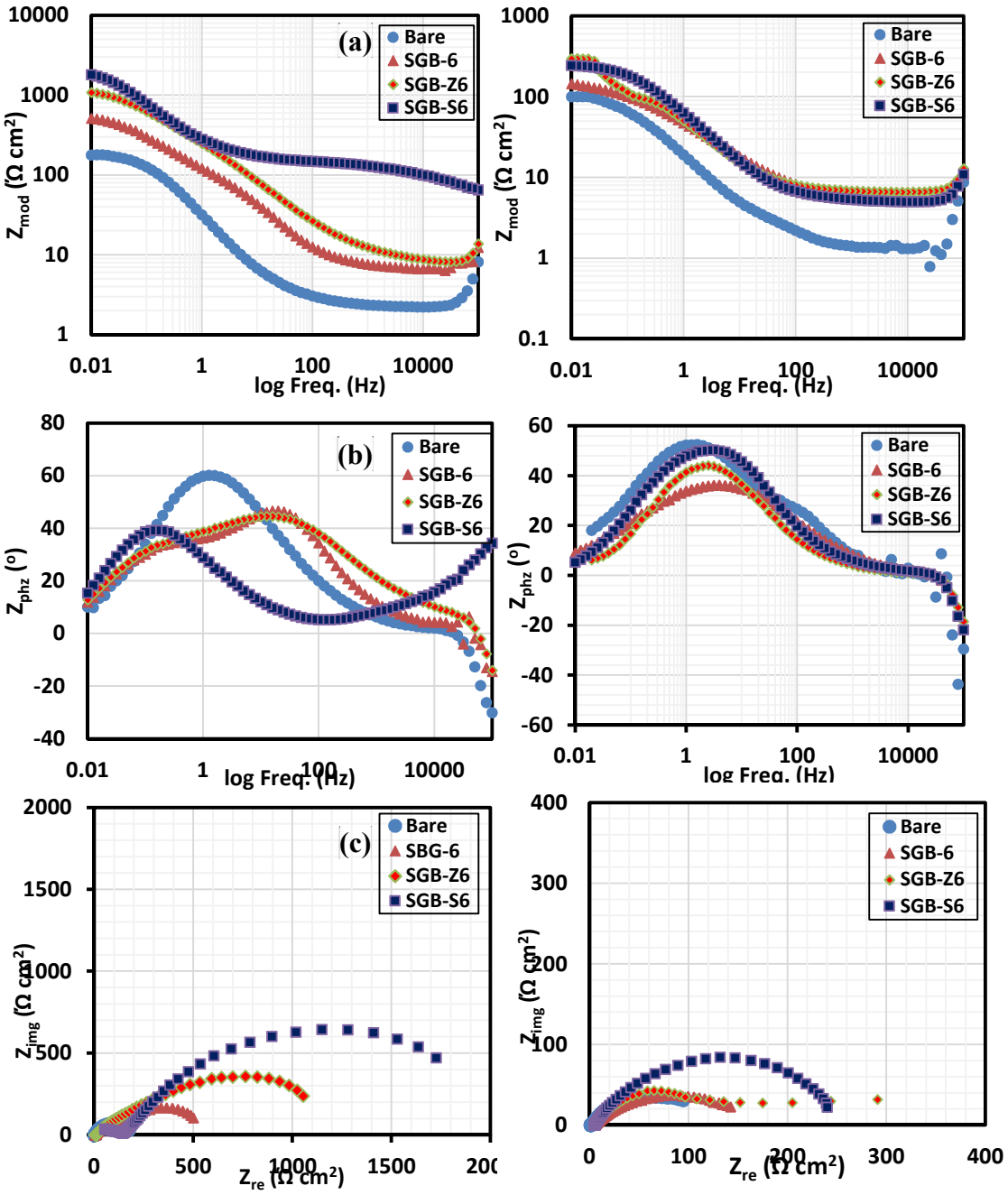

Figure 4.10 Bode module (a), Bode phase angle (b) and Nyquist (c) plots for biotic (*B. licheniformis*) coatings on mild steel compared to bare steel in 3.5 wt% NaCl after 1 h (left panel) and (b) 48 h right panel) immersion periods.

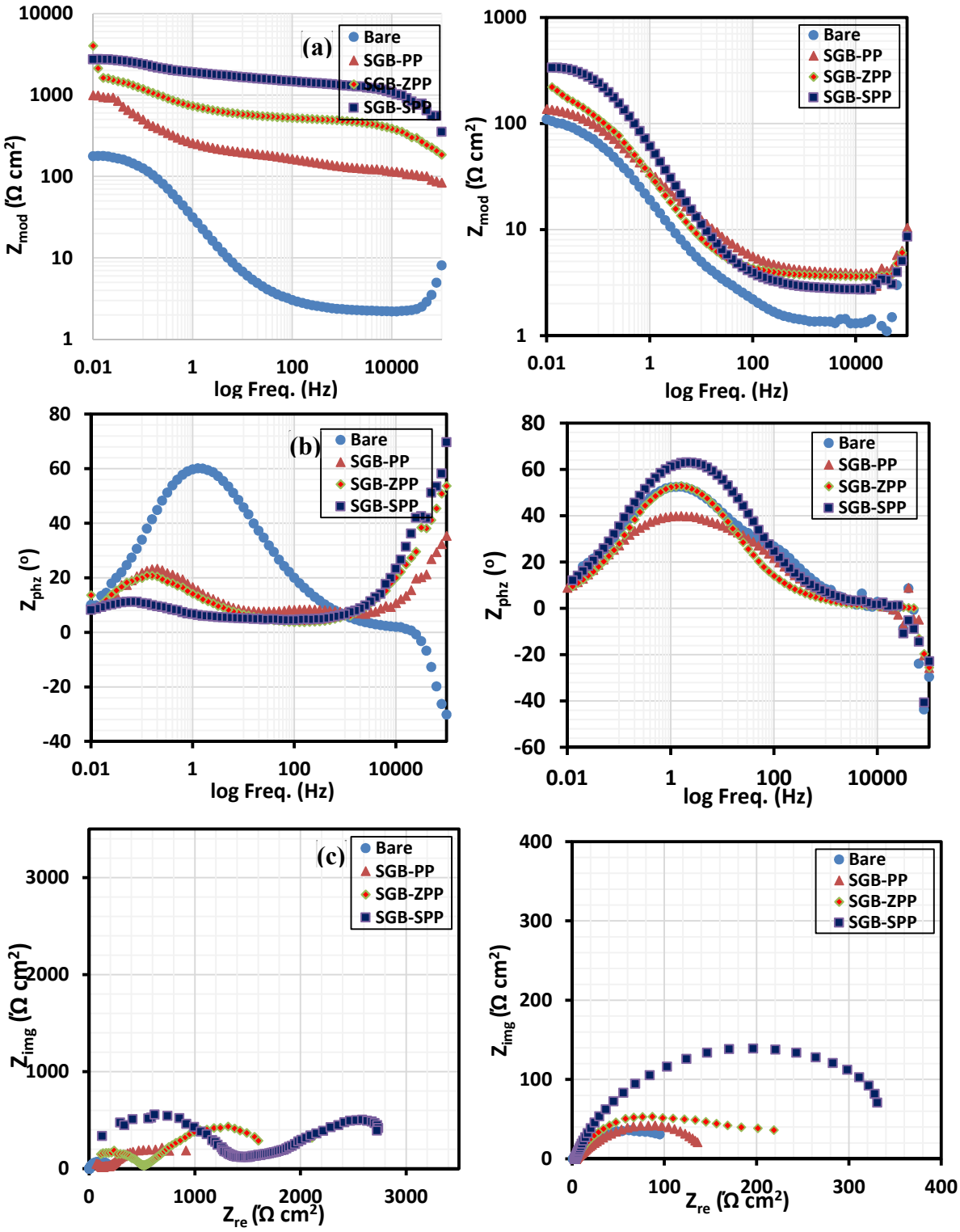

Figure 4.11 Bode module (a), Bode phase angle (b) and Nyquist (c) plots for biotic (*P. polymyxa*) coatings on mild steel compared to bare steel in 3.5 wt% NaCl after 1 h (left panel) and (b) 48 h (right panel) immersion periods.

Compare to the abiotic coatings, the sol-gel coatings encapsulated with endospores of *P. polymyxa* and *B licheniformis* (biotic coatings) demonstrated significant superior protection, especially in the presence of the two anticorrosive pigments. Just like the abiotic coatings though far lesser, the deterioration of the bulk films with prolonged immersion in 3.5 wt% NaCl is observed as the gradual reduction of R_{coat}. Values of R_{coat} for coatings encapsulated with *P. polymyxa* and *B licheniformis* endospores only (SGB-PP and SGB-6) are 969.00 and 859.7 Ω cm^2 after 1 h and 189.00 and 120.9 Ω cm^2 after 48 h. Corrosion protection increased as the biotic coatings are further functionalized with ZAPP and SAPP pigments with improved values of R_{coat} obtained for this systems of coatings. The magnitudes of R_{coat} presented in Figures 4.12 and 4.13 for SGB-Z6 and SGB-S6 are 1245.89 and 1355 Ω cm^2 after 1h; and 2001.98 and 3000.67 Ω for SGB-ZPP and SGB-SPP at the same period of exposure. Decrease in values of R_{coat} after 48 h are observed for these class of coatings after 48 h: 246.7, 300.1, 149.83 and 1785.8 Ω for SGB-Z6, SGB-S6, SGB-ZPP and SGB-SPP, respectively. In all, endospores of *P. polymyxa* showed superior protection to mild steel in the saline electrolyte compared to *B licheniformis*. While the endospores of both bacterial strains singularly improve the barrier protectives of the coatings, they also synergistically improve the bulk resistance of the coating in the presence of ZAPP and SAPP. CPE was also employed to monitor the water uptake ability of each biotic coating; and the variation of CPE_{coat} and CPE_{dl} with immersion period is presented in Figures 4.12 and 4.13 for both bacterial endospores. Increase in coating and double layer capacitances are attributed to increased water uptake, and less resistance coatings allow for the passage of corrosive ions and molecules via pore and micro-cracks.

With the trend of data in the figures, it is can be induced that biotic coating with inhibitors absorbed more water.

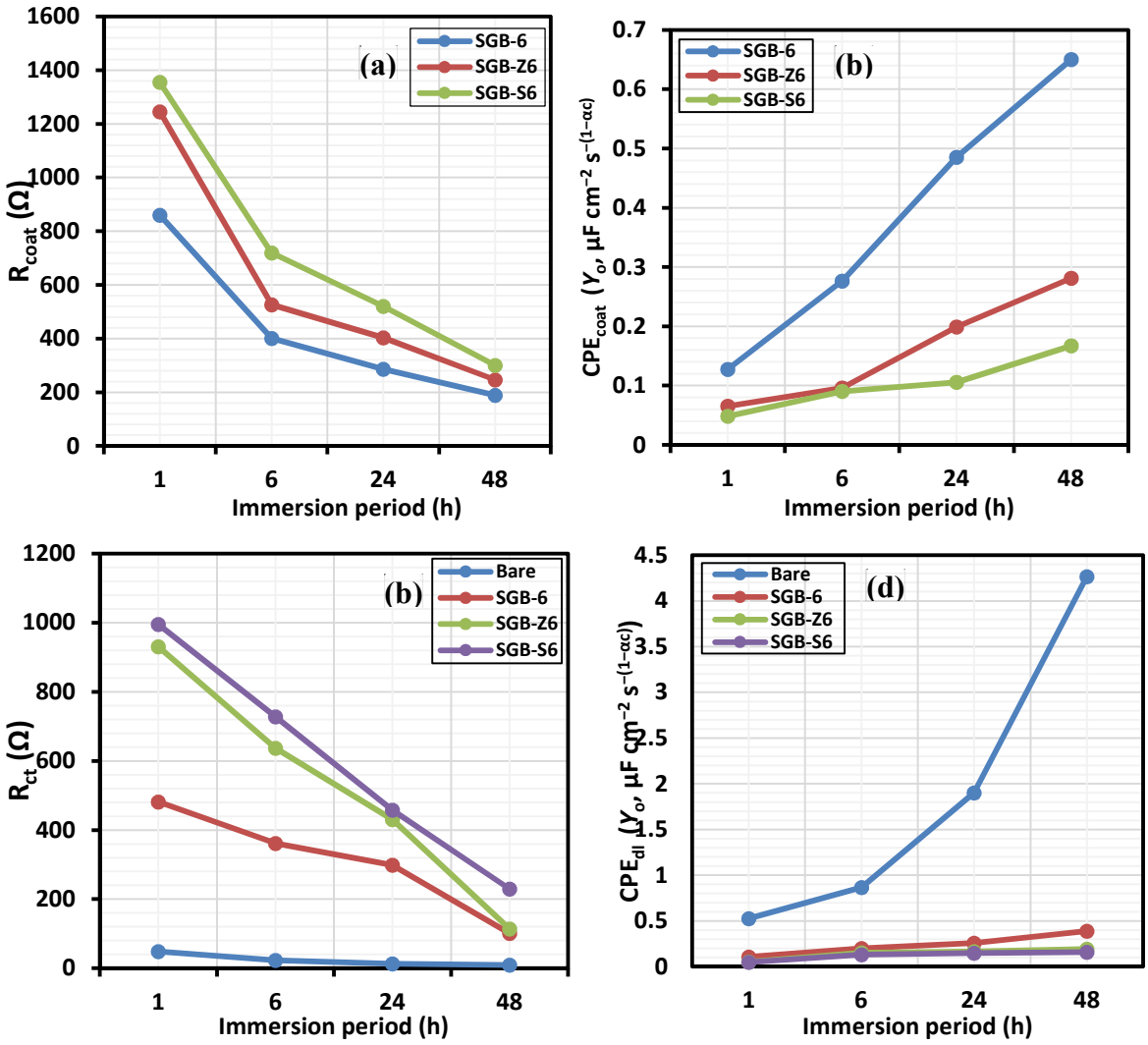

Figure 4.12 Variation in coating resistances (left panel) and capacitances (right panel) with exposure time (in days) with saline electrolyte for biotic (*B. lichenifomis* loaded) sol-gel coatings [(a) R_{coat}, (b) CPE_{coat}, (c) R_{ct}, and (d) CPE_{dl})].

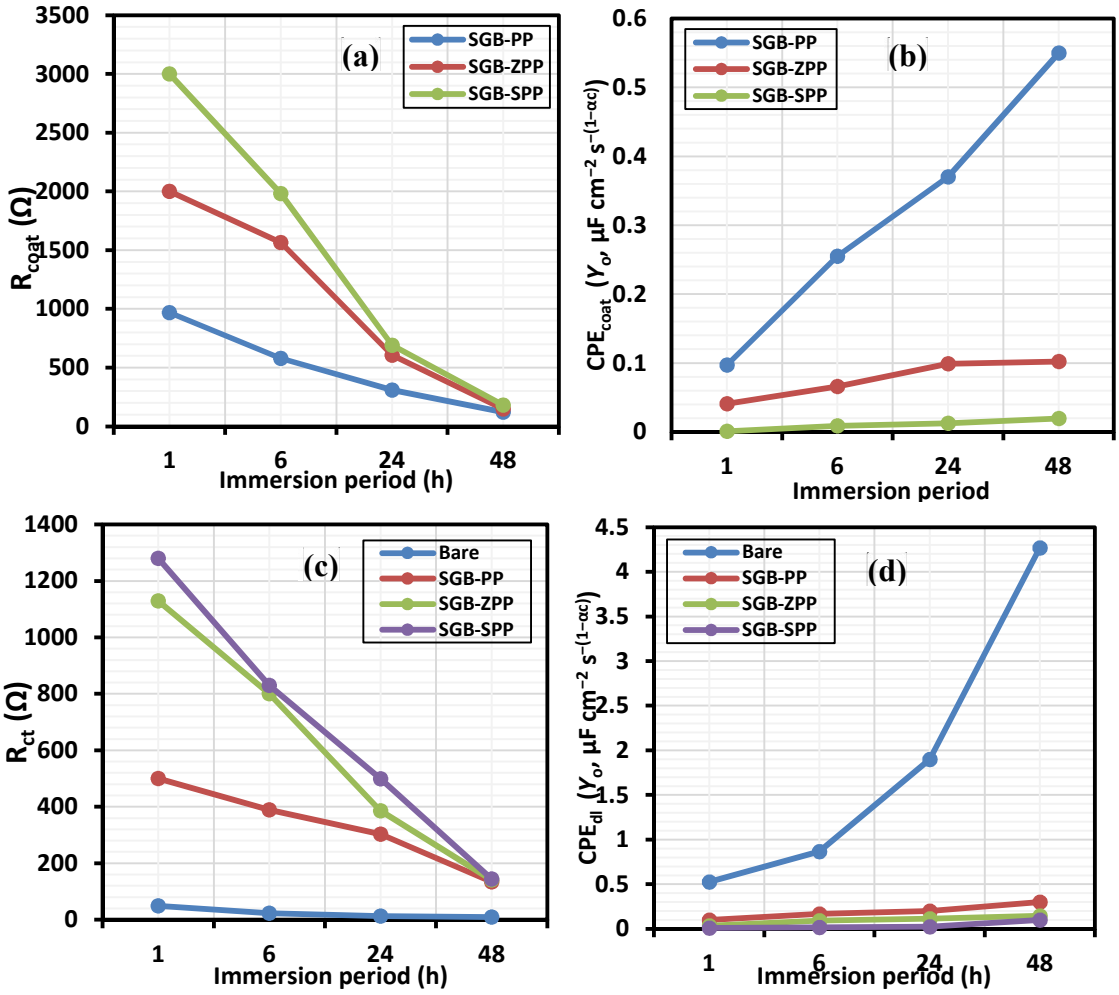

Figure 4.13 Variation in coating resistances (left panel) and capacitances (right panel) with exposure time (in days) with saline electrolyte for biotic (*P. polymyxa* loaded) sol-gel coatings [(a) R_{coat}, (b) CPE_{coat}, (c) R_{ct}, and (d) CPE_{dl})].

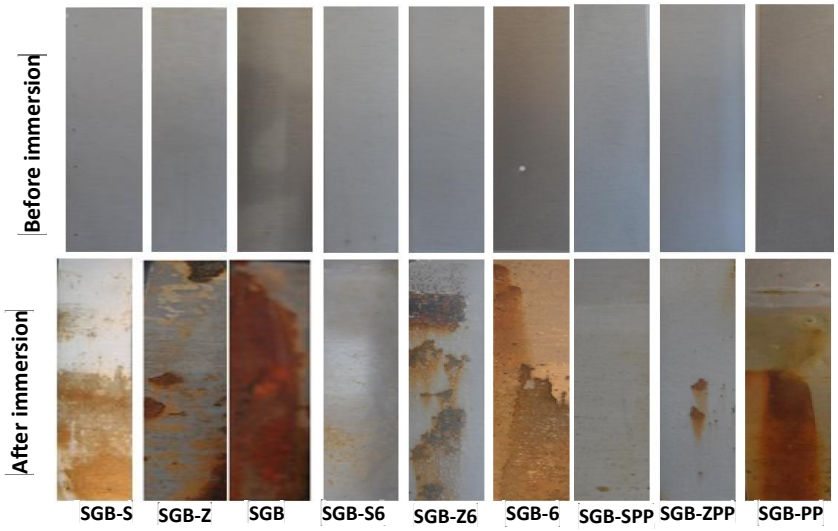

Figure 4.14 Photographs showing the appearances of defined test areas (9 cm^2) of the mild steel panels coated with abiotic and biotic sol-gel matrices before and after 48 h immersion periods in 3.5 wt% NaCl.

4.4 Field fouling trails at Whitby Harbour, UK

Whitby Harbour by the North Yorkshire seaside was chosen as the site for on-field fouling trails (throughout August 2013) since it is well known for its seasonal marine fouling episodes; most prominent in the mid summers. The presence of *P. polymyxa* and *B. lichenformis* endospores in this sol-gel coating inspired an interesting antifouling potential on immersion at Whitby Harbour as shown on the digital images for steel and aluminum in Figures 4.15 a and b. The physical appearance of both sets of coating reveals failure in protection of mild and aluminium substrates from the first week due to poor coating adhesion on steel. Independent of the anticorrosive agents in a protective sol-gel matrix, if adequate choice of precursors and reaction conditions employed for the synthesis as well as the chemistry at the metal/coating interface are not well defined, the bulk of the coating is susceptible to free passage of corrosive ions and molecules. Endospores of *P. polymyxa* and *B. lichenformis* failed to exhibit the needed antifouling properties since the sol-gel coating used for their encapsulation was not stable. These failed field results are consistent with the lab-based electrochemical data; (including the immersion test in Figure 4.15) revealing very low corrosion resistance against aerated 3.5 wt% NaCl at room temperature. The marine foulers found at the end of the 4^{th} week are dominantly green algae.

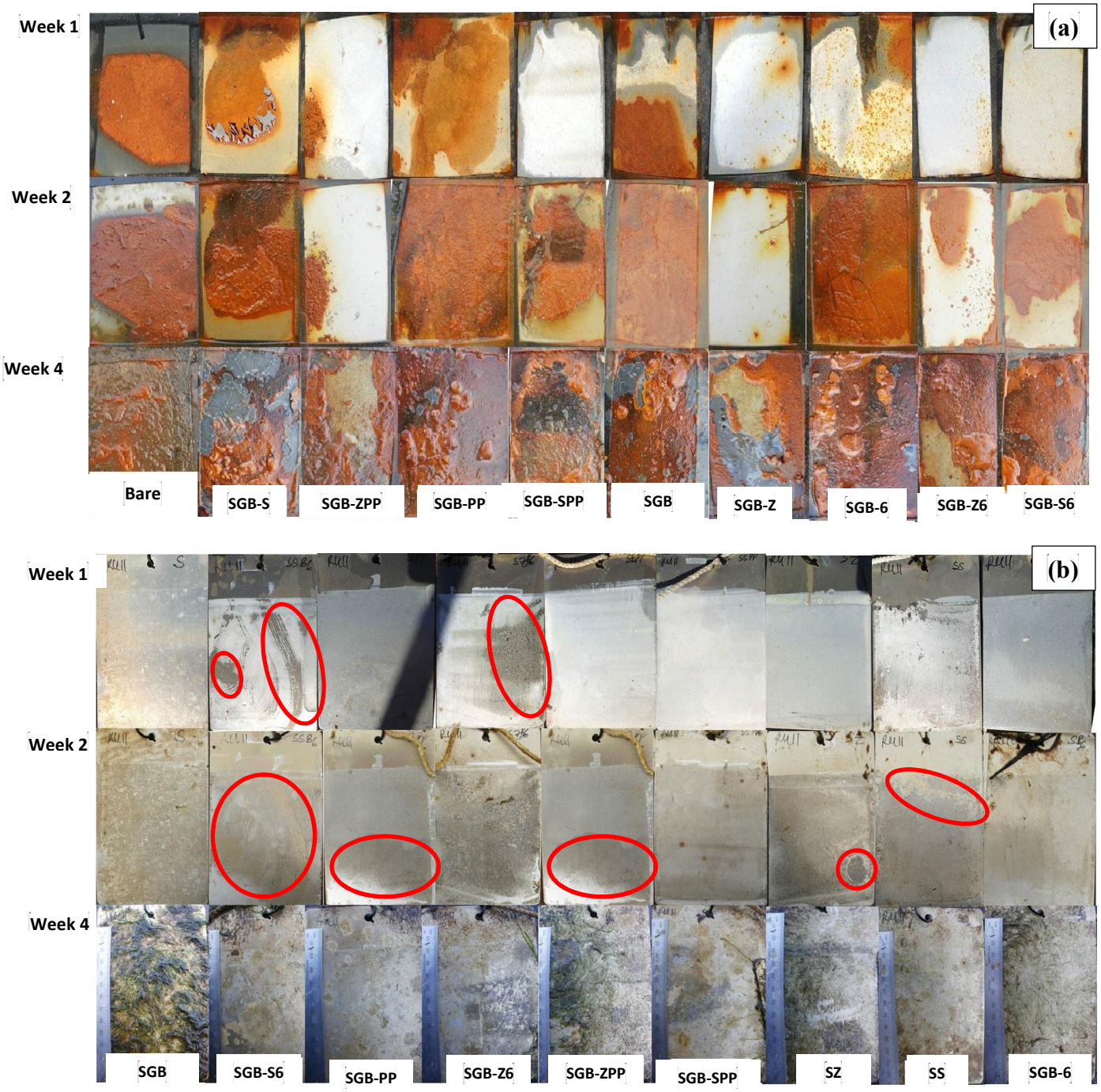

Figure 4.15 Field trial results of abiotic and biotic sol-gel coated mild steel (a) and aluminium (b) panels immersed at Whitby Harbour, UK.

4.5 Summary

The following conclusions can be drawn from the results of the electrochemical and on-field fouling trails:

1. The presence of endospores of *P. polymyxa* and *B. lichenformis*, and in combination with SAPP and ZAPP anticorrosive pigments reduces the corrosion of mild steel to a very low extent once encapsulated within this PDMS/ silica sol-gel coating matrix.
2. Failure for this coating matrix to protect corrosion in 3.5 wt% NaCl at a prolonged period of time could be link with instability in the bulk of the PDMS/silica coating and poor metal/coating adhesion due to inadequate choice of precursor chemistry.
3. The endospores of *P. polymyxa* and *B. lichenformis* remained alive in the bulk of the coating matrix to exhibit the needed anticorrosion and antifouling bioactivities as presented in the CSLM images.
4. The choice of precursors for the synthesis of barrier protective PDMS/silica coating should have involved the selection of those that will yield more compact silica bulk network and hydrophobic surfaces; reactive silicones could be excellent candidates.

CHAPTER 5

Title: Anticorrosion/antifouling properties of bacterial spore-loaded AMINO/EPOXY sol-gel type coating for mild steel in saline marine condition

5.1 A brief overview

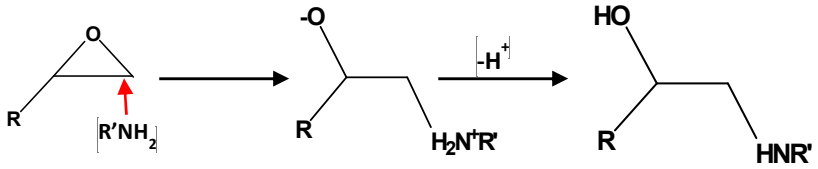

(5.1)

General mechanism for epoxy-amine cross-linking reaction

Epoxy ring-bearing precursors have been widely employed with amine-based curing agents (hardeners) in most epoxy-based protective coatings; and the ring-opening polymerization is similar to the reaction in Equation 5.1. Such coatings when combined with polydimethylsiloxane (PDMS) could have possess improved adhesion on substrates, surface energy for improved flexibility and oxidative stability and heat resistance [113]. Since this type of organic functionality on precursors predetermines their compatibility in anticorrosive sol-gel paints/resins on substrates, the functional group chemistry of these monomers needs to be understood. In this work, a bioactive additive in the form of endospores of *B. licheniformis* together with polyphosphate and molybdate based corrosion inhibitor pigments will be encapsulated into the bulk of a newly synthesized GPTMS/ aminopropylmethylsiloxane-PDMS type sol-gel coating for the simultaneous inhibition of corrosion and fouling of steel. The innovation in the sol-gel chemistry involves the ring-opening epoxy-ring with the nucleoplhilic amine group on aminopropylmethylsiloxane-PDMS type silicone precursor. GPTMS as an organically

modified type precursor will crosslink between Si-O-Si molecular chains on the bulk of the material to further enhance coating/metal chemistry, adhesion, hydrolytic stability of the final coating.

5.2 Experimental

5.2.1 Pre-treatment, reagents and sol-gel formulation method

The corrosion inhibitors used in this study were zinc aluminium polyphosphate (ZAPP) and zinc molybdate (MOLY) pigments obtained from Heucophos® ZAPP (28.1-31.0% ZnO) and MOLY-white 101 (85% $CaZnMoO_4$) (Heucotech Ltd. Co, US), respectively. The Si-based sol-gel coating was synthesized by blending Tetraorthosilicate (TEOS, Sigma-Aldrich, US), 3-glycidoxypropyltrimethoxysilane (GPTMS, SigmaAldrich, US) and 6-7% *(*Aminopropylmethylsiloxane)-dimethylsiloxane copolymer (GELEST, US) in a 10:6:4 ratio. (Aminopropylmethylsiloxane)-dimethylsiloxane copolymer is also referred to as aminopropyl-dimethicone with 6-7 mole% aminopropylmethylsiloxane with 64–200 cSt viscosity and molecular weight of 4000-5000). The mixture was stirred for an hour and a mixture of 0.5 mL 0.05 N HNO_3 (Sigma-Aldrich, US), 2 mL water and 4.5 mL isopropanol (Sigma-Aldrich, US) was then added dropwise at room temperature to induce the hydrolysis-condensation reaction. The sol-gel mixture was stirred continuously and aged for three days then finally coated on steel panels. The pH of the final coating was 3.4. All precursors involved in the sol-gel reaction were used without further purification. The sol–gel solution prepared above (SGC) was then doped individually with both ZAPP and MOLY inhibitor by suspending the appropriate inhibitor (to 5% w/v) into the solution and stirring (450 rpm) for 30 minutes, followed by sonication for an hour. These inhibitor-

doped sol-gel coatings were used as abiotic control matrices, and were labelled as SGC-Z and SGC-M, for each of ZAPP and MOLY, respectively. Table 5.1 presents the sample coding used for the variants of the inhibitor-doped abiotic coating system.

Table 5.1 Descriptive summary of the modified and unmodified coating matrices used in this study.

Coating type	Coating description	Nomenclature
ABIOTIC	Sol-gel coating only	(SGC)
	Sol-gel coating functionalized with corrosion inhibitor (ZAPP)	(SGC-Z)
	Sol-gel coating functionalized with corrosion inhibitor (MOLY)	(SGC-M)
BIOTIC	Endospores of *B. licheniformis* thermophilic strain encapsulated within the sol-gel coating	(SGC-6)
	S6 matrix further functionalized with ZAPP	(SGC-Z6)
	S6 matrix further functionalized with MOLY	(SGC-M6)

5.2.2 Spectroscopic characterization

The extent of sol-gel reaction, involving the hydrolytic conversion of alkoxy groups of the silane precursors to silanols as well as the degree of cross-linking after epoxy ring-opening polymerization with aminopropylmethylsiloxane)-PDMS was monitored using Fourier Transform infra-red (FTIR) and liquid-state nuclear magnetic resonance (^{1}H, ^{13}C and ^{29}Si NMR using DMSO as solvent) spectroscopies. NMR was acquired with a Bruker 750 spectrometer (JOEL instrument, Japan) and FTIR with Nicolet 6700 Fourier Transform (FT) Spectrometer (Thermo Electron Corporation, UK) operating in transmittance mode.

5.2.3 Preparation of *B. licheniformis* endospore suspension

The procedures for the isolation and identification of thermophilic strain of *Bacillus licheniformis* are elaborated in section 3.2.2. A single colony of the bacterium was used to inoculate a 5 mL aliquot of Tetrathionate (TT) broth and incubated (50 °C,

shaking at 180 rpm) overnight to provide a starter culture, which was used to inoculate the new flask containing fresh media. Endospores were produced from 1-litre aerobic TT culture in 2-liter flask at a constant temperature of 50 °C with an impeller speed of 200 rpm with an aeration rate of 1.5 L min^{-1}. Sporulation and lysis of mother cells were confirmed before harvesting the culture after seven days of growth. Endospores were recovered from the culture by centrifugation (17,700 ×*g* at 4 °C for ten minutes in 6×500 mL centrifuge pots) and washed five times with ice-cold water before another centrifugation trial, subsequent addition of sterile water, ice sonication and vortexing with water-saturated chloroform mixture per mL of endospore suspension [55]. The endospore suspension was adjusted to an OD_{600} of 66 with sterile distilled water before storage at ─20 °C. The *Bacillus* endospore suspension was thawed on ice at room temperature and centrifuged to remove excess chloroform. 1 mL of the prepared sol-gel was later added to diluted suspension above and sonicated for 5 seconds to separate possible aggregated endospores. Care was taken to avoid excess sonication; structural integrity of endospores was confirmed microscopically after sonication. The sol-gel bacterial/endospore suspension was then added to 10 mL of sol-gel mixture and labelled as biotic (SGC-6). This was repeated with inhibitor functionalized sol-gel coating, ZAPP and MOLY, respectively, and labelled as SGC-Z6 and SGC-M6. Table 5.1 presents a descriptive summary of the biotic and abiotic sol-gel coating matrices used in this study. The measured bacterial endospore concentration in the sol-gel solution used throughout this study was 1.98×10^6 CFU per ml (CFL/ml). This was evaluated prior to coating by measuring the optical density (OD) at 620 nm before correlating to cell forming units per millilitre (CFU/ mL) using Equation 5.2 [116].

$$Concentration\ (CFU/ml) = OD_{620\,nm} \times 472067 \qquad (5.2)$$

5.2.4 Confocal fluorescence microscopy

Confocal scanning laser microscopy was carried out using a Zeiss AxioVision confocal scanning laser microscope using a Plan Apochromat ×64 oil immersion objective. Fluorescein isothiocyanate (FITC) (488 nm) and rhodamine (543 nm) filters were used for images obtained after staining with BacLight™ Live/Dead staining kit. 1.5 cm^2 (approximately) pieces were cut from the panels, immersed in Nutrient Broth No. 2 (NB2) (at 30 °C for 24 and 48 hours), and stained using the Baclight™ Live/Dead bacterial viability stain (Invitrogen). The Baclight kit contained two DNA-binding fluorescent stains; viable cells are stained with the green fluorescent stain (Syto 9) and non-viable cells were also stained with propidium iodide. The propidium iodide bonded to the negatively-charged DNA to give red fluorescence via the damaged membranes of non-viable cells. Background fluorescence of both stains was seen since the Syto 9 green stain was able to bind to the sol-gel matrix and the propidium iodide red stain bound to the negatively-charged silanol groups within pores in the sol-gel.

5.2.5 Coating procedure

S36 mild steel panels (0.032”×3”×5”) were sonicated (Vibra-Cell Sonics and Material INC., US) with doubly distilled water, air-dried, and then stored in a desiccator. The panels were pre-cleaned with absolute ethanol before the coatings were applied. A millilitre of each of the sol-gel matrices (both modified and unmodified) was roller-coated (R K Print-Coat Instruments Ltd, UK) on each pre-treated steel panel and then allowed to cure at room temperature for 48 hours and then at 40 ºC for 24 hours. All the steel panels

were coated under a Laminar flow hood at room temperature to avoid cross contamination.

5.2.6 Electrochemical analysis

A ±10 mV amplitude voltage perturbation of the steel corrosion system over a frequency range of 100 kHz to 10 mHz was scanned with an ac signal at open circuit potential (E_{corr}) with the coated steel substrates in the solution of 3.5 wt% NaCl electrolyte. EIS Nyquist plots were obtained under potentiostatic conditions for the biotic and abiotic coated samples using a three-electrode electrochemical cell (Gamry, US). The counter and reference electrodes used were graphite and a standard calomel electrode, respectively, coupled to a Gamry Instrument potentiostat/galvanostat/ZRA (GAMRY 3000, Gamry Instruments, US) corrosion measuring system. EChem Analyst software package 6.0 was used for all the analyses, curve extrapolation, data fitting and simulations.

5.2.7 Coating and surface characterization

The measurement of the static contact angle of the individual coated metal was performed with a contact angle measurement (CAM) Instrument DSA30 (KRUSS, Deutsch, Germany) by pendant water drop for three consecutive trails. The thermal behaviour of this new hybrid sol-gel polymer was characterized with a thermogravimetric (TG) analyzer (Perkin-Elmer TGA 7) at 10 ^{o}C/min in N_2 raised to about 800 ^{o}C. Surface analytical evaluation of the coating morphology on the metal was performed using the U9320A 8500 Field Emission Scanning Electron Microscope (Agilent Technology, UK) prior to and after two weeks immersion in 3.5 wt% NaCl test solution.

5.2.8 Field trials at KFUPM beach

A field trial in a natural corrosive environment was conducted to ascertain the corrosion protection properties of the unmodified and the abiotic and bio-modified coating systems. The edges of the immersed S36 panels were covered with insulation tape leaving only a defined test area for fouling studies. The marine fouling studies were carried out in the hyper-saline seawater of KFUPM beach, Half-Moon Bay, Al Khobar, Saudi Arabia, between March and July, 2015. The temperature, pH as well as the salinity of the water body (at the point of sample immersion) recorded throughout the period of fouling studies are presented in Table 5.2.

Table 5.2 Mean values of temperature, pH, and salinity of KFUPM Beach (at the point of sample immersion) recorded throughout the 10 weeks of fouling studies.

Days	Temperature (^oC)	pH	*Salinity (ppt)
Day of immersion	28.9 ±0.1	7.6±0.2	65.8±1.0
Week 2	27.2±0.2	7.4±0.2	67.5±1.2
Week 4	28.3±0.2	7.4±0.2	66.4±0.9
Week 6	29.2±0.3	7.8±0.3	71.0±0.6
Week 8	30.8±0.2	7.7±0.2	70.2±0.8
Week 10	29.0±0.2	7.3±0.3	71.2±0.7
Week 12	31.0±0.4	7.4±0.2	71.0±0.6

Above parameters were taken in the early hours of the mornings; *Values of salinity kept increasing steadily as the hot Arabian summer approached in June; and with salinity values more than 40 ppt, KFUPM beach could be classified as being "*hyperhaline*" (very saline).

5.3 Results and discussion

5.3.1 Spectroscopic characterization

Due to the presence of multiple secondary and by-products from the sol-gel reaction of the precursors in this study, it is difficult to probe the exact route of the process, though, liquid-state NMR can help to ascertain NMR to ascertain the extent of

hydrolysis/acidification of precursors in the solution. The proton and carbon NMR of the three sol-gel precursors used in this study is presented in Figure 5.1. The proposed structure of the sol-gel (SGC) is presented in Figure 5.2. To confirm the evidence of epoxy ring-opening reaction by the amino-PDMS copolymer on the NMR of the synthesized sol-gel, amino proton peak (at 1.5 ppm) as well as those of the epoxidic protons corresponding to GPTMS were probed. The broadening of the epoxidic proton peaks at 2.7 and 3.2 ppm in Figure 5.3 (a) denotes evidence of epoxy ring-opening polymerization, and this could be attributed to the nucleophilic attack by the amino group (of which its proton peak at 1.5 ppm has disappeared). Normally, acid-catalyzed ring opening polymerization products should generate extra carbon peaks between 60 and 70 ppm, but this is not found in the ^{13}C NMR spectrum of the final sol-gel. The absence of peaks corresponding to alkylether (between 9.0─9.5 and 70 ppm), diols (at 71 ppm) and polyethylene oxide (after 74 ppm; not belonging to GPTMS) confirms that the epoxy ring in GPTMS was not due to an acid-catalyzed polymerization occurring during the sol-gel reactions, though the carbon peak at 55 ppm is suggestive of the presence of a terminal methyl ether. Figure 5.3 (b) also confirms the presence of CH_2 groups of the aminopropyl segments at 17.7 and 48.4 ppm and precisely towards 0.6, 2.5 and 2.7 ppm on the proton NMR (Figure 5.3 a). The silicon peak due to PDMS's Si-O(CH_3) group is still visible on the ^{29}Si NMR (Figure 5.4 a) spectrum of the sol-gel matrix while the disappearance of those belonging to TEOS and GPTMS precursor is an evidence of sol-gel reaction. The ^{29}Si MAS/NMR is displayed in Figure 5.4 b for the the dried sol-gel material. Figure 5.5 shows the FTIR spectrum of the sol-gel mixture collected with peaks between 3000 to 3600 cm^{-1} indicating the presence of an O–H vicinal and N-H stretching bands due to the presence silanol, reacted N-H groups

and absorbed alcohol products as well as water. The absence of IR peaks at 950─810/ 1260─1240 cm^{-1} denotes epoxy ring opening due to treatment with amino group. νSi-C(s) from PDMS group on the aminopropylmethylsiloxane)-dimethylsiloxane copolymer occurs at 1258 cm^{-1} as well as the aminopropyl residual segments at 1300-1700 cm^{-1}. IR vibrations for νSi-C (s) from PDMS group is found at 1258 cm^{-1}) while those at 1020 and 1261 cm^{-1} represent νC─N (s). For the pure silane precursors, the disappearance of peaks at 788 and 1216 cm^{-1} (corresponding to νSi─C (s)) and 928/1121 cm^{-1} (for νSi─OC (s)) denotes complete hydrolysis leading to the formation of asymmetric Si–O–Si stretching vibration at 1086 cm^{-1}, asymmetric Si–O–Si bending at 400–450 cm^{-1} and symmetric Si–O–Si bond stretching vibration at 699 cm^{-1}.The synthesized and unmodified sol-gel coating in this study was viscous and relatively clear and stable solution with pH lightly acidic (pH 3.5) showing the presence of some unreacted silane precursors. It was later modified according to the components stated in Table 5.1 and each matrix was coated on pre-cleaned mild steel substrates; and Figure 5.6 displays the appearance of the coated surfaces of each sol-gel matrix without mechanical defects.

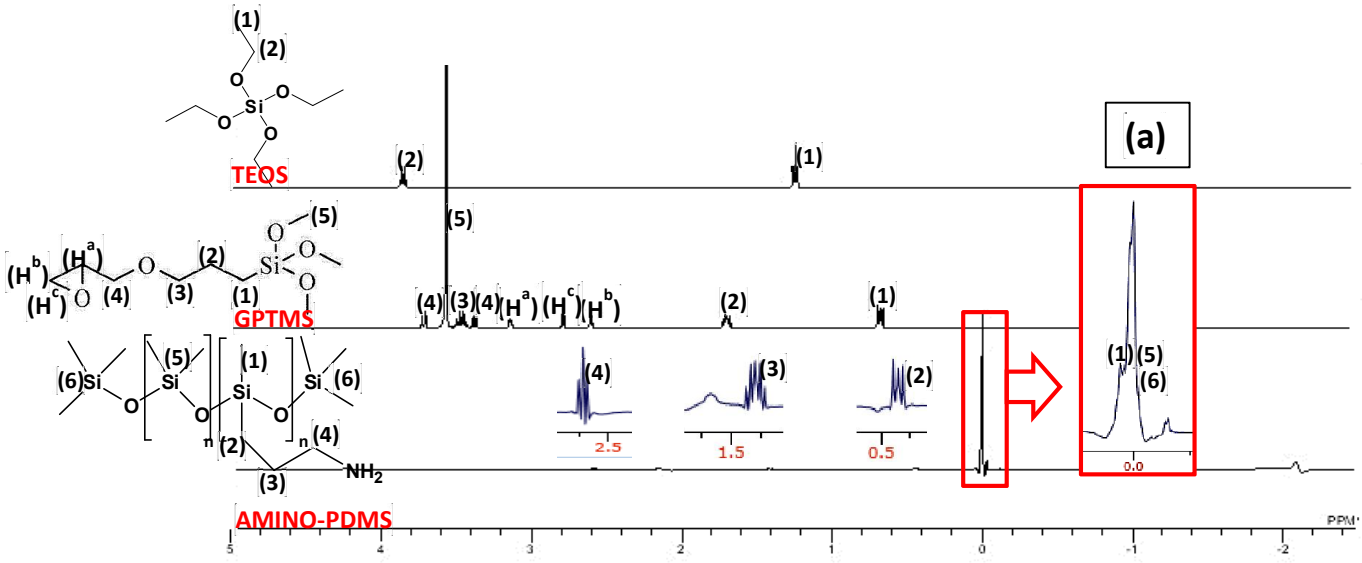

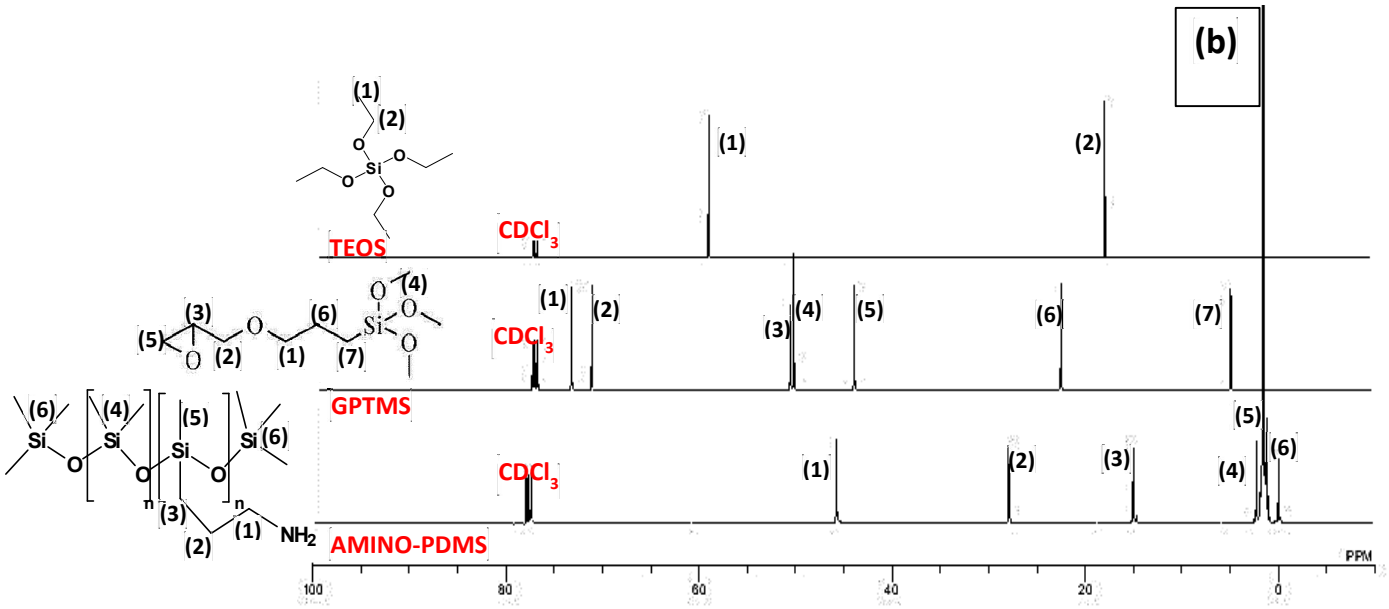

Figure 5.1 Liquid state NMR spectra (^{1}H (a) and (b) ^{13}C) of the precursors (TEOS, TMMS, GPTMS, respectively, from up to bottom) employed in this study (solvent: $CDCl_3$).

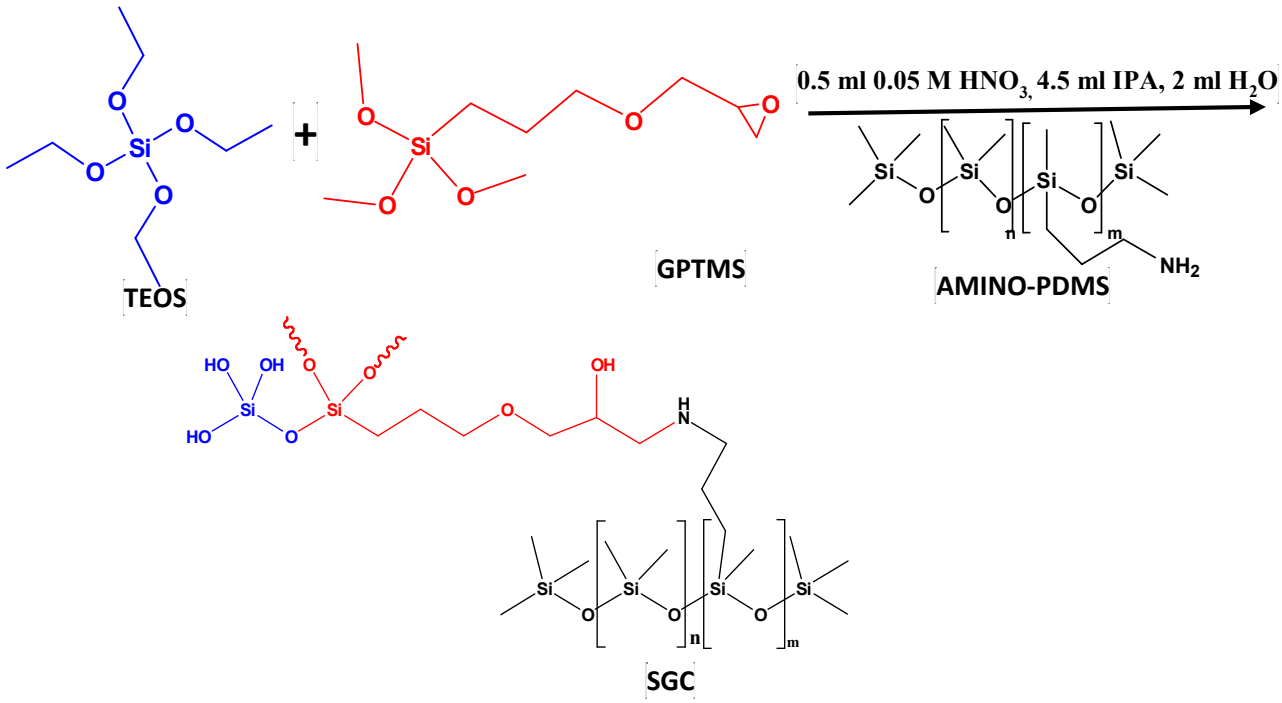

Fgure 5.2 The proposed sol-gel (SGC) reaction

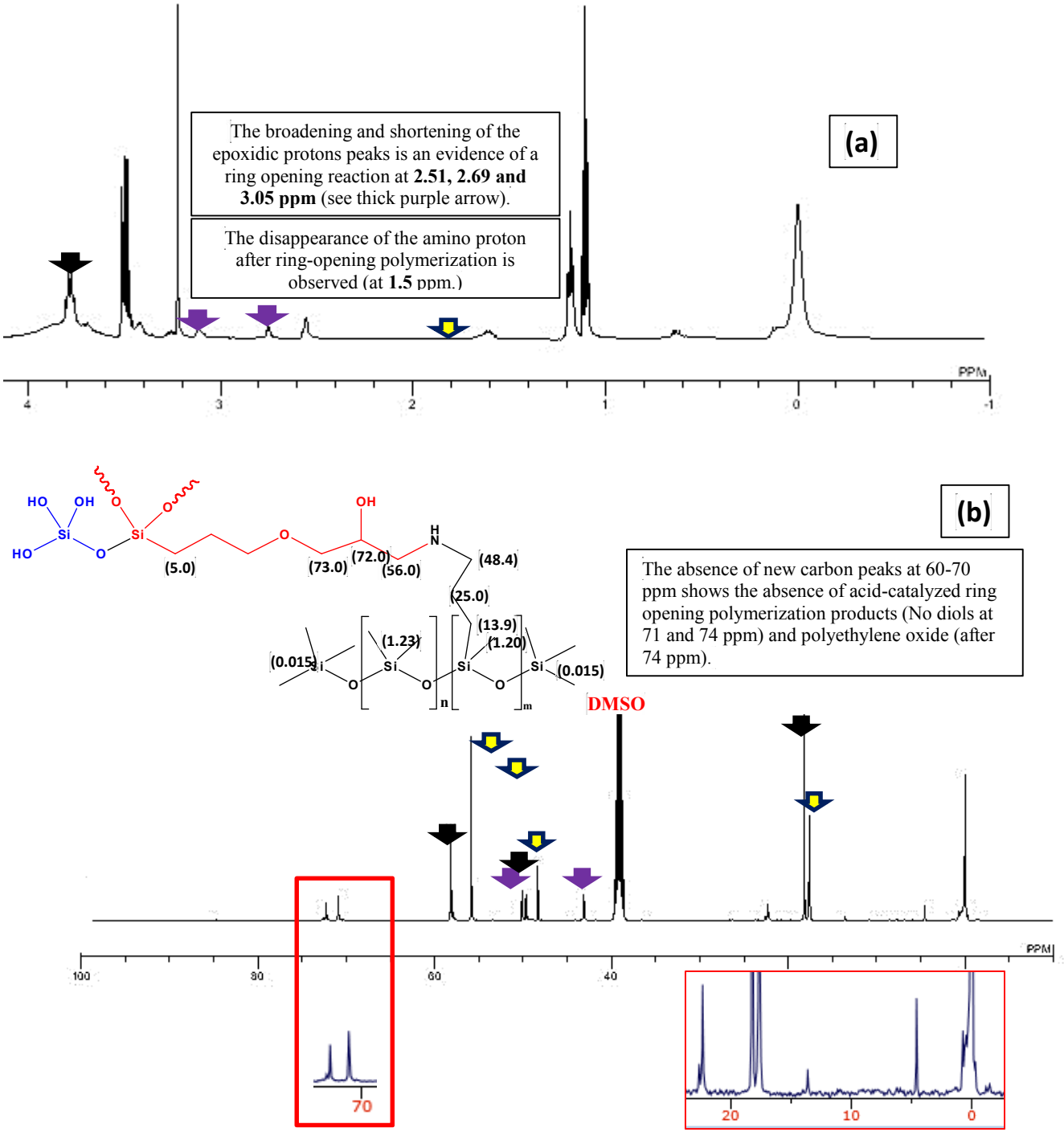

Figure 5.3 ^{1}H (a) and (b) ^{13}C NMR spectra of the as-prepared and unmodified sol-gel coating before application on metal substrate and curing procedures

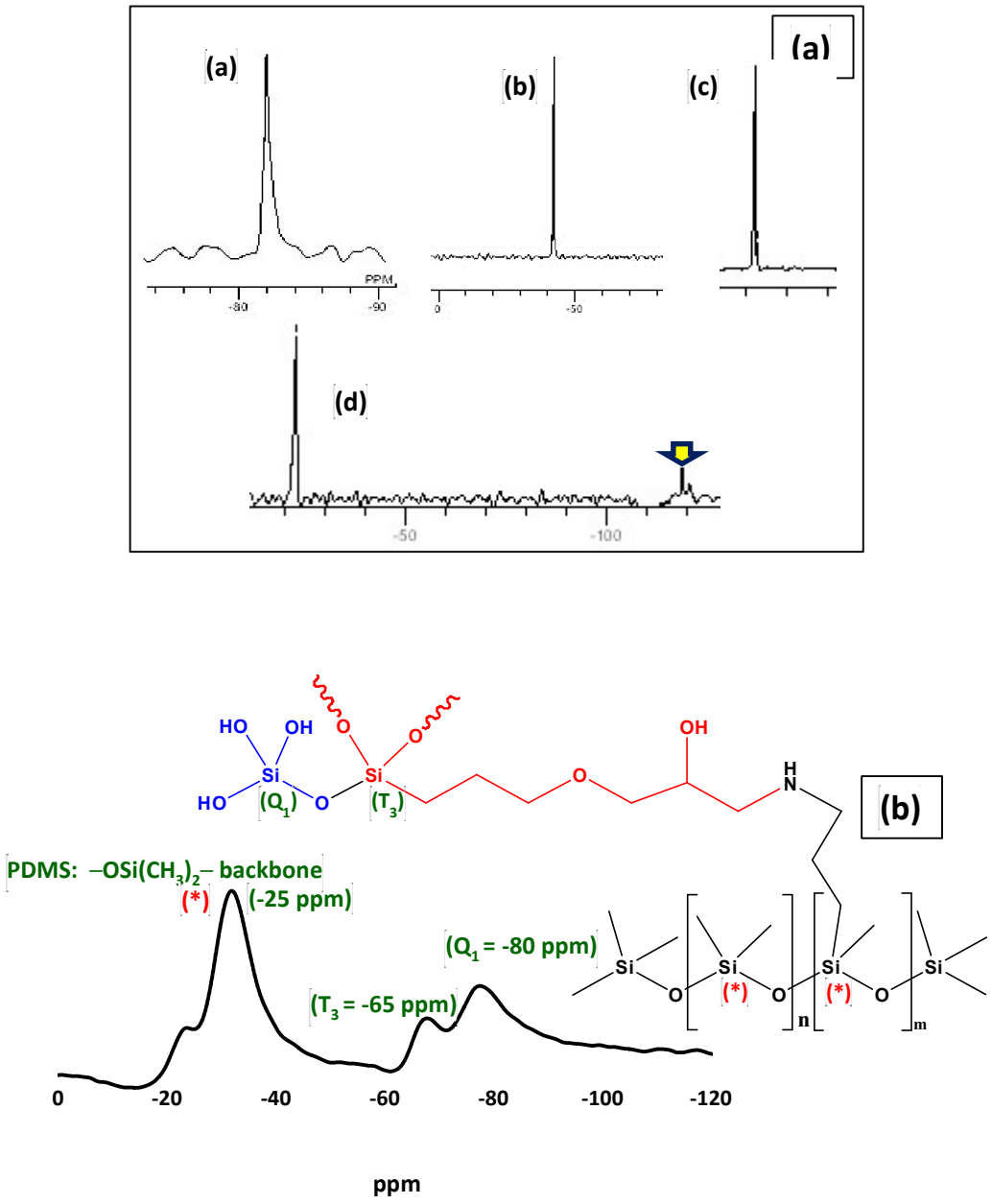

Figure 5.4 ^{29}Si Liquid (a) and MAS (b) NMR spectra of the as-prepared and unmodified sol-gel coating (Insert: ^{29}Si peaks of a, TEOS; B, GPTMS; and c, aminopropylmethylsiloxane–PDMS).

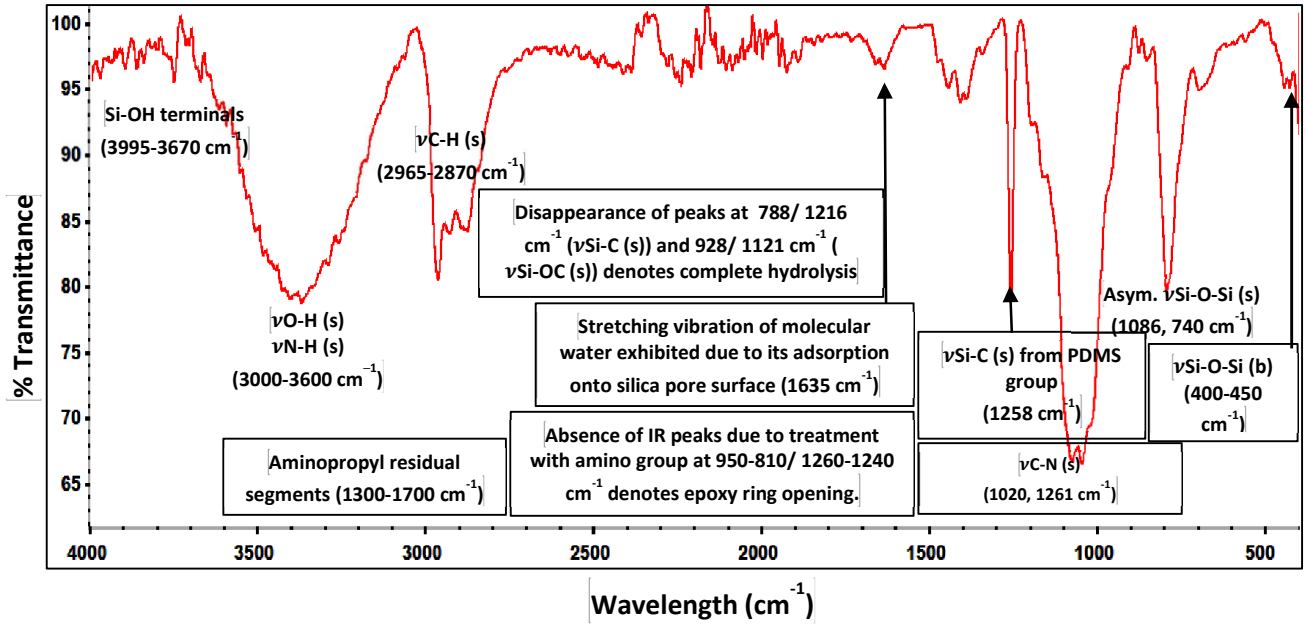

Figure 5.5 FTIR spectrum of the as-prepared and unmodified sol-gel coating before application on metal substrate.

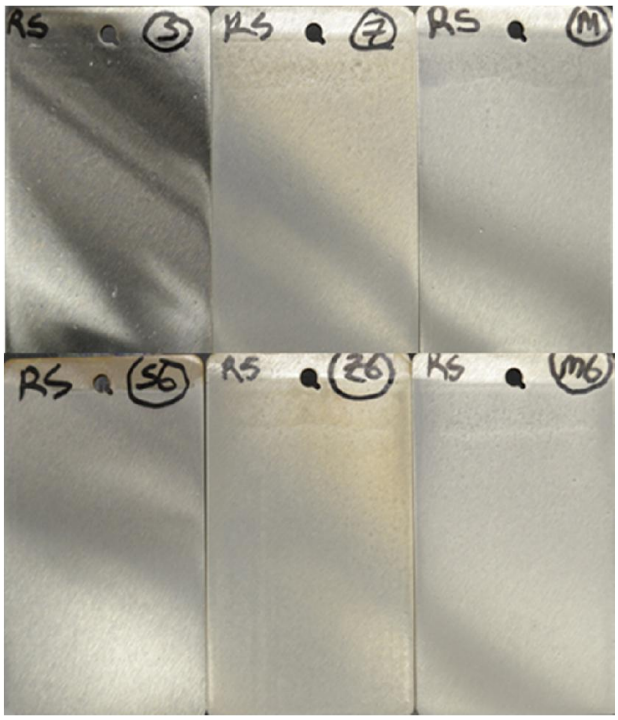

Figure 5.6 Mild steel Q panels (0.032”×3”×5”) coated with different functionalized sol-gel matrices.

5.3.2 Confocal laser scanning microscopy

To ascertain the viability of the bacterial endospores in the system of coatings and to ensure that they were alive to execute the needed physiological activities, both biotic and abiotic sol-gel solutions were inoculated in a TT agar plates [117] (Figure 5.7) as well as coated on glass slides prior to confocal laser scanning microscopy. The use of appropriate fluorescent probes and confocal scanning laser microscopy aided visualization of the viable and non-viable vegetative cell distribution within the sol-gel matrix. Bioactive coated glass samples were immersed in a nutrient solution (NB2 broth) for 24 h and then stained with the Baclight Live/Dead stain (Invitrogen) and incubated to observe cell viability of the endospores, while the abiotic samples were similarly treated and served as negative controls.

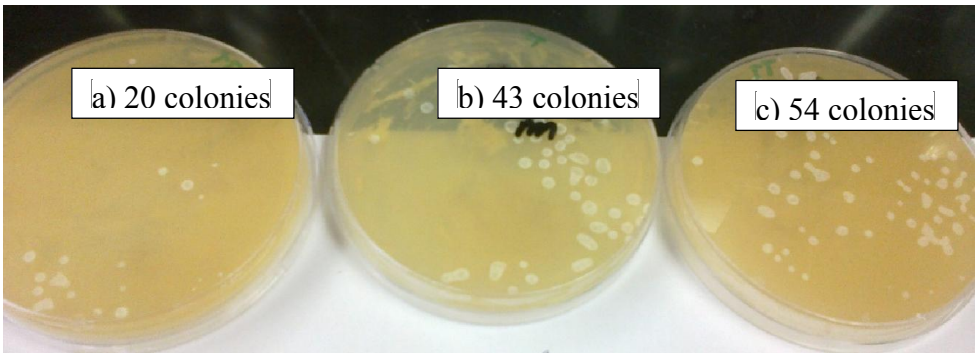

Figure 5.7 Growth of *B. licheniformis* strain No. 6 (B6) colonies from endospores in sol-gel coatings: a) Sol-gel encapsulated with B6 endospores (SGC-6), b) Sol-gel encapsulated with MOLY and B6 endospores (SGC-M6), c) Sol-gel encapsulated with ZAPP & B6 endospores (SGC-Z6).

Appropriate micrographs were collected with different optical frames as shown in Figure 5.8. As the nutrient medium contacts the endospores, bacterial cells are expected to germinate and begin to grow, and this will be accompanied by a change in cell morphology from round/oval (endospores) to rods (vegetative cells). All bioactive coated samples with and without corrosion inhibitors showed the presence of live (green) and

dead (red) endospore- and/or cell-like structures. The predominance of green rod-like cells in the biotic samples indicates viable bacterial cells in the coated samples; and being alive denotes their availability for bioactivity. The cellular clusters observed at this exposure time could be due to formation of biofilms in the early stages of growth [118]. The characteristic feature of these sol-gel matrices as shown on the confocal florescence micrographs is the presence of surface cracks and peels caused by poor coating adhesion or coating disbonding on the glass slides. Bulk pores can be seen as dark, round shapes on the micrographs for the abiotic sample. Other than the pores, the abiotic sample (SGC) has a relatively featureless appearance in comparison to the other coating samples. The confocal florescence micrographs of the abiotic coating matrices show no vegetative bacterial growth as the absence of live cells confirms that samples SGC, SGC-Z and SGC-M are actually abiotic. The background (mostly green) fluorescence observed in these images was attributed to autofluorescence of the sol-gel matrix. The green Syto 9 and red propidium iodide fluorescent probes may have bound to the negatively-charged silanol groups within the sol-gel matrix thereby creating these areas of green and also red fluorescence in the background [119].

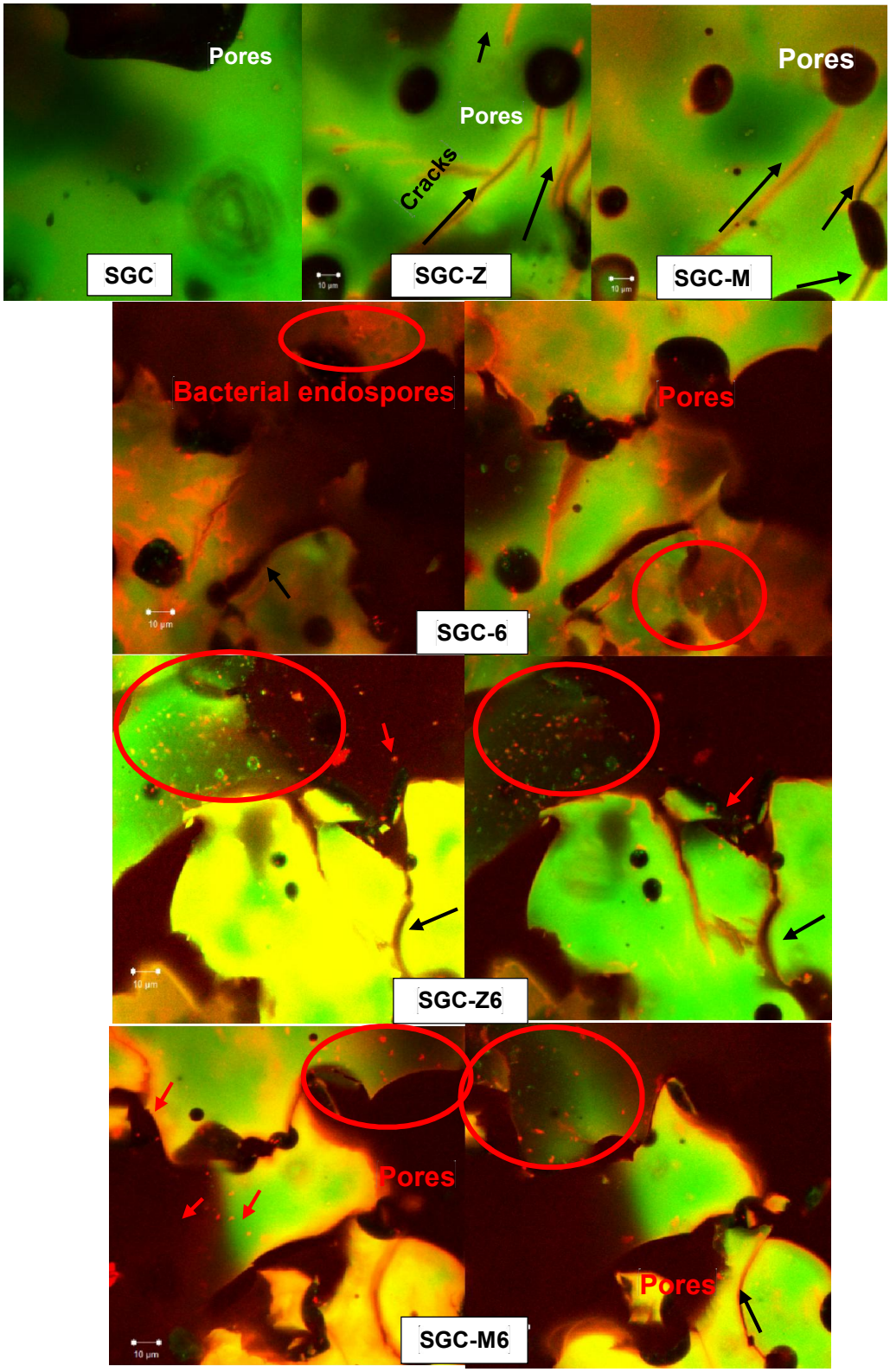

Figure 5.8 Confocal fluorescence images showing live cells in the various sol-gel coatings (the black and red bold arrows indicate the cracks and inherent bacterial vegetative cells/endospores, respectively). The stacked confocal images for the bioactive samples are presented in double panels to show clarity.

5.3.3 Thermal analysis and hydrophobicity evaluation

Thermogravimetric analysis (TGA) curve (recorded under nitrogen) for the synthesized hybrid sol-gel coating is shown in Figure 5.9 below; with weight loss (WL) being observed in few thermal regions. The evaporation of occluded/physically adsorbed or less strongly chemically bonded water molecules on the sol-gel matrix occurred between laboratory temperature and 250 ^{o}C. The magnitude of weight loss corresponding to decomposition/pyrolysis of the bridging organic groups/chains occurs around 300 ^{o}C and between 580 ^{o}C and 650◦C [120]. The differential TG (DTG) curve for this newly synthesized sol-gel coating shows typical nonlinear decomposition temperatures (T_d) around 330, 460 and 570 ^{o}C. It is adequate to mention here that the condensation reaction continued even up to thermal and curing treatments. To this end, the weight loss observed at elevated temperature could have been due to formation of 3D Si-O-Si network via condensation reactions (above 500 ^{o}C). The static water contact angle measurement of abiotic and biotic sol-gel coatings were carried out to evaluate the wetness of their surfaces, and the degree of hydrophobicity of each coating system was deduced from the result [121]. The results showed that the contact angle of the coatings increased in the following order: SGC-M6(109^{o}) > SGC-Z6(95^{o}) > SGC-6(85^{o}) > SGC-M(80^{o}) > SGC-Z(79^{o}) > SGC(75^{o}). The sol-gel containing bacterial endospores and MOLY exhibited the most hydrophobic surface (109^{o}); however the reason for this variation has not been investigated in this study (Figure 5.10 a and b), though *B. licheniformis* endospores are known to readily form surface-altering biofilms as they secrete antimicrobial substances within these biomaterials [122─125]. It can also be observed that the presence of endospores led to an increase in the coating hydrophobicity. Hence, it should be expected

that steel panels coated with high contact angle matrices should yield better corrosion protection properties since their surfaces will limit the passage of water molecules as a result of reducing the diffusion rate. The loss in the hydrophobicity of surfaces is an indication of the occurrence of more surface wetting which can lead to the onset of corrosion.

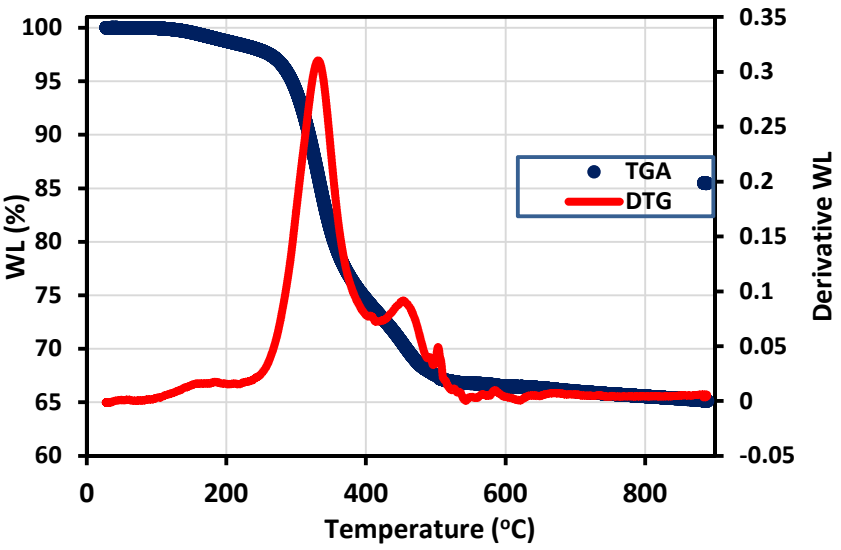

Figure 5.9. TG curves of the synthesized hybrid sol-gel (S) coating alone in N_2 atmosphere.

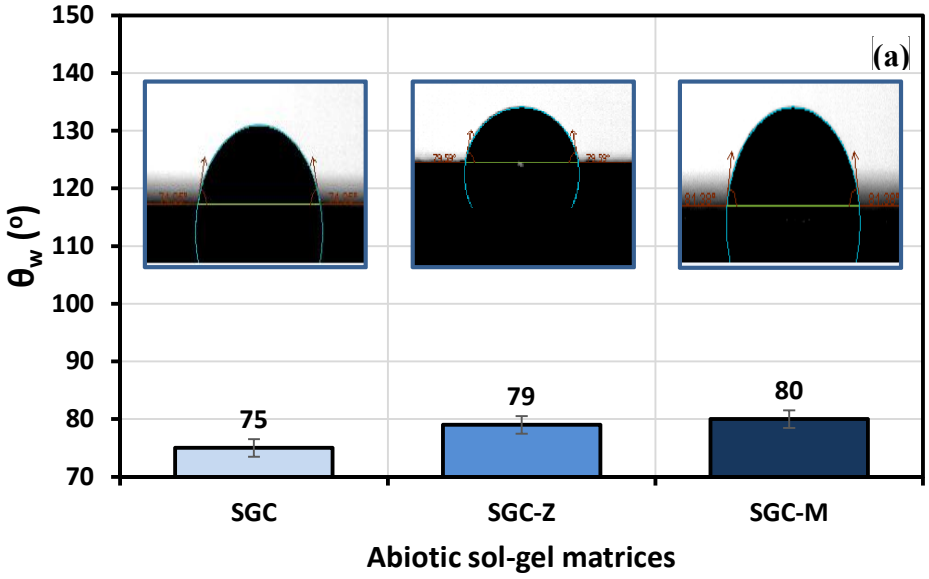

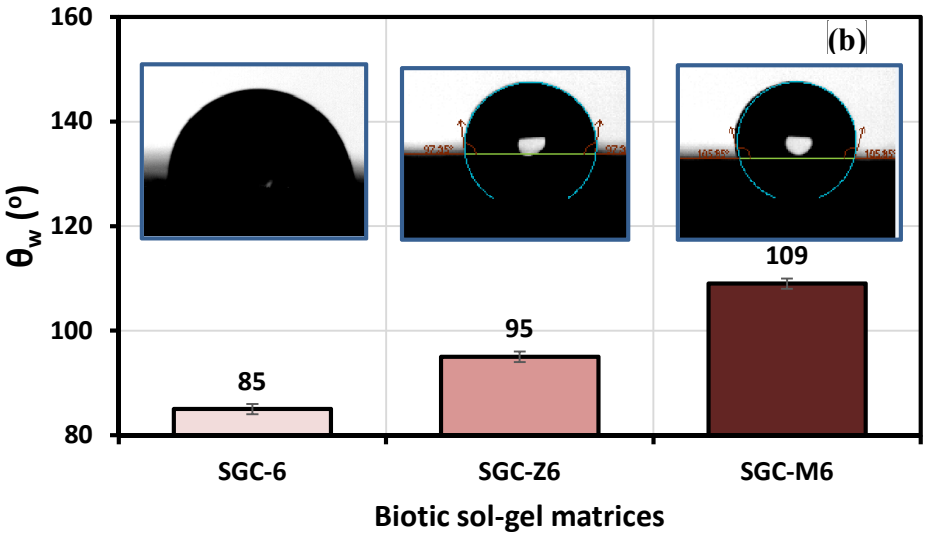

Figure 5.10 Contact angle result for steel panels coated with different sol-gel matrices; (a) abiotic and (b) biotic.

5.3.4 Electrochemical impedance spectroscopy

The electrochemical impedance response of all variant coated steel panels immersed in aerated 3.5 wt% NaCl solution was recorded periodically for 2 weeks. Comparative Nyquist curves are presented for the different coating systems at immersion periods of 24 hours in Figure 5.11 (a), 48 hours (b), and 2 weeks (c). The spectra show the presence of multiple time constants, seen as semicircles. These can be attributed to the capacitive and resistive behaviour at high and low frequencies, relating to permeation of electrolyte ions across the coating/metal interface. The varying inhibition mechanisms for these systems are related to the coating composition for each coated metal. After 24 hours, the impedance responses for the coated systems revealed the first time constant as a capacitive loop, possibly denoting that the coatings, to some extent, allowed the passage of corrosive chloride ions towards the coating/metal interface. The size of the Nyquist capacitive semi-circles are generally considered to reflect the degree of protection for each coating system. In Figure 5.11 it can be seen, that the presence of MOLY in the coating

improved the corrosion protection of steel over that of ZAPP, with and without the bacterial endospores. The presence of the encapsulated endospores in the bulk of the coating appears to increase the impedance of the coating to corrosive chloride ions, with the highest impedance observed for the MOLY-doped coating with the bacterial endospores (SGC-M6). This indicates, in terms of corrosion protection, that there is synergy between the corrosion inhibitors and the *B. licheniformis* endospores. The shapes of the Nyquist curves remain relatively unchanged after 48 h (Figure 5.11b) for all the coating systems studied indicating that there must not have been any change in the corrosion protection mechanism on prolonged immersion in the saline electrolyte. SGC-M6 maintains the largest two-time constant (ɤ) capacitive loops after 2 weeks (Figure 5.11c) showing an outstanding protection against corrosive ions at the steel surface with SGC-6 being the lesser biotic protective coating. The decrease in the impedance values of the abiotic sol-gel coating alone (SGC) is due to the failure and disbonding in the coating and subsequent passage of chloride ions to the steel surface. However, the presence of the metal-based corrosion inhibitors continues to improve the protection ability by forming passive films, this is evident from the increased Nyquist semicircles compared to the sol-gel coating alone (Figure 5.11c). After this prolonged immersion period, there are some distortions in the shapes of the capacitive loops for all the coating systems, though not vividly observed; the most reason constant phase element (CPE) was deployed in the equivalent circuits. These distortions could be directly linked with surface imperfections, such as cracks, and other previously reported interfacial unevenness.

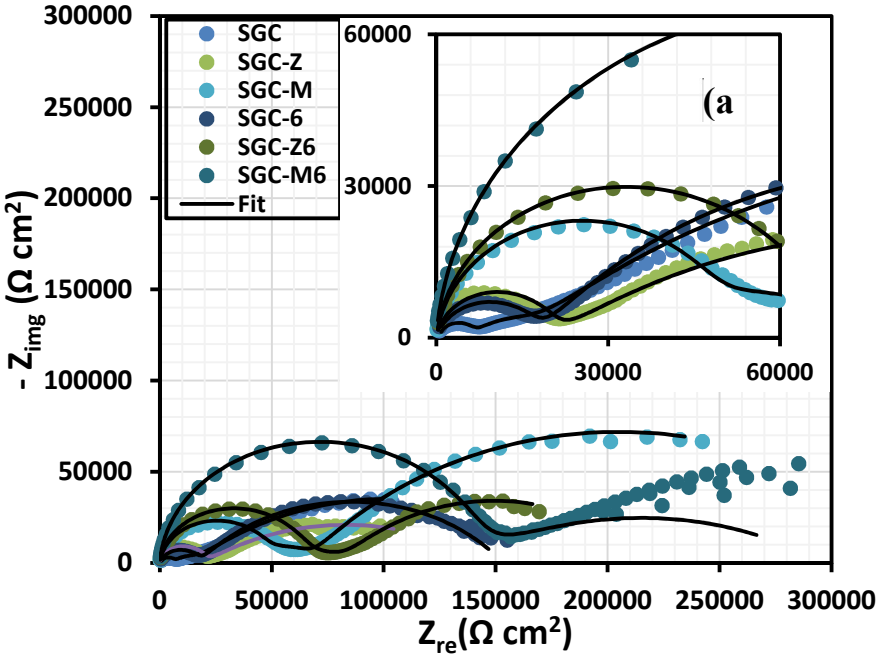
SGC
SGC-Z
SGC-M
SGC-6
SGC-Z6
SGC-M6
Fit
(a
- Z_img (Ω cm²)
Z_re(Ω cm²)
0
50000
100000
150000
200000
250000
300000
30000
60000

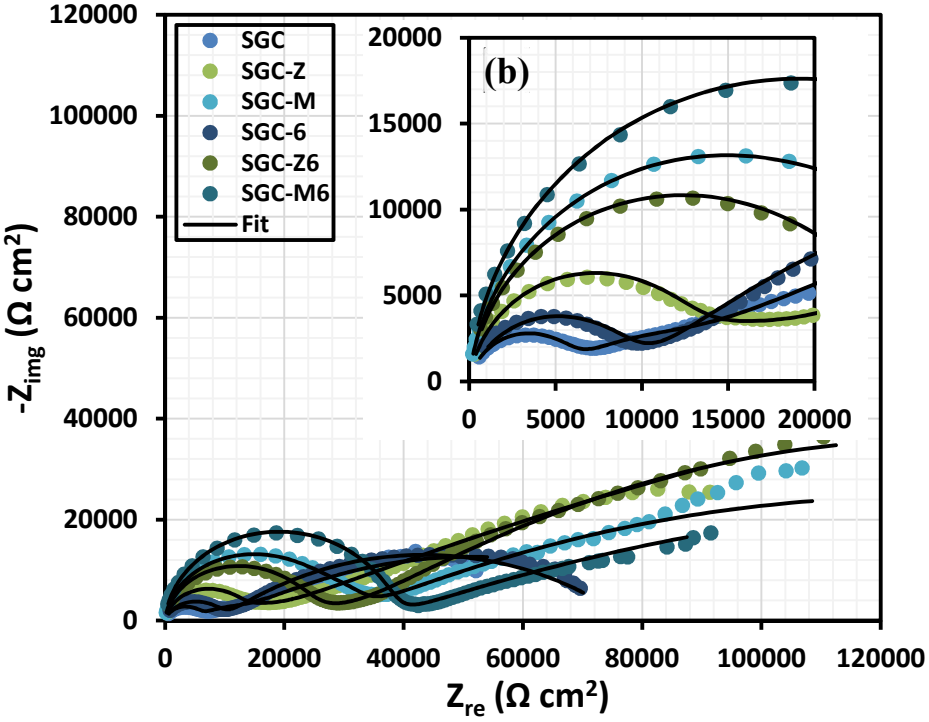
SGC
SGC-Z
SGC-M
SGC-6
SGC-Z6
SGC-M6
Fit
(b)
-Z_img (Ω cm²)
Z_re (Ω cm²)
0
20000
40000
60000
80000
100000
120000
5000
10000
15000

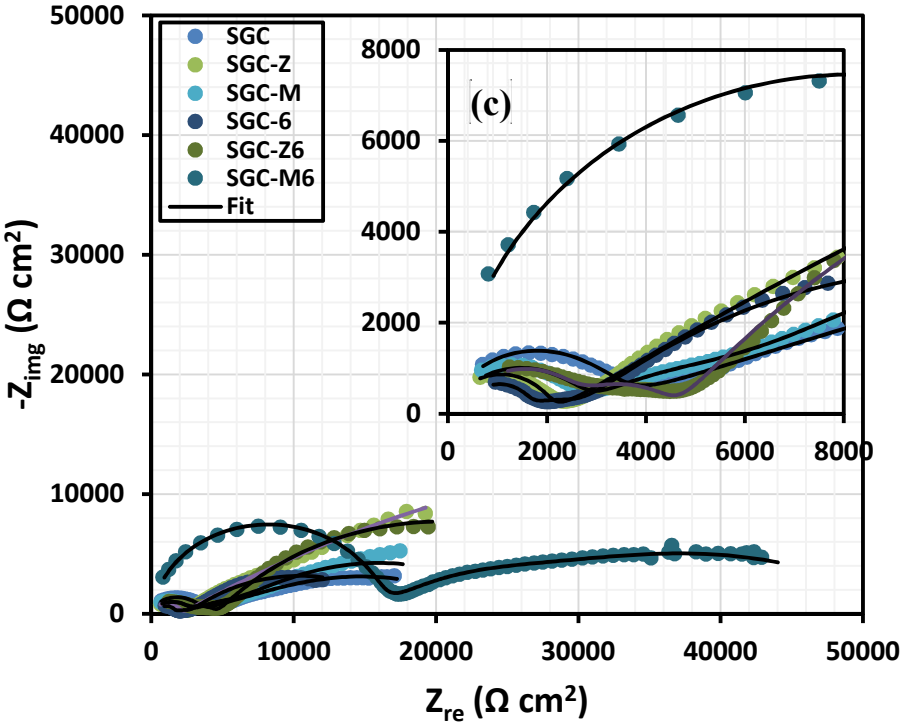

Figure 5.11 Nyquist plot of experimental data for all coating matrices after (a) 24 hours (b) 48 hours, and (c) 2 weeks of immersion in 3.5 wt% NaCl solution (insert: Nyquist curves showing Z values at higher frequencies).

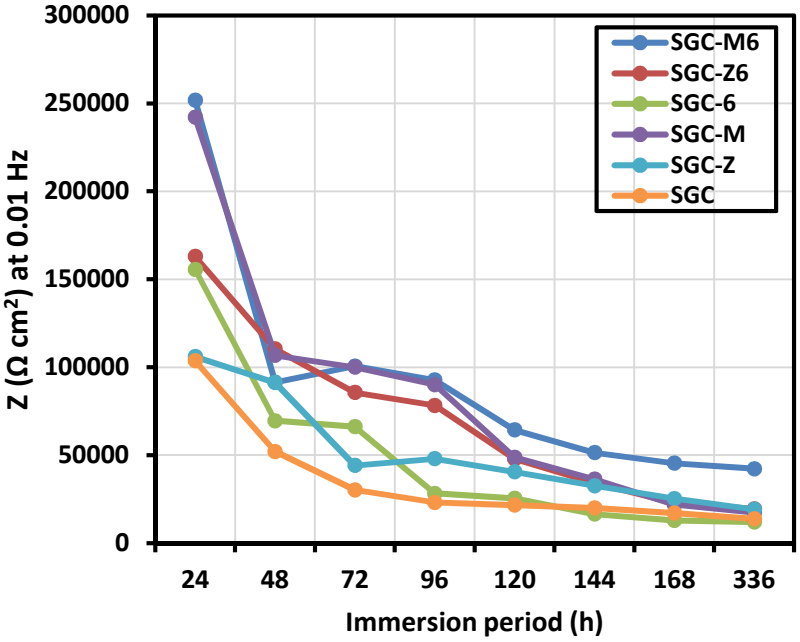

Figure 5.12 Impedance values at 0.01 Hz for all coated samples after 2 weeks of immersion in 3.5 wt% NaCl solution.

A major factor contributing to the performance of metal-type inhibitors in organic coatings is the relative solubility and stability of the inorganic pigments, and their later availability to initiate passive layer formation at the metal/electrolyte interface. These pigments are known to form precipitates of oxide or/and hydroxide passive films depending on the chemistry of the metal/electrolyte interface. The electrochemical behaviour of ZAPP has been previously reported to be linked with its critical pigment volume concentration (CPVC) values of 46.3 against 50 for MOLY [126]. The differences in impedance (Z) indicate that the passage of corrosive ions to the metal surface through the coating was impeded due to an improved interfacial barrier in the presence of these additives. The actual role of the bacteria, as an anticorrosion agent and their effect on the solubility and kinetic availability of the metal inhibitors, is currently not clear. In order to begin to assess the role of the bacteria it is necessary to determine their behaviour in the system, and in particular whether they form a biofilm and /or metabolic products by these endospores that may influence corrosion, for example by reducing the passage of water and other corrosive ions across the metal/coating interface. However, it is evident in this work that the accumulation of these bacterial endospores increases the surface hydrophobicity, so this further impeded the ionic current flow of corrosive species across the biotic coating, thereby reducing corrosion. Figure 5.12 presents the variation of electrochemical impedance (*Z*), with immersion period, measured at 0.01 Hz. Here the MOLY/bacteria coating shows a higher level of corrosion protection compared to the other coating systems at the 2 week interval. Overall the other biotic coatings also show slightly higher resistance over the same period.

Echem software is employed in experimental impedance data to the equivalent circuits shown in Figure 5.13, and the electrochemical parameters derived for the immersion periods under study have been plotted in Figure 5.13. Two-time and three-time constant equivalent circuit models are allotted to respective coating matrices for the fitting and analyzing of the experimental impedance data, with each model selected based on the respective contributions of coating systems at a particular immersion period. Multiple component circuitry with three-time constant (Figure 5.13b) is proposed for the doped or modified coating at prolonged immersion time (between 72 and 336 days). For both equivalent circuit models, the resistance and constant phase element components of each sol-gel (R_{coat} and CPE_{coat}) and interfacial (R_{ct} and CPE_{dl}) layers are being considered, at higher and lower frequencies, respectively. The second constant phase for the equivalent circuit model in Figure 5.13b represents the oxide layer (R_{ox} and CPE_{ox}). However, in this study, only the trends in R and CPE values corresponding to the first constant phase, being the sol-gel layer, are vividly discussed in a view to showing the direct impact each sol-gel layer on the corrosion protection of the metal substrate in 3.5 wt% NaCl. CPE is usually defined as $CPE = (j\omega)^{-n}/Y_o$; where n, Y_o and ω are the magnitudes of system homogeneity factor, pseudo-capacitance and angular frequency (measured in radian). The CPE components in the circuits relate to a slight deviation of the capacitance from ideality, probably due to a combination of the double layer capacitance, non-homogeneity of electrode surface and inherent pores in the coating.

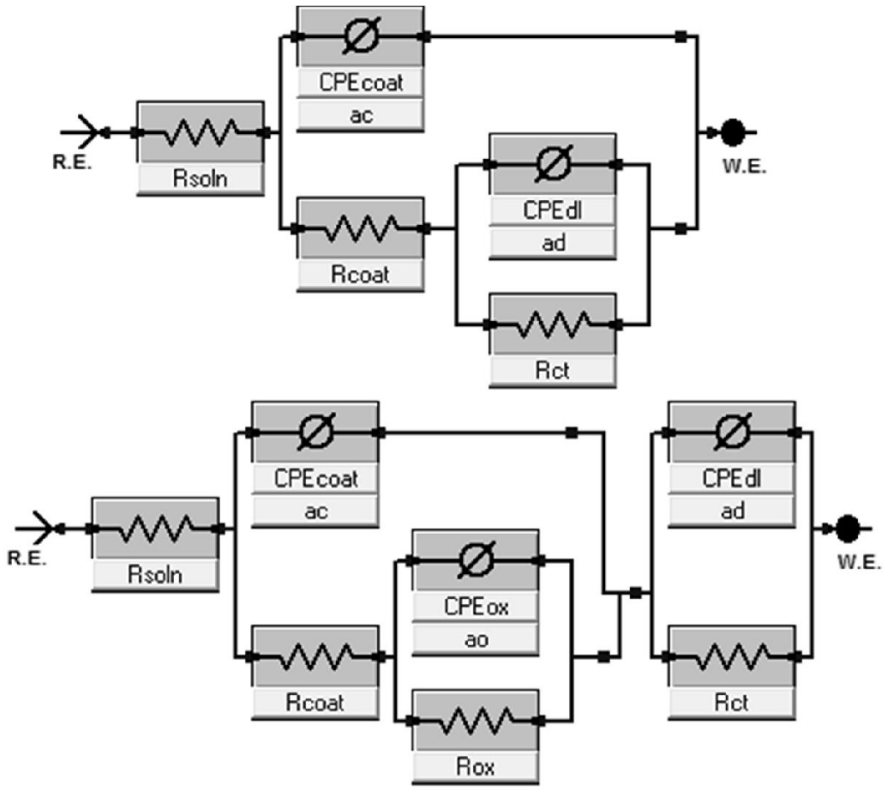

Figure 5.13 Equivalent circuit models used in fitting experimental data by Simplex method; adopted from Garmy EChem Analyst software's model editor.

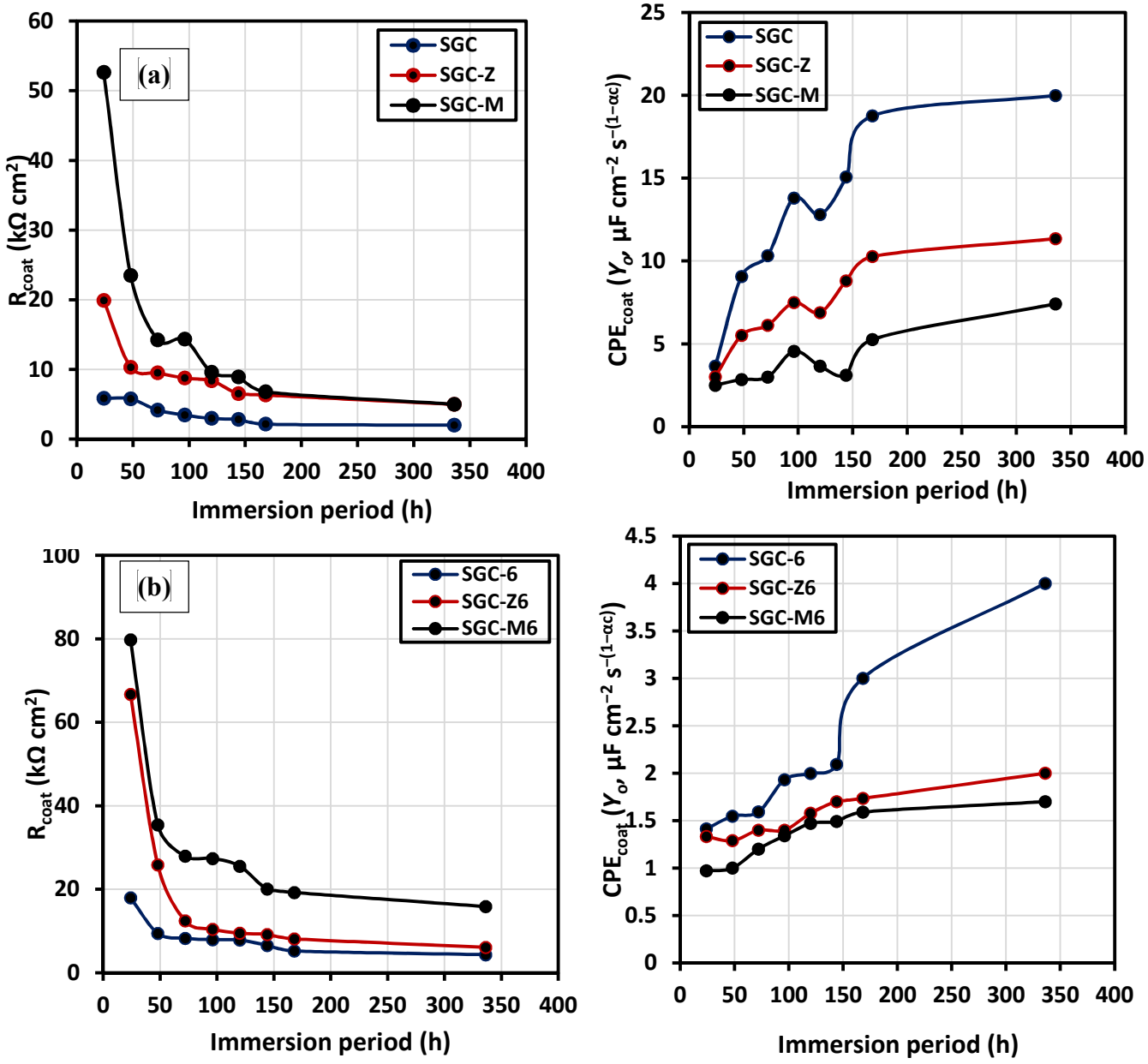

Figure 5.14 Variation in sol-gel resistances and capacitances with immersion period for abiotic (a) and biotic (b) sol-gel coatings in 3.5 wt% NaCl.

Figure 5.14 displays the changes in the values of R_{coat} and CPE_{coat} with immersion periods for the sol-gel layer of the abiotic (a) and biotic (b) coatings as proposed in the equivalent circuit models. The values of R_{coat} for SGC, SGC-Z and SGC-M are 5.6, 19.9 and 52.6 kΩ cm^2, respectively, at the first day (24 hours) of immersion in 3.5 wt% NaCl solution, magnitude of which decreases steadily with exposure time with 5 kΩ cm^2 recorded for the SGC-Z and SGC-M after two weeks (336 days). The reduction in the values of R_{coat} indicates degradation of coating for SGC, while the leaching of inhibitor pigments from the bulk of modified matrices (SGC-Z and SGC-M) occurs as the corrosive electrolyte ions reach through the sol-gel layer via created pores inherent the coatings as they gradually deteriorates in NaCl. In the same vain for the biotic coating, values of R_{coat} are found to decrease sharply between the 24th and 48th hours, and varies slightly between the third (72 h) and the seventh (168 h) day. The recorded values of R_{coat}, as presented in Figure 5.14 b, for the biotic coating are greater than the abiotic coating. At 24 hours of immersion, 17.9, 66.7 and 79.8 kΩ cm^2 are recorded for SGC-6, SGC-Z6 and SGC-M6, respectively, while magnitudes of 6.0, 6.1 and 15.9 kΩ cm^2 are observed for this same set of coatings after two weeks of immersion in 3.5% NaCl solution. The inherent pores and micro-cracks in the respective sol-gel silica networks allow for free pathways for water and corrosive ions to the surface of the metal substrate, and this could be reason for the steady decrease in the magnitude of sol-gel resistance. The biotic coatings functionalised with inhibitors (SGC-Z6 and SGC-M6) possess a double layer structure, and their greater coating resistance properties compared to the abiotic coating could be attributed to their increased multi-layered hydrophobic interface properties after endospore encapsulation. Generally, the interfacial electrolyte/water absorption (or simply water

ability) and bulk coating degradation are hugely defined by the magnitude of coating capacitance. Figure 5.14 (right panel) displays the variation in the values CPE_{coat} (measured in μF cm^{-2} $s^{-(1-\alpha c)}$) with immersion periods for the abiotic (a) and biotic (b) coatings. For both sets of coatings, abiotic and biotic, higher values of CPE_{coat} are recorded for less protective coating matrices representing high rate of water uptake as the exposure time of the coating increases. Magnitude of CPE_{coat} for biotic coating are lesser than their abiotic counterpart for all the immersion periods in this study, and CPE_{coat} for both sets of coatings are observed to steadily increase with immersion period. For the biotic coating, values of CPE_{coat} are ranged between 0.97 to 1.4 μF cm^{-2} $s^{-(1-\alpha c)}$ and 1.7 to 4.0 μF cm^{-2} $s^{-(1-\alpha c)}$ for the first day and second week of immersion; and between 2.8 to 9.1 μF cm^{-2} $s^{-(1-\alpha c)}$ and 7.4 to 19.9 μF cm^{-2} $s^{-(1-\alpha c)}$ for the abiotic coating for the same period. Poor water uptake ability of a coating denotes greater protective strength against corrosion, and the sol-gel coating encapsulated with the *B. licheniformis* endospores have shown greater corrosion inhibition in this order: SGC-M6 > SGC-Z6 > SGC-6. The coating homogeneity factor of each coating did not vary much for each coating (around 0.9) while the magnitude of the *"goodness of fit"* for the fitted experimental data were less than 10^{-3}. Similar trend was obtained for the magnitudes of the charge transfer resistance and capacitance of the double layer (not shown).

5.3.5 Surface analysis

Representative SEM micrographs for both abiotic and biotic systems, before and after immersion in 3.5 wt% NaCl ae displayed in Figure 5.15 (A and B). The sol-gel coating morphology is characterized by the presence of non-uniformly finely dispersed colloidal silica particles in the matrix (labelled with black bold arrows). After 2 week

immersion in 3.5 wt% NaCl, non-uniform cracks are observed for the abiotic (SGC) coating; this is reflected in the recorded decreased *Z* values after prolonged immersion. There are visible cracks of the surface of these coating after 2 weeks immersion in 3.5 wt% NaCl. The cause of cracks and other mechanical faults (labelled with blue dashed arrows) observed on the coated metals after prolonged immersion could be linked with the electrolyte, as well as failed adhesion [127]. The presence of surface micro-cracks leads to passage of the corrosive electrolyte to the steel and consequently localised corrosion takes place. However, the presence of the *Bacillus* endospores greatly improved the corrosion inhibition of the coating in combination with the metal inhibitors. The MOLY functionalized endospore loaded coating had fewer cracks in comparison with other coatings after 2 weeks immersion in the saline solution; the delaminated portion observed on the SGC-6 could be attributed to adhesion failure (Figure 5.15B). There was no noticeable damage on the bioactive coating system after immersion at room temperature in the aggressive saline test solution. This demonstrates a significant corrosion protection in the presence of the bacterial endospores compared to the abiotic coating. The presence of zinc and molybdate ions from the inhibitor pigments have been confirmed using EDX. The composition of these pigments obtained from EDX analysis were mainly Si (65.0%), Zn (0.9%) and Mo (0.9%) for SM and Si (38.2%), Zn (7.6%) for SZ (see Figure 5.16). This further proves that the incorporation of these inhibitor pigments into the bulk of coating was successful. Mousavifard *et al.* [126] have reported formation of passive films in the present of Zn^{+2} ions from ZAPP/ZAP inhibitors as the reason for the reduction in metal corrosion. The dissociated Zn^{2+} prevents the formation of excess OH^{-} ions (Equation 5.2) and other associated cathodic reactions at the metal/coating interface; this

could be typical of zinc aluminium polyphosphate (ZAPP) and zinc molybdate (MOLY) inhibitors, pigments with common Zn^{+2} cation. $Zn^{2+} + 2OH^{-} \rightarrow Zn(OH)_2\downarrow$

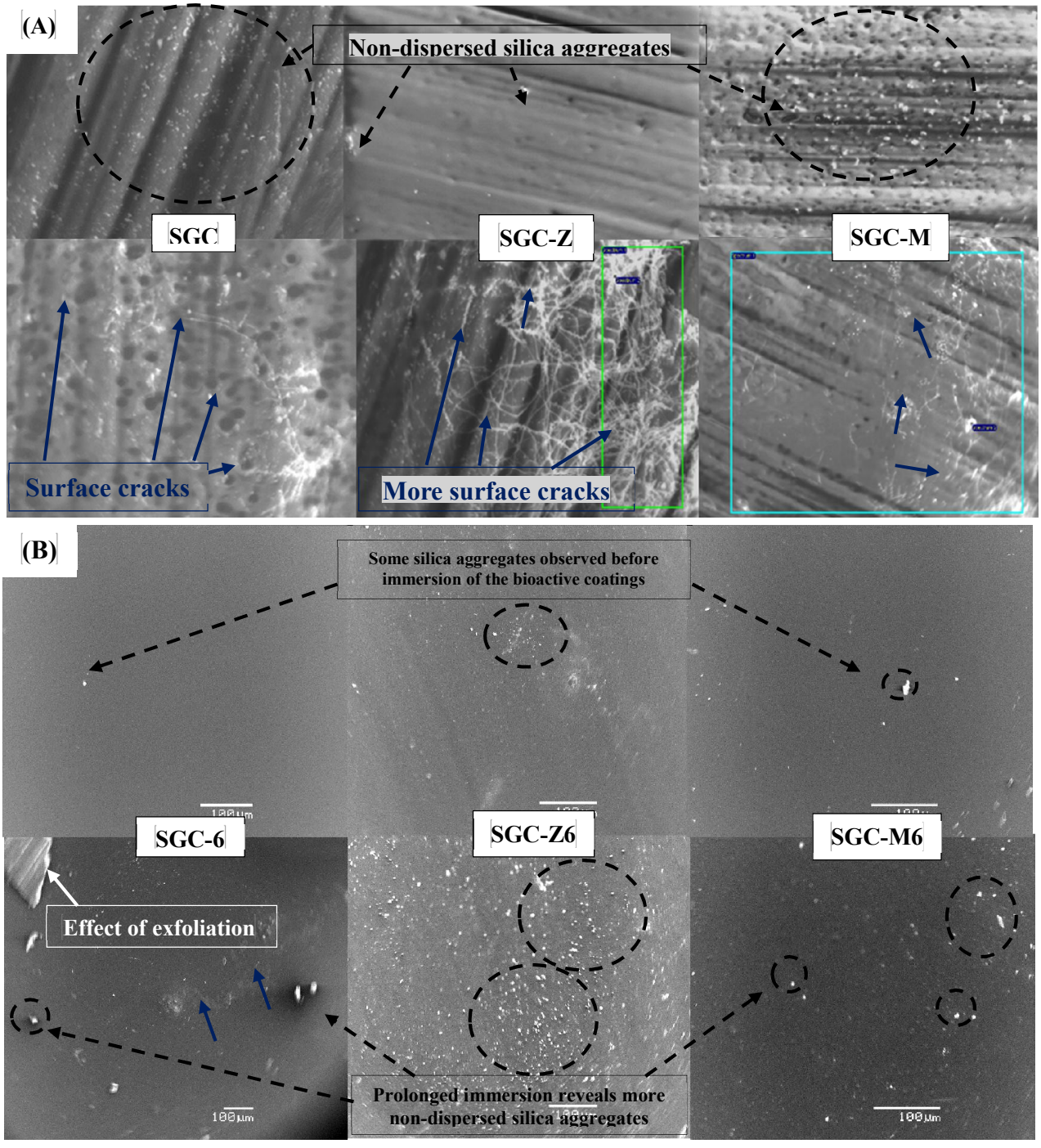

Figure 5.15 SEM micrographs of (A) biotic and (B) sol-gel coated steel coupons before (the above panel) and after (the below panel) 2 weeks immersion in 3.5 wt% NaCl solution at room temperature [blue and black (dashed) bolded arrows show surface cracks and gel particles, respectively, on the coated substrates].

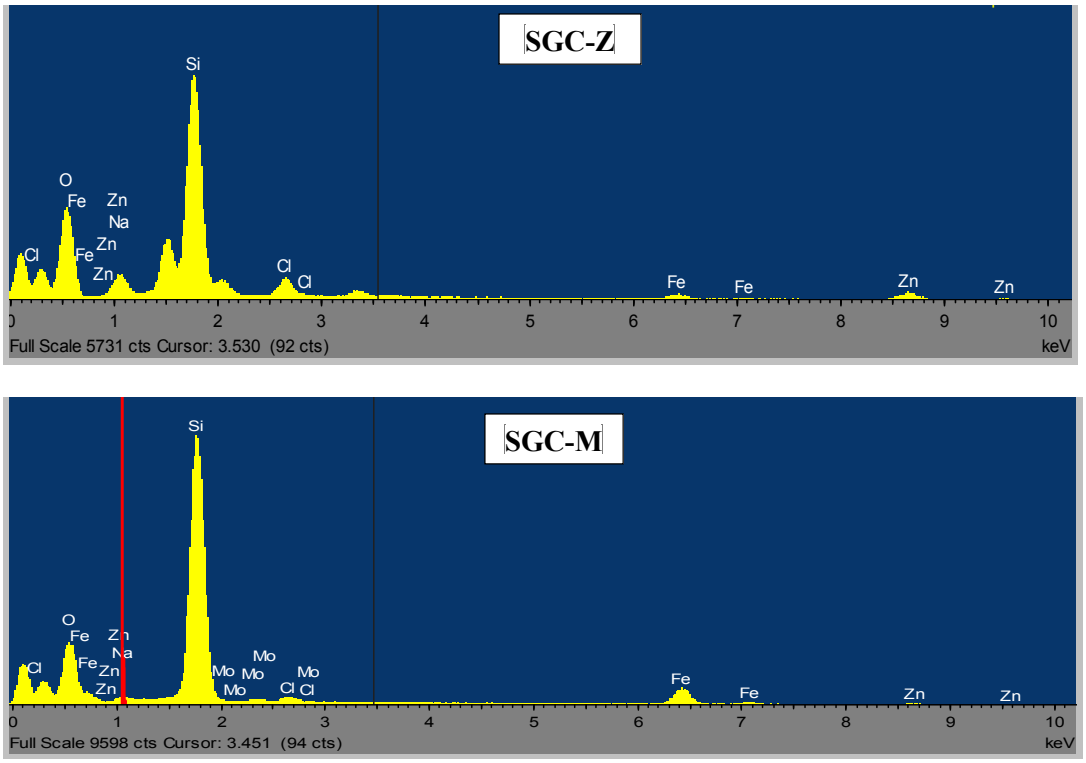

Figure 5.16 EDX: Elemental composition of SZ and SM sol-gel matrices.

5.3.6 Field trial in the marine environment

Labelled coated steel panels were submerged continuously in a natural marine environment in order to study the anticorrosive/antifouling properties of these coatings at KFUPM beach, Half Moon bay in Saudi Arabia for 12 weeks. The flow of seawater in the Eastern Province of Saudi Arabia is minimal and known for its marine macro-fouling activities and high salinity, a trait of all Gulf sea tributaries in the Sahara. For half-moon Bay (KFUPM Beach), the measured salinity values stood at 65.8─71.2 ppt between March and July 2015; this body of water could be classified as being "*hyperhaline*". Prior to sample immersion, the edges of the panels were covered with insulating tape to prevent corrosion and other oxidation processes, and also to ensure that only the indeed the test area of each substratum was submerged. Evidence of macrofouling by attachment of foulants are observed by visual inspection. Figure 5.17 shows the appearance of the

various (A) abiotic and (B) biotic coated panels, in duplicates, after every two week interval for ten weeks. An instant corrosion of the bare steel panel is observed immediately after immersion of the panels in the sea water, but not on the coated samples. Both the abiotic and the biotic sol-gel coated samples gradually decolorized and appeared dull on prolonged exposure in the saline sea water. Images collected for both sets of coatings during the earlier weeks proved that it was too early to assess corrosion and fouling phenomena. Normally for some biofouling organisms, their initial settlement on any substratum is highly influenced by the surface chemistry and topology, nutrient availability and rheology/hydrodynamics; environmental factors of which subsequent fouling population dynamics and community structure are being affected.

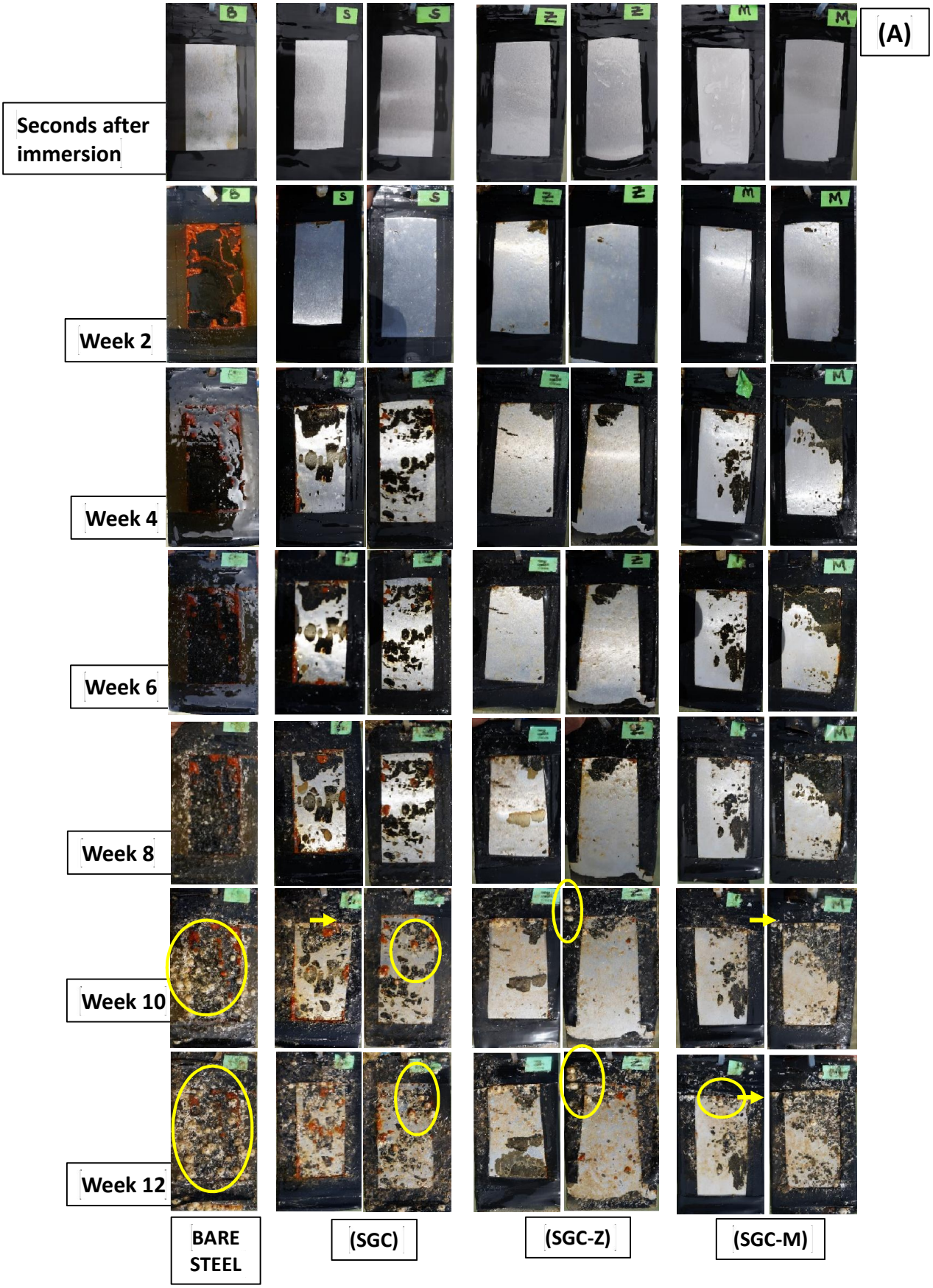
(A)
Seconds after immersion
Week 2
Week 4
Week 6
Week 8
Week 10
Week 12
BARE STEEL
(SGC)
(SGC-Z)
(SGC-M)

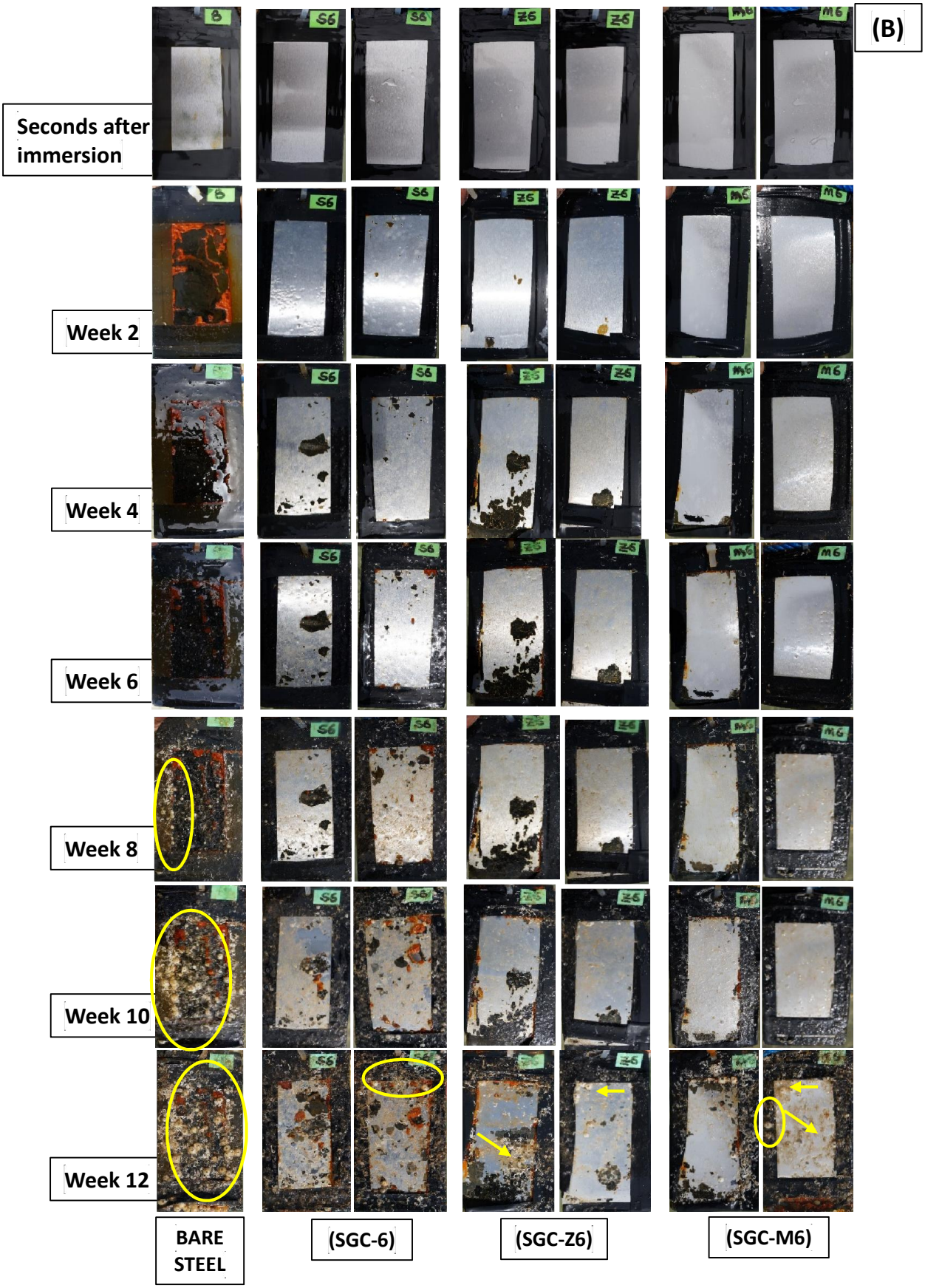

Figure 5.17 Field trial samples in duplicates: (A) Abiotic and (B) Biotic coated steel panels compared with bare/uncoated steel.

Images of the abiotic coated panels in Figure 5.17 (A) display episodes of surface pitting observed on the sol-gel coatings after two week, and this developed into severe delamination of the coatings in the proceeding weeks as fouling increases. The observed surface delamination must also have been initiated by the physical contact of the coated surfaces with sea debris (not limited to sand grains, sticks and stones) inherent in the flowing sea water which is typical of KFUPM beach. Among abiotic samples, the coating with ZAPP pigments (SGC-Z) seems to retain a relatively clear surface appearance throughout the period of study, yet the coating failed at the 8th week; both inhibitor-modified coatings (SGC-Z and SGC-M) demonstrated better anticorrosion behaviour compared to the unmodified coating (SGC) throughout the duration of the field experiment. The properties of these inhibitor (pigment)-doped coatings could be attributed to the stability of chemical species that acted as passive films thereby impeding anodic and/or cathodic reactions at the metal/solution interface. Pigment types and their product solubility, as well as their stability determines the possibility of bulk leaching from the coating. At the 8th week, newly metamorphosed juvenile barnacles are observed on the delaminated sections of the coated steel panels which later developed into full-grown hard-shelled barnacle after at the 10 and 12th weeks; they are also attached on the black insulating tape covering the edge (circles and arrows). A comparative attempt to understand the effect of inoculums of protective thermophilic strain of *B. licheniformis* endospores on the antifouling as well as the anticorrosive of this sol-gel type coating of steel has been evaluated in the same marine condition with those of the abiotic coatings. Figure 5.17 (B) presents duplicates photodigital images after ten weeks immersion for the biotic coated steel panels compared with bare/uncoated steel. The congested fouling

population on the bare steel reveals an assemblage of annelid-type polychaetes and large growing hard-shelled barnacles vivid between the 6th and 10th weeks; barnacles appear as newly metamorphosed juveniles after the 4th week. The integrity of the biotic coatings is still intact compared to their abiotic counterpart in terms of corrosion and surface pitting; surface delamination is pronounced only after the 4th week. For the biotic coating without inhibitors (SGC-6), biofouling is only vividly observed at the 12th weeks, with the endospore-loaded coatings with inhibitor (SGC-Z6 and SGC-M6) having improved antifouling and anticorrosion properties. At the 10th week, it is evident that the biotic coating demonstrated the best corrosion/fouling resistance compared to the abiotic coating. In all, the assessment of marine fouling results reveals that the protective bacterial endospores encapsulated into the sol-gel coatings demonstrate potential for antifouling activity and corrosion protection within the duration and conditions of study. The reason for the antifouling potential of these bioactive coatings could be linked with their antibiotic-type hydrophobic surfaces due to the accumulation of *B. licheniformis* endospores widely reported to secrete antimicrobial γ-polyglutamate from their biofilms [122,124,125]. The antifouling properties of these coating matrices could be further improved and made longer-lasting by varying the density of the *B. licheniformis* endospores in the coating, moderating the curing period of the coating on the steel and by optimizing other surface post-treatment procedures.

5.4 Summary

The following conclusions are drawn from the trend of experimental results:

1. The unmodified sol-gel coating synthesized in this work has protected mild against corrosion to a great extent in 3.5 wt% NaCl solution; but improved protection was realised after doping with two zinc-based corrosion inhibitor pigments and *B. licheniformis* endospores.
2. Thermophilic strain of *B. licheniformis* endospores isolated from the Gazan hot springs of Saudi Arabia encapsulated within the sol-gel matrix remained viable as revealed by the confocal laser scanning fluorescence microscopy. The presence of these bacterial endospores improved the surface hydrophobicity of the coating thereby preventing the diffusion of corrosion molecules and ions through the bulk of the coating to the metal surface; this is evident in the trend of electrochemical coating resistance and capacitance.
3. SEM micrographs shows no noticeable damage for the endospores–loaded sol-gel coatings after 2 weeks immersion at room temperature in 3.5 wt% NaCl solution, and this demonstrates significant corrosion protection in the presence of the bacterial endospores compared to the abiotic coatings. The poor performance of the inhibitor-loaded coating could be ascribed to the presence of micro-cracks within the coating.
4. The bacterial endospores possess antifouling potentials within the immersion period of study due to their foul-releasing effect; the improved corrosion and fouling resistance in the presence of these bacterial endospores could be attributed to surface hydrophobicity after spore encapsulation. Compared with the abiotic coating, the

inability of the marine foulers to settle and adhere on this biotic surface, at hypersaline condition (65.8─71.2 ppt), gives an idea of its antibiotic nature and the antimicrobial properties of the biofilm of this unique thermophilic bacterium.

5. The anticorrosion/antifouling properties of this sol-gel matrix could also be attributed to the presence of PDMS in the bulk of the matrix, offering the needed rigidity and strength to the silica network. However, the presence of aminopropylmethylsiloxane)-dimethylsiloxane copolymer in the sol-gel material did not increase the hydrophobicity of the coating without the presence of the bacterial endospores, since increased coating capacitance is observed due to the adsorption of water and corrosive ions/ molecule across the protective coating on prolonged immersion period. To solve this problem, a more careful choice of monomer precursor is needed; and the new goal should involve the synthesis of a hydrophobic sol-gel with low surface energy capable of prolong protection of mild steel by using appropriate silane monomer from the start (not a copolymer). The synthesized protective sol-gel coating should possess high water repellency (high water contact angle) even after modification with the surface active zinc-based corrosion inhibitor pigments and bacterial endospores. Fouling results of the test coatings should be compared to a typical industrial antifouling/anticorrosive coatings used in the field (oil or marine).

CHAPTER 6

Title: Enhancing water repellency for prolonged anticorrosion and antifouling applications for a new hydrophobic silica coating for mild steel

6.1 A brief overview

Chemical and engineered hydrophobic surfaces have numerous applications in various scientific fields. Table 6.1 presents some of the physical and chemical modification processes employed in achieving surfaces with this unique property. The resistance to the passage of water (and molecular oxygen in some cases) by these hydrophobic coating surfaces initiate corrosion protection since the cathodic reactions associated with these corrosive species are impeded. Such protective surfaces are designed to mimic the "lotus effect" possessed by leaves of Lotus (*Nelumbo* family) due to their high contact angles (θ_w) [128─130]. Sol–gel process remains the preferred route for the synthesis of protective coatings with hydrophobic surfaces since its reaction routes are tunable, the precursors are abundant with unique chemical properties and sol-gel products synthesized possess surface and bulk properties of a typical anticorrosive coating: self-cleaning abilities, reduced sliding angle, wettability, interfacial surface energies (surface properties); rigidity, scratch resistance, roughness, transparency (bulk properties) [131]. In the present work, a sol-gel route for synthesizing a low surface energy silica material with very hydrophobic surface (θ_w>100^o) is introduced using a hydrophobic precursor capable of ascribing reduced surface wetness to the final coating due to the presence of low alkyl groups on the monomer molecule. To keep the bulk properties of this protective sol-gel coating intact, it

will be further functionalized with anticorrosive pigments acting in dual positions as pore/crack fillers as well as corrosion inhibitors in the bulk of the coating. The following objectives will be carried: (1) the testing of the anticorrosion properties this silica coating synthesized from simple silane precursors from the start; also modified with zinc aluminium polyphosphate and zinc molybdate for prolonged steel protection (up to a month) in 3.5 wt% NaCl; (2) the evaluation of the antifouling properties of this silica coating encapsulated with *B. licheniformis* endospores in an hypersaline marine environment after prolonged immersion (up to 14 weeks).

Table 6.1 Physical and chemical modification processes employed in achieving surface hydrophobicity.

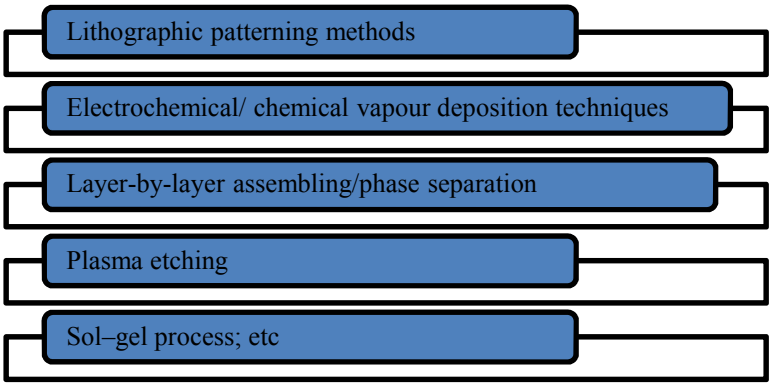

6.2 Experimental

6.2.1 Materials and preparation of hybrid coatings

Analytical-grade isopropyl alcohol (IPA) and the silane precursors were purchased from Sigma-Aldrich (US), and were used without further purification. The silane precursors (Sigma-Aldrich, US) include a tetrafunctional alkoxide, tetraethoxysilane (TEOS), 3-glycidoxypropyltrimethoxysilane (GPTMS) and dimethoxymethyl octadecylsilane (DMODS) with chemical structures shown in Figure 6.1. Inhibitor

pigments, Heucophos® *ZAPP* (white powder, zinc aluminium polyphosphate) and MOLY-white 101 (pale yellow powder, $CaZnMoO_4$) were purchased from Heucotech Ltd. Co. (US). A colloidal sol was formed from the hydrolysis of TEOS, GPTMS and DMODS in the ratio of 3:2:3 with distilled water (1 ml) stirred at room temperature at 750 rpm. Prior to this, the mixture of the precursors in the aforementioned volume ratio was pre-stirred for 30 minutes before adding the mixture of 0.25 ml 0.05 M HNO_3 (Sigma-Aldrich, US) and 1 ml Isopropyl alcohol (IPA) and water dropwise in order to avoid a fast gelation of the colloidal sol. The sol-gel mixture obtained was clear and viscous after few hours, and was left to stir overnight before modification (Figure 6.2).

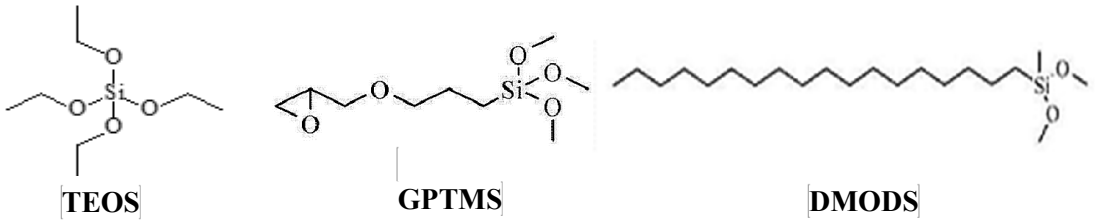

Figure 6.1. Molecular structures of the silane precursors (with its long alkyl organic chain, DMODS is a typical surface reactive molecule for LSE modifications in sol-gel coating illustrated in this study).

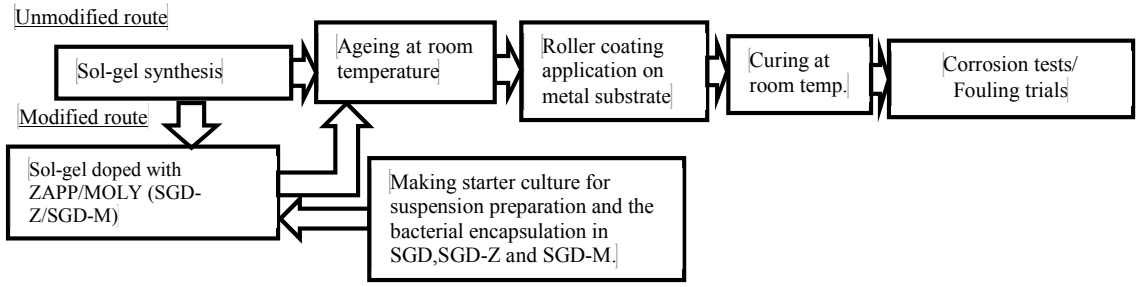

Figure 6.2 Summarized process scheme and routes for the pigment-modified and unmodified coating matrices on mild steel electrodes adopted in this study.

The resultant sol remained quite stable at 72 hours and was labelled “SGD” with a pH value of 3.0. This carefully chosen amount of water was employed as the source of hydrolysis to convert the ethoxy and methoxy groups of the silanes to their corresponding silanol groups to be monitored with NMR. Also, the volume of DMODS in excess of 1.5

ml in the presence of water precipitates colloidal silica making coating procedure impossible; 1.5 ml MTES was added for the coating used for the filed trial in order to stabilize the matrix. To 5 ml as-prepared sol-gel mixture, 2.5% w/v Heucophos® ZAPP and MOLY-white 101 anticorrosive pigments were added separately, and stirred for 30 minutes after an hour sonication (Vibra-Cell Sonics and Material INC., US). The doped-sol-gel hybrid systems were labelled SGD-Z and SGD-M, respectively, for ZAPP and MOLY inhibitors. After preparation of the bacterial endospore suspension and the concentration measured in CFU/ml (with the same method explained in Section 5.2.3), 1 ml aliquot was added to 10 mL sol-gel mixture, stirred and labelled as biotic (SGD-6). This was repeated with inhibitor functionalized sol-gel coating, ZAPP and MOLY, respectively (then labelled accordingly; SGD-Z6 and SGD-M6). The descriptive summary of the biotic and abiotic sol-gel coating matrices used in this study is similar to the one presented in Table 5.1.

6.2.2 Spectroscopic characterization and coating procedure

Before modification and finally coating in mild steel substrate, the sol-gel reaction route was probed by ^{13}C and ^{1}H NMR spectroscopy (in $CDCl_3$) using a JEOL JNM-LA500 FT NMR spectrometer (JEOL Co. Ltd., Akishima, Japan) as well as FTIR (Nicolet 6700 Fourier Transform (FT) Spectrometer (Thermo Electron Corporation, UK). The biotic and abiotic sol-gel solutions were neatly coated on mild steel substrate using a roller-coating technique (RK Print-Coat Instruments Ltd, UK) after pre-cleaning with the method periodically explained in Section 5.2.5 before curing at room temperature for 72 hours.

6.2.3 Fluorescence microscopy, TGA and contact angle measurement

The procedure of evaluating the viability of the *B. licheniformis* endospores have already been explained in Section 5.2.4 using Zeiss AxioVision confocal scanning laser microscope after staining the cells with BacLight™ Live/Dead kit. The thermal behavior of the synthesized sol-gel matrix was studied by thermogravimetry (TG) and differential TG (Perkin-Elmer TGA 7, US) at a heating rate of 10 ^{o}C min^{-1} from room temperature through to 800 ^{o}C under a nitrogen atmosphere. CAM Instrument DSA30 (KRUSS, Deutsch, Germany) was used in evaluating the water contact angle (θ_w) by static water drop method, and the results presented in this study are mean values of three trails collected at relatively closed locations on the individual films on steel. The mean and standard deviation of the results were computed with one-way Analysis of Variance (ANOVA) statistical technique, and the confidence limit was placed at 95%.

6.2.4 Scanning Electron Microscopy (SEM) and electrochemical measurements

SEM was conducted on the coated films using a U9320A 8500 Field Emission Scanning Electron Microscope (Agilent Technology, UK) instrument, operating at 15-20 kV for both surface and cross section morphologies of the coated films on mild steel surface before and after a month immersion in 3.5 wt% NaCl test solution. Electrochemical impedance experiments were carried out for all coated mild steel samples immersed in 3.5 wt% NaCl using a Reference 3000^{TM} High performance potentiostat/Galvanostat/ZRA electrochemical workstation (Gamry Instruments, US) with EChem Analyst for data analysis. The coated mild steel electrodes served as the working electrode with a 1 cm^2 geometric area in the solution of the saline electrolyte, while saturated calomel electrode

and cylindrical graphite rods were used as the reference and counter electrodes, respectively in a PTC1 Paint Test Cell. The selected test frequency range for the electrochemical impedance spectroscopy (EIS) was between 10 mHz to 100 kHz with a 10 mV excitation amplitude.

6.2.5 Field trials at KFUPM beach

A similar method previously explained in Section 5.2.8 was employed for the field trial of each coated panels, with and without the bacterial endospores, at KFUPM beach for 14 week of continuous immersion. The parameters of the seawater taken throughout the period of fouling study are presented in Table 6.2.

Table 6.2 Mean values of seawater parameters at KFUPM Beach (at the point of sample immersion) recorded throughout the 14 weeks of fouling studies.

Days	Temperature (°C)	pH	Salinity (ppt)
Day of immersion	27.7 ±0.3	7.8±0.5	69.8±1.4
Week 2	26.2±0.5	7.6±0.4	67.0±1.2
Week 4	29.8±0.6	7.5±0.6	68.2±0.8
Week 6	25.8 ±0.5	7.5±0.6	72.0±0.5
Week 8	28.3±0.3	7.8±0.4	69.2±1.3
Week 10	31.4±0.4	7.5±0.4	71.2±0.4
Week 12	28.0±0.2	7.4±0.3	73.2±1.6
Week 14	31.0±0.2	7.3±0.3	75.2±0.8

6.3 Results and discussion

6.3.1 NMR/FTIR: Sol-gel route

The presence of the electronegative ethoxy and methoxy groups on TEOS and GPTMS, respectively, brought about reactive sites to nucleophilic attack with water, hence increasing the rate of hydrolysis of the sol-gel process. In the mild acidic medium (0.05 M HNO_3), the prepared colloid contained some partially hydrolyzed precursors that could

further improve surface adhesion on the chosen substrate [132,133]. As the hydrolysis-condensation reactions proceeded, the amount of DMODS in excess of 1.5 ml in the acidic mixture precipitated colloidal silica particles. However, and to avoid this, a minimal amount of water as the source of hydrolysis and IPA (a diluent) were repeatedly stirred together with a milliliter of 0.05 M HNO_3 before initiating the reaction. The resultant liquid product formed overnight was a clear viscous sol with a pH of 3. Portions of this colloidal liquid were modified with ZAPP and MOLY, and were easily coated on pre-cleaned mild steel electrodes and cured. However, before doping, the as-prepared sol-gel matrix was characterized using NMR for possible reaction within the hydrolysable moieties of the alkoxide precursors. The silane precursors were analyzed, and Figure 6.3 displays the proton (a) and ^{13}C (b) NMR for each molecule. Isopropyl alcohol (IPA) dissolved the mixture of the silane precursors to a great extent before the acidic solution (0.05 M HNO_3) catalyzed the hydrolysis reaction and initiated the gelation process. The initial cloudy solution formed was continuously stirred until it was homogeneously clear, then it became more viscous on aging. This colloidal solution was analyzed using liquid-state NMR to ascertain the extent of hydrolysis/acidification of the sol-gel precursors, and at least probe the presence of the non-hydrolysable alkyl moiety from the DMOMS used to provide the required hydrophobicity to the coating matrix. Figure 6.4 shows the ^{1}H (a) and ^{13}C (b) NMR spectra for the sol-gel matrix after 72 hours aging at room temperature, and by direct comparison, these spectra are matched with that of the pure precursors to justify evidence of reaction. The hydrolysis of the methoxy groups on GPTMS and DMOMS was successful, and this is evident in the proton peak shortening/broadening at 3.43 ppm, as well as the disappearance of peaks from protons of the ethoxy group on

TEOS previously found at 1.23 (t) and 3.84 (q) ppm. The proposed sol-gel reaction is displayed in Figure 6.4. The C18 alkyl signature peak is still upheld in the NMR spectrum of the sol-gel matrix as a multiplet at 1.15 ppm (CH_2) as well as the broad peak at 0.56 ppm corresponding to a terminal CH_3 group. This was confirmed with the ^{13}C NMR (Figure 6.5b), with the associated peaks found at 14.3 and 29.6 ppm. Other peaks found on ^{1}H NMR spectrum may be due to water, and other intrinsic secondary hydrolysis/condensation products formed during the sol-gel reaction. The ^{13}C NMR spectrum also displays a reduced carbon peak corresponding to the reduction of the amount of hydrolysable alkoxy groups of TEOS at 57.9 and 18.1 ppm, supporting the previous assertion proposed by the ^{1}H NMR spectrum. The appearance of these peaks, and at 50.2 ppm, though reduced, suggests the presence of partially unhydrolysed methoxy groups from GPTMS or DMOMS or both, absorbed on the silica matrix. Epoxy ring opening reaction accompanying the sol-gel reaction is evident in the reduced carbon peak heights observed at 51.1 and 44.5 ppm for GPTMS at positions 3 and 5, respectively. The broadening of the epoxidic proton peaks at these positions is also an evidence of a ring opening reaction at 2.51, 2.69 and 3.05 ppm, respectively (Figure 6.5 a). ^{13}C NMR also reveals a downfield shift for carbon at position 3, suggesting an S_N2 type reaction with the NO_3^- ion of the acid, and a small resonance at 64.3 ppm characteristic of GPTMS. The additional peak formed between 60 and 70 ppm is indicative of new chemical species, possibly aldehydes, enols or ketones formed from GPTMS [134]. Bogart and Leyden [135] have previously reported that both epoxy/vicinal diols groups are likely present in the bulk of the formed silica at reduced acid pH. The proposed structure of the sol-gel

(SGC) can be observed from the spectroscopic evidence in Figure 6.5 (^{13}C NMR peaks) and 6.7 (Si ennviroment), respectively.

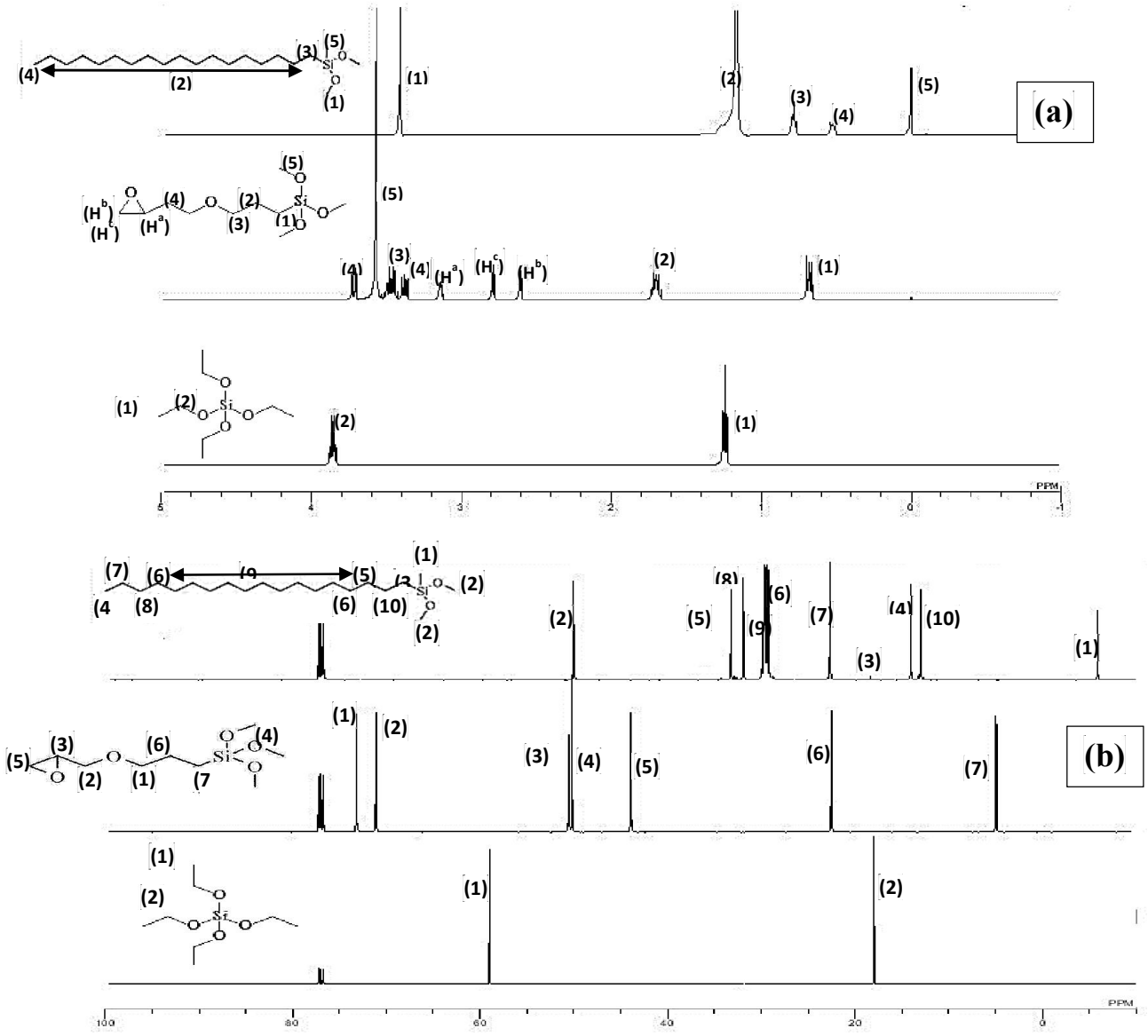

Figure 6.3 ^{1}H (a) and (b) ^{13}C NMR spectra of the precursors (DMODS, GPTMS and TEOS, respectively, from up to bottom) employed in this study (solvent: $CDCl_3$).

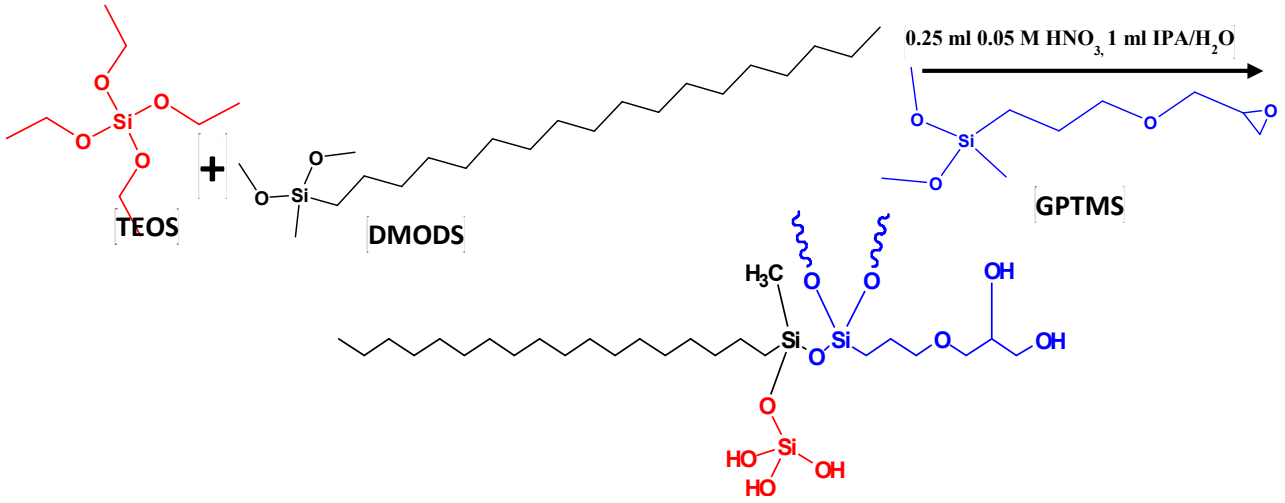

Fgure 6.4 The proposed sol-gel (SGD) reaction

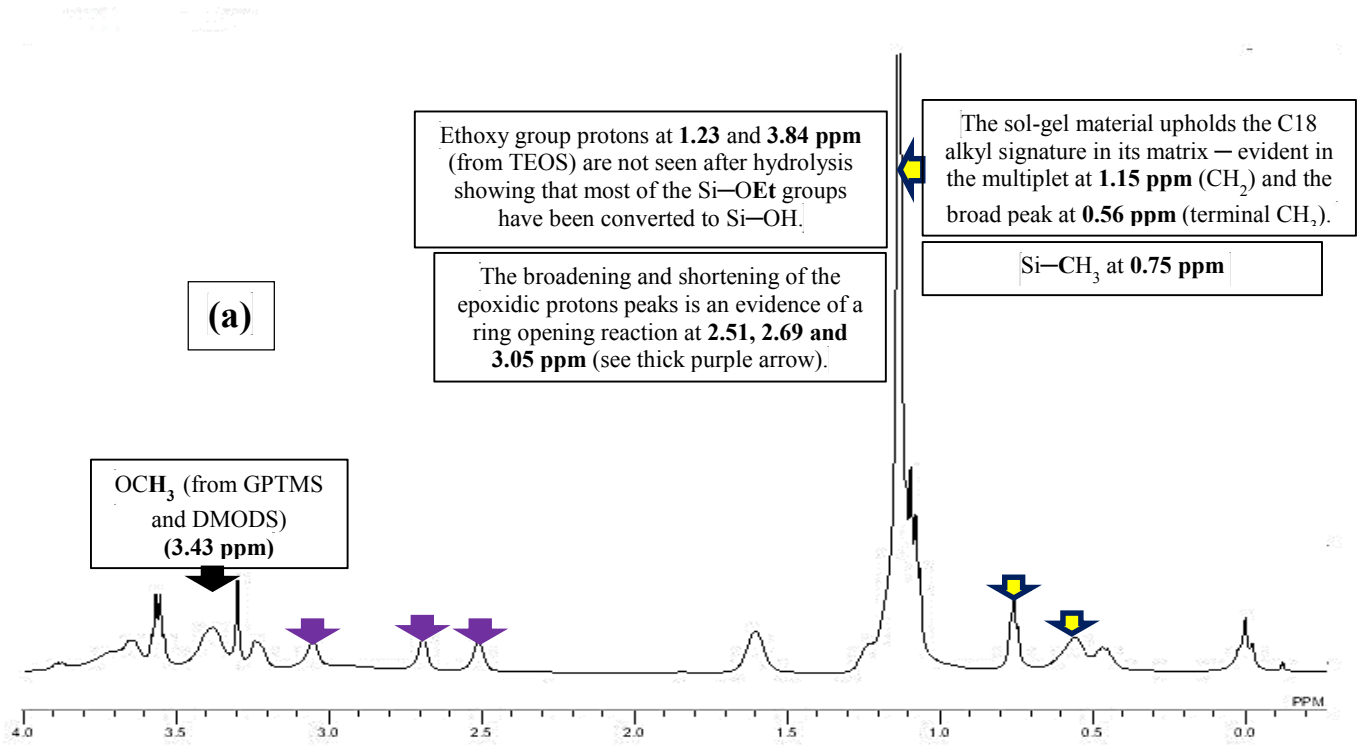

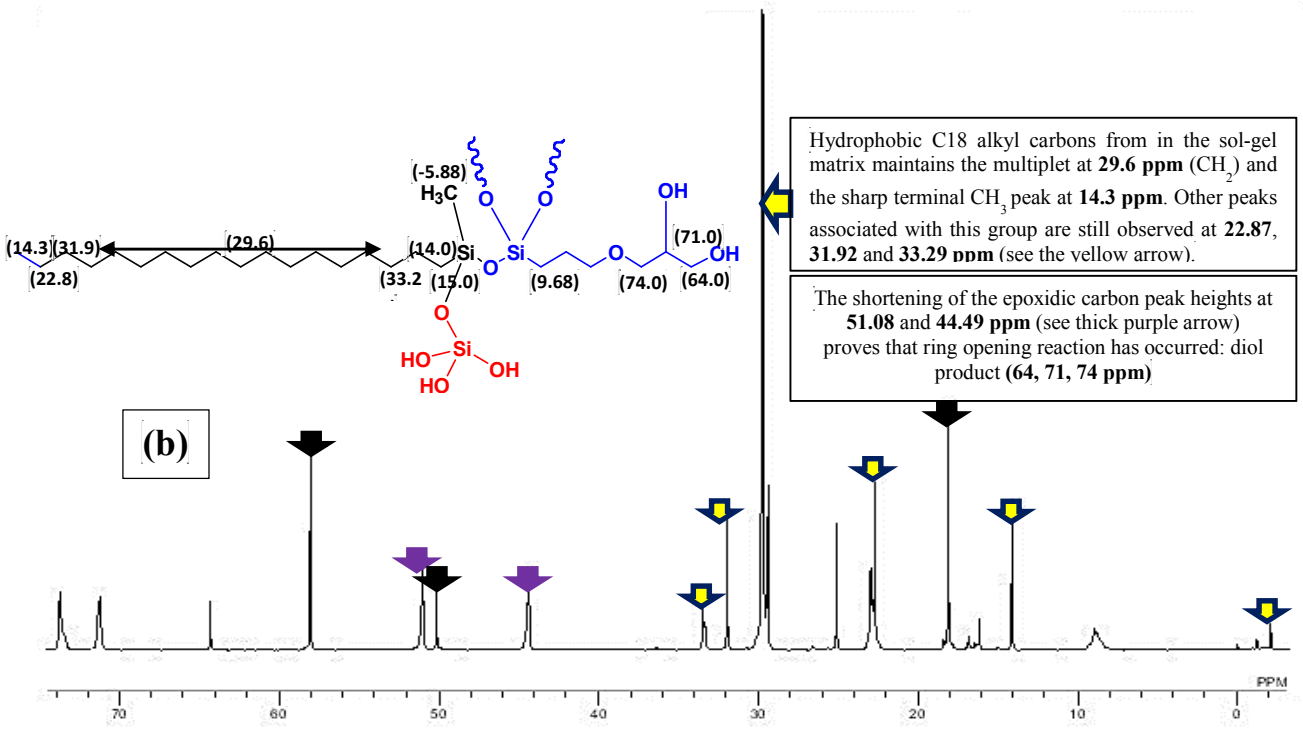

Figure 6.5 ^{1}H (a) and (b) ^{13}C NMR spectra of the as-prepared sol-gel coating after 72 h ageing at room temperature

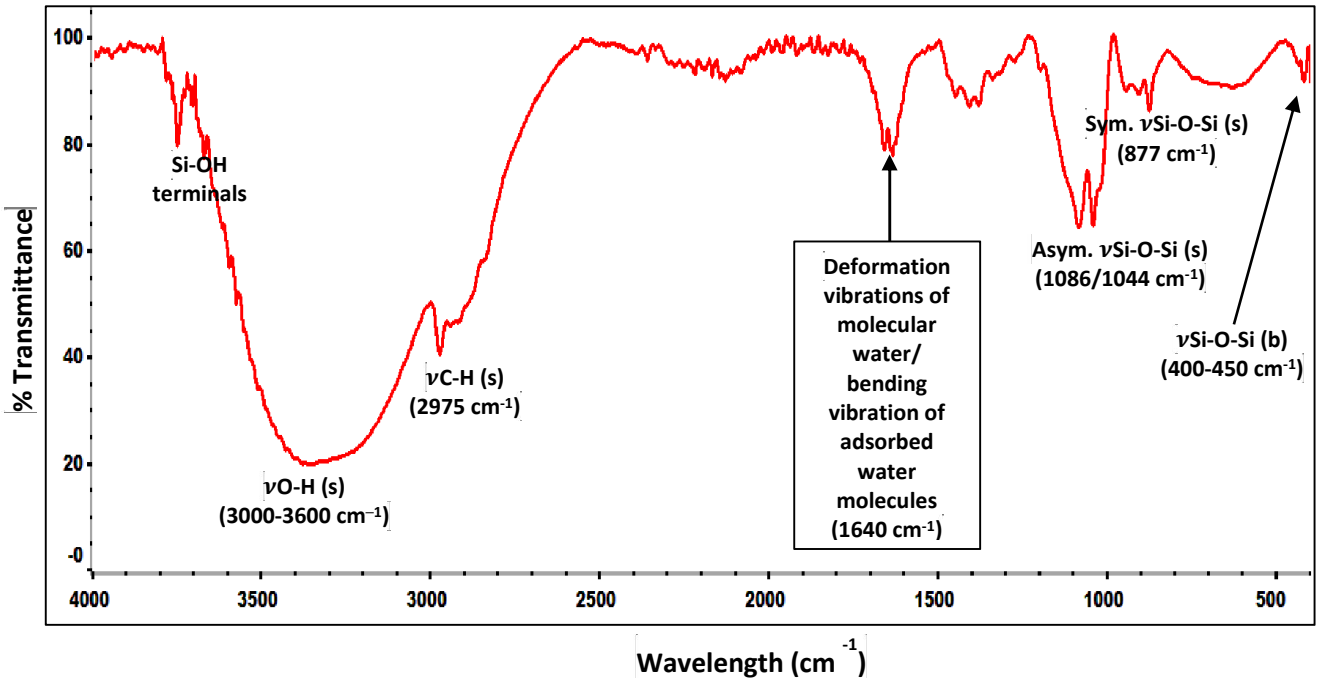

Figure 6.6 FTIR spectrum of the as-prepared sol-gel coating at room temperature.

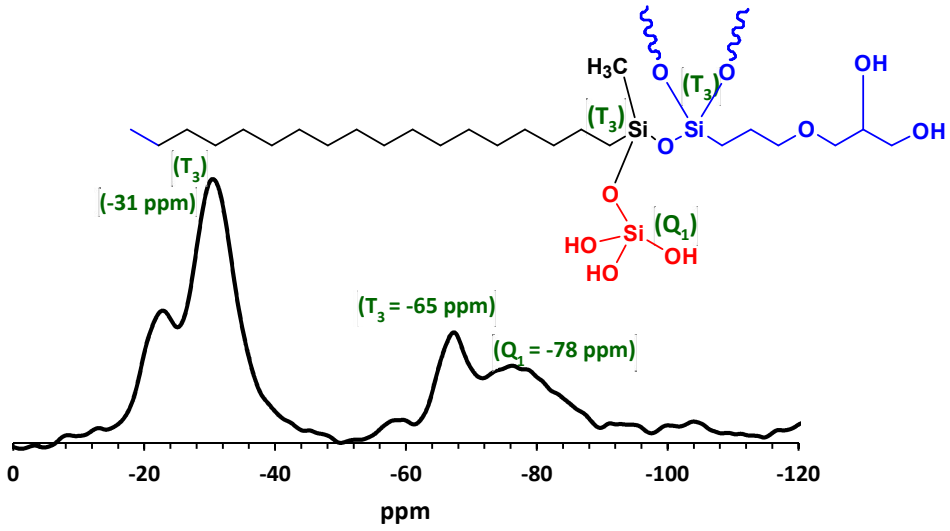

Figure 6.7 ^{29}Si MAS/NMR spectrum of the as-prepared and unmodified sol-gel coating before application on metal substrate.

FTIR spectrum (64 scans at 8 cm^{-1} resolution) was collected for the sol-gel colloid and is presented in Figure 6.6. The spectrum shows a broad peak at 3000 to 3600 cm^{-1} indicating the presence of an O–H vicinal stretching band (H connected) corresponding to the formation of silanol groups *n*(Si–OH) and/or other hydrolysis products from the RO_x groups on TEOS, GPTMS and DMODS precursors, and absorbed water [103]. Residual alcohol used as diluent (IPA) in the sol-gel reaction is known to absorb IR at this wavelength. As expected, the asymmetric Si–O–Si stretching vibration characteristic of polysiloxanic network formation being evidence condensation reaction between adjacent silanol groups is observed at 1044 and 1086 cm^{-1} [105], with similar bond bending at 420–430 cm^{-1}; while the peak at 877 cm^{-1} can be attributed to symmetric Si–O–Si bond stretching vibration [109]. Generally, the formation of silica network denotes the success of the sol-gel reactions [136,137], although some amounts of unreacted or/and partially reacted precursor species are likely to be adsorbed on the formed silica network. The shoulders at 2976 cm^{-1} and 1400 cm^{-1} denote the presence of C–H (stretching vibration

bands in the alkyl groups) and Si–C bonds, respectively, corresponding to the presence of unhydrolysed silane moieties [103,109]. Primarily, the abundance of these Si–C bonds could also be due to the presence of the long unreactive alkyl (C18) organic chain of DMODS in the colloidal silica network, and this greatly contributes to the hydrophobicity of this LSE coating. The sharp peaks at 1663.4 and 1635.8 cm^{-1}correspond to deformation vibrations of molecular water/ bending vibration of adsorbed water molecules [103]. The absence of ring-breathing vibration peak of epoxy at 1250 cm^{-1} [103] proves a successful acid-catalyzed ring opening reaction, though a few residue from adsorbed GPTMS on silica is observed around 910 cm^{-1} (asymmetric ring stretching).

6.3.2 Aqueous contact angle measurement

In this study, water droplets were placed on the surfaces of the cured coatings, and values of θ_w between the surfaces and the droplets were measured in triplicate. The degree of hydrophobicity of these surfaces were determined by the magnitude of θ_w values which remains to be a key factor in determining the corrosion barrier properties of each surface coating [108]. Figure 6.8a presents the average θ_w values of the abiotic coated electrodes by static water drop method. The unmodified sol-gel coating had a θ_w value as high as 111^o, and showed a slight increase in the presence of the Zn-based corrosion inhibitor pigments (with 4.5% increase in the presence of MOLY alone, the reason of which was not further investigated). Without the principal DMOSD precursor, the sol-gel material synthesized yields a hydrophilic surface ($\theta_w=79^o$) due to the inorganic character of the matrix dense with Si-O-Si network from TEOS thereby increasing electrolyte uptake to the metal surface. In the presence of the *B. licheniformis* endospores encapsulated within the sol-gel coating, the contact angle was observed to increase. Figure 6.8b reveals values

of θ_w as high as 108°, 114° and 124° for SGD-6, SGD-Z6 and SGD-M6, respectively. *B. licheniformis* endospores have been previously reported to readily secrete antimicrobial substances within their biofilms capable of altering the surface properties of the substrate they are attached to [121-125].The presented sol-gel route under study produces a hydrophobic organic-inorganic hybrid coating (θ_w>>100°), with a LSE surface due to the presence of the unreacted C18 alkyl group from DMODS precursor in the sol-gel network, and values of θ_w also increase in the presence of the bacterial endospores.

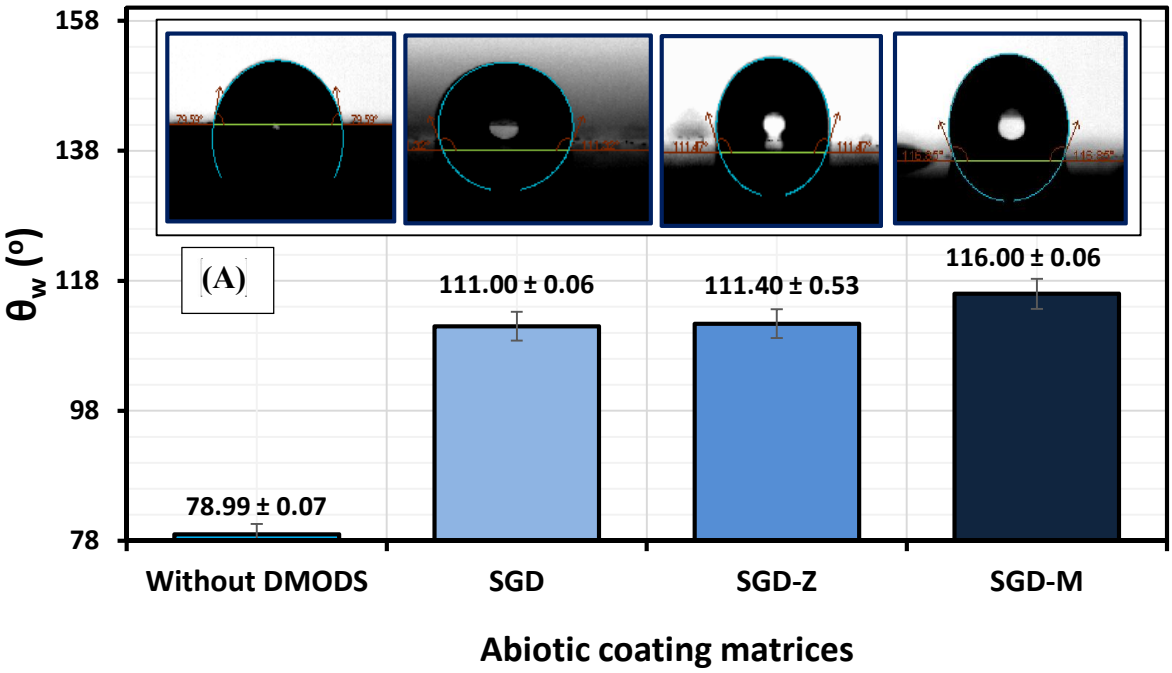

Figure 6.8A Mean water contact angle (θ_w) values of abiotic sol-gel coating synthesized with the principal precursor (DMODS) compared to the coating synthesized without DMODS.[Insert: schematic representation of the aqueous water-droplet contact angle of each coating on a static surface

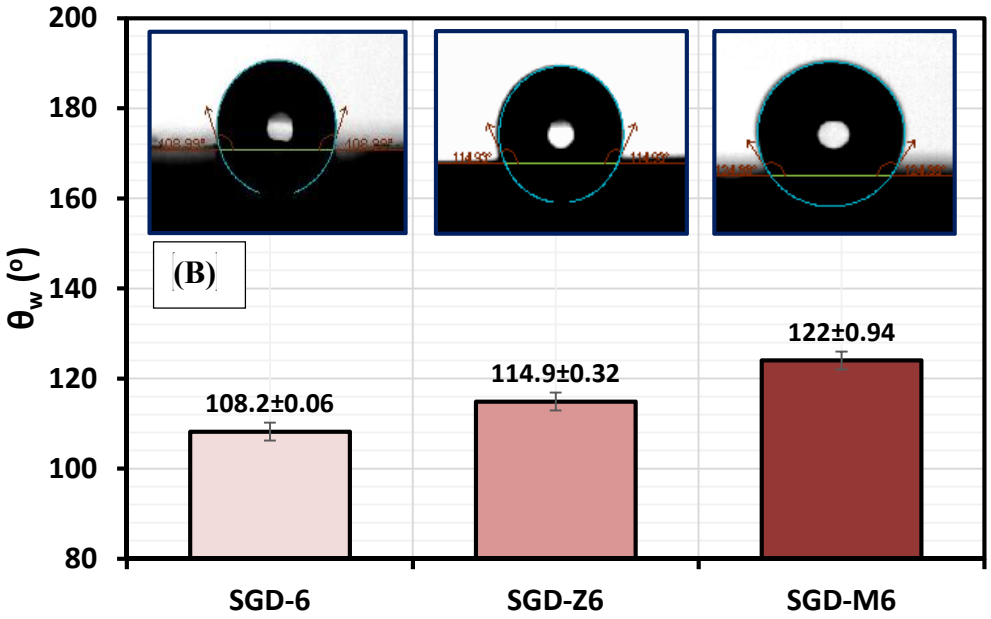

Figure 6.8B Mean water contact angle (θ_w) values of biotic sol-gel coating synthesized with the principal precursor (DMODS)

6.3.3 Confocal fluorescence microscopy

The viability of the bacterial endospores in each biotic sol-gel coating was evaluated indirectly by growing them on the TT medium; widely spread *B. licheniformis* cells are observed in Figure 6.9 after 24 h incubation at 50 ^{o}C. Clean glass slides were also coated with these biotic films, immersed in NB2 broth for a day, then stained with the Baclight Live/Dead stain (Invitrogen), and incubated to observe cell viability of the endospores. At the end of 24 h, confocal fluorescence microscopy was deployed to ascertain the bacterial growth distribution while using the abiotic coatings as the negative control.

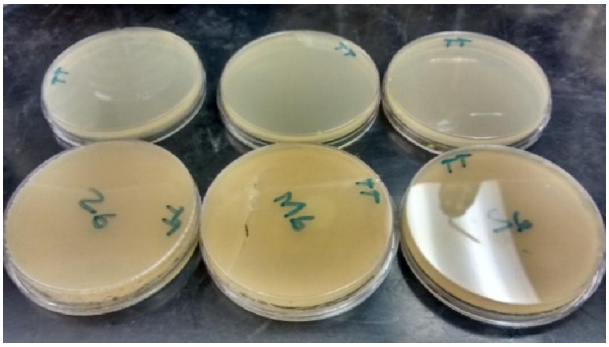

Figure 6.9 Growth of *B. licheniformis* colonies from endospores in sol-gel coatings: a) Sol-gel encapsulated with the bacterial endospores (SGD-6) and SGD-Z6 and SGD-M6, SGD-6 in combination with ZAPP and MOLY.

Cellular bacterial growth are found on the fluorescence micrographs in Figure 6.10a, and though the bright fluorescence observed in the abiotic coatings shows the presence of undissolved fluorescent dyes used during the staining procedure. The presence of bacterial cells found in the biotic coatings are characterized by rod-like cells (singly) or cellular clusters. Much bacterial growth was not observed after 24 h, so the coated glass slides were incubated overnight in NB2 before collecting the first set of fluorescence images. Figure 6.6b presents more of green rod-like cells (some of the red ones are the endospores) in the biotic samples indicating viable bacterial cells in the coated samples; and being alive denotes their availability for bioactivity.

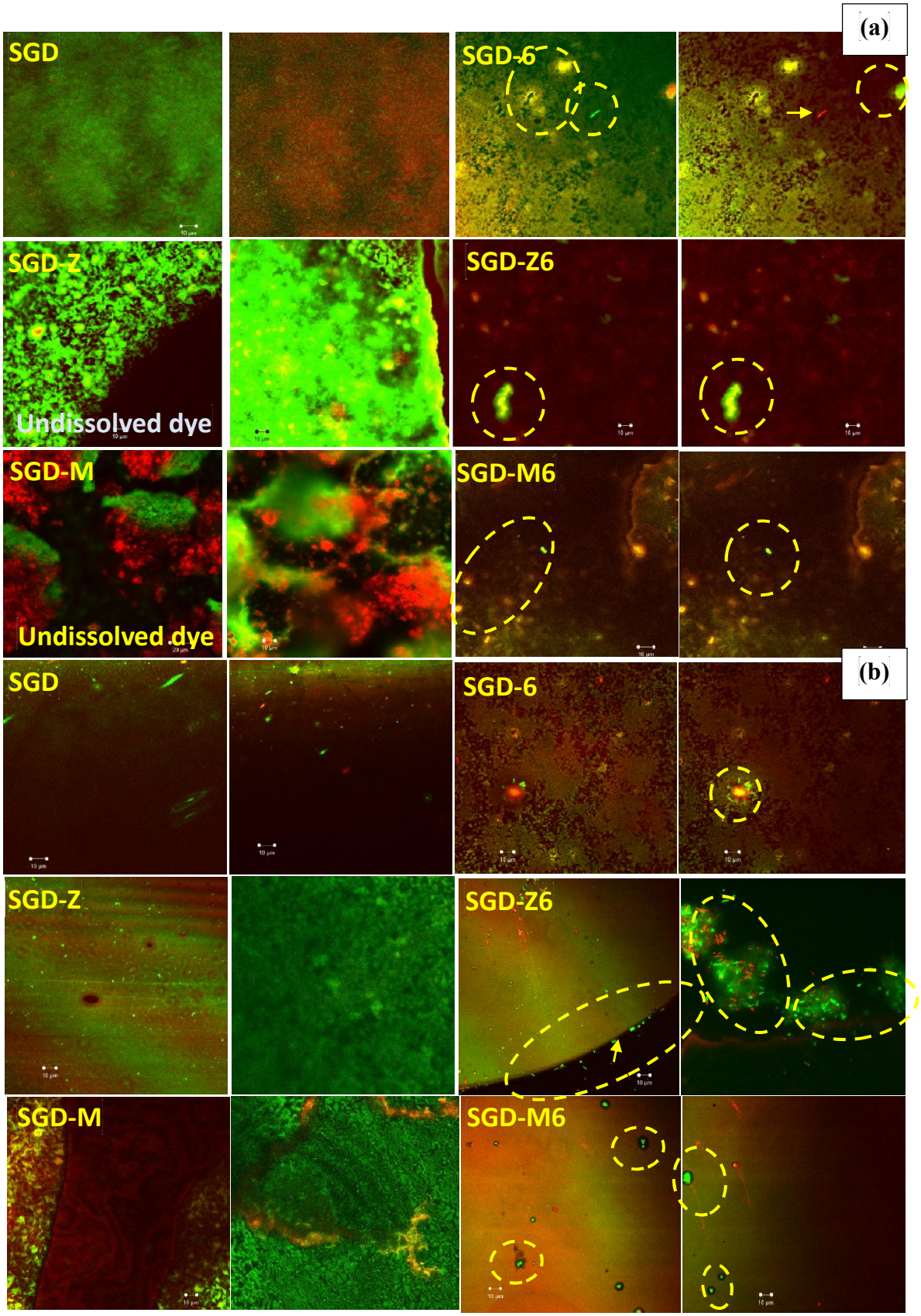

Figure 6.10. Stack confocal fluorescence images showing live cells in the various sol-gel coatings after (a) 24 h and (b) 48 h incubation in NB2 (presented in duplicates for clarity).

6.3.4 Thermogravimetric analysis

To determine the thermal stability of this new coating (SGD), the thermal gravimetric analysis (TGA) of the dried sol was performed at 10 ^{o}C min^{-1} under N_2 [229]. The weight-loss (TG) curve, as well as the differential weight-loss (DTG) plot is presented in Figure 6.11. Four main reaction stages have been clearly indicated on the thermal curve with their individual percentage weight losses determined as 4%, 15%, 5% and < 2%, respectively (Figure 6.11a). The weight losses between 50–100 ^{o}C and 100–250 ^{o}C could be ascribed to the evaporation of adsorbed water molecules and alcohols; and the weight loss at the interval of 250–375 ^{o}C could be attributed to the volatilization of small molecular oligomers and unreacted precursors [138,139] with a weight loss of 15%. The evaporation of some of these volatile components might be associated with the presence of residual silanol via incomplete polycondensation in the hybrid system. The third region (400–500 ^{o}C) could be assigned to the pyrolysis of organic chains and adjoining end groups and units, while silanol group dehydration (in the Si–O–Si framework) could have occurred above 500 ^{o}C [140]. Since DTG curves normally reveal typical temperatures of decomposition at each weight loss (thermal) region, values of corresponding thermal changes could be extrapolated for the four weight loss regions. The decomposition temperatures (T_d) of this newly prepared sol-gel coating alone (SGD) at these thermal regions are 75 and 190 ^{o}C, 375 ^{o}C (the most intense peak), 450 and 495 ^{o}C, and 600 ^{o}C as indicated on the DTG curve for this sol-gel coating. Figure 6.11b shows the TG curves for the modified (SZ and SM) coatings with three distinct thermal regions. There seems to be some shifts in values of T_d corresponding to the major weight loss (20%) region (observed at 375 ^{o}C in Figure 6.11a now shifted to 430 ^{o}C (Figure 6.7b)) attributable to the presence

of 2.5 wt % ZAPP and MOLY inhibitor pigments in the sol-gel coating, as well as possible changes in the degree of compatibility between phases in the sol-gel coatings. Apart from reasons of phase compatibility, the weight loss at this region could also be attributed the breaking down of organic chains of the hybrid sol-gel matrix containing the inhibitor pigments and the fast degradation of combustible constituents of the pigments, possibly oxides of Zn. The TG curves for SGD-Z and SGD-M show similar features with distinct values of T_d at 150 (previously observed at 190 ^oC for S coating with 5% mass loss) 430 and 510 ^oC; any other inherent difference within the curves could be due varying composition of each anticorrosive pigment. For both modified coatings, weight losses below 250 ^oC are due to the evaporation of volatile ingredients from the coating matrices. The variation in the values of T_d could be due to phase compatibility in the hybrid sol-gel matrix, and the residual ash at higher temperatures after the TGA is related to inorganic silica component of the coating [107].

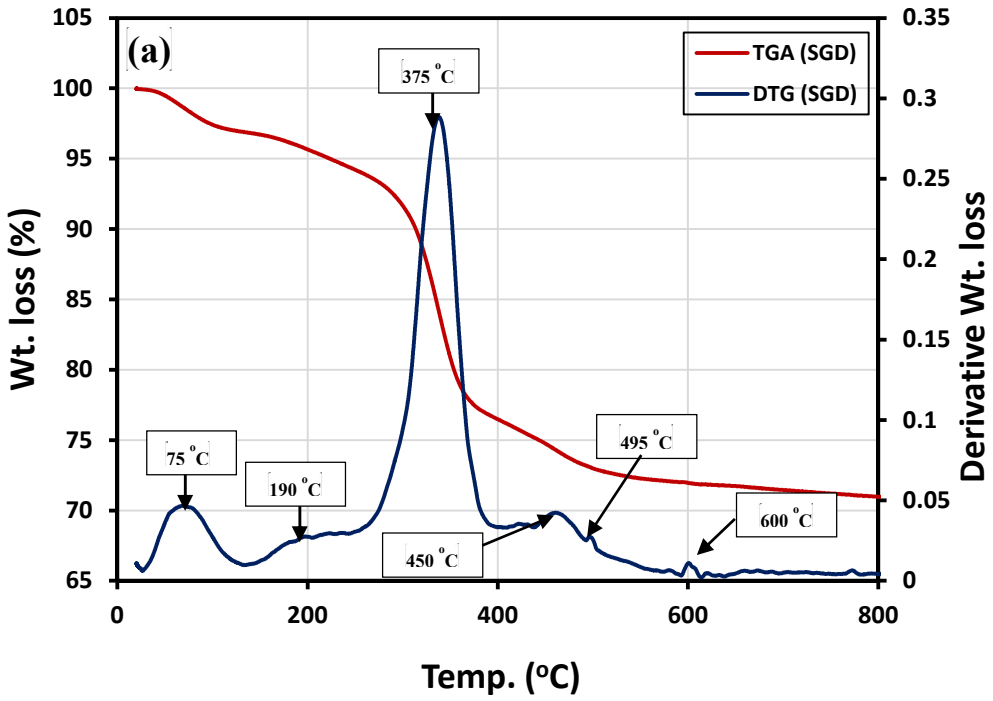

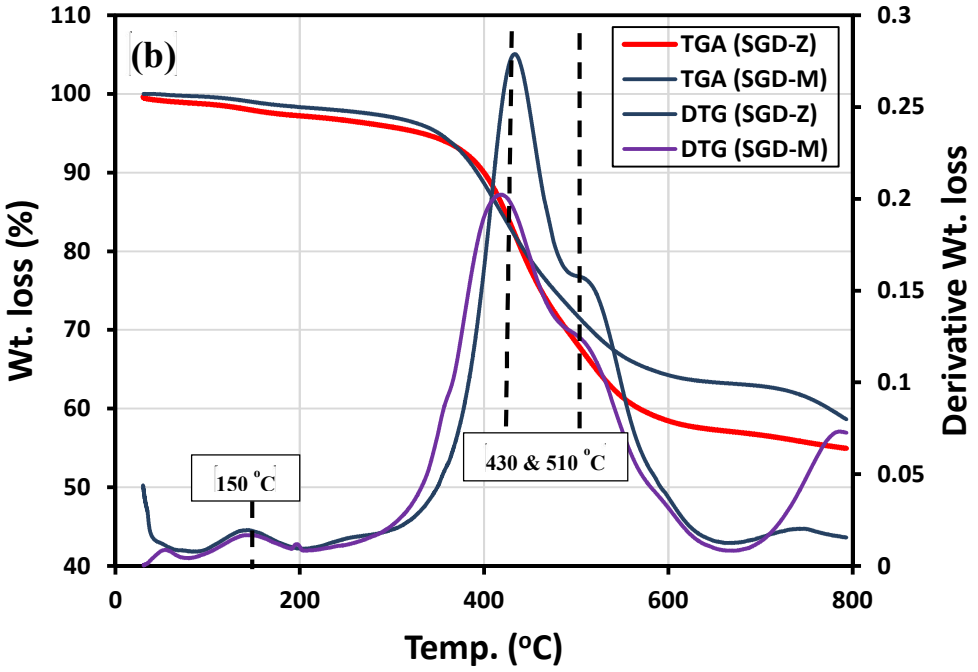

Figure 6.11 Thermogravimetric and derivative thermogravimetric curves of the dried unmodified (a, SGD) and modified (b, SGD-Z and SGD-M) sol-gel matrices obtained at a 10 °C min^{-1} heating rate under N_2

6.3.5 Coating morphology by SEM

SEM was employed to study the surface and cross section morphologies of the coatings before and after prolonged immersion in 3.5 wt% NaCl. The SEM micrographs as displayed in Figure 6.12 are without visible defects and surface cracks before immersion in the saline electrolyte. Although the appearance of each coating looks continuous, white aggregates are found on the surface of each matrix being finely divided gelled silica [184] distributed sparsely throughout the amorphous surface. However, this is the characteristic of this dual-phased "sol-gel"-type coating. It is noteworthy to explain here that these micro-sized particles are part of the complex coating matrix, and do not further increase the gross coating porosity. The cross-section areas of all the coatings appear compacted as

the coatings are firmly adhered on the metal substrate (see Figure 6.12 insert). The coating thicknesses differ slightly; 12.78 μm for the unmodified so-gel "SGD" and 10.11 and 12.04 μm for the abiotic sol-gel coating matrices, SGD-Z and SGD-M, respectively. However, after immersion in 3.5 wt% NaCl solution, the surface does not change much, though "thread-like" micro-cracks and dried NaCl crystals are found in some portions of the unmodified and modified sol-gels. The observed pitting/exfoliation on the surface of SGD-Z could have been due to unevenly disturbed sol-gel particles in the presence of ZAPP pigments. This remains a likely source of decrease in the corrosion inhibiting property of the coating, and hence, could contribute to the general reduction in the protective integrity of this coating. The micrographs for SGD-M before and after immersion in the saline electrolyte are relatively unchanged, revealing superior protective ability of this coating in the presence of corrosive chloride ions on prolonged immersion with few surface micro-cracks. The micro-cracks presented in these micrographs have threadlike and wavy patterns, and they could contribute to undefined localized anode sites and corrosion pathways in the bulk of the coating. The pitting and filiform cracks observed on the SGD-Z and SGD-M coating matrices must have been initiated by corrosive chloride ion attack on the coating on prolonged (a month) immersion in 3.5 wt% NaCl. However, metal-based corrosion inhibitors, like ZAPP and MOLY, are known to form protective passive layers at the metal/solution interfaces to further reduce these corrosion episodes [75]. These anticorrosive pigments synergistically improved the protective properties of this coating in the presence of the bacteria endospores, and this can be confirmed in the absence of surface cracks on the biotic coatings, except for the pitting found on SGD-6 matrix after 30 days immersion in 3.5 wt% NaCl. This result

reveals the anticorrosion properties of this bacteria. The coating thicknesses for the biotic sol-gel coating are: 18, 12 and 11 µm for SGD-6, SGD-Z6 and SGD-M6, respectively.

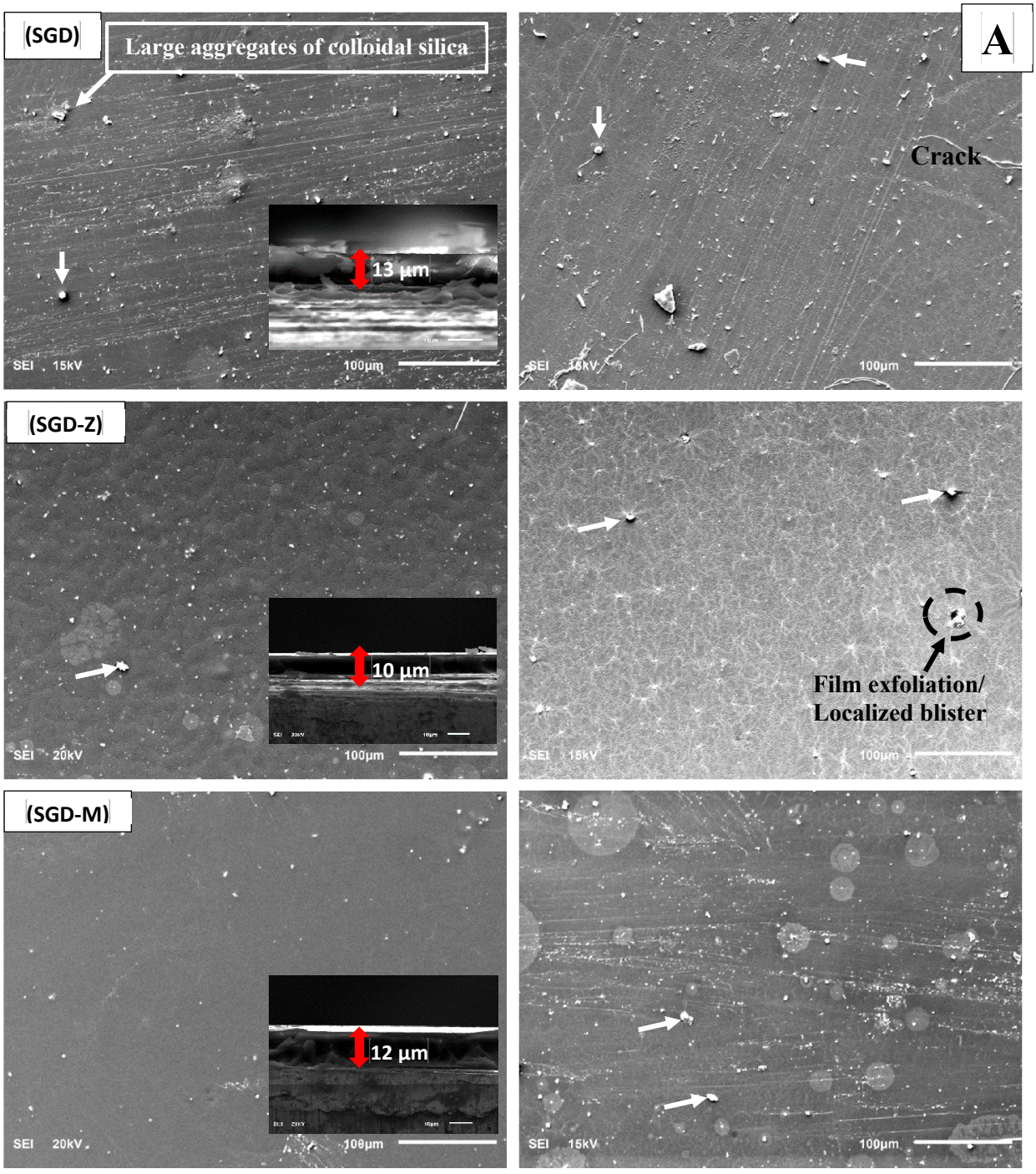

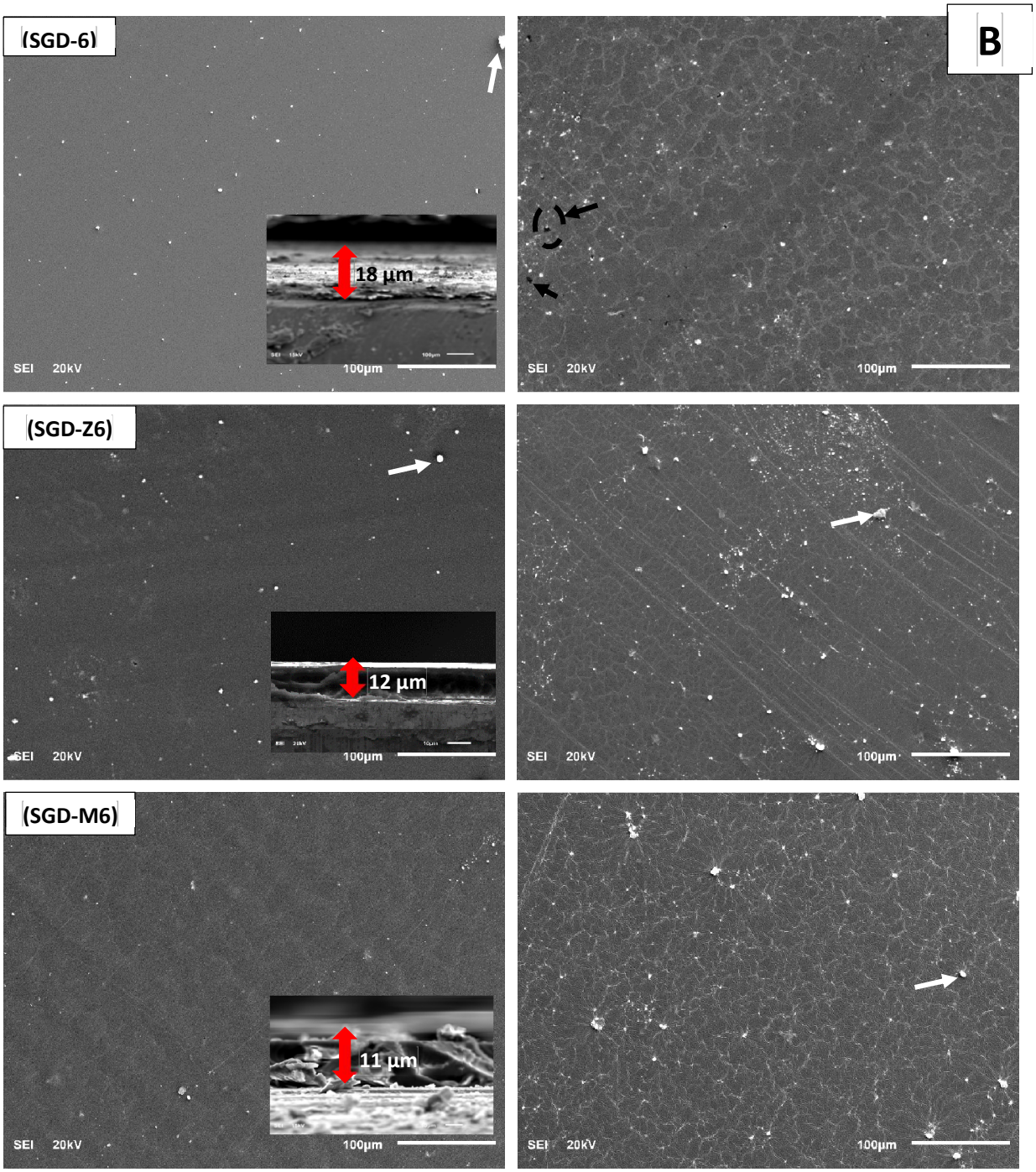

Figure 6.12. SEM micrographs of the hydrophobic coating surfaces (A) abiotic and (B) biotic; (The morphology of each coating was evaluated before (left panel) and after (right panel) a month immersion in 3.5 wt% NaCl solution at room temperature; Insert: Cross-sectional SEM images of the sol-gel hybrid matrices showing coating thicknesses).

6.3.6 Electrochemical analysis

To determine the anticorrosive mechanisms of the abiotic and biotic protective sol-gel coatings on the mild steel panels in 3.5 wt% NaCl, the electrochemical impedance spectroscopy (EIS) technique was employed for consecutive impedance measurements between 11 days and a month at E_{oc}. Impedance results were collected under potentiostatic control and are presented as Bode and Nyquist plots. Figure 6.13 presents the Bode impedance (Z_{mod}) and phase (Z_{phz}) plots for the abiotic (A) and biotic (B) sol-gel coatings after (a) 11 days (b) 20 days and (c) 30 days of immersion in 3.5 wt% NaCl aqueous solution. For both sets of coating, the Bode curves are defined by capacitive behavior at medium frequency (MF) and are characterized by slanted |Z| as well as plateaus on the phase angle curves. At 100 Hz for the 11th day of immersion, Z_{phz} ($\boldsymbol{\Phi}$) is slightly higher for the unmodified than the modified coating, with −10^o, −15^o and −17^o observed for SGD, SGD-Z and SGD-M (abiotic coating) matrices, respectively; compared with −6^o, −37^o and −38^o recorded for SGD-6, SGD-Z6 and SGD-M6 (abiotic coating). $\boldsymbol{\Phi}$ curves are with multiple maxima after a month exposure time showing vivid evidence of varying protection mechanisms; Z_{phz} ($\boldsymbol{\Phi}$) values of −52^o, −24^o and −58^o are recorded for SGD, SGD-Z and SGD-M coatings, respectively, at higher frequency (HF); for the biotic coatings, the Z_{phz} ($\boldsymbol{\Phi}$) values: −55^o, −60^o and −63^o are recorded for SGD-6, SGD-Z6 and SGD-M6 modified sol-gel matrices. Higher values of Z_{mod} are associated with higher corrosion resistance of the coating, and in this study, the MOLY functionalized sol-gel matrix encapsulated with *B. licheniformis* endospores (SGD-M6) is showing higher Z_{mod} values compared with the other biotic and abiotic coatings for every immersion period studied. This could be attributed to synergistic corrosion protection of MOLY and the

bacterial endospores. The Z_{mod} values at 0.01 Hz for the biotic coatings stands at: Z_{mod} (SGD-M6) >> Z_{mod} (SGD-Z6) > Z_{mod} (SGD-6). SM sol-gel matrix demonstrates higher protection compared to SGD-Z, evident in the higher magnitude of Z_{mod} due to the formation of more stable passive oxide film in the protective sol-gel coating. Both inhibitor modified sol-gel matrices possess higher values of Z_{mod} compared to SGD in this order: Z_{mod} (SGD-M) >> Z_{mod} (SGD-Z) > Z_{mod} (SGD). The reduction in corrosion resistance after prolonged immersion of both sets of coatings in the saline electrolyte could be attributed to the penetration of corrosive ions and molecules via micro-crack and pores as well as the solubility of anticorrosive pigments in the bulk of the sol-gel coating. Leaching of anticorrosive pigments from the bulk of the coating could also be a factor in the reduce impedance values with time [75]. For the period of immersion between the 11 days and 30 days, values of Z_{mod} at 0.01 Hz for SGD-Z and SGD-M reduced from 786 to 57 kΩ cm^2 and 1730 to 103 kΩ cm^2 while those of SGD-Z6 and SGD-M6 reduced from 5840 to 1800 kΩ cm^2 and 5850 to 1830 kΩ cm^2. The protective sol-gel coating modified (SGD-6) and unmodified (SGD) with the bacterial endospores possess Z_{mod} in the magnitude of 580 and 418 kΩ cm^2 after 11 days, 126 and 52 kΩ cm^2 after 30 days, respectively.

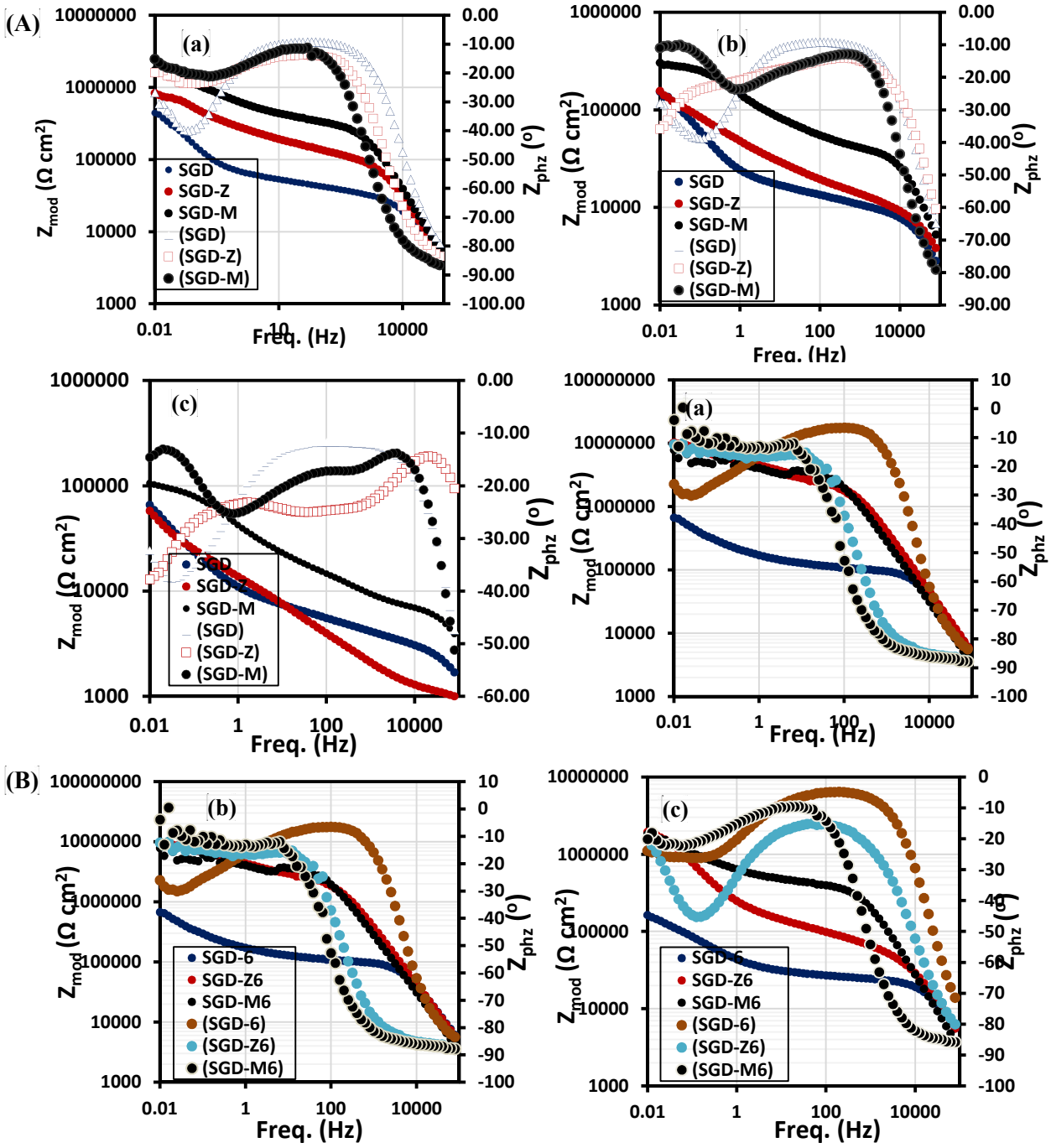

Figure 6.13. Bode (modules and phase angle) plots for (A) abiotic and (B) biotic sol-gel coated mild steel electrodes after (a) 11 days (b) 20 days and (c) a month immersion in 3.5 wt% NaCl aqueous solution. Legends with brackets () represent phase angle plots for sol-gel coatings

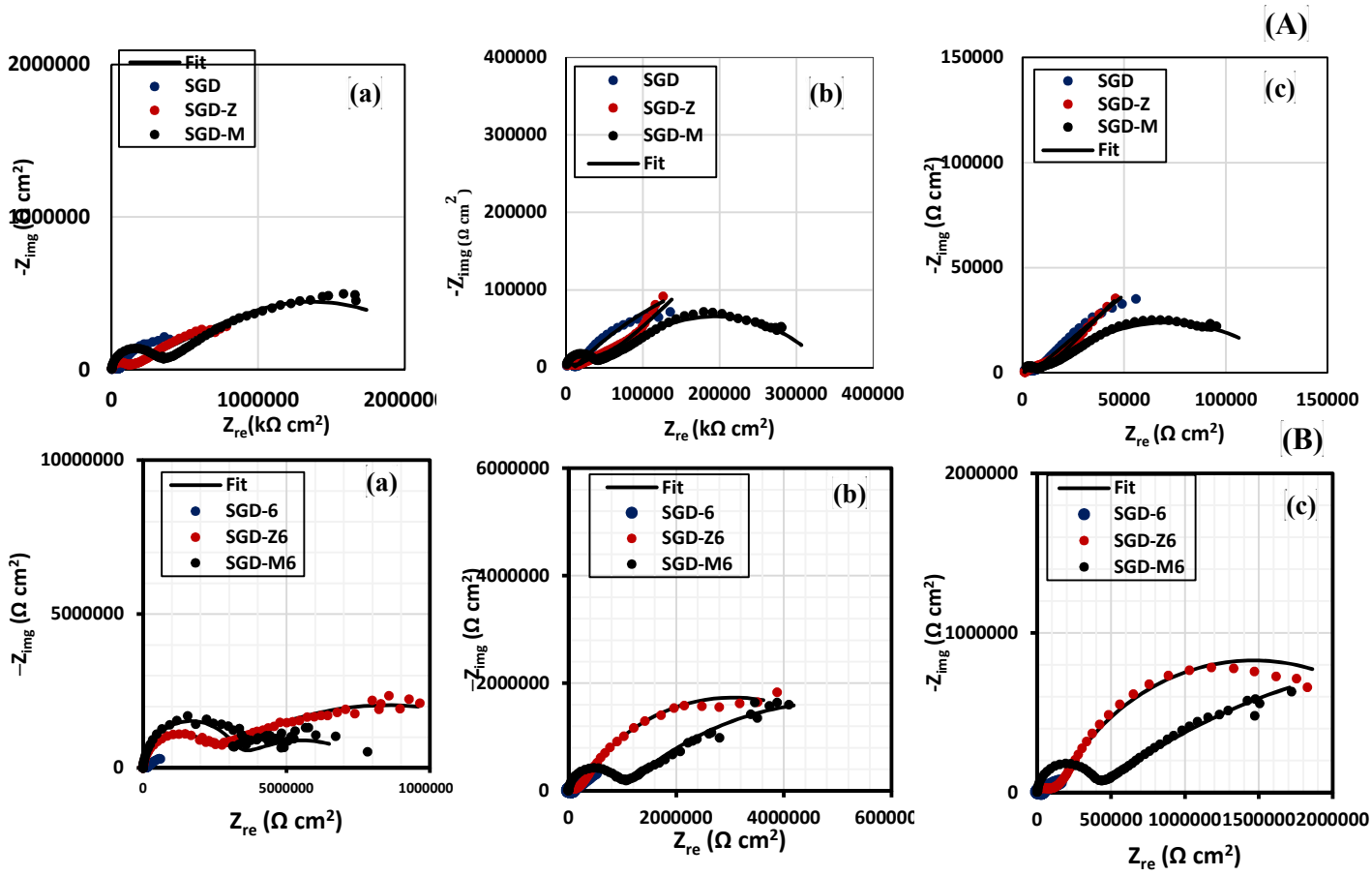

Figure 6.14. Nyquist curves (including their fittings) of abiotic (A) and (B) biotic sol-gel coated mild steel electrodes after (a) 11 days (b) 20 days and (c) a month immersion in 3.5 wt% NaCl aqueous solution.

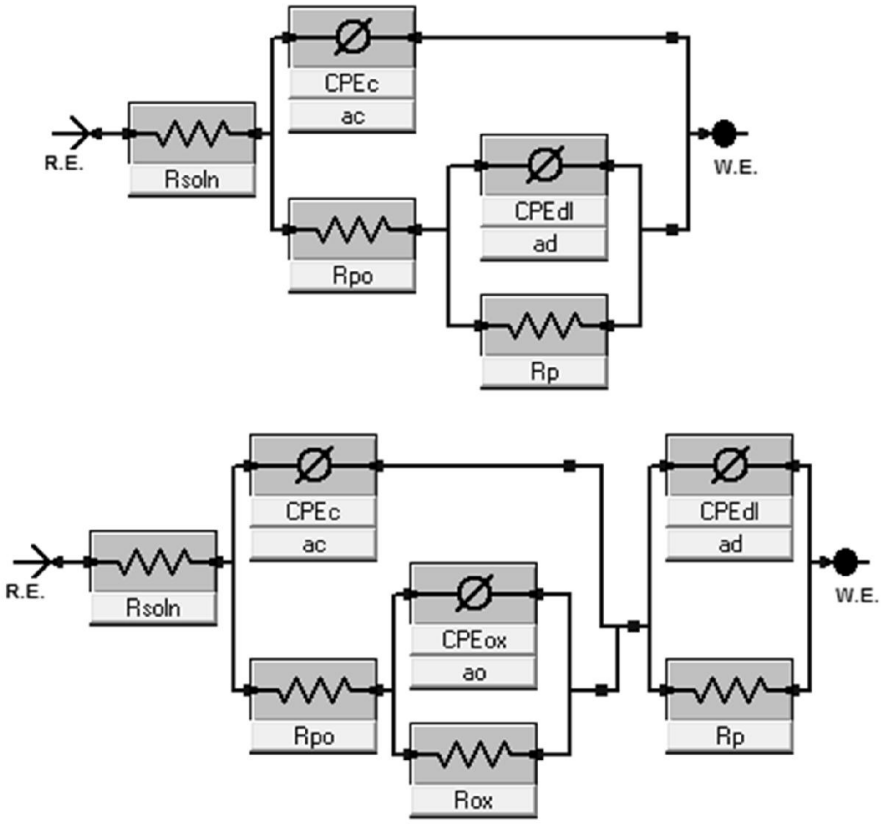

Figure 6.15. Equivalent circuit models used in fitting the experimental Nyquist curves; adopted from Garmy EChem Analyst software's model editor.

Figure 6.15 displays the Nyquist curves of the abiotic (A) and biotic (B) sol-gel coated mild steel electrodes in 3.5 wt% NaCl. As presented on the curves, wider diameters of Nyquist semi-circles are attributed of improved corrosion resistance by better protective coatings; and in this study, the modified sol-gel coating functionalized with MOLY has the widest Nyquist curve diameter among the abiotic coatings at the 11^{th} day (Figure 6.14a) of immersion in the saline electrolyte; while the MOLY functionalized sol-gel matrix encapsulated with *B. licheniformis* endospores (SGD-M6) protects more than other biotic coatings. At prolonged immersion period, the impedance curves of every coating show varying features and with reduced corrosion impedance (Z) due to the loss of protective ability of each coating. It should also be noted that the relative distortions of the Nyquist curve semi-circles may be attributed to the uneven coating textures on prolonged immersion and related surface phenomena [141] while the overall changes in the shapes of the curves on increased immersion periods are indicative of changes in the corrosion protection mechanism for each coating. Different equivalent circuit models (Figure 6.15) were employed in fitting the experimental data presented in the impedance spectra for every immersion period presented. The two-time constant ECM is used in fitting the impedance curves of both modified abiotic and biotic (only at the earlier exposure time) and unmodified (SGD) sol-gel coatings, while the three-time constant ECM is proposed for the modified abiotic and biotic coatings at prolonged immersion time. For the three-time constant ECMs, the first constant phase corresponds to the direct property of the coating (R_{po} and CPE_c) while the second and third phases represent the oxide layer (R_{ox} and CPE_{ox}) and the interphase close to the metal surface (R_p and CPE_{dl}), respectively. The ECMs are proposed with the following circuit components: the electrolyte solution

resistance (R_{soln}), the sol-gel pore resistance (R_{po}), the oxide layer resistance (R_{ox}), including their respective constant phase elements (CPEs) [142]. The electrochemical parameters are extrapolated from the circuit models, and only the magnitude of the resistor and capacitor components are used in the characterization of the barrier properties of both biotic and abiotic sol-gel coatings in this study [109]. The variation of resistance and capacitance values with immersion period for both biotic and abiotic sol-gel matrix is presented in Figure 6.16. The magnitudes of R_{po} for SGD, SGD-Z and SGD-M are 42.98, 83.24 and 276.90 kΩ cm^2, respectively, at the eleventh day of immersion in 3.5 wt% NaCl solution (Figure 6.16a), while those of SGD-6, SGD-Z6 and SGD-M6 are 98.53, 1955.89, 3096.00 kΩ cm^2. These values are observed to decrease significantly for all the coatings after 30 days. Normally for sol-gel type coatings, pores and cracks are created in the sol-gel silica network when volatile solvents evaporate during curing, and this process allows free pathways for water and corrosive ions to the surface of the metal substrate [109,143]. The values of R_{po} for the abiotic coatings are 4.6, 9.9 and 8.7 kΩ cm^2 (for SGD, SGD-Z and SGD-M, respectively) after 30 days interval and 24.20, 61.88 and 68.49 kΩ cm^2 for SGD-6, SGD-Z6 and SGD-M6, respectively. The biotic coatings functionalised with inhibitors (SGD-Z6 and SGD-M6) possess a double layer structure, and their greater coating resistance properties compared to the abiotic coating could be attributed to their increased multi-layered hydrophobic interface properties after endospore encapsulation. Reduced R_{po} values denotes deterioration of the coating integrity, and the trend in CPE values can be employed to support this assertion indirectly by monitoring the water uptake ability of the coating. The values of capacitance of the coatings, as presented in Figure 6.16b, are derived from CPE (expressed as *Y*, and measured in μF cm^{-2} $s^{-(1-\alpha c)}$). More

protective coatings possess lower values of capacitance since they absorb lower amount of corrosive solutions, including water. However, the values of the parameter keeps increasing with immersion period due to increased water uptake as the coatings are exposed to the electrolyte. The reason for this increased CPE_c with prolonged immersion could possibly be due to rise in conductivity of the electrolyte inside via the bulk of the cross-linked organic–inorganic coatings. The SGD-M6 biotic coating possesses the lowest water uptake ability, thus superior protection, with values of CPE_c increasing from 0.0008 to 0.11 µF cm^{-2} $s^{-(1-\alpha c)}$ between the 11th and the 30th day in 3.5% NaCl while SM represents a better abiotic coating with CPEc range between (0.02 to 2.11 µF cm^{-2} $s^{-(1-\alpha c)}$ within the same immersion period).

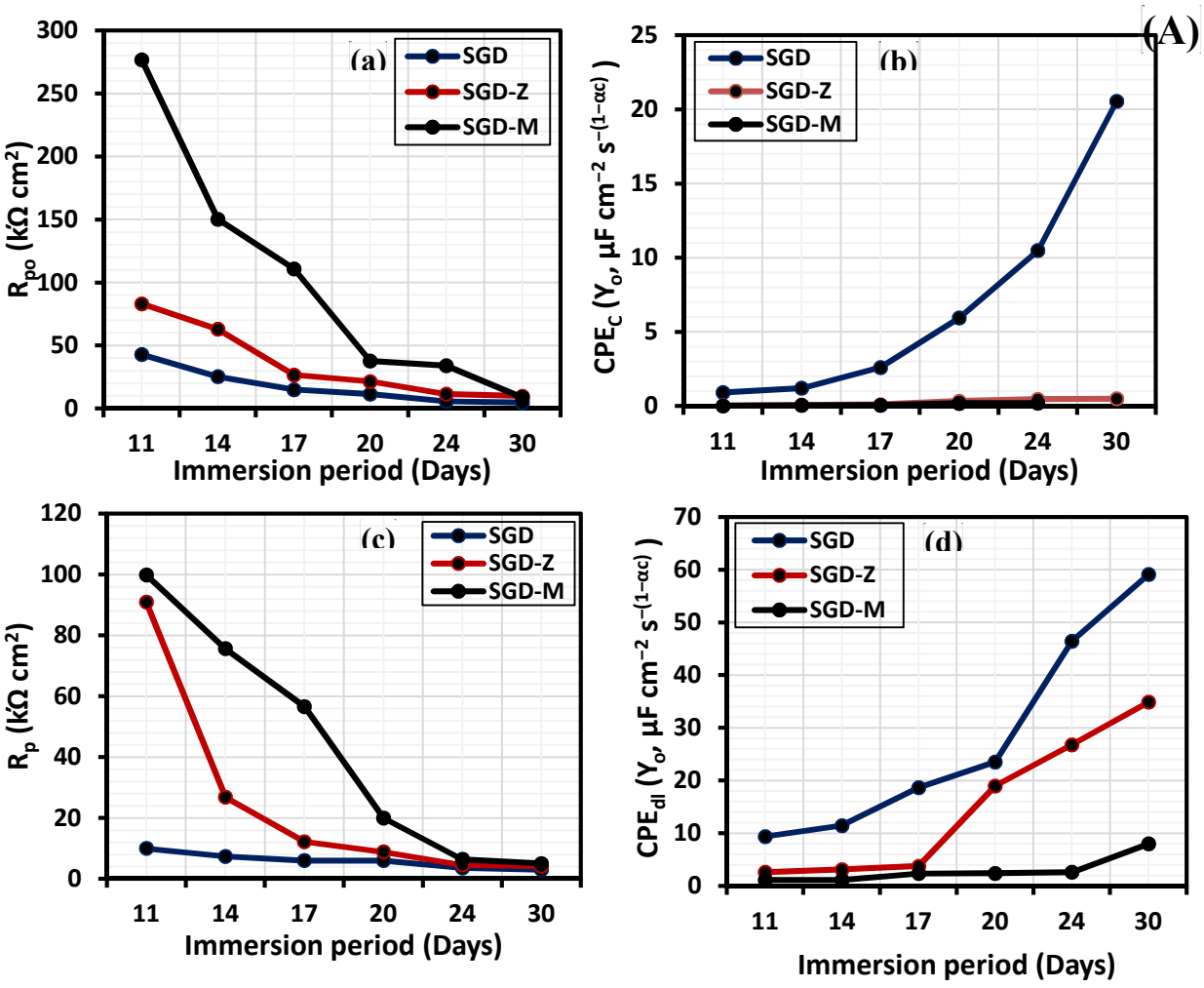

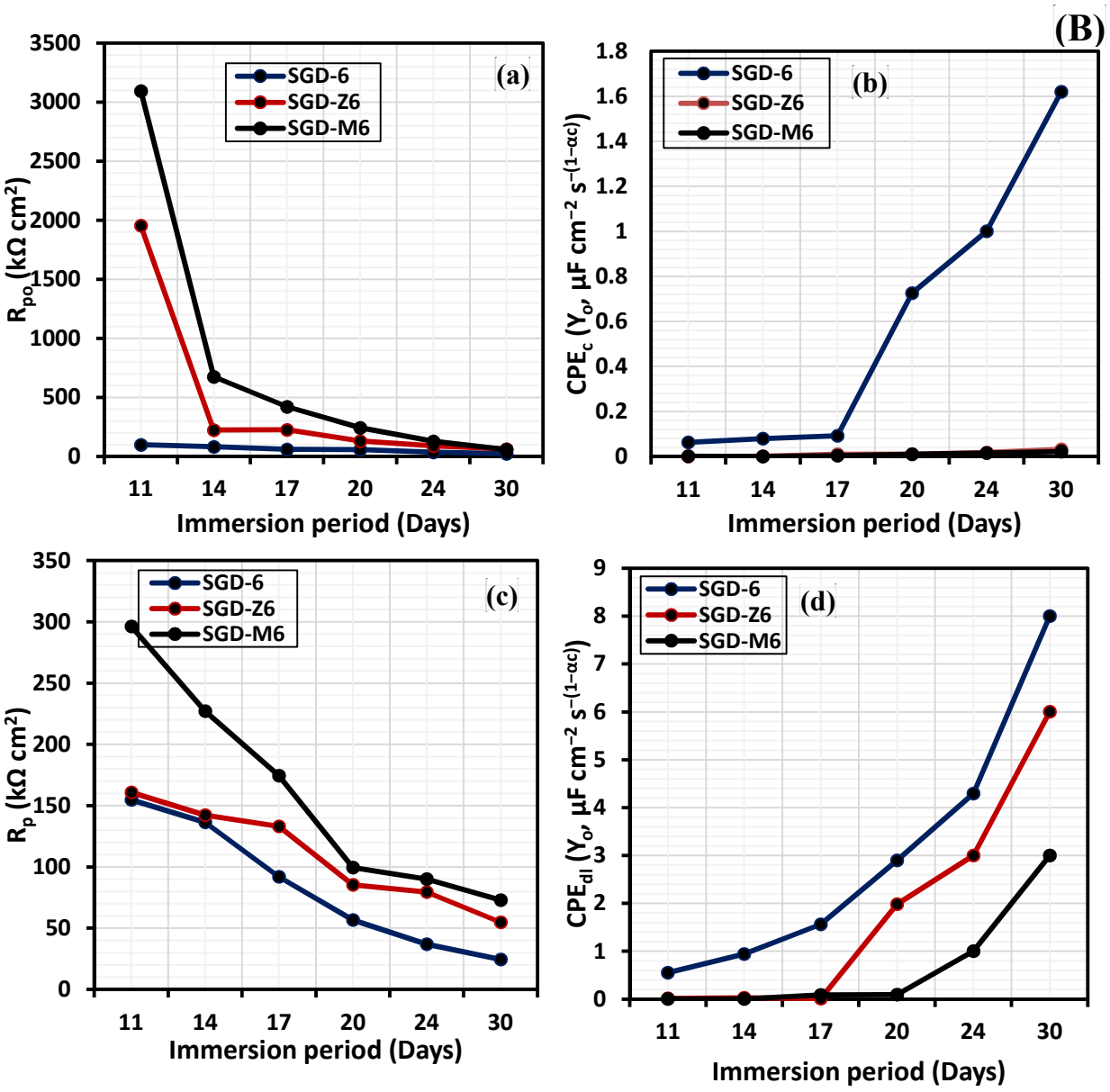

Figure 6.16. Variation in coating resistances (left panel) and capacitances (right panel) with exposure time (in days) with saline electrolyte for (A) abiotic and (B) biotic sol-gel coatings [(a) R_{po}, (b) CPE_c, (c) R_p, and (d) CPE_{dl})].

Similar trends were obtained for R_p and CPE_{dl} (employed to describe the onset of corrosion and disbonding at the metal interface) at lower frequencies. Figures 6.16c and d displays the variation of these parameters with immersion periods for the abiotic (A) and biotic (B) sol-gel coatings in 3.5 wt% NaCl. After 11 days of exposure, the highest value of R_p was recorded for the MOLY functionalized sol-gel matrix encapsulated with *B. licheniformis* endospores (SGD-M6), being the superior coating with R_p magnitude of 2963 kΩ cm^2. Other biotic coating possess R_p values of 1548 and 1600 kΩ cm^2, respectively for SGD-6 and SGD-Z6 while those of SGD, SGD-Z and SGD-M are 99.89, 99.89 and 99.89 kΩ cm^2 at the same immersion period. After 30 days, reduced R_p values were recorded, ranging between 3 and 5 kΩ cm^2 for the abiotic coatings and 7 and 24 kΩ cm^2 for the biotic coatings. The reason for this reduction with longer exposure time of the coated samples in the solution of the electrolyte could be due to the presence of coating defects that allows for the penetration of corrosive chloride ions through the coating defects. Here, the onset of corrosion is initiated as the percolated ions reach the metal/coating interface. The double-layer capacitance, CPE_{dl} is displayed on Figure 6.16 are observed to increase with prolonged immersion times. The trend of values of CPE_{dl} is similar to CPEc, and this could be also attributed the exposure of the protective sol-gel coating to corrosive molecular water and electrolyte ions, thereby favouring corrosion. Low values of CPE_{dl} are recorded for the most protective biotic coating denoting reduced uptake of water in the bulk of the coating. The variation in values of experimental electrochemical result can also be correlated with the physical appearance of the samples over the duration of immersion. Figure 6.17 displays the optical photographs showing the appearances of defined test areas (1 cm^2) of the mild steel panels coated with the biotic

and abiotic sol-gel matrices at varying immersion periods in 3.5 wt% NaCl. The gradual corrosion of the coated mild steel electrodes on prolonged immersion is observed to represent the gradual reduction in the protective performance of these coatings; this is consistent with the electrochemical reduction.

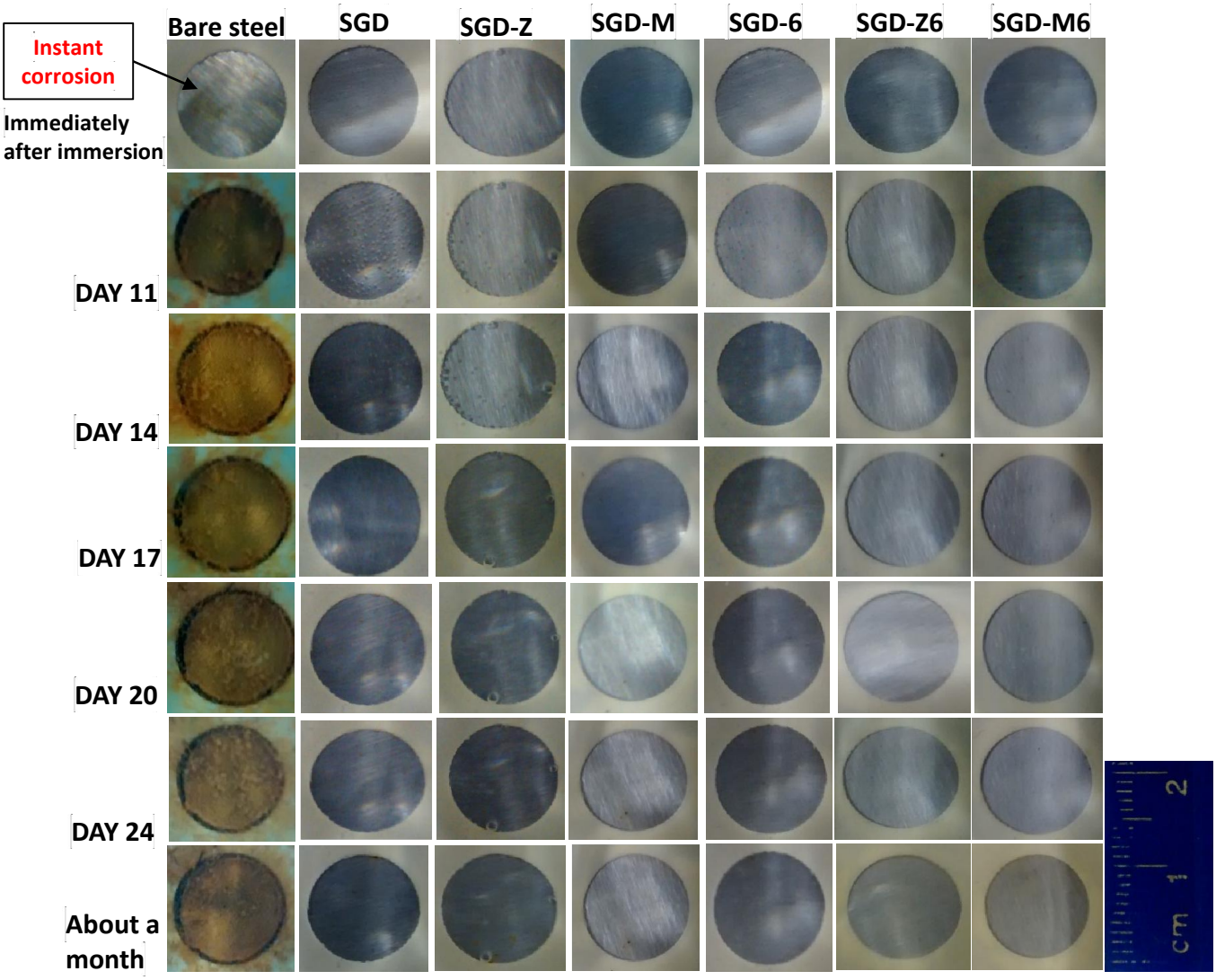

Figure 6.17 Photographs showing the appearances of defined test areas of the mild steel panels coated with the biotic and abiotic sol-gel matrices at varying immersion periods in 3.5 wt% NaCl.

6.3.7 Fouling studies at KFUPM beach

Photographs of each coated mild steel were collected periodically throughout the period of the fouling trials which lasted 14 weeks at Half Moon bay (seawater parameters are presented in Table 6.2) in Saudi Arabia. Figure 6.18 presents the appearances of the abiotic (A) and biotic (B) coated steel panels, in duplicates, with each photograph taken every two week. Evidence of macrofouling by attachment of foulants are observed by visual inspection. There was no instant corrosion on each coating, so the initial coating failure (due to failed adhesion or predominance of bulk micro-cracks and pores) immediately after immersion was not found. However, the appearance of the surface blisters at the fourth week could be attributed to the physical contact of coated surfaces with sea debris. For both sets of coatings, these blisters developed into huge delamination episodes in the later period. The surfaces of most of the inhibitor-modified coatings are still intact due to the presence of the two anticorrosive pigments; they maintained bulk rigidity which continued until the later period of immersion in the seawater. Corrosion inhibitors pigments are known to improve the mechanical properties of the coatings as well as form stable passive films capable of impeding the flow of ionic current via the coatings. Adhesion of newly metamorphosed juvenile barnacles is observed on the abiotic sol-gel coatings at the sixth week, and they continued growing into hard-shelled barnacles between the eight and fourteenth week. The adhesion and settlement of barnacles is conscious in the SGD-M coating matrix compared to other abiotic coatings, even on the edge of the panels; proving that the abiotic coatings did not possess antifouling properties. Compared to the abiotic coatings, the absence of growth of barnacle on the biotic coating (Figure 6.18 (B)) reveals that the presence of *B. licheniformis* endospores ascribes

antifouling and anticorrosion potentials to the sol-gel coatings within the duration and conditions of study. Few growths are conspicuous on SGD-Z6 and SGD-M6 coating matrices at the fourteenth week. The reason for this unique antifouling bacterial behaviour could be attributed to the secretion of antimicrobial γ-polyglutamate from the biofilms of *B. licheniformis;* this is evident in the increased surface hydrophobicity of the biotic coating in the presence of these bacterial endospores [122,124,125]. The biotic coatings in this study protected steel corrosion and fouling to a great extent compared to a fusion-bonded epoxy-based anti-corrosion coating for pipelines (Corro-Coat EP-F 1003). This commercially available coating is widely used for industrial and marine applications including the coating of subsea pipeline facilities.

(A)

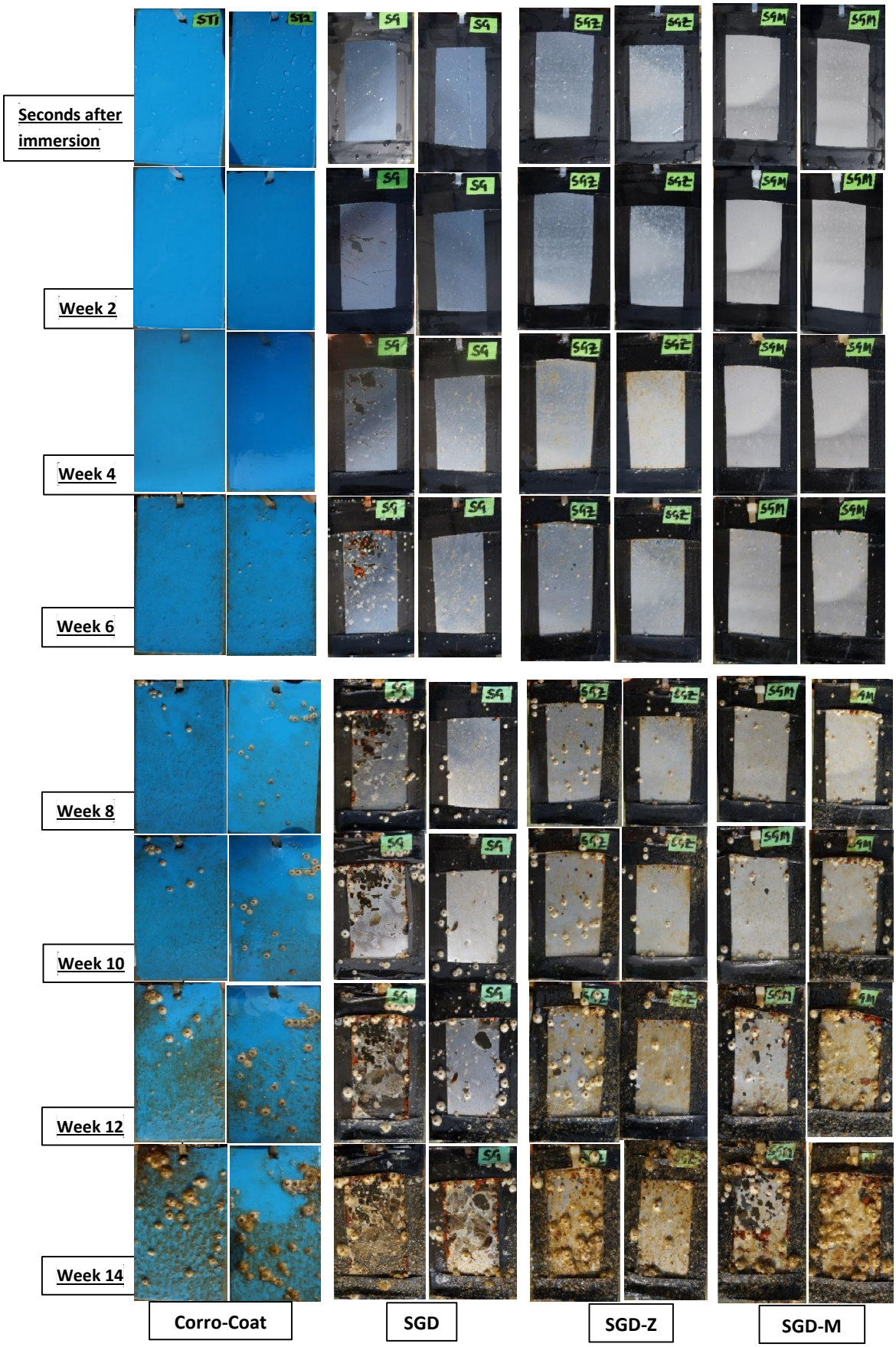
Seconds after immersion
Week 2
Week 4
Week 6
Week 8
Week 10
Week 12
Week 14
Corro-Coat
SGD
SGD-Z
SGD-M

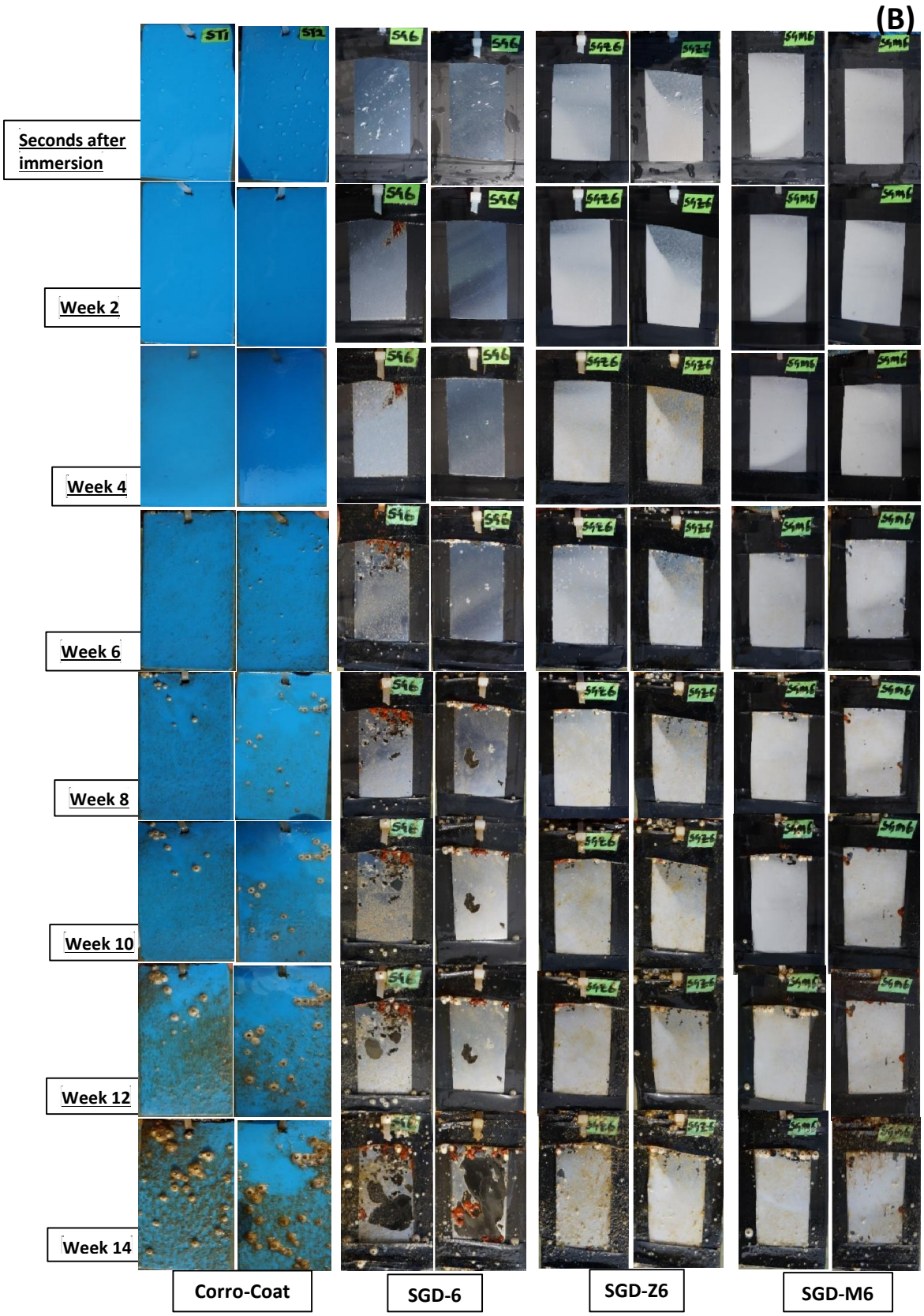

Figure 6.18. Field trial samples in duplicates: (A) abiotic and (B) biotic coated steel panels compared with Corro-Coat EP-F 1003 (a fusion-bonded epoxy-based anti-corrosion coating for pipelines; also widely used for other industrial and marine applications including the coating of subsea pipeline facilities. It is 350–500 µm thick).

6.3.8 Proposed mechanism of bacterial anticorrosion and antifouling activities

The experimental result obtained from this research concept could be further explained in Figure 6.19 below; where the settlement and subsequent adhesion of marine foulers at the surface of the protective coating is impeded by the presence of thermophilic bacterial endospores by foul-releasing mechanism. This bioactive coating simultaneously prevents metal corrosion and foul adhesion compared to the abiotic coatings, while the bare steel substrate is heavily corroded and fouled.

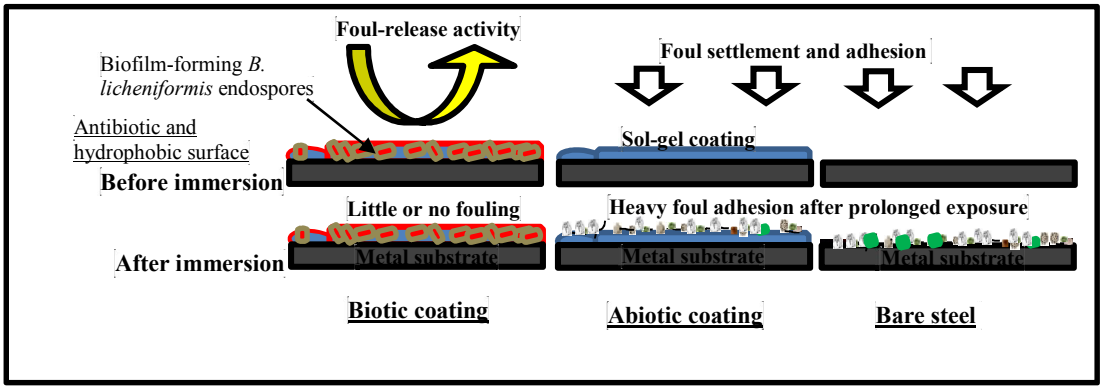

Figure 6.19. Foul-releasing mechanism in the presence of the endospores of thermophilic *B. licheniformis* strain in the sol-gel coating involves surface resistance towards foul settlement and adhesion due to the formation of bacterial biofilm with an antibiotic character.

Since the accumulation of viable *B. licheniformis* endospores in the sol-gel coating has evidently increased surface hydrophobicity, the impedance of ionic current of corrosive species at the surface of the coating is enhanced, hence corrosion is mitigated. However, the reduction in coating resistance with prolonged exposure period reveals that permeability of these corrosive ions via conductive pathways and bulk pores on the coating must be due to coating degradation and the leaching out of active coating ingredients (in this case, the bacterial endospores and corrosion inhibitors). This reduce surface wetness in the presence of the bacterial endospores could have been due to the secretion an antimicrobial type substance within their biofilms that disallowed corrosion

as well as the settlement and adhesion of marine foulers. *B. licheniformis* is widely reported to freely secrete large amounts of anticorrosive γ-polyglutamate (γ-PGM) from its biofilm into growth media as long as it is viable and alive [122,124,125,144-146]. The secreted γ-PGM is a homopolymer of glutamic acid characterized structurally by amide linkages between α-amino and γ-carboxyl functional groups of the glutamate moiety. It is known be produced between 5 and 23 g/l in any *B. licheniformis* culture, depending on pH and the availability of nutrients [122,124]. *B. licheniformis* is one of the numerous *Bacillus sp* whose biofilm has been reported to secrete extracellular antibiotic polymeric substances with corrosion inhibiting potentials like γ-PGM [125]. Ornek et al. [122] electrochemically studied aluminum pitting corrosion in a LB medium inoculated with *B licheniformis* ATCC 9945A strain. The reduction of aluminum pitting in this medium was attributed to the secretion γ-PGM by the bacterial biofilm, with 85% reduction efficiency observed compared to the sterile control in the same medium.

6.4 Summary

The following conclusions are drawn from the results of the experiments:

1. The presence of Dimethoxymethyl octadecylsilane (DMOMS; a simple silane precursor) has ascribed reduced wettability and surface energy as well as high hydrophobicity (θ_w>100^o) to this class of protective sol-gel coating (SGD). Nuclear magnetic resonance (NMR) and Fourier transform Infra-red (FTIR) spectroscopy analyses have confirmed the presence of the hydrophobic C18 alkyl moiety from DMOMS in this sol-gel coating.

2. Corrosion protection increased in the presence of *B. licheniformis* endospores (with and without anticorrosive pigments); evident in the electrochemical results as well as the scanning electron microscopy after a month immersion in 3.5 wt% NaCl solution.

3. Compared with an industrial epoxy-based anti-corrosion pipeline coating (Corro-Coat EP-F 1003), the presence of these bacterial endospores (after being encapsulated within the sol-gel coatings) have also revealed antifouling and anticorrosion potentials in a typical hypersaline marine environment within the duration and conditions of study. This unique bacterial behaviour could be attributed to the secretion of antimicrobial γ-polyglutamate from the biofilms of *B. licheniformis;* evident in the increased surface hydrophobicity of the biotic coating in the presence of these bacterial endospores.

4. Scanning Electron Microscopy revealed fewer surface cracks and defects after a month immersion of the coated metal substrates in 3.5 wt% NaCl solution for the abiotic coating, and the absence of these mechanical defects in the presence of *B. licheniformis* endospores within the sol-gel coating.

CHAPTER 7

Title: Evaluating the corrosion inhibiting role of *Bacillus licheniformis* biofilm for steel

7.1 A brief overview

The corrosion inhibition by spore-forming *gram-positive* bacteria have been widely reported in the literature for many metal substrates in both surface and ground water. These microbes alter the rate of metal dissolution as long as they remain viable in the media by reducing the concentration of oxygen at the metal surface via aerobic respiration. For this class of bacteria, the nature of their biofilms have huge influences on the overall electrochemical process as a consequence of their metabolic activities. Some biofilm-forming strains of *Bacillus brevis* and *Bacillus subtilis* can secrete antimicrobial substances (e.g. gramicidin S antibiotics) from their biofilm thereby preventing the settlement of other bacteria capable of inducing corrosion [147,148]. Arps et al. [149] have reported the corrosion reduction of some steel alloys in an artificial service water using *Bacillus* strains capable of producing polymyxins and gramicidin S. Amongst the gram-positive and spore-forming *Bacillus* species with the potency of reducing metal corrosion is *Bacillus licheniformis*.

7.1.1 *B. licheniformis*

B. licheniformis is generally a facultative anaerobic, mesophilic, gram-positive, curved or straight rod-like (*Bacillus*) motile bacterium (with pertrichous flagella/hair-like outgrowths, hence the name "licheniformis") with a full cellular size between 1.5─3.5 and 0.6─0.9 μm (Figure 7.1); it is spore- and biofilm-forming as well as apathogenic. It is

endowed with enzymes that allows for its spore (even vegetative cells) survival in harsh conditions, including temperature, solvents (e.g. NaCl) and pH (See Taxonomy in Table 7.1). This bacterium is widely found in soils and on some birds (including feathers of ducks and ground-dwelling sparrows); since many of its strains can survive at elevated temperatures, vegetative growths can still be found between 30 and 50 ^{o}C. Higher thermophilic strains can strive in the hot springs; and the strain employed in this study was isolated from the hot springs of the Saudi Arabia. It is penicillinase inducible and also known for secreting polypeptide antibiotic bacitracin (active against most gram-positive pathogenic bacteria) (http://www.tgw1916.net/Bacillus/licheniformis.html). Some strains possess proteases, lyases/ lipases and polysaccharide degrading enzymes.

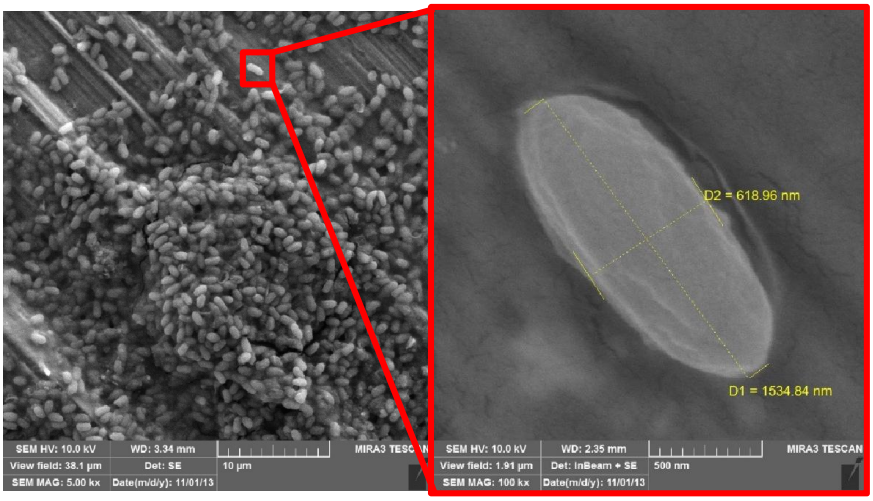

Figure 7.1 SEM micrograph showing the distribution and dimensions of vegetative *B. licheniformis* cells on steel substrate.

Table 7.1 Taxonomy of *B. licheniformis*

Phylum	*Firmicutes*
Class	*Bacilli*
Order	*Bacillales*
Family	*Bacillaceae*
Genus	*Bacullus*

Most corrosion inhibiting strains of *B. licheniformis* are biofilm-forming bacteria capable of secreting antibiotics that can act as corrosion inhibitors. Ornek et al. [122] have studied pitting corrosion of aluminum 2024 substrate in the presence of *B licheniformis* ATCC 9945A strain using in Luria Bertani (LB) medium by electrochemical impedance spectroscopy (EIS). Aluminum pitting corrosion was found to reduce by more than 85% compared to the sterile controls after a week of continuous exposure in LB medium contained in a bioreactor. Authors attributed this unique bacterial behavior to the secretion γ-polyglutamate by the bacterial biofilm in the *B licheniformis* culture at pH>6. The effect of bacterial biofilm of nitrate reducing *B. licheniformis* strain has been investigated on carbon steel [150]. The presence of the bacterial cells in the biofilm was found to produce metabolic products capable of forming pits while degrading the metal substrate in one-week exposure period. Bolton et al. [151] have reported the degradation of galvanized steel substrate (used for water storage and transportation) in the presence of *Bacillus pumilus*. Up to 70% pitting corrosion was observed via the zinc ion release, being a consequence of bacterial catalyzed activity, compared to the sterile solution. Both surface corrosion and bulk metallic pitting has been reported for isolates of *B. licheniformis* and *B. aquimaris* carbon steel in a Brazilian oil platform water by Marques et al. [152]. Authors also studied the effect of nitrate on bacterial biofilms on the corrosion rates of steel substrate monitored by weight loss in reactors. The exposure of metals to any service environment varies, and the type of bacteria they come in contact with depends on the nature of that environment and the prevalence of such microbes. Since the formation bacterial biofilms on exposure alters the chemistries of these surfaces at the substrate/solution interface, this work seeks to unravel the role of biofilm produced from

thermophilic strain of *Bacillus licheniformis* isolated from the Gazan hot spring of Saudi Arabia. The biofilm of this bacterium will be grown on stainless steel (316 L grade) and the nature of EPS as well as the possible bacterial metabolites produced from its physiological activity will be monitored chemically and electrochemically. This grade of steel (316 L) is chosen based on its susceptibility to pitting and galvanic corrosion in solutions of high ionic (e.g. chlorides) concentrations.

7.2 Experimental

7.2.1 Culture medium/composition

The sourcing of this thermophilic bacterial strain has been previously explained (Chapter 3), and in the present study, the culturing procedure in a minimal salt medium (pH 5.0) has been reported elsewhere [153]; without modification, except for the diluted water replaced by a sterile type. Components of the medium includes: 7.5 g NaCl, 10 g glucose, 0.2 g $MgSO_4 \cdot 7H_2O$, 0.01 g $FeSO_4 \cdot 7H_2O$, 1g $(NH_4)_2SO_4$, 0.5g K_2HPO. *B. licheniformis* concentration used in this study measured 2.79×10^7 CFU/ml, and 1 ml of the bacterial suspension was inoculated in 500 ml of the sterile minimal salt medium (System A; pH 4.6) and cultured at 37 ^oC for three weeks in an incubator. The other set up (System 2A; pH 3.8) had double the amount (in volume) of the bacterial suspension in System 1, and was cultured in similar condition as presented in the flow chart in Figure 7.2. The presence of NaCl in this medium enhances accelerated corrosion of steel in the presence of these bacterial endospores; the abiotic sterile solution was used as the control. Incubation was done in a closed sterile incubator devoid of external influences. Electrochemical

biocorrosion and surface analytical evaluations of the steel coupons followed at the end of the 3rd week.

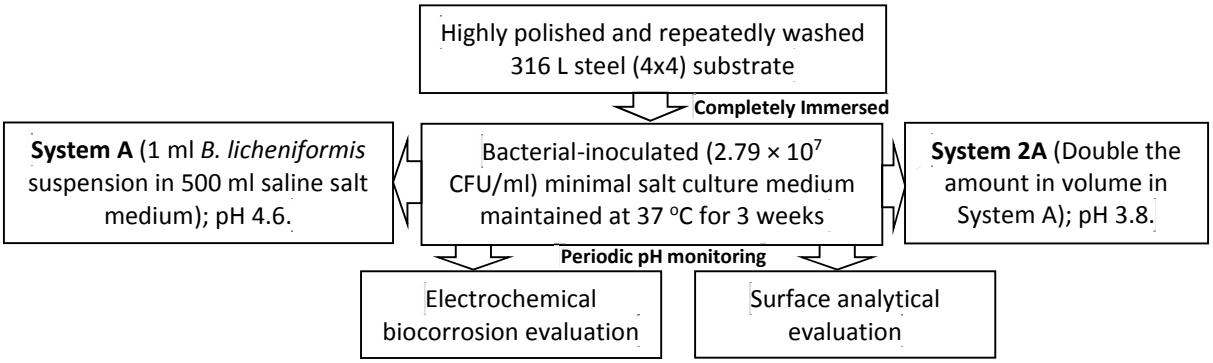

Figure 7.2. Flow chart of experiments in this bacterial study.

7.2.2 Electrochemical biocorrosion studies

The stainless steel substrate (316 L grade) used in this study was polished in a procedure previously explained in Section 3.3.1 but with 1 µm diamond paste (instead of alumina). Both ac and dc experiments were conducted using a three-electrode system with a graphite rod counter electrode (Gamry, US), the polished stainless steel coupon (4 x 4) employed as the working electrode, and a SCE reference electrode. Electrodes were assembled in a 500 ml capacity conducting cell used as the bioreactor. It contained the bacteria cell/ biofilm matrix with fresh minimal salt culture medium in which the electrochemical analyses were conducted at determined the effect of the bacterial adhesion/maturation on steel corrosion at the end of a 3 week culture period. EIS test was measured with Gamry Instrument potentiostat/galvanostat/ZRA (GAMRY 3000, Gamry Instruments, US) corrosion measuring system; ac 10 mV amplitude perturbation at E_{oc} between 100 m Hz and 100 k Hz applied via EChem Analyst software package 6.0 (Garmy, US). Tafel polarization test followed EIS analysis (on the same steel coupon), and was measured while polarizing the surface of the stainless steel electrode between ─250 and +250 mV

relative to E_{corr} (vs SCE) at a 1 mV/ s scan rate. An E ChemAnalyst software was used for the data fitting and other simulations. Before the electrochemical analyses, values of pH of the bacterial culture solution were also taken periodically from the onset of incubation until the third week, relative to the control.

7.2.3 Surface analytical evaluations

All surface analytical measurements were taken after the 3 week exposure of the steel substrate to the bacterial-inoculate minimal salt medium in order to attempt to study the morphology and chemistry of the formed bacterial biofilm. The steel coupons were removed from the bacterial inoculated culture medium to determine the chemical composition of the EPS/biofilm deposit using FTIR spectroscopy (Nicolet 6700 Fourier Transform (FT) Spectrometer (Thermo Electron Corporation, UK) in transmittance mode recorded between 400−4000 cm^{-1}, at the resolution and scan rate of 8 cm^{-1} and 64, respectively. Scanning electron microscopy (U9320A 8500 Field Emission Scanning Electron Microscope, Agilent Technology, UK) coupled with energy dispersive spectroscopy for elemental analysis (Oxford 7424 solid-state detector) was employed for the morphological/compositional study of the bacterial biofilm matrix as well as possible corrosion products on the steel surface before and after bacterial culturing. The working electrode used for the electrochemical analyses was unsuitable for microscale fluorescence imaging, so the same immersion test was conducted on ITO conductive glass slides after prolonged (about one month) immersion in a different culture medium (NB2 broth/Spizizen's salts solution with 0.1% wt/vol L-alanine and 0.5% wt/vol glucose). The glass surfaces were stained with a fluorescent dye Baclight™ Live/Dead bacterial viability stain kits (Invitrogen, USA) before observing them with a confocal laser scanning

microscope (Zeiss AxioVision confocal scanning laser microscope, UK) coupled with Plan-Apochromat 63x/1.4 Oil Ph3 objective. CLSM images from various positions were reconstructed with ZEISS Microscope Software ZEN (Zeiss, UK).

7.3 Result and discussions

7.3.1 Electrochemical analyses

The electrochemical plots of the 316 L stainless steel immersed in the culture medium containing varying concentrations of *B. licheniformis* endospores compared to the control are presented in Figure 7.3. The Nyquist curves (Figure 7.3 a) are incomplete and relatively irregular capacitive resistance semi-circle arcs for both bacterial systems (A and 2A), with System 2A having the widest diameter. With their diameters greater than the control, this represents the formation of possible bacterial biofilm on the surface of steel as well as the deposition of corrosion products beneath the biofilm. The formation of thicker bacterial biofilms on steel substrate for System 2A could be the reason for its wider Nyquist curve compared to System A [154].

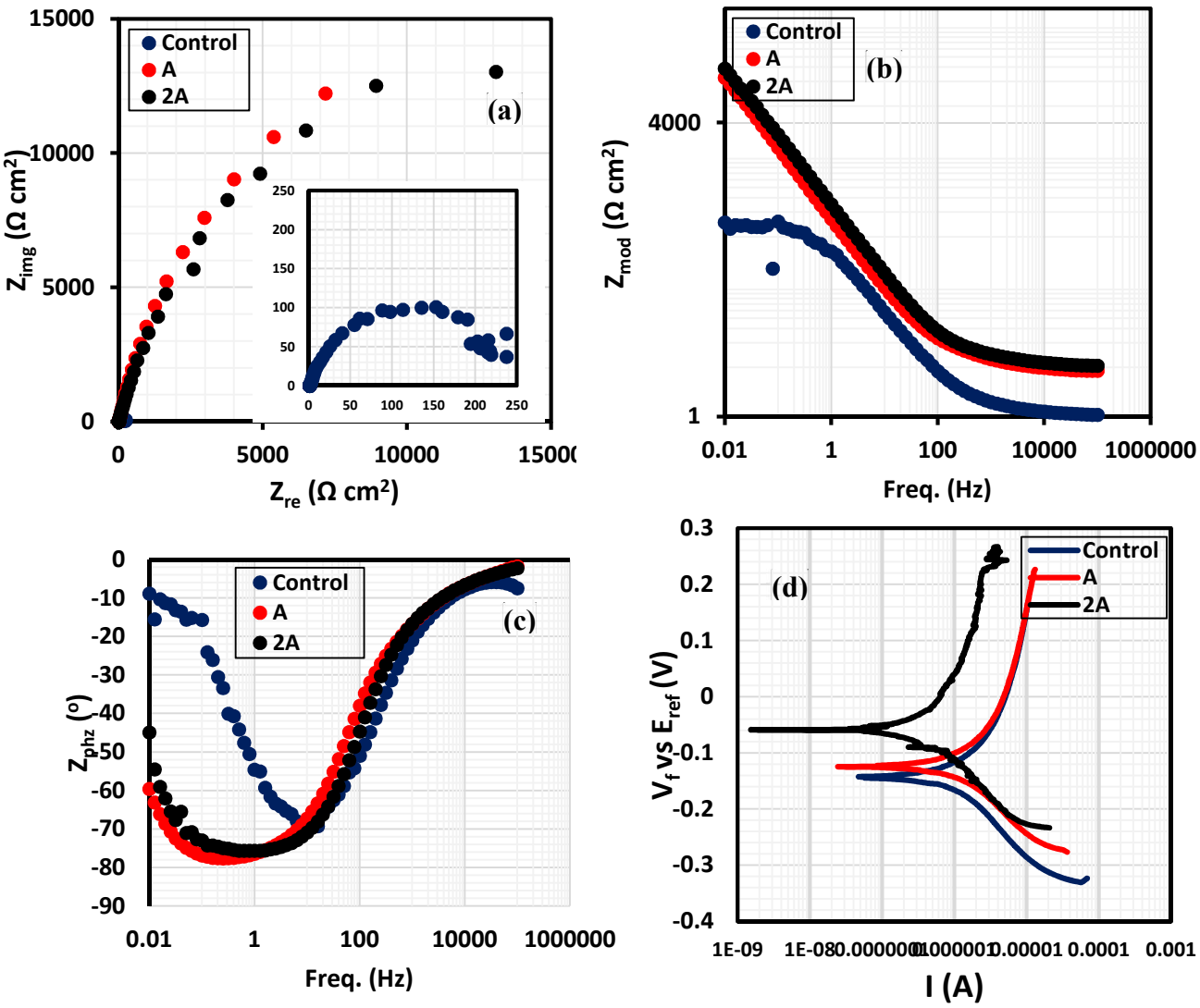

Figure 7.3 Nyquist (a), Bode (modules (b) and phase angle (c)) and potentiodyamic polarization plots for *B. licheniformis* inoculates in the culture medium compared to the control

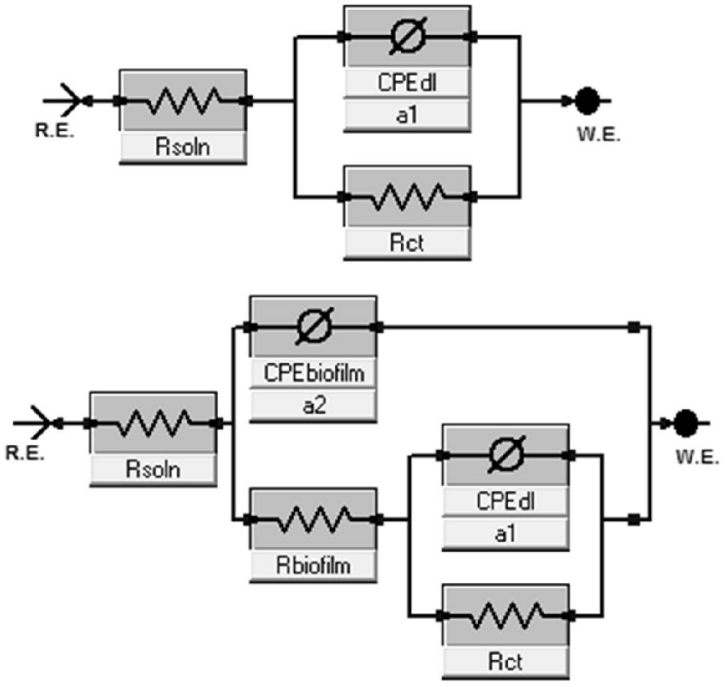

Figure 7.4. Equivalent circuit models used in fitting the experimental biofilm impedance curves; circuits are adopted from Garmy EChem Analyst software's model editor.

Apart from the Nyquist curves, it can also be observed that the total impedance (as well as the phase angle magnitude) are higher (and lower for phase angle plot) in the presence of the bacterial endospores at the same frequency than those of the control. This explains that corrosion inhibition process was enhanced by the adhesion of *B. licheniformis* biofilm on 316 L steel in the minimal salt medium. Protective bacterial biofilm capable of reducing corrosion are known to influence electrochemical reactions by forming cellular cluster thereby colonizing the metal surface [154]. Magnitudes of Z_{mod} for the abiotic and biotic systems vary significantly at all the frequencies under study, with 202, 14200 and 18500 ohm per square centimeter recorded for the control, System A and System 2A, respectively, at 0.01 Hz. Higher magnitudes of Z_{mod} represents improved protection and lower values of Z_{mod} obtained for the control denotes corrosion activation in the presence of the saline minimal salt medium without the bacterial cells. The phase angle plots (Figure 7.2 c) show distinct phase deviation in the presence of the bacteria as the biofilm

is formed on steel with minima observed between 0.01 and 1 Hz for the biotic systems and at 7.90 Hz for the control. Equivalent circuit models (Figure 7.4.) were deployed to fit the experimental biofilm impedance data; values of the electrochemical parameters derived are presented in Table 7.2.

Table 7.2 Electrochemical parameters derived from ac and dc experiments for the *B. licheniformis* inoculate in the culture medium compared to the control.

Electrochemical parameters	Control	A	2A
ac (EIS):			
R_{soln} (Ω)	1.147	4.172	4.302
$R_{biofilm}$ (kΩ)	–	3.613	77.050
$CPE_{biofilm}$ (Y_o, mF cm^{-2} s$^{-(1-\alpha c)}$)	–	0.764	0.151
a_2	–	0.84	0.85
R_{ct} (kΩ)	0.149	1.956	38.170
CPE_{dl} (Y_o, mF cm^{-2} s$^{-(1-\alpha c)}$)	1.737	0.679	0.359
a_1	0.813	0.845	0.859
CIRCUIT TYPE	**R(Q(R))**	**R(Q(R(QR)))**	**R(Q(R(QR)))**
dc (Tafel):			
I_{corr} (μA)	8.07	4.00	0.878
E_{corr} (mV)	–143	–124	–59
CR (mpy) x 10^{-3}	409.600	203.300	44.580

Magnitudes of solution resistance (R_{soln}), resistance of the biofilm layer ($R_{biofilm}$), charge transfer resistance (R_{ct}), and the capacitances of the double (CPE_{dl}) and biofilm ($CPE_{biofilm}$) layers are represented in the equivalent circuit models used in fitting the experimental impedance data of the bacterial-inoculated systems compared to control system (Table 7.2). For the abiotic (control) system, only a single adsorption layer is represented with components of R_{soln}, CPE_{dl} and R_{ct}. Solution resistance is measured between the working and reference electrodes while charge transfer resistance accounts for current leakages. Higher values of R_{soln} in the bacterial-inoculated systems compared to control could be linked with the bacterial metabolic processes occurring in the culture medium [153]; 1.147, 4.172 and 4.302 Ω are R_{soln} values for the control, System A and

System 2A, respectively. Higher values of R_{ct} and $R_{biofilm}$ for the biotic systems compared to the control denotes biocorrosion resistance of 316 L stainless steel in the saline medium [153,155]. With values of R_{ct} for the control, System A and System 2A recorded as 0.146, 1.956 and 38.170 k Ω, very compact bacterial biofilm–metal oxide layer is conceived to form at the metal surface for System 2A compared to System A; this is expected as double the amount of the bacterial suspension was used in its (2A) starter culture [153]. The formation of more thicker and compact biofilm layers on steel for System 2A must be the reason for higher $R_{biofilm}$ values compared to System A. $R_{biofilm}$ represents the formation of EPS as well as the resistance of the formed bacterial biofilm layer to the passage of ionic current of corrosive chloride ions (in combination with other aggressive ions/molecules inherent in the minimal salt medium at 37 ^{o}C) after 3 week immersion. More bacteria cells must have attached on the steel surface resulting in electron-transfer barrier; this can also be explained in terms of increased metabolic activities as more cells (thicker biofilms) are formed [156]. Constant phase element (CPE) replaces pure capacitator in the equivalent circuit so as to account for metal surface irregularities/inhomogeneity as well as those of the electrode/electrolyte interface. In this study, the trend of CPE for the bacterial-inoculated systems compared to the control, could be linked with surface inhomogeneity as the bacterial biofilm is formed on the metal surface. Values of $CPE_{biofilm}$ (and CPE_{dl}) for the System A and System 2A are 0.764 and 0.151 mF cm^{-2} $s^{-(1-\alpha c)}$ while 0.679 and 0.359 mF cm^{-2} $s^{-(1-\alpha c)}$) represents values of CPE_{dl}; lower CPE values for System 2A denote compact and denser biofilm formation on steel compared to System A [153]. Normally for most bacteria, biofilm formation begins with cellular attachment in clusters and as they colonize the surface. If surface attachment is irreversible, more complex

community of bacteria cells in the biomatrix could mature into a biofilm at a particular stage in their development depending on the availability of nutrients. EIS presents a suitable real time and online technique for monitoring biofilm formation since the application of minute voltage perturbation accompanying the technique have little or no effect on the attached bacterial cells. Polarization technique can also be used to study the same process at $E_{corr.}$ In this study, Tafel polarization method has been deployed to study the biofilm formation; the curves are presented in Figure 7.3 (d) and the extrapolated parameters enlisted in Table 7.2. The presence of bacterial-inoculated systems shift the magnitudes of potential to more positive values (anodic); with ─124 and ─59 mV recorded for both biotic systems (A and 2A, respectively) compared to the control (─143 mV). The presence of the bacterial-inoculated systems leads to reduced magnitudes of corrosion current density and corrosion rate, proving that the formation of the bacterial biofilm actually inhibited steel corrosion in the minimal salt medium. Corrosion rate stands at 400 x 10^{-3} mpy in the absence of the bacteria (control) compared to the biotic System A (203 x 10^{-3} mpy) and System 2A (44 x 10^{-3} mpy) while 8.07, 4.00 and 0.88 μA are the recorded values of corrosion current density for the control, System A and System 2A, respectively: I_{corr} (control) > I_{corr} (System A) > I_{corr} (System 2A). Results from this dc technique proves that bacterial biofilm formation inhibited steel corrosion in the minimal salt medium to a great extent; dc results are consistent with those obtained from the ac technique. The formation and maturation of this biomatrix led to reduction in pH of the medium as the more cells adhere on the steel substrate; and Figure 7.5 shows reducing culture media pH containing as more metabolic products are formed from inherent physiological bioactivity in the presence of the bacterial-inoculated systems (compared to

the control) for 316L at with exposure periods [153]. These products (alongside inorganic nutrients in the culture) supported the protective biofilm formation on surface of the metal. It was pertinent to complement the electrochemical technique with surface analytical evaluation of the adhering biofilm on the surface of the steel substrate especially, as the cellular growth continues in the minimal salt medium containing the needed nutrients.

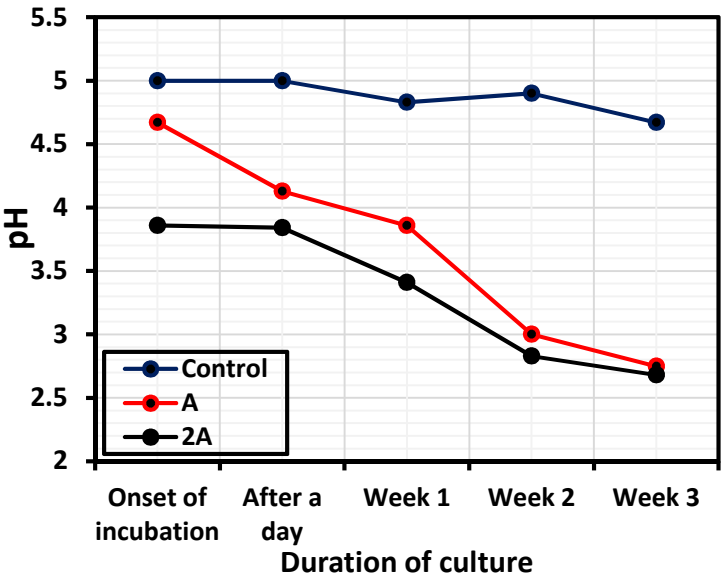

Figure 7.5. Variation in culture media pH containing *B. licheniformis* inoculates (compared to the control) for 316L corrosion at different exposure periods.

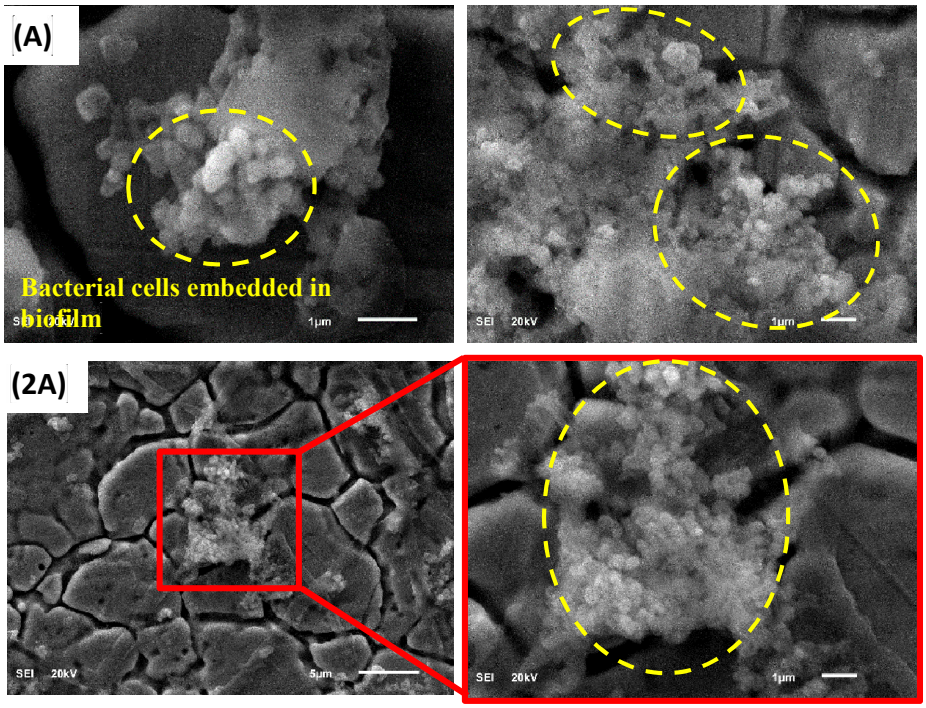

Figure 7.6 SEM images showing the *B. licheniformis* biofilms formed on 316L coupons after 3 weeks immersion in the culture medium.

7.3.2 Surface analyses

The *B. licheniformis* biofilms formed on 316L coupons after 3 weeks immersion in minimal salt culture medium are presented in the SEM micrographs in Figure 7.6. The biofilms are relatively compact and thick groups of bacterial cells enclosed in an EPS matrix on the metal substrate. As expected, the assemblage these gram-positive bacterial cells are grouped in colonies attached in no regular manner within the phase boundaries of the austenitic stainless steel as its microstructure is exposed. The biofilms on each biotic system still show imprints of rod-like (some appear round) shaped bacterial cells excepted of *B. licheniformis*. The SEM images for each bacterial-inoculate (Systems A and 2A) also reveal exposed grain boundaries properly delineated by the corrosive chloride ions of the saline etchant (the minimal salt medium); few pits are also observed. Pitting sites must have been much without the diffusional resistance caused by the formation of the bacterial biofilm matrix (cells, EPS, and inorganic solid phases) as well as the influence of its

metabolic physiological activity. The presence of these biofilms of the surface of the steel substrate immersed in the culture medium inhibited corrosion by limiting molecular oxygen diffusion at the cathodic sites as well as inhibit electron transfer from the anodic ferrous sites on the substrate [157]. EPS helps in binding the biofilm matrix to the metal surface, and the inhibiting properties of its constituents (polysaccharides, proteins, nucleic acids and phospholipids) must also have contributed to corrosion reduction of steel in the saline medium [153,158]. The thicknesses of the biofilms formed from both biotic systems cannot be comparable at this point, but the electrochemical results have shown superior perform of System 2A compared to System A due to the presence of double bacterial cells in the starter culture.

The functional group chemistry of the attached *B. licheniformis* biofilm on 316L coupons after 3 weeks immersion in culture medium is probed with FTIR in this study, and the spectra are displayed in Figure 7.7. The IR peaks characteristic of typical bacterial EPS are displayed on the spectra for System A and System 2A being a prove biofilm formation on steel; both spectra have no distinct difference (in shapes, intensity and position of IR absorption) since they originate from the EPS of the same bacterium.

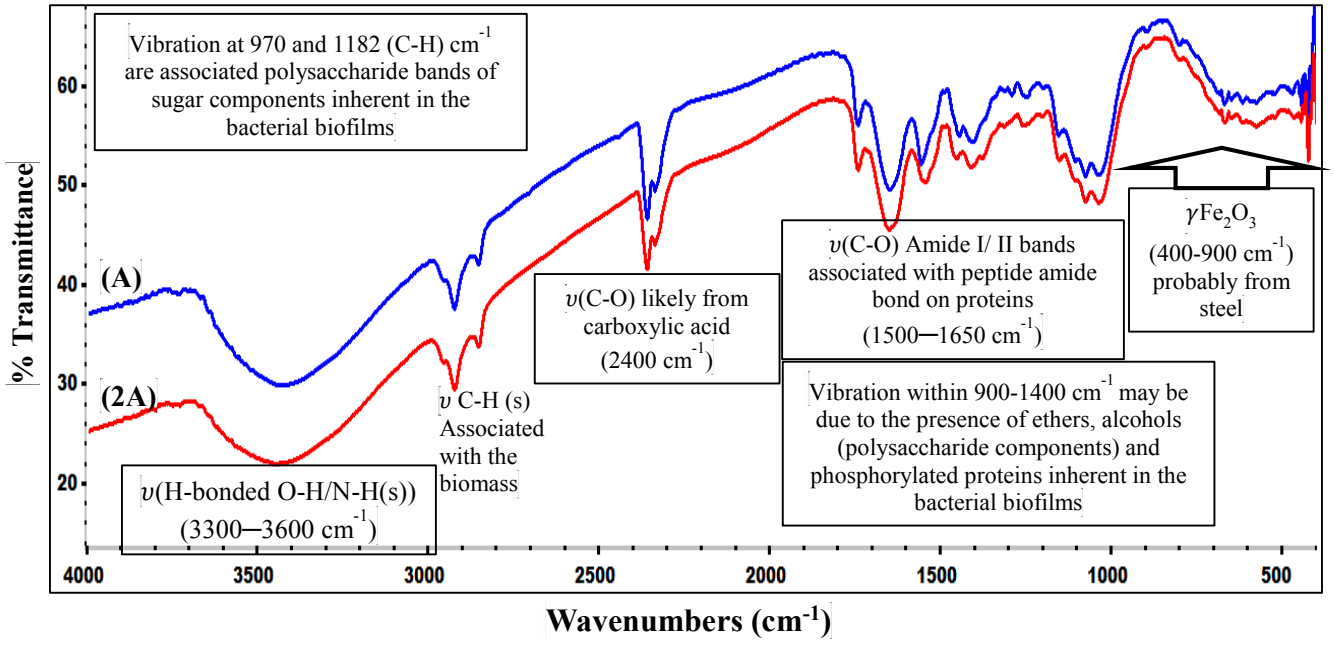

Figure 7.7. FTIR spectra of *B. licheniformis* biofilm formed on 316L coupons after 3 weeks immersion in culture medium.

Absorption peaks stretching between 1400 and 1900 cm^{-1} represent the protein portion of the bacterial EPS [153]. The appearance of C─O associated with peptide amide bonds (amide I and II at 1550 and 1650 cm^{-1}, respectively) on proteins are visible between 1500 and 1650 cm^{-1}; usually, this IR peaks are normally used in probing repetitive peptide amide functional groups in proteins. The resolution of IR peaks associated with protein and sugar could be problematic since peaks of amide II are usually less intense than amide I, and the presence of EPS's polysaccharides possesses a C–O stretching vibrational modes around this region (1610 cm^{-1}), and this may interfere with that of amide 1 [158,159]. Sugar bands are observed between 970 and 1180 cm^{-1} while peaks at between 2900 and 3000 cm^{-1} are C–H stretching vibrations associated with the bacterial biomass. While studying total sugar contents in dried bacterial samples with FTIR, Marcotte et al. [159], opined that IR peaks of polysaccharides can be identified by probing absorption peaks of functional groups characteristic of alkanol, alkanals, alkanones, alkanoic acids and even ethers. They suggested that the ratios of the peak area of polysaccharides and

amide II (or C–H stretching) can indicate the content of sugar in the dried bacterial biomass. IR vibration peak within 900─1400 cm^{-1} may be due to the presence of ethers, alcohols (polysaccharide components) and phosphorylated proteins inherent in the bacterial biofilms (C–OH, C– O–C bonds). υ(C-O) likely from carboxylic acid is present at 2400 $cm^{-1}$and the H-bonded O─H/N-H stretching vibrations (from a sugar/proteins or just from adsorbed molecular water) are visible between 3300 and 3600 cm^{-1}. γ─Fe_2O_3 (from the steel substrate) absorbs between 400−900 cm^{-1} [153]. FTIR results proves that the EPS biomatrix is dominantly proteins and polysaccharides; yet no further experiment was conducted to ascertain the bio-polymeric type inherent in the matrix. The structure of the biofilm as well as the chemistry of the EPS binding it to the substrate predetermines the ability of a biofilm-forming bacterium to act promote MIC or MIC inhibition (MICI) [153] and even transmit disease [160].

Figure 7.8 shows the SEM micrographs of the 316L steel coupon surfaces before and after the 3 weeks immersion in culture medium containing biofilm/ bacterial growths (compared with the control). The polished marks on the bare non-immersed coupon are still visible in some portions, but after immersion in the sterile minimal salt medium, the grain boundaries are exposed (and without corrosion products). In mild corrosive medium, due to the presence of special metallic constituents (like Ni, Cr and Mo) in stainless steel is known to form passive inhibiting layer that disallows further surface or bulk corrosion. However, the observed pitting on the passivated surface must have been due to the presence of corrosive chloride ions (present in the culture medium) as the metal is immersed continuously for a period of 3 weeks. In this medium, the steel substrate could not quickly re-passivate in the medium as the chloride ions attack the metal surface. A pit

is formed when the passive layer (cathodic) is penetrated by the corrosive ions as the rest of the metal becomes totally anodic. The surface of the steel coupon in the bacterial-inoculated systems do not corrode as much as the control proving the formation of *B. licheniformis* biofilm contributed to corrosion reduction to a great extent [153]. The EDX spectra (Figure 7.8; right panel) for both biotic and abiotic systems show the biofilm/corrosion products' components comprising of mainly oxide deposits of Cr and Fe [153], and the metals displayed on each spectrum are predominantly from the 316 L steel substrate itself.

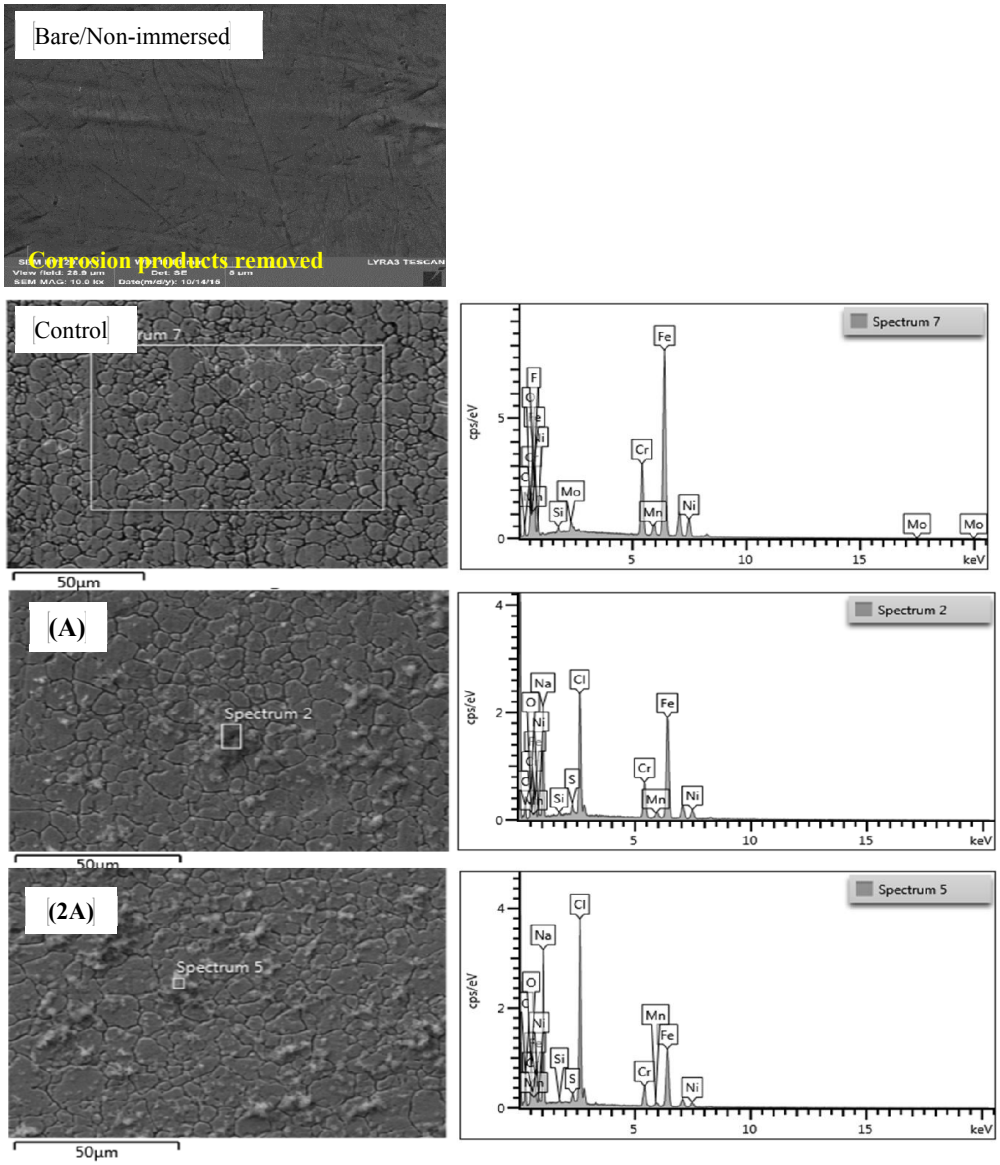

Figure 7.8 SEM/EDX micrographs showing the surfaces 316L steel coupons as *B. licheniformis* biofilms are formed on the substrate before and after 3 weeks immersion in culture medium containing biofilm/ bacterial growths.

Evidence of *B. licheniformis* growth from 100 µL of each biotic system of *B. licheniformis* suspension in the culture medium (on TT media after incubation at 50 ºC overnight) was observed at the end of the 3 weeks as presented in Figure 7.9. Compare to the control (without growth), the bacterial-inoculated systems show distinct bacterial growth colonies; 2 and 13 visible colonies for System A and System 2A, respectively; this proves presence of the bacteria cells in the culture medium even after 3 weeks. Since the steel substrate

used in this study was unsuitable for microscale fluorescence imaging of viable bacterial cells in the biofilm matrix, the same immersion test was conducted on ITO conductive glass slides immersed in a different culture medium (NB2 broth/Spizizen's salts solution with 0.1% wt/vol L-alanine and 0.5% wt/vol glucose). The glass substrates were stained with fluorescent dye (Baclight™ Live/Dead bacterial viability stain kits, Invitrogen, USA) before imaging. Figure 7.10 presents CLSM images of attached *B. licheniformis* cells/ biofilms on ITO conducting glass slides after a short and prolonged immersions in the modified culture medium. The absence of bacterial cells as observed on the CLSM micrograph of the control proved that this system is abiotic (a); supporting the electrochemical results and the findings from other surface analytical evaluations. Bacterial biofilm is observed in the bacterial-inoculate system after a brief culture period (b) and more cellular clusters as the duration of culture increases (c); proving that compact and thick bacterial biofilm formed on the ITO conducting glass slides on prolonged immersion in the bacterial culture.

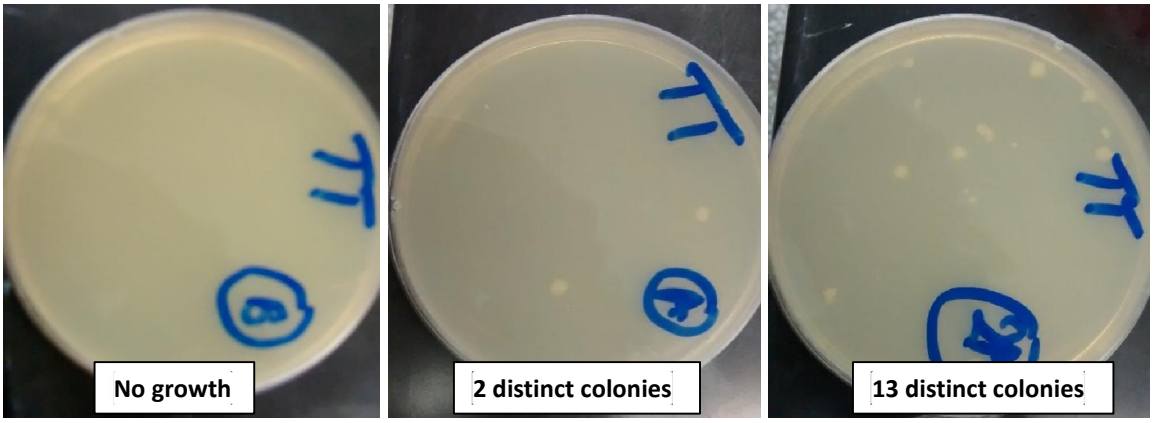

Figure 7.9. Evidence of bacterial growth from 100 µL of each *B. licheniformis* inoculate in the culture medium (in TT media after incubation at 50 °C for 18-24 hours).

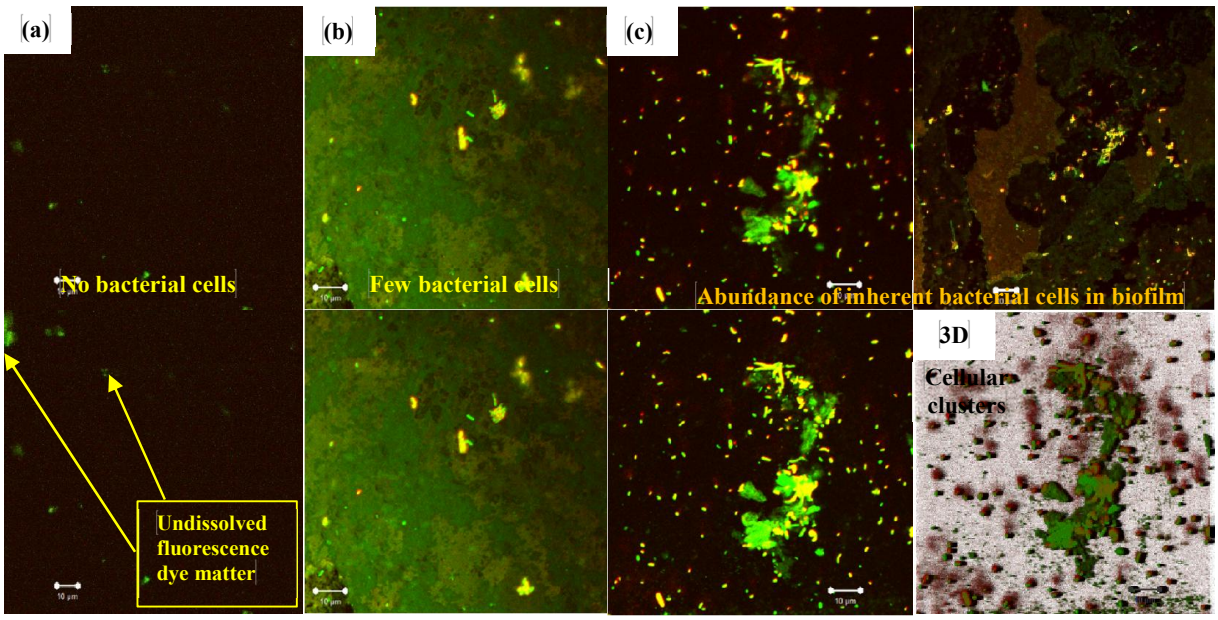

Figure 7.10. CLSM images of attached *B. licheniformis* cells/ biofilms on ITO conducting glass slides after (a) a short and (b) prolonged (about one month) immersion in culture medium (NB2 broth/Spizizen's salts solution with 0.1% wt/vol L-alanine and 0.5% wt/vol glucose).

7.4 Summary

The following conclusions were drawn from the results of the experiments:

1. Higher values of R_{soln} in the bacterial-inoculated systems compared to control could be linked with the bacterial metabolic processes occurring in the culture medium.
2. With values of R_{ct} for the control, System A and System 2A recorded as 0.146, 1.956 and 38.170 kΩ; this could be attributed to the formation of compact bacterial biofilm–metal oxide layer on the metal surface for System 2A compared to System A; this is expected as double the amount of the bacterial suspension was used in its (System 2A) starter culture.
3. The formation of more thicker and compact biofilm layers on steel for System 2A must be the reason for higher $R_{biofilm}$ values compared to System A. $R_{biofilm}$

represents the formation of EPS as well as the resistance of the formed bacterial biofilm layer to the passage of ionic current of corrosive chloride ions (in combination with other aggressive ions/molecules inherent in the minimal salt medium at 37 ^{o}C) after 3 week immersion.

4. The presence of the bacterial-inoculated systems led to reduced magnitudes of corrosion current density and corrosion rate, proving that the formation of the bacterial biofilm actually inhibited steel corrosion in the minimal salt medium. The variation in the magnitude of I_{corr} is in this order: I_{corr} (control) > I_{corr} (System A) > I_{corr} (System 2A).

5. SEM and CLSM images of the bacterial-inoculate show relatively compact and thick biofilm (groups of bacterial cells enclosed in an EPS matrix) proving that corrosion inhibition of the metal substrate was due to the formation of these bacterial biofilms on its surface; FTIR results suggests that the EPS biomatrix could be dominantly proteins and polysaccharides.

CHAPTER 8

Summary, conclusion and recommendations for future work

8.1 Summary and conclusion

For the first time, the foul-releasing and anticorrosion potentials of bacterial endospores of a thermophilic and apathogenic strain of *B. licheniformis* isolated from the hot Gazan springs of the Saudi Arabia have been studied. Endospores of this gram-positive bacterium were encapsulated within some newly synthesized protective sol-gel coatings in other to test for their ability to reduce marine fouling and corrosion of S36-grade mild steel in saline medium. From the results of the experiments conducted, the following can be summarized for all the systems of sol-gel coating:

1. The unmodified sol-gel coatings synthesized in this work have protected mild against corrosion to a great extent in 3.5 wt% NaCl solution; but improved protection is realised after doping them with corrosion inhibitor pigments and *B. licheniformis* endospores.
2. The *B. licheniformis* endospores encapsulated within every the sol-gel matrix remained viable as revealed by the confocal laser scanning fluorescence microscopy.
3. The presence of these bacterial endospores improved the surface hydrophobicity of the coating thereby preventing the diffusion of corrosion molecules and ions through the bulk of the coating to the metal surface; this is evident in the trend of electrochemical coating resistance and capacitance. Even in the absence of the bacterial endospores,

higher corrosion protection is obtained for sol-gel coating with hydrophobic surfaces (those with reduced surface energies).

4. For all sol-gel coating matrices synthesized in this study, corrosion resistance (or the protection efficiency) in 3.5 wt% NaCl is in this order:

Inhibitor modified biotic (in the presence of the bacterial endospores) >>> Inhibitor modified abiotic >> unmodified sol-gel coatings

5. Surface and bulk nano- and nicro-cracks are revealed on the endospores–loaded sol-gel coatings after prolonged immersion at room temperature in 3.5 wt% NaCl solution though not as much as they are on the abiotic modified and unmodified coatings; this demonstrates significant corrosion protection in the presence of the *B. licheniformis* endospores compared to the abiotic coatings.
6. The bacterial endospores possess antifouling potentials within the immersion period of study due to their foul-releasing effect; the improved corrosion and fouling resistance in the presence of these bacterial endospores could be attributed to surface hydrophobicity after spore encapsulation. Compared with the abiotic coating, the inability of the marine foulers to settle and adhere on this biotic surface, at hypersaline condition, gives an idea of its antibiotic nature and the antimicrobial properties of the biofilm of this axenic thermophilic bacterium strain.
7. The formation of more thicker and compact biofilm layers (bacterial cells enclosed in an EPS matrix) on steel substrate by bacterial-inoculate system on steel in appropriate saline culture medium reveals one of mechanisms of anticorrosion and antifouling activities of *B. licheniformis*. FTIR analysis of the attached EPS biomatrix reveals dominant proteins and polysaccharides composition.

8.2 Recommendations for future work

Based on the difficulties encountered in this work, and the quest to foster a better understanding of this experimental concept, the following has been suggested for further analyses in the future:

1. Protective sol-gel coatings capable of reducing corrosion in acidic and alkaline media should be synthesized and tested for mild steel.
2. The extent of sol-gel reactions depends on precursor types, but the exact routes of reaction are not defined since hydrolysis and condensation reactions as well as other side reactions occur simultaneously. To this end, the structure of the material cannot be obtained. Yet, the elucidation of the structural make up of these sol-gel materials is needed, including X-ray diffraction with more spectroscopic evaluations.
3. In this work, the reason for the bacterial anticorrosion and antifouling activities has been attributed to the hydrophobicity as well as the antibiotic surface in the presence of *B. licheniformis* endospores encapsulated within the sol-gel coatings. This could be due to the secretion of extracellular antibiotic polymeric substances with corrosion inhibiting potentials like anticorrosive γ-polyglutamate in some appreciable amount; this assertion should be proven by bacterial culturing and the subsequent chemical extraction of this homopolymer of glutamic acid from the biofilm. The antimicrobial nature of the bacterial biofilm should be tested comparatively with those of the extracted γ-polyglutamate from the same bacterial culture.

4. To ascertain the antifouling properties of these sets of protective coatings, fouling test should be repeated in the different seasons (including autumn, fall and winter, not just summer). Though the presence of barnacles, polychaetes and other macro-foulers are predominant in the summer, climatic changes could promote or reduce the formation of other marine foulers.
5. The use of primers is also recommended for prolong immersion in a typical marine enviorment.

References

[1] E.R.A. Lima, T. Jiang, J. Wu, A theoretical study of colloidal forces near amphiphilic polymer brushes, *Colloids and Surfaces A: Physicochem. Eng. Aspects* 384 (2011) 115─120.

[2] M.R. Detty, R.A. Ciriminna, F.V. Bright, M. Pagliaro, Environmentally Benign Sol-Gel Antifouling and Foul-Releasing Coatings, *Accounts of Chemical Research* 47 (2) (2014) 678–687.

[3] J. Schumacher, M. Carman, T. Estes, A. Feinberg, L. Wilson, M. Callow, J. Callow, J. Finlay, A. Brennan, Engineered antifouling microtopographies – effect of feature size, geometry, and roughness on settlement of zoospores of the green alga *Ulva, Biofouling* 23(1) (2007) 55─62.

[4] J.E. Gittens, T.J. Smith, R. Suleiman, R. Akid, Current and emerging environmentally-friendly systems for fouling control in the marine environment, *Biotechnology Advances* 31 (2013) 1738─1753

[5] M. Ebelmen, Sur les combinaisons des acides borique et silicique avec les ethers. *Annl Chim Phys* 16 (1846) 129–166

[6] M. Ebelmen, B. Bouquet, Sur les combinaisons des acides borique et silicique avec les ethers. *Annl. de Chim et de Phys III*. Ser. XL/16 (1846) 129.

[7] D. Segal, Chemical Synthesis of Advanced Ceramic Materials Cambridge University Press,UK, pp 58-78.

[8] S.M. Attia, J. Wang, G. Wu, J. Shen, J. Ma., Review on Sol-gel derived coating: process, techniques and optical application, *Journal of Material Science and Technology* 18 (3) (2002) 211─218.

[9] E. Wallström, H.T. Jespersen, K. Schaumburg, A new concept for anti-fouling paint for Yachts, *Progress in Organic Coatings* 72 (2011) 109─114.

[10] S. Dire, F. Babonneau, Sol-gel precursors: a spectroscopic study of transesterification reactions between silicon and titanium alkoxides, *Journal of Non-Crystalline Solids* 167 (1994) 29-36.

[11] B. Alonso, D. Massiot, M. Valentini, T. Kidcho, P. Innocenzi, Design of hybrid organic–inorganic materials through their structure control: The case of epoxy bearing alkoxides, *Journal of Non-Crystalline Solids* 354 (2008) 1615–1626.

[12] D. Wang, G.P. Bierwagen, Sol–gel coatings on metals for corrosion protection, *Progress in Organic Coatings* 64 (2009) 327─338.

[13] R.B. Figueira, C.J.R. Silva, E.V. Pereira, Hybrid sol–gel coatings for corrosion protection of hot-dip galvanized steel in alkaline medium, *Surface & Coatings Technology* 265 (2015) 191─204.

[14] M. Gobara, H. Kamel, R. Akid, A. Baraka, Corrosion behaviour of AA2024 coated with an acid-soluble collagen/hybrid silica sol–gel matrix, *Progress in Organic Coatings* 89 (2015) 57–66.

[15] M. Criadoa, I. Sobrados, J.M. Bastidas, J. Sanz, Steel corrosion in simulated carbonated concrete pore solution its protection using sol–gel coatings, *Progress in Organic Coatings* 88 (2015) 228–236.

[16] E. Borovin, E. Callone, R. Ceccato, A. Quaranta, S. Dire, Adsorptive properties of solegel derived hybrid organic/inorganic coatings, *Materials Chemistry and Physics*, 147 (2014) 954─962.

[17] R.V. Lakshmi, T. Bharathidasan, P. Bera, B.J. Basu, Fabrication of superhydrophobic and oleophobic sol–gel nanocomposite coating, *Surface & Coatings Technology* 206 (2012) 3888─3894.

[18] T.J. Lee, S.H. Kwon, B.K. Kim, Biodegradable sol–gel coatings of waterborne polyurethane/gelatin chemical hybrids, *Progress in Organic Coatings* 77 (2014) 1111─1116.

[19] A. Roy, S.S. Singh, M.K. Datta, B. Lee, J. Ohodnicki, P.N. Kumta, Novel sol–gel derived calcium phosphate coatings on Mg4Y alloy, *Materials Science and Engineering B*, 176 (2011) 1679─1689.

[20] B. Mahltig, H. Haufe, H. Bottcher, Functionalisation of textiles by inorganic sol–gel coatings, *Journal of Materials Chemistry A,* 15 (2005) 4385–4398.

[21] S.D. Wang, B.J. Lin, C.C. Hsieh, C.C. Lin, Application of superhydrophobic sol gel on canvas, *Applied Surface Science* 307 (2014) 101─108.

[22] M. Zaharescu, L. Predoana, A Barau, D. Raps, F Gammel, N.C Rosero-Navarro, Y.Castro, A Durán, M Aparicio, SiO_2 based hybrid inorganic–organic films doped with TiO_2–CeO_2 nanoparticles for corrosion protection of AA2024 and Mg-AZ31B alloys, *Corrosion Science* 51 (2009) 1998–2005.

[23] H.R. Jeon, J.H. Park, M.Y. Shon, Corrosion protection by epoxy coating containing multi-walled carbon nanotubes, *Journal of Industrial Engineering Chemistry* 19 (2013) 849─853.

[24] A. Gergely, E. Pfeifer, I. Bertóti, T. Török, E. Kálmán, Corrosion protection of cold-rolled steel by zinc-rich epoxy paint coatings loaded with nano-size alumina supported polypyrrole, *Corrosion Science* 53 (2011) 3486─3499.

[25] F. Ansari, R. Naderi and C. Dehghanian, Improvement in the corrosion resistance of stainless steel 304L in sodium chloride solution by a nanoclay incorporated silane coating, *RSC Advances*, 5 (2015) 706.

[26] R. Sharmila, N. Selvakumar, K. Jeyasubramanian, Evaluation of corrosion inhibition in mild steel using cerium oxide nanoparticles, *Materials Letters* 91 (2013) 78─80.

[27] S.A.S. Dias, S.V. Lamaka, C.A. Nogueira, T.C. Diamantino, M.G.S. Ferreira, Sol–gel coatings modified with zeolite fillers for active corrosion protection of AA2024, *Corrosion Science* 62 (2012) 153─162.

[28] A.S. Kousalya, A. Kumar, R. Paul, D. Zemlyanov, T.S. Fishe, Graphene: An effective oxidation barrier coating for liquid and two-phase cooling systems, *Corrosion Science*, 69 (2013) 5─10.

[29] Z, Ma, C.C. Li, H.M. Wei, D.Q. Ding, Silica sol-gel anchoring on aluminum pigments surface for corrosion resistance based on aluminum oxidized by hydrogen peroxide, *Dyes and Pigments* 114 (2015) 253─258

[30] P. Pi, C. Liu, X. Wen, L. Zheng, S. Xu, J. Cheng, Improved performance of aluminum pigments encapsulated in hybrid inorganic–organic films, *Particuology* 19 (2015) 93─98

[31] L. Li, P. Pi, X. Wen, J. Cheng, Z. Yang, Optimization of sol–gel coatings on the surface of aluminum pigments for corrosion protection, *Corrosion Science* 50 (2008) 795─803.

[32] R. Supplit, U. Schubert, Corrosion protection of aluminum pigments by sol–gel coatings *Corrosion Science* 49 (2007) 3325─3332.

[33] Y. Zhang, H. Ye, H. Liu, K. Han, Preparation and characterisation of aluminium pigments coated with silica for corrosion protection, *Corrosion Science* 53 (2011) 1694─1699.

[34] A.N. Khramov, N.N. Voevodin , V.N. Balbyshev , R.A. Mantz, Sol–gel-derived corrosion-protective coatings with controllable release of incorporated organic corrosion inhibitors, *Thin Solid Films* 483 (2005) 191─196.

[35] A. Kakaroglou, B. Nisol, T. Hauffman, I.D. Graeve, F. Reniers, G.V. Assche, H. Terryn, Incorporation of corrosion inhibitor in plasma polymerized allyl

methacrylate coatings and evaluation of its corrosion performance, *Surface & Coatings Technology* 259 (2014) 714─724.

[36] N. Voevodin, N.T. Grebasch, W.S. Soto, F.E. Arnold, M.S. Donley, Potentiodynamic evaluation of sol-gel coatings with inorganic inhibitors, *Surface and Coatings Technology* 140 (2001) 24─28.

[37] R. Naderi, M.M. Attar, Cathodic disbondment of epoxy coating with zinc aluminum polyphosphate as a modified zinc phosphate anticorrosion pigment, *Progress in Organic Coatings* 69 (2010) 392─395.

[38] S.M. Mousavifard, P.M. Nouri, M.M. Attar, B. Ramezanzadeh The effects of zinc aluminum phosphate (ZPA) and zinc aluminum polyphosphate (ZAPP) mixtures on corrosion inhibition performance of epoxy/polyamide coating, *Journal of Industrial and Engineering Chemistry* 19 (2013) 1031─1039.

[39] M.R. Heydarpour, A. Zarrabi, M.M. Attar, B. Ramezanzadeh, Studying the corrosion protection properties of an epoxy coating containing different mixtures of strontium aluminum polyphosphate (SAPP) and zinc aluminum phosphate (ZPA) pigments, *Progress in Organic Coatings* 77 (2014) 160─167.

[40] R. Naderi, M.M. Attar, Electrochemical study of protective behavior of organic coating pigmented with zinc aluminum polyphosphate as a modified zinc phosphate at different pigment volume concentrations, *Progress in Organic Coatings* 66 (2009) 314─320.

[41] R. Naderi, M.M. Attar, Electrochemical assessing corrosion inhibiting effects of zinc aluminum polyphosphate (ZAPP) as a modified zinc phosphate pigment, *Electrochimica Acta* 53 (2008) 5692─5696.

[42] X. Lu, Y. Zuo, X. Zhao, Y. Tang, The influence of aluminum tri-polyphosphate on the protective behavior of Mg-rich epoxy coating on AZ91D magnesium alloy, *Electrochimica Acta* 93 (2013) 53─64.

[43] S. Papavinasam (2014) "Monitoring external corrosion", Corrosion control in the oil and gas industry, Elsevier, Dhu'l-H. 10, 1434 AH - Science pp. 715-750.

[44] J.G. Speight (2014) "Corrosion monitoring and control; Chapter 6", Oil and Gas Corrosion Prevention: From Surface facilities to refineries, Gulf Professional Publishing, Jum. I 12, 1435 AH - Science pp. 109-149.

[45] C.S. Gudipati, M. Greenlief, J.A. Johnson, P. Prayongpan, K.I. Wooley, Hyperbranched Fluoropolymer and Linear Poly(ethylene glycol) Based

Amphiphilic Crosslinked Networks as Efficient Antifouling Coatings: An Insight into the Surface Compositions, Topographies, and Morphologies, *Journal of Polymer Science: Part A: Polymer Chemistry* 42 (2004) 6193─6208.

[46] J.A. Mielczarski, E. Mielczarski, G. Galli, A. Morelli, E. Martinelli, E. Chiellini, The Surface-Segregated Nanostructure of Fluorinated Copolymer-Poly(dimethylsiloxane) Blend Films, *Langmuir* 26(4) (2010) 2871─2876.

[47] M. Berglin, K.J. Wynne, P. Gatenholm, Fouling-release coatings prepared from α, ω-dihydroxypoly(dimethylsiloxane) cross-linked with (heptadecafluoro-1,1,2,2-tetrahydrodecyl)triethoxysilane, *Journal of Colloid and Interface Science* 257 (2003) 383─391.

[48] I. Marabotti, A. Morelli, L.M. Orsini, E. Martinelli , G. Galli, E.Chiellini, E.M. Lien , M.E. Pettitt , ME. Callow, J.A. Callow, S.L. Conlan, R.J. Mutton, A.S. Clare, A. Kocijane, C. Donike, M. Jenko, Fluorinated/siloxane copolymer blends for fouling release: chemical characterization and biological evaluation with algae and barnacles, *Biofouling* 25 (6) (2009) 481─493.

[49] M.A. Grunlan, N.S. Lee, F. Mansfeld, E. Kus, J.A. Finlay, J.A. Callow, M.E. Callow, W.P. Weber, Minimally Adhesive Polymer Surfaces Prepared from Star Oligosiloxanes and Star Oligofluorosiloxanes, *Journal of Polymer Science: Part A: Polymer Chemistry* 44 (2006) 2551─2566.

[50] Mera, A. E.; Wynne, K. J. Fluorinated silicone resin fouling release composition. US6265515, 2001.

[51] W.R. Lampe, A.A. Moore, K.R. Hartley, Marine foulant release coating, US 4861670 A, 1989.

[52] E. Martinelli, S. Agostini, G. Galli, E.Chiellini, A. Glisenti, M.E. Pettitt, M.E. Callow, J.A. Callow, K. Graf, F.W. Bartels, Nanostructured Films of Amphiphilic Fluorinated Block Copolymers for Fouling Release Application, *Langmuir* 24 (2008) 13138─13147.

[53] S. Krishnan, N. Wang, C.K. Ober, J.A. Finlay, M.E. Callow, J.A. Callow, A. Hexemer, K.E. Sohn, E.J. Kramer, D.A. Fischer, Comparison of the Fouling Release Properties of Hydrophobic Fluorinated and Hydrophilic PEGylated Block Copolymer Surfaces: Attachment Strength of the Diatom *Navicula* and the Green Alga Ulva, *Biomacromolecules* 7 (2006) 1449─1462.

[54] M. Wouters, C. Rentrop, P. Willemsen, Surface structuring and coating performance Novel biocidefree nanocomposite coatings with anti-fouling and fouling-release properties, *Progress in Organic Coatings* 68 (2010) 4─11.

[55] R. Akid, H. Wang, T.J. Smith, D. Greenfield, J.C. Earthman, Biological Functionalization of a Sol–Gel Coating for the Mitigation of Microbial-Induced Corrosion, *Advanced Functional Material* 18 (2008) 203─211.

[56] J. Gittens, H. Wang, T. J. Smith, R. Akid, D. Greenfield, Biotic Sol-Gel Coating For The Inhibition Of Corrosion In Seawater, *ECS Transactions* 24 (1) (2010) 211─229.

[57] Premkumar, R., Sagi,E., Rozen, R., Belkin, S., Modestov, A., Lev, O. Fluorescent Bacteria Encapsulated in Sol−Gel Derived Silicate Films, *ChemMatters*. 14 (2002) 2676─2686.

[58] W. Ghach, M. Etienne, P. Billard, F.P.A. Jorand, A. Walcarius, Electrochemically assisted bacteria encapsulation in thin hybrid sol–gel films, *Journal of Materials Chemistry B* 1 (2013) 1052─1059.

[59] L.L. Hench, J.K. West, The Sol-Gel Process, Chemical Reviews 90 (1990) 33-72.

[60] E. Salahinejad, M.J. Hadianfard, D.D. Macdonald, M. Mozafari, D. Vashaee, L. Tayebi, A new double-layer sol–gel coating to improve the corrosion resistance of a medical-grade stainless steel in a simulated body fluid, *Materials Letters* 97 (2013) 162─165.

[61] M. Norouzia, A.A. Garekan, Corrosion protection by zirconia-based thinfilms deposited by a sol–gel spin coating method, *Ceramics International* 40 (2014) 2857─2861.

[62] J.B. Cambon, F. Ansart, J.P. Bonino, V. Turq, Effect of cerium concentration on corrosion resistance and polymerization of hybrid sol–gel coating on martensitic stainless steel, *Progress in Organic Coatings* 75 (2012) 486─493.

[63] M. Fedela, M. Poelman, M. Zago, C. Vandermiers, D. Cossement, M.G. Olivier, F. Deflorian, Influence of formulation and application parameters on the performances of a sol–gel/clay nanocomposite on the corrosion resistance of hot-dip galvanized steel. Part II. Effect of curing temperature and time, *Surface & Coatings Technology* 274 (2015) 9─17.

[64] E. Certhoux, F. Ansart, V. Turq, J.P. Bonino, J.M. Sobrino, J. Garcia, J. Reby New sol–gel formulations to increase the barrier effect of a protective coating against the corrosion of steels, *Progress in Organic Coatings* 76 (2013) 165–172.

[65] S. Kirtay, Preparation of hybrid silica sol–gel coatings on mild steel surfaces and evaluation of their corrosion resistance, *Progress in Organic Coatings* 77 (2014) 1861─1866.

[66] S. Omar, F. Repp, P.M. Desimone, R. Weinkamer, W. Wagermaier, S. Ceré, J.. Ballarre, Sol–gel hybrid coatings with strontium-doped 45S5 glass particles for enhancing the performance of stainless steel implants: Electrochemical, bioactive and *in vivo* response, *Journal of Non-Crystalline Solids* 425 (2015) 1–10

[67] M. Criado, I. Sobrados, J.M. Bastidas, J. Sanz, Steel corrosion in simulated carbonated concrete pore solution its protection using sol–gel coatings, *Progress in Organic Coatings* 88 (2015) 228–236.

[68] M.J. Juan-Díaz, M. Martínez-Ibánez, M. Hernández-Escolano, L. Cabedo, R. Izquierdo, J. Suay, M. Gurruchaga, I. Goni. Study of the degradation of hybrid sol–gel coatings in aqueous Medium, *Progress in Organic Coatings* 77 (2014) 1799─1806.

[69] I. Pavlovska, K. Malnieks, G. Mezinskis, L. Bidermanis, M. Karpe, Hard TiO_2–SiO_2 sol–gel coatings for enamel against chemical corrosion, *Surface & Coatings Technology* 258 (2014) 206─210.

[70] A. Duran, A. Conde, A. Gomez-Coedo, T. Dorado, C. Garcıa, S. Cere, Sol–gel coatings for protection and bioactivation of metals used in orthopaedic devices, *Journal of Materials Chemistry* 14 (2004) 2282─2290.

[71] F. Ansari, R. Naderi, C. Dehghanian, Improvement in the corrosion resistance of stainless steel 304L in sodium chloride solution by a nanoclay incorporated silane coating, *RSC Advances* 5 (2015) 706─716.

[72] R. Okner, A.J. Domb, D. Mandler, Electrochemically deposited poly(ethylene glycol)-based sol–gel thin films on stainless steel stents, *New Journal of Chemistry* 33 (2009) 1596–1604.

[73] R. Okner, G. Favaro, A. Radko, A.J. Domb, D. Mandler, Electrochemical codeposition of sol–gel films on stainless steel: controlling the chemical and physical coating properties of biomedical implants, *Physical Chemistry Chemical Physics* 12 (2010) 15265–15273.

[74] P. Kiruthika 1 , R. Subasri, A. Jyothirmayi, K. Sarvani, N.Y. Hebalkar, Effect of plasma surface treatment on mechanical and corrosion protection properties of UV-curable sol-gel based GPTS-ZrO2 coatings on mild steel, *Surface & Coatings Technology* 204 (2010) 1270–1277.

[75] H. Wang, R.Akid, Encapsulated cerium nitrate inhibitors to provide high-performance anti-corrosion sol–gel coatings on mild steel, *Corrosion Science* 50 (2008) 1142─1148.

[76] G. Ruhi, O.P. Modi, A.S.K. Sinha, I.B. Singh, Effect of sintering temperatures on corrosion and wear properties of sol–gel alumina coatings on surface pre-treated mild steel, *Corrosion Science* 50 (2008) 639–649.

[77] S.K. Tiwari, R.K. Sahu, A.K. Pramanick, R.Singh Development of conversion coating on mild steel prior to sol gel nanostructured Al_2O_3 coating for enhancement of corrosion resistance, *Surface & Coatings Technology* 205 (2011) 4960–4967.

[78] N. Asadi, R. Naderi, M. Saremi, Determination of optimum concentration of cloisite in an eco-friendly silane sol-gel film to improve corrosion resistance of mild steel, *Applied Clay Science* 95 (2014) 243–251.

[79] E. Nouri, M. Shahmiri, H.R. Rezaie, F. Talayian, Investigation of structural evolution and electrochemical behaviour of zirconia thin films on the 316L stainless steel substrate formed via sol–gel process, *Surface & Coatings Technology* 205 (2011) 5109─5115.

[80] R. Akid, M. Gobara, H. Wang, Corrosion protection performance of novel hybrid polyaniline/sol–gel coatings on an aluminium 2024 alloy in neutral, alkaline and acidic solutions, *Electrochimica Acta* 56 (2011) 2483─2492.

[81] H. Wang, R. Akid, M. Gobara, Scratch-resistant anticorrosion sol–gel coating for the protection of AZ31 magnesium alloy via a low temperature sol–gel route, *Corrosion Science* 52 (2010) 2565–2570.

[82] H. Wang, R. Akid, A room temperature cured sol–gel anticorrosion pre-treatment for Al 2024-T3 alloys, *Corrosion Science* 49 (2007) 4491─4503.

[83] M. May, H.M. Wang, R. Akid, Effects of the addition of inorganic nanoparticles on the adhesive strength of a hybrid sol–gel epoxy system, *International Journal of Adhesion & Adhesives* 30 (2010) 505–512.

[84] R. Suleiman, M. Mizanurrahman, N. Alfaifi, B. El Ali, R. Akid, Corrosion resistance properties of hybrid organic–inorganic epoxy–amino functionalised polysiloxane based coatings on mild steel in 3.5%NaCl solution, *Corrosion Engineering, Science and Technology*, 48(7) (2013) 525─529.

[85] R. Suleiman, M. Khaled, H. Wang, T. J. Smith, J. Gittens, R. Akid, B. Mohamad El Ali, A. Khalil, Comparison of selected inhibitor doped sol–gel coating systems for

protection of mild steel, *Corrosion Engineering, Science and Technology* 49(3) (2014) 189─196.

[86] R.M. Suleiman, Corrosion protective performance of epoxy-amino branched polydimethylsiloxane hybrid coatings on carbon steel, *Anti-Corrosion Methods and Materials* 61(6) (2014) 423─430.

[87] M.E. Callow, J.E. Callow, Marine biofouling: a sticky problem, *Biologist* 49 (2002) 4–10.

[88] L.D. Chambers, J.A. Wharton, R.J.K. Wood, F.C. Walsh, K.R. Stokes, Techniques for the measurement of natural product incorporation into an antifouling coating. *Progress in Organic Coatings* 77 (2014) 473–484.

[89] Office of Naval Research Corporate Strategic Communications; "New Hull Coatings Cut Fuel Use, Protect Environment", Story Number: NNS090605-04; Release Date:6/5/2009;1:45:00PM (http://www.navy.mil/submit/display.asp?story_id=45984).

[90] M. Salta, J. Warton, P. Stoodley, S. Dennington, L. Goodes, S. Werwinski, U. Mart, R. Wood, K. Stokes, Designing biomimetic antifouling surfaces. *Philosophical Transactions of the Royal Society* 368 (1929) (2008) 4729─4754.

[91] I. Omae, Organotin antifouling paints and their alternatives. *Applied Organometallics Chemistry* 17 (2003) 81─105

[92] R.W. Revie, E.D. Verink Jr. (2011) Chapter 7. Simplified Procedure for Constructing Pourbaix Diagrams; in: Uhlig's Corrosion Handbook (3rd Edition), John Wiley & Sons, Inc., Hoboken, New Jersey, US. DOI: 10.1002/9780470872864.ch7.

[93] M. A. Khiyami, E. A. Serour, M. M. Shehata and A. H. Bahklia, *African Journal of Biotechnology* 11 (2012) 4053─4062.

[94] R. M. M. Abed, A. Al-Thukair and D. de Beer, Bacterial diversity of a cyanobacterial mat degrading petroleum compounds at elevated salinities and temperatures, *FEMS Microbiology Ecology* 57 (2006) 290─301.

[95] Z. A. Mohamed, Toxic cyanobacteria and cyanotoxins in public hot springs in Saudi Arabia, *Toxicon*, 51 (2008) 17─27.

[96] A. Khalil, Isolation and characterization of three thermophilic bacterial strains (lipase, cellulose and amylase producers) from hot springs in Saudi Arabia, *African Journal of Biotechnology*, 10 (44) (2011) 8834─8839.

[97] P. Miquel, Monographie d'un bacille vivant au-dela de 70 ºC, *Ann Micrographic* 1 (1888) 3.

[98] A. Khalil, G. Anfoka and S. Bdour, *World Journal of Microbiology and Biotechnology*, 19 (2003) 239─241.

[99] B.L. Bramfitt, Structure/Property Relationships in Irons and Steels, Metals Handbook Desk Edition, 2nd Edition (J.R. Davis, Editor) p. 153─173; 1998 ASM International, US.

[100] T.J. Horr, G.D. Reynolds, I. Wark, The reactions of 3-glycidoxypropyltrimethoxysilane in acidic solutions on polymerization and in the presence of silica, *Journal of Adhesion Science and Technology* 11 (1997) 995─1009.

[101] T.H. Lee, E.S. Kang, B.S. Bae, Catalytic Effects of Aluminum Butoxyethoxide in Sol-Gel Hybrid Hard Coatings, *Journal of Sol-Gel Science and Technology* 27 (2003) 23─29.

[102] P. Innocenzi, C. Figus,T. Kidcho, M. Valentini, B. Alonso, M. Takahashi, Sol-gel reactions of 3-glycidoxypropyltrimethoxysilane in a highly basic aqueous solution, *Dalton Transactions* (2009) 9146─9152.

[103] I.R. Fontinha, M.M. Salta, M.L. Zheludkevich, M.G.S. Ferreira, EIS Study of Amine Cured Epoxy-silica-zirconia Sol-gel Coatings for Corrosion Protection of the Aluminium Alloy EN AW 6063, *Portugaliae Electrochimica Acta* 31 (2013) 307─319.

[104] B. Riegel, S. Plittersdorf, W. Kiefer, N. Hiisingb, U. Schubert, Raman spectroscopic analysis of the sol-gel processing of $RSi(OMe)_3/Si(OMe)_4$ mixtures, *Journal of Molecular Structure* 410-411 (1997) 157─160.

[105] M.S. Oliver, K.Y. Blohowiak, R.H. Dauskardt, Molecular structure and fracture properties of ZrOx/Epoxysilane hybrid films, *Journal of Sol-Gel Science and Technology* 55 (2010) 360─368.

[106] Wahab, M., Guo, W., Cho, W., Ha, C., Synthesis and Characterization of Novel Amorphous Hybrid Silica Materials. *Journal of Sol-Gel Science and Technology* 27 (2003) 333─341.

[107] E. Bakhshandeh, A. Jannesari, Z. Ranjbar, S. Sobhani, M.R. Saeb, Anti-corrosion hybrid coatings based on epoxy–silica nano-composites: Toward relationship between the morphology and EIS data, *Progress in Organic Coatings* 77 (2014) 1169─1183.

[108] X. Zhang, F. Zheng, L. Ye, P. Xiong, L. Yan, W. Yang, B. Jiang, A one-pot sol–gel process to prepare a superhydrophobic and environment-resistant thin film from ORMOSIL nanoparticles, *RSC Advances* 4 (2014) 9838.

[109] M.J. Juan-Díaz, M. Martínez-Ibánez, M. Hernández-Escolano, L. Cabedo, R. Izquierdo, J. Suay, M. Gurruchagaa, I. Goni. Study of the degradation of hybrid sol–gel coatings in aqueous medium, *Progress in Organic Coatings* 77 (2014) 1799─1806.

[110] M. Criado, I. Sobrados, J. Sanz, J.M. Bastidas, Steel protection using sol–gel coatings in simulated concrete pore solution contaminated with chloride, *Surface & Coatings Technology* 258 (2014) 485–494.

[111] H. Hassannejad, T. Shahrabi, F. Malekmohammadi, A. Shanagi, M. Aliofkhazraei, A. Oskuie, Effect of cerium doping on corrosion resistance of amorphous silica–titanium sol–gel coating, *Current Applied Physics* 10 (2010) 1022─1028.

[112] M. Criado, I. Sobrados, J. Sanz, J.M. Bastidas, Steel protection using sol–gel coatings in simulated concrete pore solution contaminated with chloride, *Surface & Coatings Technology* 258 (2014) 485─494.

[113] X.M. Zhang, L. Li, Y. Zhang, Study on the Surface Structure and Properties of PDMS/PMMA Antifouling Coatings, International Federation for Heat Treatment and Surface Engineering 20th Congress Beijing,China,23-25 October 2012, *Physics Procedia* 50 (2013) 328─336.

[114] D.A. Jones, Principles and Prevention of Corrosion, Prentice-Hall Inc., New Jersey, 1996.

[115] Korenblum, E., Sebastián, E., Paiva, M., Coutinho, C., Magalhães, F., Peyton, B., Seldin, L. Action of antimicrobial substances produced by different oil reservoir *Bacillus* strains against biofilm formation. *Applied Microbiology and Biotechnology* 79 (2008) 97─103.

[116] M. Mehanna, R. Basséguy, M.L. Délia, A. Bergel, Effect of *Geobacter sulfurreducens* on the microbial corrosion of mild steel, ferritic and austenitic stainless steels, *Corrosion Science* 51 (2009) 2596─2604.

[117] J. Gittens, H. Wang, T. J. Smith, R. Akid and D. Greenfield, in *Fifth International Symposium on Advances in Corrosion Protection by Organic Coatings*, eds. M. Kendig and D. Scantlebury, 2010, pp. 211─229.

[118] N. D. Vejar, M. I. Azocar, L. A. Tamayo, E. Gonzalez, J. Pavez, M. Gulppi, J. H. Zagal, X. Zhou, F. Santibaez and G. E. Thompson, Antibiofouling Properties of

Sol-Gel Type Polymers for Aluminium Alloys: Biocorrosion Protection Against *Pseudomonas Aeruginosa, Int. J. Electrochem. Sci* 8 (2013) 12062─12077.

[119] D. Tronelli, E. Maugini, F. Bossa, S. Pascarella, Structural adaptation to low temperatures − analysis of the subunit interface of oligomeric psychrophilic enzymes, *FEBS Journal* 274(17) (2007) 4595─4608.

[120] M. A. Wahab, W. Guo, W.J. Cho, C.S. Ha, Synthesis and Characterization of Novel Amorphous Hybrid Silica Materials, *Journal of Sol-Gel Science and Technology* 27 (2003) 333─341.

[121] H. Jeon, J. Park and M. Shon, Corrosion protection by epoxy coating containing multi-walled carbon nanotubes, *Journal of Industrial and Engineering Chemistry* 19 (2013) 849─853.

[122] D. Ornek, A. Jayaraman, B.C. Syrett, C.H. Hsu, F.B. Mansfeld, T.K. Wood, Pitting corrosion inhibition of aluminum 2024 by Bacillus biofilms secreting polyaspartate or γ-polyglutamate, *Applied Microbiology and Biotechnology* 58 (2002) 651─657.

[123] S.G. Batrakov, T.A. Rodionov, S.E. Esipov, N.B. Polyakov, V.I. Sheichenko, N.V. Shekhovtsov, S.M. Lukin, N.S. Panikov, Y.A. Nikolaev, A novel lipopeptide, an inhibitor of bacterial adhesion, from the thermophilic and halotolerant subsurface Bacillus licheniformis strain 603, *Biochimica et Biophysica Acta*, 1634 (2003) 107─115.

[124] Y.H. Ko, R.A. Gross, Effects of glucose and glycerol on γ-poly(glutamic acid) formation by *Bacillus licheniformis* ATCC 9945a, *Biotechnology and Bioengineering* 57 (1998) 430–437.

[125] K.A. Zarasvand, V.R. Rai, Microorganisms: Induction and inhibition of corrosion in metals, *International Biodeterioration & Biodegradation*, 87 (2014) 66─74.

[126] S. M. Mousavifard, P. M. Nouri, M. M. Attar and B. Ramezanzadeh, The effects of zinc aluminum phosphate (ZPA) and zinc aluminum polyphosphate (ZAPP) mixtures on corrosion inhibition performance of epoxy/polyamide coating, *Journal of Industrial and Engineering Chemistry*, 19 (2013) 1031─1039.

[127] A. S. Hamdy, D. P. Butt and A. A. Ismail, Electrochemical impedance studies of sol–gel based ceramic coatings systems in 3.5% NaCl solution. *Electrochimica Acta*, 52 (2007) 3310-3316.

[128] T. Darmanin, F. Guittard, Recent advances in the potential applications of bioinspired superhydrophobic materials, *Journal of Materials Chemistry A* 2 (2014) 16319-16359.

[129] B.N. Sahoo, B. Kandasubramanian, Recent progress in fabrication and characterization of hierarchical biomimetic superhydrophobic structures, *RSC Advances*, 4 (2014) 22053-22093.

[130] Y.L. Linda, Q. Wu, X.C. Shao, H.Y. Wang, C.C. Zheng, C. Wong, Hierarchical structured sol–gel coating by laser textured template imprinting for surface superhydrophobicity, *Soft Matter* 8 (2012) 6232─6238.

[131] D. Kumar, X. Wu, Q. Fu, J.W.C. Ho, P.D. Kanhere, L. Li, Z. Chen, Hydrophobic sol–gel coatings based on polydimethylsiloxane for self-cleaning applications, *Materials and Design* 86 (2015) 855─862.

[132] K.A. Manjumol, L. Mini, A.P. Mohamed, U.S. Hareesh, K.G.K. Warrier, A hybrid sol–gel approach for novel photoactive and hydrophobic titania coatings on aluminium metal surfaces, *RSC Advances* 3 (2013) 18062─18070.

[133] K. Balachandran, R. Venkatesh, R. Sivaraj, Synthesis of nano TiO_2-SiO_2 composite using sol–gel method: effect on size, surface morphology and thermal stability, *International Journal of Engineering Science and Technology* 2 (2010) 3695─3700.

[134] A. Paula, V. Pereira, W.L. Vasconcelos, R.L. Orefice, Novel multicomponent silicate/poly(vinyl alcohol) hybrids with controlled reactivity, *Journal of Non-Crystalline Solids* 273 (2000) 180─185.

[135] G.R. Bogart, D.E. Leyden, Spectroscopic investigation of the hydrolysis of glycidoxypropylsilane bound to silica surfaces, *Journal of Chromatography* 483 (1989) 209─221.

[136] G. Verma, S.K. Dhoke, A.S. Khanna, Polyester based-siloxane modified waterborne anticorrosive hydrophobic coating on copper. *Surface & Coatings Technology* 212 (2012) 101─108.

[137] S. Peng, Z. Zeng, W. Zhao, H. Li, J. Chen, J. Han, X. Wu. Novel functional hybrid silica sol–gel coating for copper protection via *in situ* thiol–ene click reaction, *RSC Advances* 4 (2014) 15776–15781.

[138] X. Zhang, Y.Y. Wu, S. Y. He, D. Z. Yang, Structural characterization of sol–gel composites using TEOS/MEMO as precursors, *Surface and Coating Technology* 201 (2007) 6051–6058.

[139] K. H. Wu, C. M. Chao, C. J. Yang, T. C. Chang, Synthesis and characterization of polydimethylsiloxane-cured organically modified silicate hybrid coatings, *Polymer Degradation and Stability* 91 (2006) 2917–2923.

[140] T. C. Chang, Y. T. Wang, Y. S. Hong, Y. S. Chiu, Organic–inorganic hybrid materials. V. Dynamics and degradation of poly(methyl methacrylate) silica hybrids, *Journal of Polymer Science, PartA:Polym.Chem*. 38 (2000) 1972–1980.

[141] S.A. Umoren, Y. Li, F.H. Wang, Synergistic effect of iodide ion and polyacrylic acid on corrosion inhibition of iron in H_2SO_4 investigated by electrochemical techniques, *Corrosion Science* 52 (2010) 2422–2429.

[142] S.J. Garcia, J. Suay, Optimization of deposition voltage of cataphoretic automotive primers assessed by EIS and AC/DC/AC, *Progress in Organic Coatings* 66 (2009) 306–313.

[143] A. Shakeri, H. Abdizadeh, M.R. Golobostanfard, Synthesis and characterization of thick PZT films via sol–gel dip coating method, *Applied Surface Science* 314 (2014) 711–719.

[144] D. Ornek, T.K. Wood, C.H. Hsu, Z. Sun, F. Mansfeld, *Corrosion science* 58 (2002) 761–767.

[145] D. Ornek , T.K. Wood, C.H. Hsu, F. Mansfeld, Corrosion control using regenerative biofilms (CCURB) on brass in different media, *Corrosion Science* 44 (2002) 2291–2302.

[146] F. Mansfeld, H. Hsu, D. Ornek, T. K. Wood, B. C. Syrett, *Journal of the Electrochemical Society*, 149 (2002) B130-B138.

[147] R. Zuo, T. K. Wood, Inhibiting mild steel corrosion from sulfate-reducing and iron-oxidizing bacteria using gramicidin-S-producing biofilms*, Applied Microbiology and Biotechnology* 65 (2004) 747-753.

[148] A. Jayaraman, F.B. Mansfeld, T.K. Wood, Inhibiting sulfate-reducing bacteria in biofilms by expressing the antimicrobial peptides indolicidin and bactenecin*, Journal of Industrial Microbiology and Biotechnology* 22 (1999) 167-175.

[149] P.J. Arps, J.C. Earthman, L.C. Xu, B.C. Syrett, R. Green, T. Wood, F.B. Mansfeld, Field Evaluation of Corrosion Control Using Regenerative Biofilms (CCURB). CORROSION/03. NACE International, San Diego, CA. Paper no. 03714 (2003).

[150] D. Xu, Y. Li, F. Song, T. Gu, Laboratory investigation of microbiologically influenced corrosion of C1018 carbon steel by nitrate reducing bacterium *Bacillus licheniformis*, *Corrosion Science* 77 (2013) 385–390.

[151] N. Bolton, M. Critchley, R. Fabien, N. Cromar, H. Fallowfield, Microbially influenced corrosion of galvanized steel pipes in aerobic water systems, *Journal of Applied Microbiology* 109 (2010) 239–247.

[152] J.M. Marques, F.P. deAlmeida, U. Lins, L. Seldin, E. Korenblum, Nitrate treatment effects on bacterial community biofilm formed on carbon steel in produced water stirred tank bioreactor *World Journal of Microbiology and Biotechnology* 28 (2012) 2355–2363.

[153] H.Z. Wadood, A. Rajasekar, Y.P. Ting, A.N. Sabari, Role of Bacillus subtilis and Pseudomonas aeruginosa on Corrosion Behaviour of Stainless Steel, *Arabian Journal of Science and Engineering* 40 (2015) 1825–1836.

[154] H. Zhang, Y. Tian, J. Wan, P. Zhao, Study of biofilm influenced corrosion on cast iron pipes in reclaimed water, *Applied Surface Science* 357 (2015) 236–247.

[155] E. Miranda, M. Bethencourt, F. Botana, M. Cano, J. SánchezAmaya, A. Corzo, J.G. De Lomas, M.L. Fardeau, B. Ollivier, Biocorrosion of carbon steel alloys by an hydrogenotrophic sulfate-reducing bacterium *Desulfovibrio capillatus* isolated from a Mexican oil field separator, *Corrosion Science* 48 (2006) 2417–2431.

[156] A. Dheilly, I. Linossier, A. Darchen, D. Hadjiev, C. Corbel, V. Alonso, Monitoring of microbial adhesion and biofilm growth using electrochemical impedancemetry, *Applied Microbiology and Biotechnology* 79 (2008) 157–164.

[157] I.T. Vargas, M.A. Alsina, J.P. Pavissich, G.A. Jeria, P.A. Pastén, M. Walczak, G.E. Pizarro, Multi-technique approach to assess the effects of microbial biofilms involved in copper plumbing corrosion, *Bioelectrochemistry* 97 (2014) 15–22.

[158] A. Rajasekar, Y.P. Ting, Microbial corrosion of aluminum 2024 aeronautical alloy by hydrocarbon degrading bacteria *Bacillus cereus* ACE4 and *Serratia marcescens* ACE2 *Ind. Eng. Chem. Res*. 49 (2010) 6054–6061.

[159] L. Marcotte, G. Kegelaer, C. Sandt, J. Barbeau, M. Lafleur, An alternative infrared spectroscopy assay for the quantification of polysaccharides in bacterial samples, *Anal. Biochem.* 361 (2007) 7–14.

[160] M.O. Suraju, S.L. Barnes, S. Sanamvenkata, M. Esmaeili, S. Shishodia, J.A. Rosenzweig, The effects of indoor and outdoor dust exposure on the growth,

sensitivity to oxidative-stress, and biofilm production of three opportunistic bacterial pathogens, *Science of The Total Environment* 538 (2015) 949–958.

Vitae

Name : Ubong Monday Eduok

Nationality : Nigerian

Date of Birth :7/26/1982

Email : ublook@yahoo.com/ umeduok@gmail.com

Address :C/o Dr. Saviour A. Umoren, Department of Chemistry, University of Uyo, Akwa Ibom, Nigeria

Academic Background :

- **PhD; Chemistry,** King Fahd University of Petroleum and Minerals, KSA, 2015.
  Research Focus: Fouling/corrosion inhibition with immobilized thermophilic bacterium in novel protective sol-gel coatings for steel ***(with Dr. M. Khaled/ Dr. R. Suleiman).***
- **M.Sc.; Analytical Chemistry,** University of Uyo, Nigeria, 2011.
  Research Focus: Effect of iodide ions on the corrosion inhibition performance of Sida acuta on steel ***(with Dr. S.A. Umoren)****.*
- **B.Sc.; Applied Chemistry,** University of Uyo, Nigeria, 2006.
  Research Focus: Corrosion inhibition by Polymer blends for Aluminium ***(with Dr. S.A. Umoren)****.*

AWARDS AND FELLOWSHIPS

- Saudi Arabian Government Graduate Fellowship for International Scholars tenable at King Fahd University of Petroleum and Minerals (KFUPM), KSA.
- Best Graduating M.Sc. Student, University of Uyo, Nigeria, 2011 (on basis of academic performance and published works).
- Second Best Graduating Student Chemistry/ School of Science, University of Uyo, 2006 (on basis of academic performance).

EXPERIENCES

Researcher/Lecturer; Department of Chemistry, King Fahd University of Petroleum/ Minerals, KSA; (2012-2015).

- Engaged in full-time corrosion/ biocorrosion research.
- Taught several classroom and lab-based chemistry courses allotted by the registrar.

- Assisted in administering (including grading) freshmen chemistry and other school examinations.
- Assisted in other departmental duties and student course registrations.

Research assistant; Materials and Corrosion Protection Research Laboratory, University of Uyo, Nigeria; (2011-2012) (with Dr. S.A Umoren).

- Developed metal inhibition systems with plant extracts and polymers (natural and synthetic); synthesized organic coatings and investigated materials corrosion and corrosion inhibition mechanisms on conventional and modified amorphous and crystalline surfaces.
- Developed expertise in the use of electrochemistry techniques for corrosion monitoring; scanning probe and microscopy to characterize corrosion morphology.
- Published some research articles with my Professor.

Teaching and Research assistantship, Chemistry, University of Uyo, Nigeria; (2008-2011)).

- Lectured and mentored freshmen chemistry, laboratory usage, and instrumentation.
- Designed various corrosion monitoring procedures for metal oxidation processes in various inhibition systems (Natural and Synthetic).
- Researched in the area of municipal soil and water quality assessment, and general environmental assessment.
- Acquired skills in editing conference proceedings and research project reports.
- Have to my credit some scientific journal and conference papers (details provided).
- Developed interest in fulltime field and laboratory-based research surface science and electrochemistry.

RESEARCH REVIEW ENGAGEMENTS

- Chemical Engineering Communications (Taylor and Francis).
- Journal of Environmental Chemical Engineering (Elsevier).
- Journal of Adhesion Science and Technology (Springer).
- Material Research Innovation (Springer).

AFFILIATED PROFESSIONAL SOCIETIES

- Member, National Association of Corrosion Engineers (NACE International).
- Member, American Chemical Society.
- Member, Electrochemical Society

SELECTED RESEARCH PUBLICATIONS

(1) **Ubong Eduok**, Rami Suleiman, Mazen Khaled, Robert Akid (2016). Enhancing water repellency and anticorrosion properties of a hybrid silica coating on mild steel, *Progress in Organic Coatings,* **93**, 97-108.

(2) **Ubong Eduok**, Rami Suleiman, Mazen Khaled, Thomas J. Smith, Jeanette Gittens, Robert Akid, Bassam El Ali, Amjad Khalil (2015). Anticorrosion/antifouling properties of bacterial spore-loaded sol-gel type coating for mild steel in saline marine condition: A

case of thermophilic strain of *Bacillus licheniformis*, *RSC Advances,* **5** (114), 93818-93830.

(3) Saviour A. Umoren, Edu Inam, Aniekan A. Udoidiong, Ime B. Obot, **Ubong M. Eduok,** Kyoung-Woong Kim (2015). Humic Acid from Livestock Dung: Ecofriendly Corrosion Inhibitor for 3SR Aluminum Alloy in Alkaline Medium, *Chemical Engineering Communications*, 202 (2), 206-216.

(4) S.A. Umoren, **U.M. Eduok**, M.M. Solomon (2014). Effect of polyvinylpyrrolidone–polyethylene glycol blends on the corrosion inhibition of aluminium in HCl solution, *Pigment & Resin Technology*, **43**(5), 299 –313.

(5) **U.M. Eduok**, S.A. Umoren, A.P. Udoh, (2012). Synergistic inhibition effects between leaves and stem extracts of *Sida acuta* and iodide ion for mild steel corrosion in 1 M H_2SO_4 solutions, *Arabian Journal of Chemistry*, **5**, 325–337.

(6) A.U. Israel, **U.M. Eduok**, E Inam, Kyoung-Woong Kim (2012). The role of pH in metal ion removal using coir dust and its modified extract resins, *Geosystem Engineering*, 15 (4), 269-279.

(7) U.J. Etim, S.A. Umoren, **U.M. Eduok** (2012). Coconut coir dust as a low cost adsorbent for the removal of cationic dye from aqueous solution, *Journal of Saudi Chemical Society*, http://dx.doi.org/10.1016/j.jscs.2012.09.014.

(8) S.A. Umoren, **U.M. Eduok**, A.U. Israel, I.B. Obot, M.M. Solomon (2012). Coconut coir dust extract: a novel eco-friendly corrosion inhibitor for Al in HCl solutions, *Green Chemistry Letters and Reviews*, **5**(3), 303-313.

(9) S.A. Umoren, **U.M. Eduok**, M.M. Solomon, A.P. Udoh, (2011). Corrosion inhibition by leaves and stem extracts of *Sida acuta* for mild steel in 1 M H_2SO_4 solutions investigated by chemical and spectroscopic techniques, *Arabian Journal of Chemistry*, doi:10.1016/j.arabjc.2011.03.008.

(10) S.A. Umoren, **U.M. Eduok** and E.E. Oguzie, (2008). Corrosion Inhibition of Mild Steel in 1 M H_2SO_4 by Polyvinyl Pyrrolidone and Synergistic Iodide Additives, *Portugaliae Electrochimica Acta*, **26**(6), 533-546.

SELECTED CONFERENCE PRESENTATIONS

(1) **Ubong Eduok**, Rami Suleiman, Jeanette Gittens, Mazen Khaled, Thomas J. Smith, Robert Akid, Bassam El Ali, Amjad Khalil. "Electrochemical Assessment of Corrosion Performance of Novel Hybrid Sol-gel Coatings", Submitted for presentation at the 16th Middle East Corrosion Conference and Exhibition to be held at the Gulf Hotel, Bahrain from the 8th to 11th February, 2016. (Session resources; to be organized by NACE International);

(2) Rami Suleiman, **Ubong M. Eduok**, Bassam El-Ali, "Corrosion Resistance of Novel Hybrid Sol-Gel Coating on Mild Steel in 3.5% NaCl solution", presented at the 19th International Corrosion Congress held at Jeju Island, South Korea from the 2nd to 6th November, 2014.

(3) **Ubong M. Eduok**, Rami Suleiman, Mazen Khaled, Amjad Khalid, Robert Akid, "An improved corrosion resistant sol-gel film for steel protection in saline solution: Bioelectrochemical assay", presented at the Gordon aqueous corrosion conference (Tools and Techniques for Corrosion Assessment) held at Colby-Sawyer College, New London, US from the 7th to 13th July, 2014.

(4) **Ubong M. Eduok**, Rami Suleiman, Mazen Khaled, "Electrochemical corrosion evaluation of a novel doped-sol-gel coating for LCS substrate in saline meduim" presented at the 15th Middle East Corrosion Conference and Exhibition held at the Gulf Hotel, Bahrain from the 3rd to 5th February, 2014. (Session resources; organized by NACE International);

WORKSHOPS

(1) **"Certificate of completion"** for a workshop organised by the Elsevier, Netherlands (Publishing Connect Webinar). Theme: "How reviewers look at your paper" presented by Jaap van Harten, Executive Publisher, Elsevier held on the October 2014.

(2) **"Certificate of attendance"** for a workshop organised by the Information Technology Centre, KFUPM, KSA. Theme: "Microsoft Exchange and Lync: messaging and collaboration platforms" sponsored by Microsoft and Global Knowledge held on the September 11th, 2012.

(3) **"Certificate of completion"** for a workshop organised by the Elsevier, Netherlands (Publishing Connect Webinar). Presented by Jaap van Harten, Executive Publisher, Elsevier held on the 21 August, 2015.
- Theme 1: "How Reviewers become Editors"
- Theme 2: "Peer review in Asia: special tips for Reviewers"
- Theme 3: "Why get involved in peer review?"

HOBBIES

Event planning and organization; poetry and music.

DATE/PLACE OF BIRTH

26th July 1982 / Calabar, Nigeria.

REFEREES (avaliable on request)